INVESTIGATION OF CHEMOMETRICS METHODS

FOR CHARACTERISING

DRIFT PHENOMENA IN ICP-AES

by

ANA MARÍA MARCOS-DOMÍNGUEZ

A thesis submitted to the University of Plymouth

in part fulfilment for the degree of

DOCTOR OF PHILOSOPHY

DEPARTMENT OF ENVIRONMENTAL SCIENCES

FACULTY OF SCIENCES

In collaboration with the
BRITISH GEOLOGICAL SURVEY

FEBRUARY 2001

COPYRIGHT STATEMENT

INVESTIGATION OF CHEMOMETRICS METHODS

FOR CHARACTERISING DRIFT PHENOMENA IN ICP-AES

ANA MARÍA MARCOS-DOMÍNGUEZ

ABSTRACT

The objective of this study was to fully characterise drift phenomena in inductively coupled plasma atomic emission spectroscopy (ICP-AES) in order to develop novel correction procedures to aid routine analysis. Long-term drift of the analytical signal continues to be a potential disadvantage when using ICP-AES and often necessitates regular recalibration.

The long-term stability of three commercially available instruments was studied using in each case a range of analyte and intrinsic plasma emission lines. Long-term fluctuations were observed which generated drift bias of up to 20% on the initial values. The drift patterns were characterised and found to be qualitatively reproducible. In most cases, similar long-term fluctuations were observed independent of the analyte or nature of the emission line. In addition, high inter-element correlation was observed on the long-term fluctuations even when sequential acquisition was employed.

In order to study the fundamental causes of drift, the effect of two key instrumental parameters, i.e. the RF power and the nebuliser gas flow rate were studied with respect to the stability of the signal. Different drift patterns were found depending on the working conditions. Classical statistical methods and a multi-way approach, PARAFAC, were then employed to describe the system.

The use of internal standards to correct for drift has also been investigated, but found to be of benefit only under certain defined conditions (i.e. robust conditions, high RF power and low nebuliser flow rate). At soft conditions, low RF power and medium to high nebuliser flow rate, the system is very unstable and internal standardisation is not fully effective as a correction method. For such conditions, a novel correction procedure has been developed, which employs the drift pattern of one intrinsic plasma line (i.e. an argon line) and a correction factor which is specific for each emission line. The drift values were reduced from around 20% before correction to better than ±2% following the described protocol.

Finally, the effects of chemical matrices on the long-term stability of the emission signals have been evaluated. Three synthetic matrices were prepared simulating nitric, soil and water matrices. The stability of the instrument when working with these matrices at both robust and soft conditions was found to be poor, especially when the solution was matched with the soil matrix. The use of more robust conditions did not improve the long-term stability of the emission signals.

The outcome of this study proved to be a better understanding of drift phenomena and a novel method for drift correction.

ACKNOWLEDGEMENTS

AUTHOR'S DECLARATION

At no time during the registration for the degree of Doctor of Philosophy has the author been registered for any other University award.

This study was financed with the aid of a studentship from the University of Plymouth and carried out in collaboration with the British Geological Survey.

Relevant scientific seminars and conferences were regularly attended at which work was often presented. Several papers have been published.

Signed:...

Dated: ...27. l. FEB l 2.001

TABLE OF CONTENTS

TABLE OF TABLES

TABLE OF FIGURES

CHAPTER 1

INTRODUCTION

1.1 THE ATOMIC SPECTRA

The most commonly used techniques for the determination of trace concentrations of metals in samples are based on atomic spectroscopy. These techniques involve electromagnetic radiation that is absorbed and/or emitted from atoms of a sample. The electromagnetic radiation is a type of energy that is transmitted through space at the speed of light. It can be defined by both wavelength and frequency. Figure 1.1 shows the different regions of the electromagnetic spectrum and the type of excitation that gives rise to each region.

FIGURE 1.1: THE ELECTROMAGNETIC SPECTRUM.

	Molecular Rotation		Molecular Vibration	Electronic Excitation				Core-Electron Excitation				Nuclear Excitation	
Radio	Microwave		Far Infrared	Near Infrared	Visible	Ultraviolet	Vacuum Ultraviolet	X - Ray				γ - Ray	Cosmic Rays

| 1 | 10^{-1} | 10^{-2} | 10^{-3} | 10^{-4} | 10^{-5} | 10^{-6} | 10^{-7} | 10^{-8} | 10^{-9} | 10^{-10} | 10^{-11} | 10^{-12} | 10^{-13} | 10^{-14} |

Wavelengths (m)
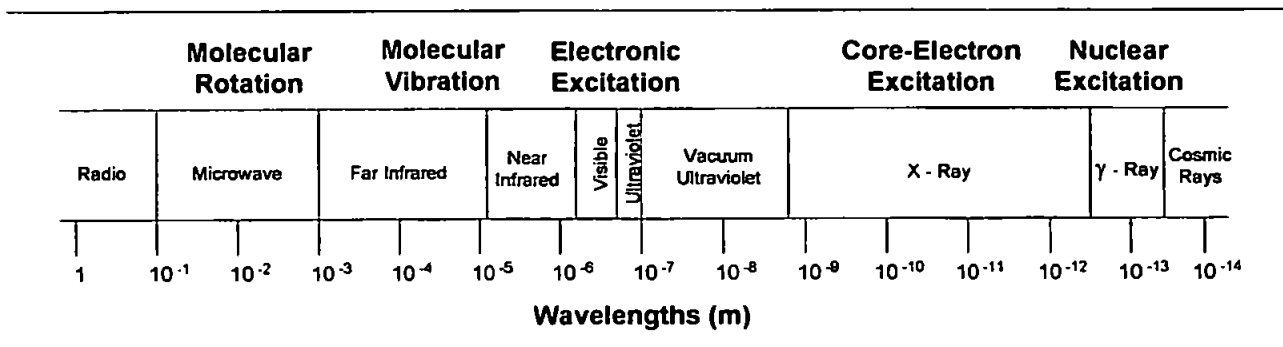
The atomic spectrum originates from energy transitions in the outer electronic shells of free atoms and ions. Atomic emission spectrometry (AES), atomic absorption spectrometry (AAS) and the atomic fluorescence spectrometry (AFS) are the three branches of analytical spectrometry, which provide analytical information from atomic spectra in the optical region of the electromagnetic spectrum, the ultraviolet and the visible, between 160 and 800 nm.

FIGURE 1.2: SCHEMATIC REPRESENTATION OF AAS, AES AND AFS

Atomic Absorption Spectroscopy	Atomic Emission Spectroscopy	Atomic Fluorescence Spectroscopy
E_j ⎯⎯⎯⎯ Absorption of radiation E_0 ⎯⎯⎯⎯	E_j ⎯⎯⎯⎯ Absorption of heat or chemical reaction — Emission of radiation E_i	E_j ⎯⎯⎯⎯ Absorption of radiation — Emission of radiation E_i ⎯⎯⎯⎯
$$v_{jo} = \frac{E_j - E_o}{h}$$	$$v_{ji} = \frac{E_j - E_i}{h}$$	$$v_{ji} = \frac{E_j - E_i}{h}$$
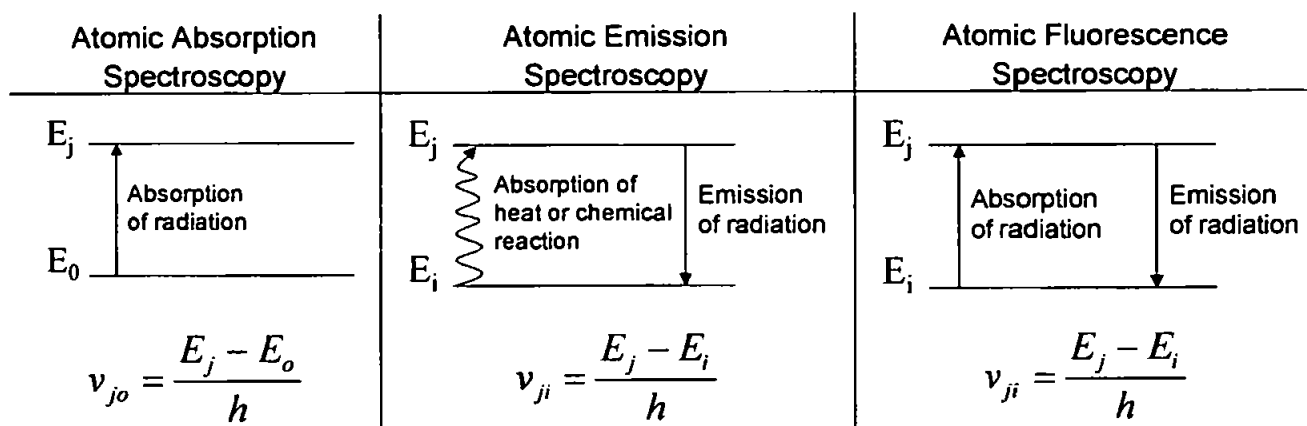
The emission and absorption of light by an analyte is associated with the transition of an electron from one energy level to another. The transition probability governs the intensity of the line, as does the concentration of the analyte in the sample. By using atomic spectroscopy techniques, meaningful qualitative and quantitative information can be obtained. Qualitative information is related to the wavelengths at which the radiation is absorbed or emitted while quantitative information can be acquired from the amount of radiation absorbed or emitted.

1.2 ICP-AES: AN OVERVIEW

Inductively coupled plasma atomic emission spectroscopy, ICP-AES, is a powerful analytical tool widely used for routine analysis. The method is based on atomic emission spectroscopy coupled with an ICP (Inductively Coupled Plasma) source.

1.2.1 ATOMIC EMISSION SPECTROSCOPY (AES):

The technique is based on the measurement of light emitted by chemical species after the absorption of energy. A source of energy promotes the outer electron from the ground state into an excited state. The excited atom then relaxes to the ground state and releases its excess energy as a photon of visible or ultraviolet light.

The difference in energy between the upper (E_m) and the lower (E_k) level defines the wavelength of the radiation that is involved in that transition:

$$h\nu = E_m - E_k$$

EQUATION 1.1

where h is the Planck's constant. In AES, wavelength (λ) is commonly used instead of frequency such that:

$$\lambda = c / \nu$$

EQUATION 1.2

where c is the velocity of the light (2.998×10^8 ms^{-1}). In atomic spectroscopy, wavelengths are usually expressed in nm (10^{-9} m). The intensity (I) of the transition is proportional to:

- the difference in energy between the upper and the lower level of the transition
- the population of electrons in the upper level, n_m
- the transition probability, A, between the upper and the lower level.

Thus:

$$I \propto (E_m - E_k)n_m A$$

The Boltzmann equation (Equation 1.3) relates the population of two quantum energy levels, assuming thermodynamic equilibrium conditions:

	Where:
$$\frac{n_m}{n_k} = \frac{g_m \exp\left(\frac{-E_m}{kT}\right)}{g_k \exp\left(\frac{-E_k}{kT}\right)}$$	n_m, n_k are the populations of the energy levels E_m, E_k g_m, g_k are the statistical weight of each level k is the Boltzmann constant ($k = 1.38 \times 10^{-23} JK^{-1}$) T is the temperature of the radiation source, the excitation temperature (K)

EQUATION 1.3

In order to relate the population of the excited levels, n_m, to total population, N, it is possible to sum the terms $g_m exp(-E_m/kT)$ for all possible levels. The partition function, Z, is defined as:

$$Z = g_o + g_1 \exp\left(\frac{-E_1}{kT}\right) + ... + g_m \exp\left(\frac{-E_m}{kT}\right) + ...$$

EQUATION 1.4

Using the partition function, the Boltzmann law may be modified to:

$$\frac{n_m}{N} = \frac{g_m \exp\left(\frac{-E_m}{kT}\right)}{Z}$$

EQUATION 1.5

This equation allows us to relate the intensity of the transition to the total population, and thus to the concentration of the species giving rise to the transition:

$$I = \Phi\left(\frac{hc g_m AN}{4\pi\lambda Z}\right) g_m \exp\left(\frac{-E_m}{kT}\right)$$

EQUATION 1.6

where Φ is a coefficient to account for the emission being isotropic over a solid angle of 4π steradian.

When a radiation source is stable enough to provide a constant temperature, the partition function Z will remain constant, and the number of atoms will be proportional to the

concentration. For a given emission line of an element, g_m, A, λ and E_m are constant. Therefore, I is proportional to the concentration and quantitative analysis can be conducted. Figure 1.3 shows the excitation, ionisation and emission process schematically. The horizontal lines of the diagram represent the energy levels of an atom.

FIGURE 1.3: ATOMIC AND IONIC EMISSIONS
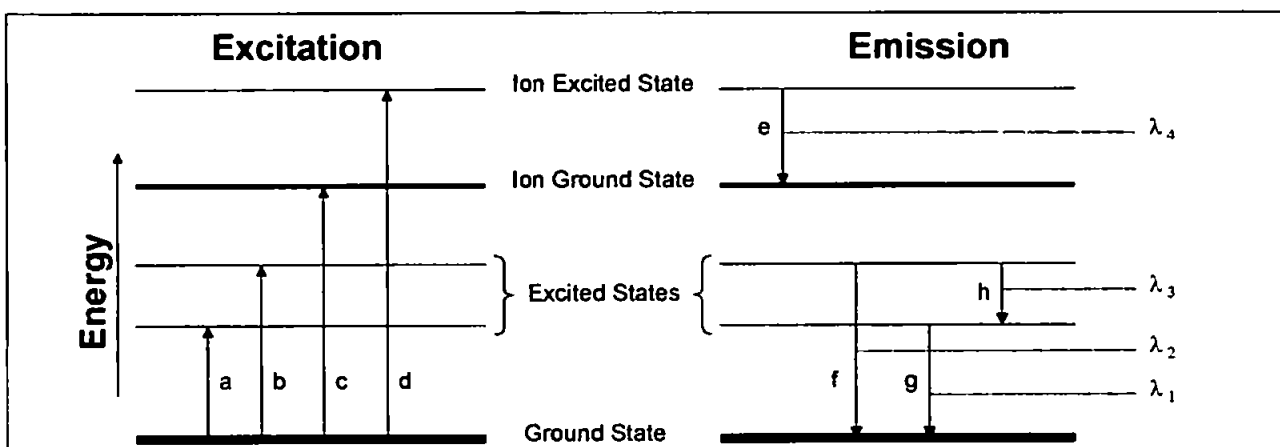
In Figure 1.3, transitions **a** and **b** represent atomic excitation, while **c** is the ionisation step and **d** ion excitation. The transitions **f**, **g** and **h** result from atomic species generated *atomic emissions:* λ_1, λ_2 and λ_3. The transition **e**, departing from an ionic state generates an ionic emission line, λ_4.

1.2.2 THE INDUCTIVELY COUPLED PLASMA

The inductively coupled plasma discharged used for optical emission is a stable high energy source and was first described by Greenfield[1] and Wendt[2]. Since then, adoption of the ICP source for analytical purposes has been widespread as its offers low detection limits, freedom from interference and long linear ranges compared to other sources of emission such as flames, arks and sparks.

An ICP discharge is obtained when a high-frequency field is applied to a gas such as argon. The plasma is created above a torch consisting of three concentric tubes through which the gas is directed tangentially. At the top of the torch, a 2 to 5 turn copper coil, *the load coil*, is connected to a radio frequency (RF) generator. When RF power is applied to the load coil, an alternating current oscillates within the coil at a rate corresponding to the frequency of the generator. In most ICP instruments, this frequency is either 27.12 or 40.68 MHz. This oscillation induces RF magnetic and electric fields in the area about the load coil. A spark is applied to the gas flowing through the torch and some electrons are stripped out from the gaseous atoms. These electrons are then accelerated by the magnetic field in circular paths around the coil causing collisions with other gaseous atoms and further electrons are emitted. This collisional ionisation of the gas continues in a chain reaction to form the plasma. A plasma can be defined as a partially ionised gas formed by atoms, electrons and ions that is macroscopically neutral. The ICP discharge is sustained within the torch and load coil by the RF energy, which is continually transferred. The plasma appears as a very intense, brilliant white, teardrop-shaped discharge.

The reason argon is most often used in the ICP discharge is related to its noble characteristics. Argon as a noble gas is a mono-atomic element with a high ionisation energy and chemically inert. Therefore:

- A simple spectrum is obtained (no molecular species)

- Argon has the capability to excite most of the elements of the periodic table

- No stable compounds are formed between argon and the analytes.

Other noble gas such as helium[3,4] have also been used in ICP systems although helium used is more commonly in ICP mass spectrometry[5,6]. The use of gas mixtures has also been reported[7,8].

The Excitation Process in Ar Plasmas

The high-frequency field produced by the RF generator accelerates the electrons, which ionised the argon gas:

$$e + Ar \rightarrow Ar^+ + e + e$$

The argon ions then recombine with the electrons to form excited argon atoms:

$$e + Ar^+ \rightarrow Ar^* + h\nu$$
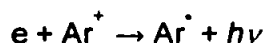
The plasma acts as a reservoir of energy and transfers this energy to the analytes to complete two processes: the sample atomisation and the partial ionisation of the analyte atoms (M) and excitation of the ions and the atoms to higher-energy states. The duration of these processes are quite different; while the atomisation of the sample is a relatively long process (a few milliseconds), the ionisation and excitation are very fast process.

Various ionisation and excitation processes have been suggested[9,10]. The main ionisation processes are:

- charge transfer ionisation: $\quad\quad Ar^+ + M \rightarrow M^{++} + Ar$

- electron impact ionisation $\quad e\,(fast) + M \rightarrow M^+ + e\,(slow) + e(slow)$

- Penning ionisation $\quad\quad\quad Ar^m + M \rightarrow M^{++} + Ar$

and the main excitation processes are:

- electron impact excitation $\quad\quad e + M \rightarrow M^* + e$

- ion-electron radiative recombination $\quad M^+ + e \rightarrow M^* + h\nu$

The ICP Temperature

Plasma temperatures range from 6000 to 10000K depending on the distance to the coil (Figure 1.4). These temperatures, which are much higher than those obtained by other excitation methods, i.e. flames and furnaces, not only improve the excitation and ionisation efficiencies but also minimise chemical interferences.

FIGURE 1.4: TEMPERATURE REGIONS OF AN ICP
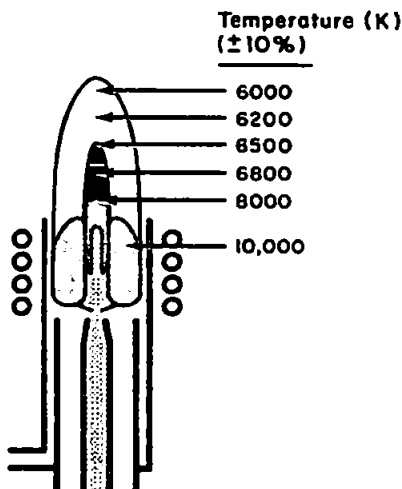
Plasma is composed of species with very large differences in mass: electrons and heavy Ar atoms and ions, participating in different processes. Therefore, at the particle level, several temperatures are involved in plasma. Temperatures defined as occurring in the plasma are:

- The kinetic temperature, T_{kin}, is related to the motion of particles and could be defined as the temperature of the system for the state of the complete thermodynamic equilibrium.

- The excitation temperature, T_{exc}, describes the Boltzman equilibrium, i.e. governs the population in the excite levels.

- The ionisation temperature, T_{ion}, describes the Saha equation, i.e. the equilibrium between two successive ionisation states.

- The electron temperature, T_e, is related to the velocity of the free electrons in the plasma.

- The rotation temperature, T_{rot}, is related to the vibration-rotational excitation of molecules or radicals that could still be present in the ICP.

ICP plasma belongs to the category "thermal plasmas". A thermal plasma should be close to local thermodynamic equilibrium (LTE), i.e. all temperatures involve in the different processes occurring should be similar. Practically this is not the case and it is observed that:

$$T_{rot} < T_{exc} < T_{ion} < T_o$$

Methodologies to provide detailed temperature information including absolute line intensity measurements and laser pertubated plasma probes are described elsewhere[11-13]. In addition,

a detailed overview of the subject has been made by Mermet[14]. However, regardless of the type of temperature, an increase is usually observed when the power increases, the carrier gas flow rate decreases and the generator frequency decreases. A similar trend is observed for the electron density. This means that small changes in the operating conditions can lead to totally different plasma in terms of kinetic and excitation temperatures, tolerance to solvent loading and therefore in emission intensities and matrix effects. Methods to evaluate the state of the plasma at different operating conditions have been suggested, among them are the plasma perturbation and the magnesium intensity ratio.

The ionic-to-atomic line intensity ratio of the same element[15] is a simple experiment, which provide information of the operating conditions of the ICP. The aim is to calculate a theoretical ratio assuming LTE and to compare it to an experimental ratio. Usually atomic lines are not very sensitive to a change in the excitation conditions, while ionic lines are. Their ratio allows the normalisation of the behaviour of the ionic line compared to the atomic line. In addition, if the two lines are close in terms of wavelength, their intensity ratio will be independent of the detector conditions. Magnesium has been used for these purposes[16] and particularly the emission lines: Mg II 280.270 nm (or Mg II 279.553 nm) and Mg I 285.213 nm. Under the LTE assumption, the theoretical value of the ratio varies between 10 and 14 for an electron population normally observed in an ICP. Experimental values of the magnesium ratio range from 1 to 14. When the experimental ratio is above a value of 8, so-called robust conditions are obtained, which means that complete atomisation, excitation and ionisation processes are expected. Under these operating conditions, which usually imply a high RF power and a low carrier gas flow rate, matrix affects are minimised[17,18]. In contrast, when the ratio is below 4, processes are not optimised and the ICP is subject to large matrix effects.

Plasma perturbation by **power modulation**[19,20] has been use to provide information about the energy transfer occurring in the plasma from the load coil to the analyte. Different modulation techniques have been tried, including sinusoidal modulated power[21], amplitude

modulated power[22] or pulsed modulation[20]. Diagnoses have been performed following the behaviour of various test elements, and of special note is the different time-dependent behaviour observed between argon and analyte lines.

1.2.3 THE ICP-AES TECHNIQUE

The ICP-AES instrument can be divided in three areas: the sample introduction system (pump, nebuliser and spray chamber), the excitation area (RF generator and torch) and the signal resolution area (spectrophotometer and detector). A schematic diagram of an ICP-AES instrument is shown in Figure 1.6. The sample solution is nebulised and introduced as an aerosol into the ICP discharge via the nebuliser and the spray chamber. The plasma then desolvates, dissociates, atomises and excites the elements presents in the sample, Figure 1.5. This results in the emission of light at different frequencies depending on the elements present in the sample. The light is then separated by the optical system into discrete wavelengths, and the intensity of light is measured at a wavelength, which is unique to the element of interest. Since the concentration of an element is proportional to the intensity of the light produced, after calibration, the software of the spectrometer calculates the correlation and quantifies the results.

FIGURE 1.5: FATE OF A SAMPLE DROPLET AFTER INTRODUCTION IN AN ICP DISCHARGE
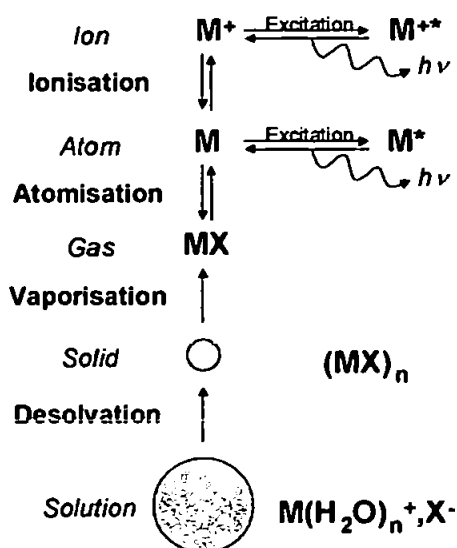
FIGURE 1.6: ICP-AES SCHEMATIC DIAGRAM
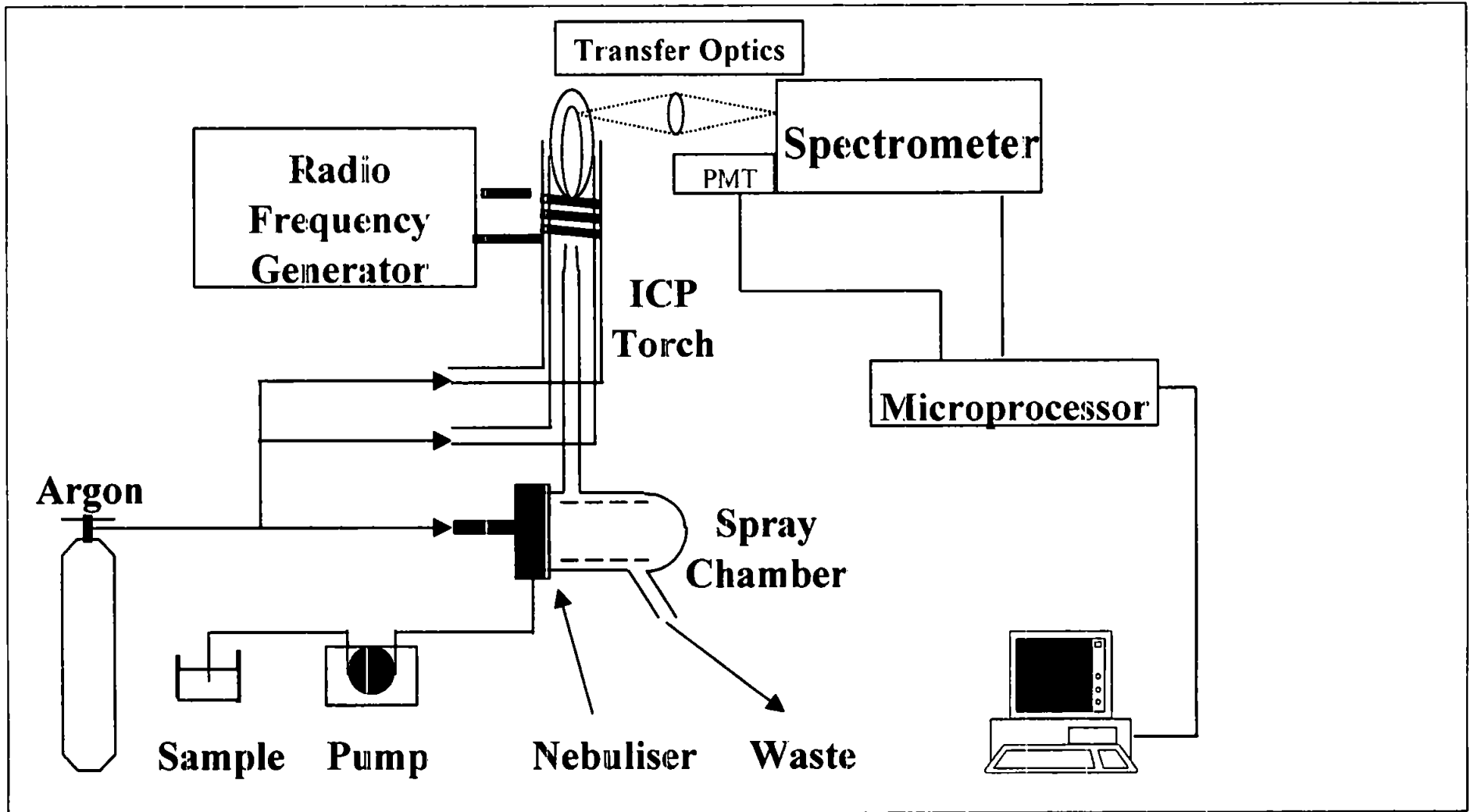
1.2.4 INSTRUMENTATION

Many efforts have been made to develop and improve the different parts of ICP-AES instruments. In the following pages, the basic components of an ICP-AES instrument are described and some of the most recent improvements reported.

The Excitation Area: RF generators, Induction Coil and Torches

The RF generator is a device that is used to provide the power for the generation and sustain the plasma discharge. The generator is an oscillator that produces an alternating current at a desired frequency. There are two basic types of RF generator: free running and crystal controlled. The power required for a AES measurements ranges between 600 and 1800 W, however, the typical operating powers are from 1000 to 1500 W. The frequency of operation of a RF generator is several MHz, although most commercial instruments use either 27.12 or 40.68 MHz. The use of higher frequency generators has been reported, e.g. 56, 64 or even 148 MHz, but these are not common. Traditionally, most instruments were run at 27.12 MHz, however recently manufacturers tend to utilise the 40.68 MHz generator, since this generator offers improved coupling efficiency and a reduction in the continuum background[23].

The RF power is transferred to the argon gas by a water-cooled copper load coil that surrounds the top of the torch. The coil configuration will determine the shape and the size of the plasma. If the coil is of wide diameter, the plasma tends to be larger. If the coil has several turns, the plasma will be extended. Moreover, the coil has to be configured so that the turns are as close as possible to maintain a uniform field but not so close as to form discharges between them. Typically, a three-turn copper coil is used.

The third part of the excitation area of an ICP is the torch. The basic design of an ICP torch is shown in Figure 1.7. The torch consists in three concentric tubes, the outer two usually made of quartz and the inner, the injector, is made either of quartz or ceramic. The principal gas flow of the plasma, is delivered tangentially through the outer tube. This gas provides the

plasma working gas and separates the plasma from the walls of the torch. A second tangential flow is directed through the intermediate tube, called the intermediate or auxiliary gas. The central gas is the nebuliser flow, which carries the sample aerosol through the injector to the base of the plasma. The most commonly used torch today has an outer diameter of 20 mm and is known as the Fassel torch.

FIGURE 1.7: SCHEMATIC DIAGRAM OF A TYPICAL TORCH

Plasma / Coolant gas in

Auxiliary / Intermediate gas in

Nebuliser / Carrier gas in
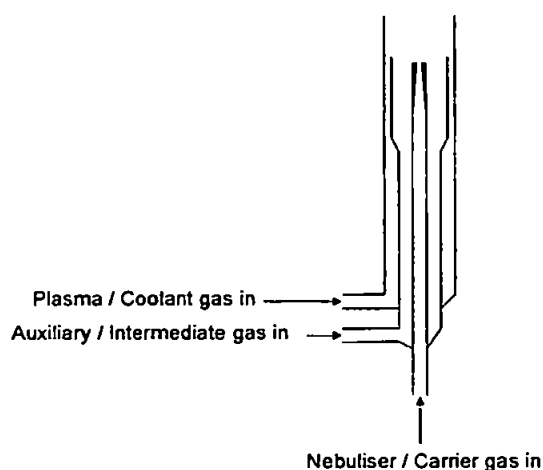
Numerous workers have modified the Fassel-torch design in order to improve performance or minimise running costs. For instance, the mini- and micro-torches were developed to allow the use of lower argon flows[24,25]. These are basically smaller versions of the Fassel torch, sometimes also known as low-flow torches. The mini-torch has a diameter of approximately 13 mm, a coolant gas flow rate of 8 Lmin^{-1} and typically is used with a RF power of 1 kW[26]. The micro-torch[27] is an even smaller version first developed by Weiss et al.[28]. It is 9mm in diameter and operates with a coolant flow rate of 6.4 Lmin^{-1} and a power of 500 W. The performance obtained by such torches is similar to the standard Fassel design[29,30]. However, they are often susceptible to blocking by solutions with high solid content[31]. Applications of such torches can be found in the literature and comparisons of such torches have also been reported[32,33]. Larger torches than the Fassel design have also been developed. Recently, a 22mm torch design has been reported[34].

Other modified torches available are the partially or total de-mountable torches. It has became very common that manufacturers provide torches from which the injector can be easily removed and replaced with another of a different design or made of a different material. Total de-mountable torches may also be designed, but they can be difficult to re-assemble in the correct alignment.

The torch disposition in ICP-AES instrument is usually radial. However, commercially axially viewed plasmas are now available. The basic instrumentation for use with axial and radial plasmas is similar. One of the differences is that axially viewed plasmas required a shear gas across the top of the plasma to prevent burning or condensation forming on the optics of the instrument. In terms of performance, axial viewed plasmas provide lower limits of detection and more emission lines can be observed[35,36]. Several reports have been published comparing the two plasma configurations[37,38] and applications[39-41]. A concise review on the present status of the axial viewed ICP has been recently published[42].

Sample Introduction and Transport

The sample solution is usually introduced into the torch as an aerosol. The solution is first pumped by a peristaltic pump into the nebuliser where it is transformed into a stream of droplets. The smaller the droplets, the more sample reaches the plasma.

Many different nebulisers have been developed in order to improve transport efficiency and to minimise matrix effects. The most commonly used nebulisers are pneumatic nebulisers, based on the Venturi effect. Among the pneumatic nebulisers, the concentric glass pneumatic nebuliser is the most common. It consists of an outer glass tube through which gas (typically argon) flows at a rate of 0.5 to 1.5 $Lmin^{-1}$. The gas rushing across the end of the tube causes a drop in pressure, which leads to the liquid sample being drawn through the sample tube. On reaching the end of the tube, the sample is shattered into a nebular by the flowing gas[43]. The main disadvantage of this nebuliser is that the tip is easily blocked when sample solutions contain a high solid content.

Other types of pneumatic nebulisers also exist: the cross flow, Babington and its modifications (the V-groove, Ebdon and de Galan). These nebulisers are more tolerant to suspended soils and are therefore more appropriate for the majority of sample types. In addition they are usually made of corrosion resistant materials, which allows the use of HF or NaOH without any adverse effects. In the cross flow nebuliser (Figure 1.8a) two capillaries meet at right angle, one carrying the sample and the other carrying the argon. The high speed argon flow serves to create the aerosol. In the V-groove nebuliser (Figure 1.8b) the sample flows down a groove which has a small hole in the centre for the nebuliser gas. Argon flowing through the hole shears the liquid layer of sample on the groove and forms a nebular.

FIGURE 1.8: THE V-GROOVE AND THE CROSS-FLOW NEBULISERS

A) Cross-Flow Nebuliser	B) V-Groove Nebuliser
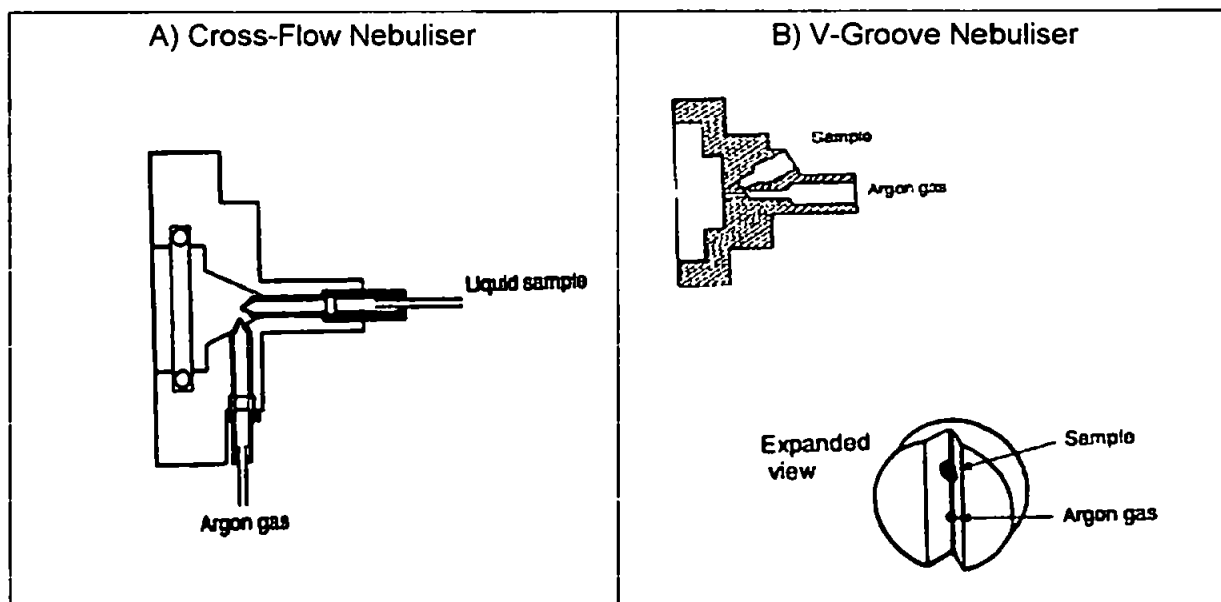
A further type of nebuliser is the ultrasonic nebuliser. These nebulisers form an extremely fine aerosol and therefore offer a much higher transport efficiency (i.e. ~20%). Using ultrasonic nebulisation, the limits of detection for many analytes can be improved by a factor of 10. However, ultrasonic nebulisers also have several disadvantages. They are expensive, require their own RF generator and they may suffer memory effects. Nevertheless, many applications of such nebulisers can be found in the literature[44-48]. Their use in the in the study of matrix and acid effects[49-52] has been the subject of several publications.

Many other nebuliser designs such as the Frit-type nebulisers, the electro-spray and the thermo-spray nebulisers, direct sample insertion nebulisers, are described elsewhere[53]. A comparison of different nebuliser devices has also been reported[54,55].

After nebulisation the sample aerosol is introduced into the spray chamber. The main role of the spray chamber is to act as droplet-size filter to ensure that only the smallest droplets reach the plasma by removing the larger ones to drain. A secondary function of the spray chamber is to dampen noise originating from the peristaltic pump. Numerous designs of spray chamber have been developed however in practice, the most widely used is the Scott-double pass design as shown in Figure 1.9.

FIGURE 1.9: A SCOTT-DOUBLE PASS SPRAY CHAMBER*.
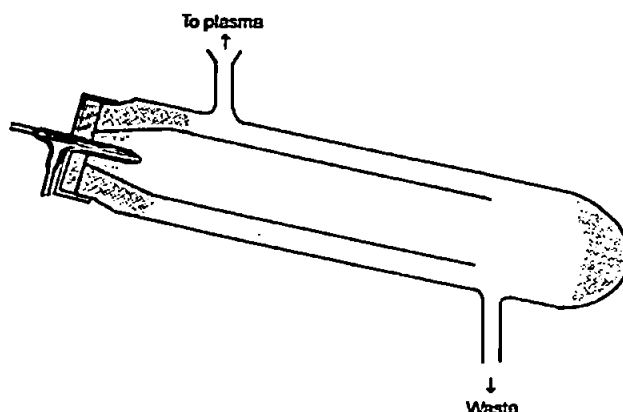
*The shaded parts represent the "dead space" areas.

The main problems associate with the Scott-double pass design is that it is usually made of glass. This material can be attacked by some reagents (e.g. HF) and may adsorb some trace analytes. Moreover, the existence of "dead spaces" may lead to appreciable memory effects. A review of the processes occurring within the spray chamber has been published by Sharp[56]. Other spray chambers designs include the single pass, the cyclone and the impact Bead[53], the fast cleaning[57] and the heated spray chambers[58,59]. Evaluations of the performance of different spray chambers have also been reported[60].

The Detection System: Spectrometers, Detectors and Data Process

The role of the spectrometer is to isolate the analytical wavelength of interest from the light emitted from the plasma source. The separation of the light into its component wavelengths is normally achieved using a diffraction grating. A diffraction grating is a reflection surface with very closely space lines etched onto the surface at a density between 600 to 4200 lines per millimetre. Light striking the grating is diffracted at an angle according to the wavelength of the light. There are three types of diffraction grating: ruled, holographic and echelle. The echelle grating[61] has become the most popular in ICP-AES systems because it offers very good efficiency in each of the spectral orders and an improved resolution by using higher spectral orders.

The dispersed light is then focussed by the spectrometer onto an exit plane or circle to allow certain wavelengths to pass to the detector while blocking out others. There are two types of spectrometers, reflecting the number of exit slits, i.e. monochromators and polychromators. Polychromators use several exits slits and detectors in the same spectrometer, while a monochromator uses one exit slit and one detector. Monochromators allow multi-element analysis by rapidly slew-scan from one emission line to another. However, in more modern instruments, the echelle –type polychromator is the more common[61,62].

The detector is used to measure the intensity of the emission line once it has been isolated by the spectrometer. Traditionally, the photomultiplier tube (PMT) has been the more widely used in ICP-AES. A PMT consist of a vacuum tube containing a photo- sensitive cathode and a series of dynodes set at successively more positive potential until an anode is reached. When the isolated wavelength strikes the PMT cathode, this emits electrons, which are accelerated down the dynode chain. Each time an electron impacts on a dynode several electrons are emitted to initiate an avalanche effect, which amplifies the signal. The electrical current measured at the anode is directly proportional to the radiation reaching the PMT. However, new types of detectors have been developed and are now becoming more popular. The solid state detectors have a high quantum efficiency (over 40%) and a very low dark

current effect[1], but similar detection limits, sensitivities and linear ranges to PMT-based instruments. There are two types of solid state detectors, the charge-coupled device (CCD) and the charge-injection device (CID). A detailed description of how these devices work can be found elsewhere[63].

The electrical signal produced by the detector is amplified and converted to digital form before inputting into a microcomputer. Finally it is the microcomputer that gives the read-out and processes all the data.

1.2.5 PERFORMANCE CHARACTERISTICS AND APPLICATIONS

Inductively coupled plasma atomic emission spectrometry is a well established technique for routine analysis. Multi-element determinations, high selectivity and limits of detection below the μg g^{-1} level have led to a wide range of applications in areas of food sciences, environmental and clinical analysis.

<u>Figures of Merit</u>

Among the figures of merit of any analytical technique accuracy, precision and long-term stability are of prime concern. In addition sensitivity, selectivity and the number of elements that can be determined will condition the applicability of the technique.

The trueness of a measurement can be defined as the agreement of the mean value of a series of replicates with the accepted (true) value. Precision refers to both repeatability and reproducibility. Repeatability is the closeness agreement in a short time period between successive results obtained with the same material under the same conditions, whereas, reproducibility involves a change of at least one parameter.

---

[1] *The dark current effect of a multiplier refers to the signal generated in the absence of any photons.*

Degradation of precision in ICP-AES determinations is mainly due to the presence of flicker and shot noise[64-66]. Shot noise is observed wherever a current involves the movement of electrons across a junction such is in a PMT. Shot noise can be minimised by using long integration times[67]. Flicker noise originates in the sample introduction process. It is a multiplicative noise, this means that the noise magnitude is proportional to the magnitude of the signals. The multiplicative nature of the flicker noise allows that any element can be used as internal standard to compensate for it, provided that simultaneous measurements of the analyte and the internal standard are carried out[64,66,68].

Degradation in accuracy usually originates from systematic errors, such as drift phenomena. The idea of drift has to be related to the notion of reliability. The reliability of an analytical method can be defined as its ability to provide accurate and precise data. When an instrumental method is *not reliable with time*, it said that it drifts. Drift can therefore be defined as a systematic trend in the results as a function of time. Two major causes are associated to the degradation of accuracy and long-term stability in ICP-AES signals[69]: changes in the energy transfer between the generator and the plasma, and changes in the aerosol formation. Uncontrolled fluctuations in the instrumental parameters, matrix mismatching or temperature variations may promote such changes. Drift phenomena, being the main subject of this thesis, will be discussed further in the different chapters so as to cover drift causes and correction methods.

In term of sensitivity, ICP-AES is characterised by low detection limits of the order of 1 to 100 ng ml^{-1} and a large linear dynamic range (up to six orders of magnitude). Many elements from the periodic table of elements can be determined by ICP-AES. Exceptions include intrinsic plasma species, e.g. argon, hydrogen and oxygen, man-made elements, which are often short-lived or very radioactive and some other elements such us F, Cl and noble gases, for which the ICP offers insufficient energy for excitation.

In 1995, Mermet *et al.*[70] reported the performance of several ICP-AES instruments, all at that time commercially available. The figures of merit under study were the wavelength range, the

selectivity or line resolution, the repeatability, the long-term stability of signals, the robustness versus matrix effects, the limits of detection and the accuracy of measurements and calibration processes. These figures of merit where obtained by simple experimental diagnosis described by the same authors elsewhere[71,72]. The results of this study are described in Table 1.1.

TABLE 1.1: FIGURES OF MERIT FOR ICP-AES INSTRUMENTS[70]

FIGURE OF MERIT	DIAGNOSIS	OUTSTANDING RESULTS	WORST RESULTS
Limit of Detection	Signal to Background ratio using Ni^{231nm} at 1 mg l^{-1}	> 30	< 2
Selectivity	Using Ba 230 nm line	< 5 pm	> 16 pm
Number of elements	Wavelength Range	120–770 nm	190–450 nm
Warm up period	Time necessary to obtain a stable signals (fluctuations within the short term rsd)	< 15 min	> 90 min
Repeatability	RSD of the signal Mg(I) 285nm (15 replicates)	< 0.2 %	> 1.2 %
Long-term Stability	RSD of signals Ba^{455nm}, Zn^{206nm}, Ar^{404nm} (over 20 replicates, 14.5 min)	< 1%	> 10 %
Robustness	Mg(II)/Mg (I) Ratio	> 10	< 4

Unfortunately, currently not all the commercial instruments cover all the outstanding capabilities described in Table 1.1. Therefore, research continues on the area of diagnosis and improvement of ICP-AES instrumentation.

Applications

Application of the ICP-AES technique can be found in many different areas from geological and environmental analysis to food or medical science. Geological applications of ICP-AES involve the determination of major, minor and trace elements in soils, rocks and sediments. Many environmental applications of this technique can be found in the literature related to the analysis of water quality, industrial sewage and pollution dust. Biological and clinical

applications include the determination of trace metals in animal and human tissues and blood. This has can be applied to medical research and forensic analysis[73]. ICP-AES has also been widely used to determine the metal content of many foods and beverage to obtain nutritional information and for food authentication. Periodical reviews of ICP-AES applications can be found in the Atomic Spectroscopy Updates[74-76].

1.2.6 SPECTRAL INTERFERENCES AND MATRIX EFFECTS

No analytical technique is free of interferences, and ICP-AES in not an exception. Among the more common interferences that can affect an ICP-AES analysis are spectral interferences and matrix effects.

Spectral Interferences

Spectral interferences, also called background interferences, may be caused either by an increase in the continuum background emission or as a line overlap. Although modern ICP-AES instruments provide a fairly good selectivity and high resolution, rare-earth elements and some line-rich elements e.g. Mo, Ta, have been found to result in severe spectral interferences[77-79]. The spectral interferences encountered in ICP-AES when analysing environmental materials have also been studied[80].

In terms of correction, background shifts can be easily compensated by subtraction of the background adjacent to the line. A review was recently published about the use of mathematical procedures for background correction in ICP-AES[81]. Line overlaps may occur as direct line overlaps or because of nearby lines. In the first case, the best solution is to use an alternative line. For partial overlaps several correction methods have been suggested. The more common is the inter-element correction (IEC), which uses the emission intensity of the interferent element at another wavelength and apply a predetermined correction factor to the results. Nolte[82] has evaluated five different correction methods for spectral line overlap:

parabolic fit calculation of peak maximum, on-peak measurement, matrix matching, inter-element correction, and a chemometric technique (Multi-component Spectral Fitting). The latter technique gave best results with respect to accuracy, reproducibility, and detection limits. Danzaki *et al.*[83] have developed a practical method to estimate spectral interferences and to select optimum analytical lines in ICP-AES depending on the matrix composition and the amounts of the analyte present on the samples.

Matrix Effects

The high temperatures reached in the plasma results in most samples being completely atomised, and therefore the technique suffers from few chemical interferences. However, the nature of sample introduction system makes this technique very sensitive to transport effects. Such effects are caused by different physical characteristics between standards and samples, e.g. changes in viscosity, volatility or surface tension. This can result in different nebulisation and sample transport efficiencies, and manifest as apparent suppression or enhancement in the analytical signal.

Matrix effects can be defined as the changes in the behaviour of the system induced by the sample predominant species. Acids and easily ionised elements are the most common matrices in elemental analysis by ICP-AES. Acids are usually employed for sample preparation and stabilisation. Their effects on emission signals can be classified in two groups:

- the physical effects arising from the properties that acids confer to the solution

- and the acid effects in the excitation area, in the plasma.

Acids effects have been mainly studied in terms of aerosol formation. In such a way, the influence of acid effect on the sample introduction system has been evaluated[52] and compared when using different nebulisers[84] and different spray chambers[60,85].

The influence of the operating conditions on the magnitude of acid effects has also been reported[85-89]. Authors agreed on the convenience of using the so-called "robust conditions",

i.e. high RF power and low nebuliser flow, to record a common effect on the signal intensity, regardless of the energy line: the acid effects are only due to a change in the aerosol formation and transport. A review on the subject has been recently published[90].

Other commonly present matrices in ICP-AES analysis include the alkali and the alkali earth metals, also called easily ionised elements (EIE). The presence of large excess of EIE in an excitation source increases the electron density and therefore may shift the ionisation equilibrium versus the neutral atom. This would lead to an enhancement of atomic emissions and a partial suppression of ionic emissions. Although plasmas have a high electron density and are not expected to be vulnerable to small changes in the electron density, EIE interferences have been observed. Blades and Horlick[91] have made a survey of the EIE effects in plasmas. They observed two different effects depending on the region of the plasma. Low in the plasma discharge, the presence of EIE enhances emissions due to an increase of the collisional excitation. Meanwhile, at higher areas of the discharge, emission intensities are partially suppressed by EIE due to ambipolar diffusion. According to the authors, this applies for both atomic and emission lines. More recently, Al-Ammar[92] suggested that the dominant cause for matrix interference in ICP-AES when using common plasma operating conditions, were the inelastic collisional deactivation of the analyte excited state. Further studies on the EIE effects in fundamental terms, i.e. electron density, plasma temperatures, have been published by Olesik[93], Tripkovic[94] and Hanselman[95,96]. In these works, attention was also given to the effects caused by non-easily ionised elements, such as Cd, Ba or Zn. The influence of the aerosol formation on EIE effects has also been object of recent research[97,98]. Galley and Hieftje[99] reviewed the EIE effects on both axial and radial instrument to find optimal conditions to minimise such interferences. As in the case of acid effects, many authors[17,18,89,100] agree with the importance of selecting robust operating conditions to minimise the matrix interactions. Mermet[101] concluded that under robust conditions, matrix effects resulting from a change in the plasma conditions, i.e., temperature, electron number density and spatial distribution of the various species, are minimised to the

same extent, regardless of the element and line. The remaining depressive effect is assigned to the sample introduction system, and it was demonstrated that the effect occurs during aerosol transport and filtering. Matrix effects from sodium[18,39,100], potassium[102] and calcium[103,104] have been extensively studied. Traditional methods to overcome matrix effects include matrix matching, internal standardisation, standard addition, or modification of the sample introduction system such as eliminate the spray chamber or use a desolvatation systems. Sadler et al.[105] published a paper comparing some of these procedures when determine trace metals in soils. Other approaches have also been suggested, however the extend of their usage is more limited. A predictive model of plasma matrix effects in ICP-AES has been developed by Ramsey[106] assuming that analytes are affected to a degree dependent on the total excitation potential. Thompson et al. have suggested two new methods for matrix correction: the iterative power adjustments[107] and the extrapolation to infinite dilution[108]. Al-Ammar extended the correction method CAIS[109](common analyte internal standard) to correct for non-spectroscopic matrix effects in ICP-AES measurements[110]. The application of a full-factorial design experiment for characterising and correcting matrix effects due to Ca and Mg has also been reported recently[111].

The effects of chemical matrices on long-term stability will be subject of study in Chapter 5.

1.3 CHEMOMETRICS OVERVIEW

Chemometrics has been defined by Massart *et al.*[112] as "the chemical discipline that uses mathematics, statistics and formal logic:

- to design or select optimal experimental procedures,

- to provide maximum relevant chemical information by analysing chemical data,

- and to obtain knowledge about chemical systems."

In other words, chemometrics is concerned with formal methods for the selection and optimisation of analytical methods and procedures and for the interpretation of data. According to the definition, chemometrics procedures can be proved useful at any point in an analysis, from the first conception of an experiment, through to the interpretation and classification of the data, even prediction or forecasting future results.

Chemometrics methods may be classify in four groups:

- For experimental planning and optimisation: Experimental design procedures

- For exploratory analysis: pattern recognition and classification methods.

- For calibration process: Multivariate regression methods.

- For learning purposes: Artificial intelligence, expert systems and neural networks.

Many texts have been published on the subject. Among them can be highlighted *"Chemometrics a text book"*[113], which provide an accessible mathematical approach to the subject, applied texts such as *"Chemometrics in Environmental Analysis"* by Einax *et al.*[114] and the Brereton compilation[115]. A more recent and complete text form are the two volumes *"Handbook of Chemometrics and Qualimetrics"*[116,117].

Most chemometrics models are based on multivariate analysis. The term multivariate analysis, as usually applied by chemometricians, defines any statistical, mathematical or graphical approach, which considers multiple variables simultaneously. In the following sections, a brief description of the more common chemometrics methods is presented.

1.3.1 EXPERIMENTAL DESIGN

Whenever experimentation is considered, one should first decide which experiments should be carried out. The data can be collected from various sources or designed with a specific purpose in mind. Experimental design is a strategy to gather empirical knowledge. The purposes of experimental design approaches are:

- Efficiency: Get more information from a fewer number of experiments

- Focusing: Collect only the information you are interested on.

Experimental design can be applied to investigate a phenomenon in order to gain understanding or to improve performance. By planning experiments, the influence of different parameters can be considered simultaneously in a systematic way.

There are four steps in building an experimental design:

1. Define an objective to the experiment, e.g. "better understand" or "sort out important variables" or "find optimum".

2. Define the variables that will be controlled during the experiment (design variables), and their levels or ranges of variation.

3. Define the variables that will be measured to describe the outcome of the experimental runs (response variables).

4. Choose among the available standard designs the one that is compatible with the objective, number of design variables and levels, and has a reasonable cost.

Generating an experimental will provide a list of all experiments to perform, to gather enough information for the initial purposes. There are two different types of designs: screening designs and optimisation designs. Full or Fractional Factorial designs and Plackett-Burman designs are the more common screening designs, while Central Composite Designs are the most common optimisation design. Detail information on this subject can be found elsewhere[118,119].

1.3.2 PATTERN RECOGNITION AND CLASSIFICATION METHODS

Traditional methods to explore results include graphical data display and descriptive statistics. However, these methods are seriously limited when many variables are employed to describe the same object or sample. Chemometrics and particularly patterns recognition techniques may help to explore large data tables. Such methods seek to identify regularities and similarities present in the data. The main applications of pattern recognition techniques are:

- to reduce the number of variables to better visualise the data.

- to detect structure in the relationships between variables in order to classify objects.

Classification and data reduction methods are part of the chemical pattern recognition.

Data Reduction Methods

Large data tables contain a huge amount of information, much of which is partially hidden because the of the high complexity of the data, i.e. many dimensions would be required to visualise and interpret the data effectively. One of the primary goals of chemometrics is to reduce the number of dimensions needed to accurately portray the characteristics of the data set. There are a wide variety of methods available to do this, either by selecting an important subset of the original variables, or by creating a set of new variables, which are more efficient than the originals in describing the data. The creation of new variables can be approached in several ways; two of these are projection and mapping. Projection is the more common technique and involves using weighted linear combinations of the original variables to define a new, smaller set of variables, which contain nearly the same information as the original variables. The most frequently used projection technique is principal component analysis (PCA). Mapping is similar to projection, but the transformations considered in this case are non-linear. These non-linear methods often seek to preserve certain properties in the data,

such as inter-point distances, while performing a dimensional reduction. Mapping results can be difficult to interpret, however, and they are not as important as the projection methods.

Principal component analysis, PCA, is a projection based dimension reduction method that assimilates information to variation. PCA finds the maximum variations in the data and forms new variables known as Principal Components (PCs), such that:

- Each successive PC accounts for as much of the remaining variability as possible.

- Each new variable must be uncorrelated, i.e. orthogonal, to all other variables.

PCA requires a data matrix, D_{ik}, containing i rows that correspond to the samples and k columns that correspond to the variables. The output of PCA will be in the form of two matrices and some statistical information. The first of these is called "*the score matrix*" which contains values for each sample on each principal component. These are known as <u>scores</u>. The other, "*the loading matrix*", contains coefficients used to compute the new principal components from the original variables and are known as <u>loadings</u>.

	Where:
$$S_{ij} = D_{ik} \times L_{kj}$$ **EQUATION 1.7**	**D** is the Data matrix. **S** is the Score matrix **L** is the Loading matrix **i** are the samples. **k** are the variables. **j** are the principal components.

Factor analysis is another data reduction method also based on principal components. First, a PCA is performed on the data. Secondly, the number of significant new components or factors is determined in order to assimilate them to a physically meaningful process. Detailed description of this methodology can be found in the book "*Factor analysis in chemistry*" by Malinowsky[120].

Classification Methods

Classification of samples is one of the principal goals of pattern recognition. Classification methods can be divided into unsupervised and supervised approaches, the difference being that supervised methods require a training set of samples with known origin or class.

Cluster analysis is probably the most common unsupervised classification method. The term cluster analysis encompasses a number of different classification algorithms, which can be used to develop taxonomies. The aim of this approach is to identify similar characteristics in a group of observations. Several algorithms may be used to create the clusters. The most commonly used algorithms are hierarchical methods that construct tree-like structures. Hierarchical cluster analysis has been described in detail by Massart and Kaufmann[113]. The result of a cluster analysis is normally displayed graphically as a dendrogram. Objects that are most similar are joined together at the top levels of such a diagram. Some examples of algorithms used in hierarchical clustering methods are the *Nearest Neighbour*, the *Furthest Neighbour*, the *Centroid* based, the *Median* based, the *Group Average* and the *Ward's* distance.

Supervised classification methods require two steps:

1. Modelling step: Build one separate model for each class;

2. Classifying new samples: Fit each sample to each model and decide whether the sample belongs to the corresponding class.

The modelling stage implies that the analyst has identified enough samples as members of each class to be able to build a reliable model. It also requires enough variables to describe the samples accurately. The actual classification stage uses significance tests, where the decisions are based on statistical tests performed on the object-to-model distances.

Linear discriminant analysis, LDA, is a supervised pattern recognition method that forms linear combinations of independent (predictor) variables, which become the basis for group classifications. Applying and interpreting discriminant analysis is similar to regression

analysis, where a linear combination of measurements for two or more independent variables describes or predicts the behaviour of a single dependent variable. The most significant difference is that discriminant analysis is used for problems where the dependent variable is categorical whereas in regression the dependent variable is metric.

The objectives for applying discriminant analysis include:

- determining if there are statistically significant differences among two or more groups

- establishing procedures for classifying units into groups

- determining which independent variables account for most of the difference in two or more groups.

SIMCA, Soft Independent Modelling of Class Analogy, is a PCA based method which provides more rigorous classifications than LDA. A principal component analysis is performed for each class in the training set. Unknown samples are then compared to the class models and assigned to classes according to their analogy to the training samples.

1.3.3 MULTIVARIATE REGRESSION METHODS

Regression is a generic term for all methods attempting to fit a model to observed data in order to quantify the relationship between two groups of variables. The fitted model may then be used either to describe the relationship between the two groups of variables, or to predict new values. Univariate regression uses a single predictor, which is often not sufficient to model a property precisely. Multivariate regression takes into account several predictive variables simultaneously, thus modelling the property of interest with more accuracy.

Multiple Linear Regression (MLR) is a well-known statistical method based on ordinary least squares regression. It estimates the model coefficients by the equation:

$$B = (X^T X)^{-1} X^T Y$$ EQUATION 1.8

This operation involves a matrix inversion, which leads to collinearity problems if the variables are not linearly independent. Incidentally, this is the reason why the predictors are

called independent variables in MLR; the ability to vary independently of each other is a crucial requirement for variables used as predictors with this method. MLR also requires more samples than predictors, otherwise the matrix cannot be inverted.

Principal Component Regression (PCR) is a two-step procedure that first decomposes the X-matrix by PCA, then fits an MLR model, using the PCs instead of the raw data as predictors.

Partial Least Squares - or **Projection to Latent Structures** - (PLS) models both the X- and Y-matrices simultaneously to find the latent variables in X that will best predict the latent variables in Y. These PLS-components are similar to principal components, and are usually also referred to as PCs.

A tutorial review on the subject has been recently published by Brereton[121].

1.3.4 TIME SERIES

Time series may also be included in the area of chemometrics. The objective of these techniques is to highlight characteristics of the data in terms of time, such as seasonal effects, cyclic changes, trends, errors, outliers, or turning points. Among the more common methods are the smoothing and filtering techniques to remove the random fluctuations. Moving average or exponential smoothing are simple techniques to remove short-term fluctuation or seasonal effects from a date series. An example of a data filter is the Kalman filter. Kalman filters have been extensively employed to remove random noise from spectroscopy signals[122].

The CUCUM series is another example of time series were the data are integrated in order to highlight the presence and nature of a trend in a data series. The opposite process is called the differentiation of a time series and can remove a linear or higher order trend in the data.

Other methods employed in time series analysis are correlation and regression techniques. Traditional correlation compares in a *"parallel"* way two series of data. For example, the

intensities of line A at time t_1, t_2, t_3, are compared to the intensities of line B at the same measurement times: t_1, t_2, t_3 and so on. Other ways to compare variables also exist, for instance variables can be compared with respect to change of τ (lag) in time. One could imagine that in the relationship between cause and effect in an environmental accident a dead time or a lag exists. In such case, correlation can be calculated by introducing a "lag time". The magnitude of the 'causing' variable will be compared with the magnitude of the 'affected' variable after the dead time τ, i.e. the cause variable measured at time t_1, t_2, t_3 will be related to the affected one measured at times $(t_1+\tau)$, $(t_2+\tau)$, $(t_3+\tau)$.

A detail description of the subject can be found in Chapter 6 from Einax *et al.*[114] and in the Chatfield manual[123].

1.3.5 A Step Further: The N-Way Approach

Although most traditional chemometric techniques are concerned with two-way data matrices, many chemical systems may require higher orders of arrays. Consider for instance, the determination of a number of metals in various samples and at different pH. Such data could be arranged in a three-way structure, indexed by sample, element and pH. This kind of problem could require a pattern recognition technique or a multivariate calibration. A traditional solution was to unfold the higher order data sets to form a two-dimension data matrix and then apply common chemometrics methods. This has a number of disadvantages, since the n-way structure is lost and such methods use a higher number of parameters. Multi-way analysis can tackle an n-dimension data sets without the need of unfolding. Smilde[124] has published a review on the use of three-way analysis. There are a number of multi-way methods available to study three and higher orders data sets: Tucker, PARAFAC, N-PLS are the more common.

PARAFAC, parallel factor analysis[125-127] is a decomposition method for 3 or higher orders of array, and can be compared to principal component analysis (PCA). Similar to PCA, the aim is to retain the maximum amount of information from the data but represent it in a smaller number of components or factors. Using PARAFAC the algorithm is extended to higher modes, 3, 4 or in general N-way data sets. A tutorial course on PARAFAC can be found on the internet[128].

The structural model of a two-way PCA is a bilinear model (Equation 1.9). Likewise a PARAFAC model of a three-way array is defined by the structural model described in Equation 1.10.

$$x_{ij} = \sum_{f=1}^{F} a_{if} b_{jf} + e_{ij}$$

EQUATION 1.9

$$x_{ijk} = \sum_{f=1}^{F} a_{if} b_{jf} c_{kf} + e_{ijk}$$

EQUATION 1.10

Where:

x_{ijk} Data in object i of variable j at condition k

i,j,k Variables respectively along the first, second and third dimension

f, F Principal Components or Factors

a,b,c Model loadings on first, second and third dimension

e Model error

A decomposition of the data is made into triads or trilinear components. The results of a PARAFAC analysis are given as N-loading matrices, one for each mode studied. In a three way data set, three loading matrices will be obtained A, B and C. The trilinear model is found to minimise the sum of squares of the residuals e_{ijk} in the model. Equation 1.10 may be represented graphically as in Figure 1.10.

FIGURE 1.10: GEOMETRICAL REPRESENTATION OF A PARAFAC ANALYSIS.
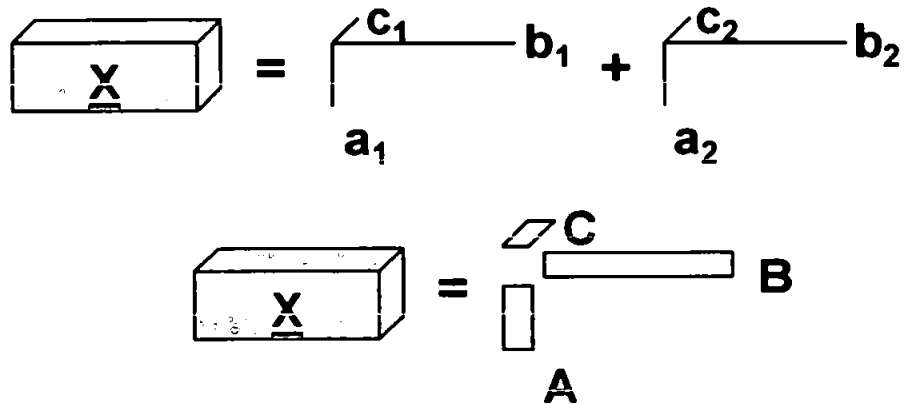
It should be stressed that the reason for using a multi-way method is not to obtain a better fit for the data, but rather a more adequate, robust and interpretable model, based on a smaller number of parameters. For example, in order to calculate an F-component PCA model to a IxJxK array, we would need first to unfold the data to a IxJK matrix and then applied a PCA, the solution of which will consist of $F(I+JK)$ parameters (Figure 1.11).

FIGURE 1.11: DIFFERENCES IN THE DATA DISPOSITION BETWEEN PARAFAC AND PCA
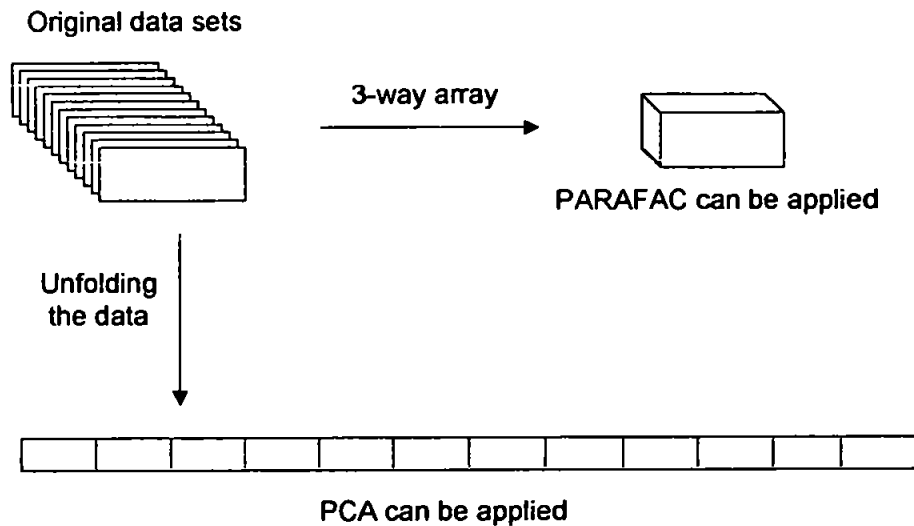
A corresponding PARAFAC model with an equal number of components would consist of only $F(I+J+K)$ parameters. Clearly the PCA model will be more difficult to interpret because a much higher number of parameters are implied.

An another advantage of PARAFAC versus unfolded PCA is the uniqueness of the solution. In bilinear methods, the solutions present rotational freedom. This is not the case with PARAFAC; the estimated model cannot be rotated without a loss of fit.

Tucker Models[129] involve calculating weight matrices corresponding to each of the dimensions (A,B,C), together with a "core" box or array (G), which provides a measure of magnitude.

FIGURE 1.12: GEOMETRICAL REPRESENTATION OF A TUCKER3 MODEL
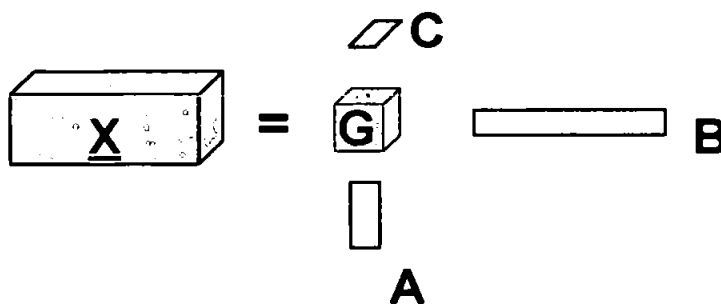
Mathematically, this can be expressed by:

$$x_{ijk} = \sum_{d=1}^{D}\sum_{e=1}^{E}\sum_{f=1}^{F} a_{id}b_{je}c_{kf}g_{def} + e_{ijk}$$

EQUATION 1.11

These models are called three-mode principal component analysis. As with PCA, they have rotational freedom and hence are not structurally unique. A comprehensive course in the subject may be obtained from the internet[130].

N-PLS[131,132], N-way partial least squared, is a the three-way version of the PLS. In N-PLS, the n-way array of independent variables is decomposed into a trilinear model similar to PARAFAC. However, the model is not fitted in a least squared sense but is design to describe the maximum covariance of the dependent and the independent variables. This is achieved by simultaneously fitting a multilinear model for the dependent variables, a multilinear model of the independent variables, and a regression model relating the two decomposition models.

1.3.6 ARTIFICIAL INTELLIGENCE AND NEURAL NETWORKS

Artificial intelligence applications in chemistry have been considered by many to be chemometrics techniques. Artificial intelligence aims to provide "silicon assistants", virtual colleagues or experts to assist in solving chemical problems. Self-optimising instruments, automated structural elucidation and perhaps even automatic chemometrics analysis are the aims of research in this field. Expert systems and neural networks are examples of applications of artificial intelligence. An introduction to the subject focussed on analytical chemistry problems was published by Salin et al.[133].

Expert systems are computer programs that are intended to support tasks at an expert level. These programmes combine quantitative parameters and qualitative rules, also called heuristic rules, to simulate the human reasoning process.

Artificial Neural Networks, ANN, are analytic techniques modelled after the processes of learning in the cognitive system and the neurological functions of the brain. Therefore, as with a human brain, they are capable of predicting new observations (on specific variables) from other observations (on the same or other variables) after executing a process of so-called learning from existing data. Artificial neural networks are models that do not presume any underlying relationship in the data, thus they can be used to model non-linear chemical systems.

ANN models the relationship between the input independent variables and the output dependent variables by using weighted sums of transforms. The first step is to design a specific network architecture (that includes a specific number of "layers" each consisting of a certain number of "neurons"). The size and structure of the network needs to match the nature (e.g., the formal complexity) of the investigated phenomenon. Because the latter is obviously not known very well at this early stage, this task is not easy and often involves a multiple "trial and error" approach. The new network is then subjected to the process of "training." In this phase, neurones apply an iterative process to the number of inputs (variables) to adjust the weights of the network in order to optimally predict (in traditional

terms one could say, find a "fit" to) the sample data on which the "training" is performed. After this phase of learning from an existing data set, the new network is ready and it can then be used to generate predictions. An overview on the use of this technique for chemical analysis has been reported by Bos[134].

1.4 APPLICATIONS OF CHEMOMETRICS

Many applications of chemometric models in analytical chemistry have been reported. An early review on the subject was published by Brereton[135] in 1987. Since then, the use of chemometrics among the analytical community has increased, mainly due to the huge amounts of information that can be obtained from computed assisted analytical instrument. Some recent publications are reviewed here.

- The use of experimental design in analytical chemistry for screening[136], optimisation[137] and quantification[138] have been reviewed.

- Pattern recognition and classification techniques are probably the most used in analytical chemistry. Cluster analysis, PCA, LDA and SIMCA have been used to differentiate three brands of Spanish wines from the Galician region using their metal content. Other beverages and foods have been also classified and/or authenticate using chemometrics methods and their metal content, often determined by spectroscopy analysis. Examples are the authentication of the geographical origin of tea[139], determination of the quality of olive oils[140], the classification of coffees[141], wines[142] and rices[143,144]. Other application include classification of pottery[145], determination of trace metal distribution in soils[146,147], screening for drugs of abuse[148] or study the pollution of industrial soils[149]. PCA has also been applied for more fundamental studies. For instance, Cave employed a PCA model to improve short-term precision in ICP-AES[150]. Factor and cluster analyses were employed to evaluate heavy metal deposition in pine trees[151]. SIMCA applications are mainly used with NIR spectroscopy for the identification of pharmaceutical

excipients[152,153]. Authentication of meat product has been carried out using mid-infrared spectroscopy in conjunction with PLS and SIMCA[154].

- Multivariate regression methods are also widely used in analytical chemistry. One of the most prolific areas of study is instrument calibration. Sadler *et al.*[155] suggest a multi-line calibration for ICP-AES using PCR. Multivariate calibration has been successfully applied to high interfering chemical systems[156]. Cladera *et al.*[157] uses MLR and neural networks to resolve overlapped voltammetric signals

- Time series and in particular filtering techniques have been extensively used in spectroscopy analysis. Examples are the use of Kalman filter for multivariate calibration[158], for drift correction[159] for data reduction[160] or for resolving partially overlapping peaks[157].

- Multi-way methods, although still less common than 2-way chemometrics models, have been used with complex data systems. Although, PARAFAC was originally employed in psychometrics[161], several applications of PARAFAC in chemical systems have now been reported. Most of these corresponded to the decomposition process in excitation-emission fluorescence spectroscopy for data treatment[162,163] and also for instrument optimisation[164]. Applications of PARAFAC to high performance liquid chromatography (HPLC) coupled with different detectors [165,166] have been reported, as have applications for the chemical industry[167-171].

- The use of neural networks and expert systems in chemical systems is increasing. Salin has reported various applications of expert systems in ICP-AES, including line selection expert systems[172,173] and autonomous ICP-AES instrumentation[174-176]. Neural networks have also been applied to different systems, often for pattern recognition and classification proposes. A comparison of the performance of ANN and more common chemometrics approaches has been made[177] and applications of ANN for the classification of alloys[178] using the glow emission spectra, the classification of Italian olive

oils using its fatty oil composition and the classification of French wines[142] according to their trace metal composition have all been reported.

In addition, several reviews have been published on the subject of the application chemometrics. Brown[179] reported in 1998 the current trends in the data handing procedures in chemistry and chemical engineering. More focussed is the work by Van Veen *et al.*[81], which reviewed the procedures developed over the last decade, based on convolution, differentiation, Fourier transforms, correlation, expert systems, neural networks, principal component analysis, projection methods, Kalman filtering, multiple linear regression and generalised standard additions applied to ICP-AES data.

1.5 DESCRIPTION OF THE PROJECT

The main objective of this study as indicated by the thesis title, was to characterise the drift phenomena in ICP-AES measurements using chemometrics methods.

The ICP-AES technique has been reported to suffer from poor long-term stability, and subsequently from drift error, when used for analysis over several hours. The causes of drift have been directly related to small variations in the instrumental parameters[72,180,181]. Most work to date has studied the drift phenomena using only a few lines at a time. However, modern ICP-AES instruments offer the possibility to analyse several dozen lines simultaneously, a feature which facilitates true multi-element analysis. Moreover, auto-sampler devices are now often coupled to the instrument allowing the analyst to automatically process hundreds of samples. Thus, ICP-AES instruments can now generate huge data sets in a matter of hours, and so the application of chemometrics become a key tool to explore and interpret the ICP-AES data. In this study, an attempted has been made to simulate as closely as possible "real" analysis by monitoring the long-term stability in emission signals over several hours, simultaneously on many lines. The causes of drift have been investigated and particular attention has been given to the effect of the instrumental parameters on the long-term stability of the emission intensities.

In terms of correction, many different approaches have been suggested to overcome drift effects. Most of these employ one or several internal standards to compensate for drift bias. However, several disadvantages are associated with the use of internal standards to improve data quality. For internal standardisation to work well, samples and calibration solutions need to be carefully matched with the internal standard elements. This is time consuming, may be expensive and a potential source of contamination. One of the goals of the present work was therefore to study the potential of using intrinsic plasma lines to monitor and correct for drift. The term "intrinsic plasma lines" refers to emission lines generated from species intrinsically present in the plasma, i.e. argon, nitrogen and water fragments, hydrogen, oxygen and

hydroxyl groups. The use of such lines to correct for drift avoids the need for internal standardisation and associated problems.

In this thesis, the drift problem associated with ICP-AES instruments is tackled in four stages. First, an experimental study was undertaken to evaluate the magnitude and characteristics of the long-term stability (Chapter 2). Secondly, a further more detailed investigation of the causes of the drift phenomena was undertaken (Chapter 3) and used to attempt drift correction (Chapter 4). The final experimental chapter describes the effect of complex chemical matrices on long-term stability (Chapter 5).

CHAPTER 2

INITIAL STUDIES

2.1 INTRODUCTION

The objective of this chapter is to provide an overview of drift phenomena from an experimental point of view. Previous work has been reported on the area of drift evaluation. Carre et al.[72] suggested a drift diagnosis for a sequential ICP-AES instrument based on the observation of the behaviour of three emission lines: Ba (II) 455.403, Zn (II) 206.200 and Ar(I) 404.442. These lines were selected because of their excitation characteristics. The Ba 455 nm has a low energy sum, and therefore should not be very sensitive to changes in the power. On contrast, the Zn 206 line is a very hard line and was expected to show a high sensitivity to any change in the power supply. However, both lines would have a similar

behaviour when there is a change in the nebulisation efficiency. Finally the argon line should be relative insensitive to sample transport variations but sensitive to energy fluctuations. Several drift diagnoses were performed varying the experiment duration and the warming up period in three different instruments. Long-term stability was found to vary considerably from one instrument to another. According to the authors, the analysis of the drift patterns of those three emission lines allowed the main causes of drift to be determined. In particularly, if the origin of the problem was the in nebulisation or in the excitation process.

To study the long-term stability of the sequential ICP-AES available in our labs, five "drift diagnoses" were performed. The number of lines under study was increased in comparison with previous work, to cover a wide spectrum range and both atomic and ionic lines. The first objective was to determine the magnitude of the drift error on our instrument in order to decide if a drift correction procedure is required. Secondly, it will be necessary to determine if a long-term degradation effect is common for all the emission lines or related to the nature of emission which may condition the drift error. This point will be critical when attempting drift correction by internal standard methods. Moreover, the study of variation on the long-term behaviour of atomic and ionic emission lines could allow the causes of instability to be explained. Finally, the potential use of intrinsic plasma lines, i.e. argon or oxygen, as internal standards to correct for drift will be investigated. The results obtained from this study are compiled and discussed in this chapter.

2.2 EXPERIMENTAL

2.2.1 METHODOLOGY

A test solution containing fifteen elements at 10 mgl^{-1} was repeatedly analysed by ICP-AES over a period up to 5 hours without re-calibration. Such "drift diagnosis" was repeated five times, in order to estimate the reproducibility of the drift phenomena.

Sample Preparation

A multi-element standard solution was prepared using 1000 mgl⁻¹ Titrisol ampoules (Merck, Darmstadt, Germany). The solution contained fifteen elements at 500 mgl⁻¹:

Al, Ba, Ca, Cd, Co, Cr, Cu, Fe, Mg, Mn, Na, Ni, Pb, Ti, Zn

Five litres of 10 mgl⁻¹ test solution were prepared by diluting the above multi-element standard, thus the same solution was employed for the five diagnosis. The test solution was matched with a 2% nitric matrix using HNO_3 Aristar (BDH, Poole, Dorset, UK).

2.2.2 INSTRUMENTATION

A Liberty 200 sequential ICP-AES instrument (Varian, Cheshire, UK) was employed to perform the five drift diagnoses. This is a radial viewed plasma with a vacuum-path monochromator offering a wavelength range of 160-940 nm, and a sequential data acquisition. The instrumental parameters employed are detailed below:

TABLE 2.1: INSTRUMENTAL PARAMETERS.

Generator	40 MHz
RF Power	1 kW
Plasma Gas Flow	15.0 Lmin⁻¹
Auxiliary Gas Flow	1.5 Lmin⁻¹
Nebuliser Pressure	150 KPa (~ 1.0 Lmin⁻¹)
Pump Speed	20 r.p.m. (~ 1.0 mLmin⁻¹)
PMT Voltage	650 V *(500V for Ca)*
Viewing Height Optimisation	SBR *(Ca & Mg by intensity)*
Stabilisation Time	10 s
Integration Time	3 s
Number of Replicates	3 readings

Wavelength calibration was performed prior to each analysis using the system mercury lamp. The emission intensities from eighteen analyte lines and four intrinsic plasma lines were monitored. The analyte emission lines used for this study are listed in Table 2.2:

TABLE 2.2: ANALYTE EMISSION LINES

ELEMENT	TYPE OF LINE	λ (nm)	INTENSITY I_n/I_b	EE = λ (eV)	IP (eV)	EP + IP (eV)
Al	ATOMIC	396.152	10.5	3.13	—	3.1
Ba	IONIC	455.403	230	2.72	5.21	7.9
Ca	IONIC	393.366	89.0	3.15	6.11	9.2
Cd	ATOMIC	228.802	110	5.42	—	5.4
Cd	IONIC	214.438	120	5.78	8.99	14.7
Co	IONIC	228.616	43.0	5.42	7.88	14.3
Cr	IONIC	267.716	42.0	4.63	6.77	$\geq$ 11.4
Cu	ATOMIC	324.754	56.0	3.82	—	3.8
Fe	IONIC	259.940	48.0	4.77	7.90	$\geq$ 12.7
Mg	IONIC	279.553	195	4.44	7.65	12.0
Mn	IONIC	257.610	220	4.81	7.43	12.2
Na	ATOMIC	589.592	43.0	2.10	—	2.1
Ni	IONIC	231.604	15.0	5.35	7.64	$\geq$ 13.0
Pb	ATOMIC	405.783	11.0	3.06	—	4.4
Pb	IONIC	220.353	70.0	5.62	7.42	14.7
Ti	IONIC	337.280	45.0	3.68	6.83	10.5
Zn	ATOMIC	213.856	170	5.80	—	5.8
Zn	IONIC	206.200	51.0	6.01	9.39	15.4

Where:

EE   Transition Emitted Energy. (By calculation)

IP   First Ionisation Potential. (From Handbook of Physics and Chemistry, CRC Press, 77th Edition, 1997)

EP+IP   Excitation Potential. (Handbook of Spectroscopy Vol.1, PW Robinson. CRC Press, 1974)

I_n/I_b Ratio to net analyte intensity to background intensity. (From Handbook of ICP-AES, CRC Press, 1981)

In addition to the analyte lines, four intrinsic plasma lines were studied in order to evaluate the potential of using such lines to monitor long-term instability (Table 2.3).

TABLE 2.3: INTRINSIC PLASMA LINES STUDIED.

ELEMENT	TYPE OF LINE	λ (nm)	EE = λ (eV)	IP (eV)	EP + IP (eV)
Ar	ATOMIC	763.511	1.62	—	?
Ar	ATOMIC	811.531	1.53	—	13.0
OH (band)	IONIC	309.446	4.01	13	?
O	ATOMIC	777.193	1.60	—	10.7

It should be noted that each measurement took approximately eight minutes to be completed due to the sequential acquisition system employed. In addition, a couple of minutes for washing were allowed between measurements. Thus there was a total delay of ten minutes between any two determinations. The total time allowed for each drift diagnosis experiment was 5h; thus 30 replicate determinations were performed.

A final important factor to be considered is temperature. Although the instrument optic system works under temperature controlled conditions, the laboratory room was not air-conditioned and thus, stable room temperature could not be achieved. For this reason, the room temperature was checked during each experiment in order to identify any effect that this factor may have on the drift phenomena.

Table 2.4 summarises the temperature intervals at which each experiment was performed.

TABLE 2.4: TEMPERATURE CONDITIONS

	$T_{MINIMUM}$ (°C)	$T_{MAXIMUM}$ (°C)
Drift Diagnosis 1	23.0	25.5
Drift Diagnosis 2	19.0	23.5
Drift Diagnosis 3	23.0	25.5
Drift Diagnosis 4	27.0	30.0
Drift Diagnosis 5	25.0	27.0

2.3 RESULTS AND DISCUSSION

2.3.1 DRIFT CHARACTERISATION

<u>Magnitude of the Drift Phenomena</u>

Each drift diagnosis experiment generated a data set that could be presented as a data matrix with the 23 columns for the emission lines and the 30 rows to represent replicate determinations.

The first factor measured on the data sets was the magnitude of the drift error with time. Drift error has been expressed as a percentage from the relative bias between the emission intensity of wavelength *i* at time *t*, and its intensity at the first measurement when *t* equals zero.

$D_{i,t}(\%) = \dfrac{I_{i,t} - I_{i,t_0}}{I_{i,t_0}} \times 100$	$D_{i,t}$ is the drift error on measuring λ_i at time t. $I_{i,0}$ is the emission intensity of λ_i at time $t = 0$. $I_{i,t}$ is the emission intensity of λ_i at time t.	**Equation 2.1**

Table 2.5 shows the maximum values of drift encountered on each line during the five diagnoses. It can be observed that the maximum drift values vary from one experiment to another and from line to line, but all show around 10–15 % error. In addition, the emission intensities decrease with time in every case. The magnitude of the drift error in this experiment suggests that either a drift correction procedure or recalibration must be used.

TABLE 2.5: MAXIMUM VALUES OF DRIFT ERROR OBSERVED (%).

Emission Lines Monitored			DRIFT DIAGNOSIS				
			1	2	3	4	5
Al	I	396.152	-19	-7	-14	-9	-10
Ba	II	455.403	-16	-11	-14	-8	-5
Ca	II	393.366	-15	-10	-19	-11	-10
Cd	I	228.802	-13	-7	-12	-9	-7
Cd	II	214.438	-11	-7	-11	-7	-8
Co	II	228.616	-10	-9	-12	-8	-8
Cr	II	267.716	-12	-8	-14	-10	-10
Cu	I	324.754	-17	-9	-11	-8	-8
Fe	II	259.940	-14	-10	-15	-10	-10
Mg	II	279.553	-11	-8	-13	-9	-10
Mn	II	257.610	-15	-9	-12	-7	-11
Na	I	589.592	-17	-8	-12	-9	-10
Ni	II	231.604	-15	-7	-14	-9	-9
Pb	I	405.783	NO DATA	-9	-14	-7	-10
Pb	II	220.353	-12	-8	-12	-9	-10
Ti	II	337.280	-18	-11	-15	-10	-12
Zn	I	213.856	-11	-7	-14	-8	-10
Zn	II	206.200	-5	-7	-12	-8	-10
Ar	I	763.511	-8	-3	-7	-8	-8
Ar	I	811.531	-10	-6	-7	-10	-8
OH	II	309.446	-13	-8	-1	0	-6
O	I	777.193	-6	-3	-4	-2	-5

These values are considerably higher to those obtained by Mermet[70,72] on the assessment of the ICP-AES technique. In that work, values of long-term stability ranged between 1 to 10% were observed. However there, values were determined by calculating the rsd of 20 replicates measured on an average time of 15 min. In this work, the time of study has been increased in order to cover the expected duration of a real experiment.

Trends in Long-Term Stability

More important than the actual magnitude of the drift error, would be to record any specific trend on the intensity fluctuations over time. In order to observe the trends, drift errors for every line were plotted against time. Figure 2.1 summarises these plots.

FIGURE 2.1: DRIFT PLOTS OF THE FIVE DRIFT DIAGNOSES.
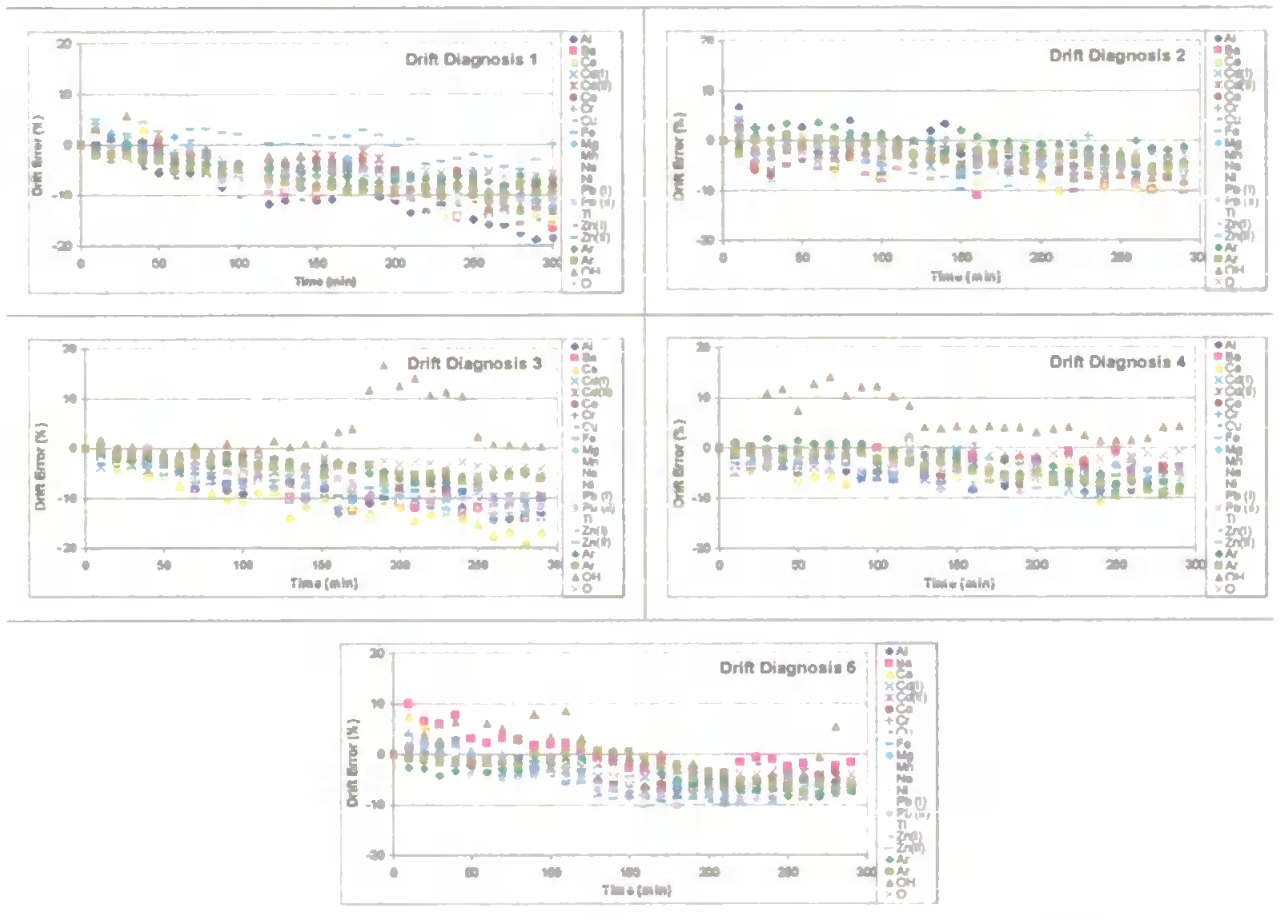
From the plots in Figure 2.1, several observations may be made. First, the drift phenomenon is qualitatively reproducible. All the five diagnosis produced similar plots and drift bias of the same order of magnitude. Secondly, the long-term instability on the signals follows a marked trend towards lower intensity values with slow fluctuations. This kind of intensity degradation could be due either from a slight decrease in the energy transfer from the plasma to the aerosol or from a decrease in the sample introduced into the system. In terms of the intrinsic plasma lines, it should be noted that these lines follow a rather similar drift pattern to the rest of analyte emissions. Only the OH band emission shown a considerably different behaviour

over time. This would support the idea of using such lines for drift correction. However, this similarity needs to be investigated further before any firm conclusions can be made.

2.3.2 APPLICATION OF CHEMOMETRIC METHODS TO DRIFT STUDY

Time Series

The study of trends on the drift plots can be approached in a more systematic way by using time series analysis. Among the techniques available, probably the most suitable for emphasising the presence of a trend is the integration of the data points. A series can be integrated by calculating the cumulative sum[114] (CUSUM) which integrates the deviations from the mean of the series:

$$CUSUM(t) = \sum_{i=1}^{t} x(i) - t\bar{x}$$

Where:

$\bar{x}$ refers to mean value of x

$x(i)$ refers to the value of x at time i.

EQUATION 2.2

When applying the CUSUM technique on a time series, any trend will be identified, i.e. a linear trend will appear as a parabola. In this study, the five data sets were reprocessed and the cumulative sums calculated. As expected, the plots obtained were downwards parabolas, i.e. *"the trend on the series was noted to be linear and negative"*.

Some examples of CUSUM plots are presented Figure 2.2.

FIGURE 2.2: EXAMPLE OF CUSUM INTEGRATION OF THE DRIFT TRENDS.

Another way to mathematically underline the presence of a trend on a data series would be to compare the common relative standard deviation of the data points to the successive relative standard deviation[66,72,182].

NORMAL RSD (%)

$$RSD_A^{nor} = \dfrac{\sqrt{\dfrac{\sum\limits_{i=1}^{n}\left(I_{A,i} - \overline{I_A}\right)^2}{n-1}}}{\overline{I_A}} \times 100$$	**EQUATION 2.3**

SUCCESSIVE RSD (%)

$$RSD_A^{suc} = \dfrac{\sqrt{\dfrac{\sum\limits_{i=1}^{n-1}\left(I_{A,i+1} - I_{A,i}\right)^2}{2(n-1)}}}{\overline{I_A}} \times 100$$	**EQUATION 2.4**

Where:

$I_{A,i}$ refers to the intensity of analyte line A at replicate i

$I_{A,i+1}$ refers to the intensity of analyte line A at replicate $(i+1)$

$\overline{I_A}$ refers to the average intensity of analyte A

n is the total number of measurements or replicates

In the absence of a trend, both relative standard deviations would be comparable. However, when a trend is present, the calculation of the successive rsd gives smaller values than the normal rsd.

TABLE 2.6: COMPARISON OF NORMAL AND SUCCESSIVE RSD (%).

			DRIFT DIAGNOSIS									
			1		2		3		4		5	
			rsd_{nor}	rsd_{suc}	rsd_{nor}	rsd_{suc}	rsd_{nor}	rsd_{suc}	rsd_{nor}	rsd_{suc}	rsd_{nor}	rsd_{suc}
Al	I	396.152	5.9	1.3	3.1	2.3	4.6	1.4	3.2	1.4	3.4	1.2
Ba	II	455.403	5.4	2.0	3.2	2.4	4.4	1.9	2.4	2.3	3.7	1.8
Ca	II	393.366	5.8	1.7	3.4	2.7	5.4	1.6	2.6	2.0	4.5	1.7
Cd	I	228.802	4.2	1.0	2.3	1.8	3.4	1.2	2.4	1.9	3.1	0.9
Cd	II	214.438	3.2	1.3	2.5	1.9	3.3	1.5	1.6	1.5	3.4	0.9
Co	II	228.616	3.6	1.4	2.2	1.9	3.5	1.4	2.2	2.1	3.0	1.1
Cr	II	267.716	4.2	1.5	3.3	2.8	4.2	1.6	2.5	2.1	3.7	1.2
Cu	I	324.754	4.8	1.6	3.0	1.9	3.7	1.5	2.6	2.0	3.0	1.5
Fe	II	259.940	4.9	1.1	3.0	2.2	4.3	2.0	2.4	1.6	4.2	1.5
Mg	II	279.553	4.3	1.3	2.5	2.1	4.0	1.6	2.7	2.4	3.7	1.4
Mn	II	257.610	4.8	1.4	2.8	1.9	4.3	1.6	2.2	1.8	3.9	1.2
Na	I	589.592	5.6	1.2	2.7	2.5	3.8	1.8	2.7	1.8	3.5	1.5
Ni	II	231.604	5.0	1.5	2.8	2.0	4.6	2.1	2.7	1.7	4.5	1.3
Pb	I	405.783	2.9	1.2	3.1	2.5	4.6	1.7	2.0	1.2	3.5	1.3
Pb	II	220.353	4.0	1.5	2.2	1.3	3.4	1.6	2.3	2.1	3.4	1.2
Ti	II	337.280	6.4	1.6	3.2	2.2	5.0	1.8	3.0	2.2	4.6	1.3
Zn	I	213.856	3.6	1.3	2.5	1.9	3.7	1.1	2.3	1.6	3.5	1.0
Zn	II	206.200	2.6	1.3	2.3	1.6	3.3	1.6	2.0	1.7	3.4	1.0
Ar	I	763.511	2.6	0.8	1.8	1.3	2.0	0.8	3.2	1.2	2.9	0.9
Ar	I	811.531	3.2	0.7	2.0	0.9	2.0	0.9	3.1	1.0	2.7	0.8
OH	II	309.446	5.3	2.4	2.5	0.6	5.1	1.9	4.1	1.9	6.1	3.4
O	I	777.193	1.9	0.3	1.0	0.6	1.3	0.5	0.6	0.4	1.4	0.3

As expected, the successive rsd values are considerably lower than the normal rsd, thus identifying the presence of a trend.

Some examples of the data generated are presented in Figure 2.3.

FIGURE 2.3: DIFFERENCES BETWEEN NORMAL AND SUCCESSIVE RSD IN VARIOUS LINES.
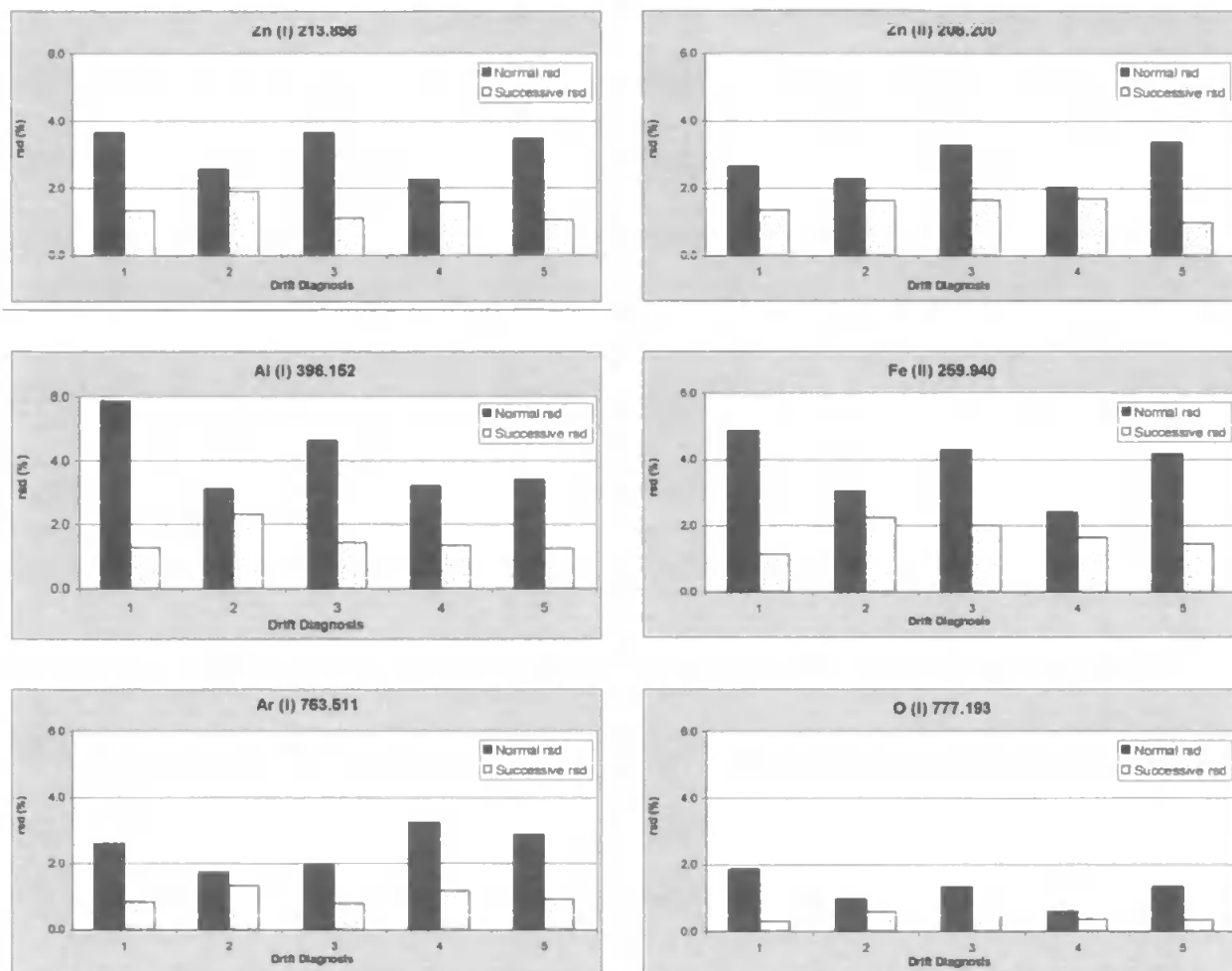
Trends can be noted for both atomic and ionic lines. Although, intrinsic plasma lines show less pronounced fluctuations over time, i.e. lower rsd values, the difference between the normal and the successive rsd can be clearly observed.

Correlation Study of the Drift Diagnoses: Influence of the Emission Nature on the Drift

The long-term behaviour of the emission intensities was studied according to the nature of the line. For example, any relationship between drift phenomena of an emission line and the energetic characteristics of the electronic transition causing such emission was studied

Correlation is a classical way to express similarity. Correlation parameters have been employed previously to evaluate the potential of internal standardisation[64,65,182,183], to study

the fluctuations arisen from the sample introduction system[68,184], to improve precision[185]. More recent applications of correlation methods include the use of cross-correlation for spectral pattern recognition in an expert system[186] or the study of time correlation at different instrumental conditions[187].

The correlation coefficient, r, quantifies the linear relationship between two variables[112].

$$r(x,y) = \frac{\text{cov}(x,y)}{s_x s_y} = \frac{\left[\sum_{i=1}^{n}(x_i - \bar{x})(y_i - \bar{y})\right]/(n-1)}{\sqrt{\left[\sum_{i=1}^{n}(x_i - \bar{x})^2 \sum_{i=1}^{n}(y_i - \bar{y})^2\right]/(n-1)^2}}$$

Equation 2.5

The correlation coefficient is bounded between −1 and +1. Absolute values of correlation close to the unity reflect a strong linear relationship between two variables.

A quick way to calculate the correlation coefficient between all the variables of a data set consists in build the correlation matrix of the data set. The correlation matrices can be calculated using the auto scaled data obtained from Equation 2.6.

$$R = \frac{1}{(n-1)} \times D_{AS}^{T} \times D_{AS}$$

Where:

R is the correlation matrix

D_{AS} is the auto-scaled data matrix.

D^{T}_{AS} is the transpose of D_{AS}.

n the number of variables

Equation 2.6

The auto-scaled data is obtained by subtracting the mean and dividing by the standard deviation SD_A:

$$I_{A,n}^{AS} = \frac{I_{A,n} - \bar{I_A}}{SD_A}$$

Equation 2.7

This transformation produces data with zero mean and unity standard deviation.

The correlation matrices of the five drift diagnoses performed on the sequential instrument were calculated in this way. A strong linear relation between some of the emission lines monitored was found.

Table 2.7 shows the correlation matrix obtained for the first data set. Very high correlation is observed between most of the lines, r ~ 90%. No meaningful difference is observed between atomic and ionic lines. The only line showing a lower level of correlation is the ionic emission of Zn, r~75%, and to a lesser extent, the ionic line of Cd. These two lines are the hardest lines in the data set. In terms of intrinsic plasma lines, similar levels of correlation are observed, r > 80%, and again Zn^{II} and Cd^{II} have poor correlation.

TABLE 2.7: CORRELATION MATRIX OF DRIFT DIAGNOSIS 1.

D.D.1	Al	Ba	Ca	Cd(I)	Cd(II)	Co	Cr	Cu	Fe	Mg	Mn	Na	Ni	Pb(I)	Pb(II)	Ti	Zn(I)	Zn(II)	Ar	Ar	OH	O
Al	1.00																					
Ba	0.94	1.00																				
Ca	0.94	0.95	1.00																			
Cd(I)	0.95	0.90	0.94	1.00																		
Cd(II)	0.84	0.81	0.81	0.87	1.00																	
Co	0.87	0.83	0.88	0.93	0.89	1.00																
Cr	0.93	0.94	0.95	0.93	0.82	0.85	1.00															
Cu	0.92	0.90	0.91	0.94	0.88	0.89	0.90	1.00														
Fe	0.96	0.94	0.95	0.96	0.87	0.89	0.95	0.94	1.00													
Mg	0.94	0.92	0.92	0.93	0.83	0.85	0.96	0.92	0.97	1.00												
Mn	0.94	0.94	0.94	0.94	0.84	0.86	0.97	0.93	0.96	0.95	1.00											
Na	0.95	0.93	0.94	0.94	0.84	0.88	0.96	0.95	0.97	0.98	0.96	1.00										
Ni	0.95	0.91	0.92	0.94	0.90	0.86	0.93	0.90	0.95	0.95	0.95	0.95	1.00									
Pb(I)	xxx	xxx	xxx	xxx	xxx	xxx	xxx	xxx	xxx	xxx	xxx	xxx	xxx	xxx								
Pb(II)	0.92	0.89	0.91	0.95	0.89	0.92	0.92	0.90	0.96	0.92	0.92	0.93	0.92	xxx	1.00							
Ti	0.96	0.94	0.93	0.92	0.86	0.84	0.94	0.92	0.95	0.94	0.94	0.95	0.94	xxx	0.90	1.00						
Zn(I)	0.92	0.87	0.90	0.92	0.89	0.87	0.90	0.92	0.92	0.91	0.89	0.93	0.93	xxx	0.90	0.93	1.00					
Zn(II)	0.76	0.74	0.77	0.76	0.84	0.78	0.79	0.73	0.81	0.79	0.78	0.79	0.84	xxx	0.75	0.80	0.85	1.00				
Ar	0.88	0.82	0.88	0.87	0.71	0.77	0.88	0.88	0.89	0.86	0.86	0.90	0.81	xxx	0.88	0.84	0.85	0.59	1.00			
Ar	0.88	0.82	0.85	0.87	0.70	0.78	0.86	0.87	0.88	0.85	0.84	0.90	0.81	xxx	0.85	0.86	0.86	0.58	0.96	1.00		
OH	0.87	0.86	0.88	0.88	0.76	0.80	0.88	0.87	0.90	0.85	0.87	0.87	0.85	xxx	0.86	0.89	0.84	0.70	0.88	0.85	1.00	
O	0.96	0.91	0.91	0.95	0.81	0.87	0.93	0.95	0.95	0.93	0.94	0.97	0.92	xxx	0.92	0.95	0.92	0.72	0.92	0.94	0.91	1.00

The correlation matrix corresponding to the second drift diagnosis is shown in Table 2.8. A lost of correlation between all lines is observed and the average correlation falls to values around 70%. Especially important is the absence of correlation between the long-term behaviour of analyte lines and argon lines. Only water species, i.e. OH and O emission lines, maintain a level of similarity with most of the emission lines monitored.

TABLE 2.8: CORRELATION MATRIX OF DRIFT DIAGNOSIS 2.

D.D 2	Al	Ba	Ca	Cd(I)	Cd(II)	Co	Cr	Cu	Fe	Mg	Mn	Na	Ni	Pb (I)	Pb (II)	Ti	Zn(I)	Zn(II)	Ar	Ar	OH	O
Al	1.00																					
Ba	0.69	1.00																				
Ca	0.70	0.87	1.00																			
Cd(I)	0.68	0.72	0.71	1.00																		
Cd(II)	0.72	0.76	0.74	0.82	1.00																	
Co	0.48	0.60	0.59	0.78	0.63	1.00																
Cr	0.73	0.70	0.67	0.75	0.84	0.65	1.00															
Cu	0.74	0.70	0.65	0.65	0.69	0.56	0.78	1.00														
Fe	0.70	0.64	0.65	0.69	0.79	0.54	0.78	0.65	1.00													
Mg	0.67	0.66	0.60	0.71	0.79	0.65	0.80	0.58	0.66	1.00												
Mn	0.71	0.76	0.76	0.80	0.84	0.60	0.80	0.79	0.88	0.65	1.00											
Na	0.77	0.72	0.66	0.75	0.76	0.66	0.78	0.66	0.68	0.83	0.71	1.00										
Ni	0.81	0.69	0.66	0.69	0.78	0.54	0.82	0.77	0.85	0.70	0.83	0.74	1.00									
Pb (I)	0.80	0.65	0.63	0.74	0.68	0.64	0.69	0.55	0.63	0.67	0.84	0.72	0.73	1.00								
Pb (II)	0.82	0.79	0.80	0.76	0.75	0.65	0.75	0.81	0.76	0.78	0.79	0.77	0.81	0.74	1.00							
Ti	0.72	0.72	0.57	0.60	0.69	0.52	0.60	0.61	0.71	0.71	0.63	0.62	0.72	0.65	0.77	1.00						
Zn(I)	0.77	0.62	0.66	0.79	0.87	0.56	0.79	0.68	0.74	0.79	0.78	0.79	0.83	0.69	0.77	0.65	1.00					
Zn(II)	0.65	0.66	0.61	0.76	0.84	0.60	0.71	0.58	0.73	0.74	0.73	0.79	0.73	0.63	0.74	0.68	0.87	1.00				
Ar	0.12	0.04	0.07	0.30	0.18	0.11	0.01	0.28	0.13	0.09	0.17	0.00	0.12	0.13	0.27	0.15	0.25	0.23	1.00			
Ar	0.34	0.38	0.40	0.47	0.35	0.26	0.24	0.53	0.33	0.25	0.40	0.25	0.36	0.26	0.52	0.31	0.40	0.33	0.85	1.00		
OH	0.71	0.65	0.73	0.70	0.67	0.47	0.57	0.73	0.65	0.55	0.68	0.57	0.74	0.58	0.84	0.62	0.74	0.65	0.54	0.78	1.00	
O	0.77	0.76	0.75	0.78	0.79	0.52	0.64	0.64	0.63	0.65	0.66	0.69	0.68	0.65	0.81	0.64	0.75	0.75	0.33	0.55	0.85	1.00

The correlation matrix of drift diagnosis 3 (Table 2.9) shows higher correlation coefficients between all the analyte lines, r > 80%. In terms of the intrinsic plasma lines, both of the argon lines studied present some correlation with the analyte lines, r ~ 75%, however, the oxygen line shows the lowest correlation coefficients. The OH emission, as already detected on the drift plots, follows a complete different trend and thus no correlation is observed.

TABLE 2.9: CORRELATION MATRIX OF DRIFT DIAGNOSIS 3.

D.D 3	Al	Ba	Ca	Cd(I)	Cd(II)	Co	Cr	Cu	Fe	Mg	Mn	Na	Ni	Pb (I)	Pb (II)	Ti	Zn(I)	Zn(II)	Ar	Ar	OH	O
Al	1.00																					
Ba	0.91	1.00																				
Ca	0.95	0.92	1.00																			
Cd(I)	0.88	0.87	0.88	1.00																		
Cd(II)	0.92	0.87	0.91	0.89	1.00																	
Co	0.84	0.81	0.84	0.92	0.86	1.00																
Cr	0.94	0.89	0.91	0.91	0.89	0.87	1.00															
Cu	0.89	0.88	0.92	0.89	0.92	0.88	0.90	1.00														
Fe	0.92	0.88	0.91	0.87	0.85	0.79	0.92	0.87	1.00													
Mg	0.93	0.86	0.93	0.85	0.91	0.85	0.91	0.91	0.92	1.00												
Mn	0.92	0.86	0.90	0.90	0.90	0.89	0.95	0.93	0.93	0.94	1.00											
Na	0.93	0.88	0.91	0.87	0.87	0.83	0.91	0.87	0.90	0.93	0.91	1.00										
Ni	0.94	0.88	0.92	0.88	0.87	0.82	0.92	0.88	0.94	0.92	0.92	0.92	1.00									
Pb (I)	0.94	0.84	0.90	0.87	0.89	0.84	0.92	0.89	0.90	0.94	0.94	0.89	0.92	1.00								
Pb (II)	0.67	0.79	0.66	0.82	0.83	0.78	0.88	0.83	0.82	0.88	0.88	0.90	0.84	0.85	1.00							
Ti	0.95	0.93	0.92	0.92	0.92	0.88	0.95	0.90	0.92	0.92	0.95	0.92	0.93	0.94	0.84	1.00						
Zn(I)	0.95	0.90	0.95	0.90	0.92	0.84	0.89	0.90	0.87	0.95	0.90	0.90	0.92	0.88	0.93	0.87	1.00					
Zn(II)	0.88	0.84	0.86	0.88	0.87	0.83	0.91	0.89	0.87	0.91	0.90	0.88	0.85	0.90	0.87	0.89	0.90	1.00				
Ar	0.80	0.73	0.81	0.71	0.76	0.65	0.73	0.78	0.71	0.72	0.74	0.75	0.71	0.74	0.75	0.74	0.77	0.70	1.00			
Ar	0.82	0.78	0.84	0.81	0.77	0.78	0.79	0.83	0.73	0.77	0.78	0.75	0.78	0.80	0.74	0.81	0.84	0.74	0.88	1.00		
OH	-0.41	-0.35	-0.31	-0.40	-0.44	-0.33	-0.32	-0.39	-0.39	-0.36	-0.45	-0.34	-0.37	-0.45	-0.30	-0.48	-0.39	-0.35	-0.59	-0.48	1.00	
O	0.94	0.89	0.92	0.88	0.89	0.82	0.93	0.92	0.91	0.93	0.92	0.93	0.92	0.94	0.88	0.93	0.93	0.88	0.75	0.79	-0.33	1.00

Table 2.10 shows the correlation matrix of the forth data set. The values obtained tend to be low and similar to those obtained with the second drift diagnosis. The average correlation coefficient falls to around 60%, however some exceptions can be noted. For example, there are some lines which present similar behaviour, i.e. Al, Cr, Fe, Mg, Mn, Na, Ni. Concerning

plasma lines, there is no correlation between OH lines and the rest of the emission lines, however some correlation is observed with the other plasma lines studied.

TABLE 2.10: CORRELATION MATRIX OF DRIFT DIAGNOSIS 4.

DD 4	Al	Ba	Ca	Cd(I)	Cd(II)	Co	Cr	Cu	Fe	Mg	Mn	Na	Ni	Pb(I)	Pb(II)	Ti	Zn(I)	Zn(II)	Ar	Ar	OH	O
Al	1.00																					
Ba	0.59	1.00																				
Ca	0.62	0.75	1.00																			
Cd(I)	0.72	0.60	0.41	1.00																		
Cd(II)	0.29	0.38	0.27	0.48	1.00																	
Co	0.48	0.46	0.26	0.79	0.48	1.00																
Cr	0.73	0.43	0.33	0.71	0.62	0.61	1.00															
Cu	0.61	0.46	0.43	0.58	0.51	0.61	0.59	1.00														
Fe	0.81	0.47	0.39	0.79	0.54	0.63	0.66	0.60	1.00													
Mg	0.71	0.56	0.35	0.78	0.57	0.72	0.60	0.60	0.65	1.00												
Mn	0.60	0.46	0.37	0.73	0.37	0.53	0.74	0.50	0.82	0.70	1.00											
Na	0.60	0.57	0.47	0.64	0.56	0.60	0.63	0.68	0.79	0.88	0.87	1.00										
Ni	0.81	0.55	0.47	0.62	0.56	0.66	0.82	0.64	0.88	0.80	0.75	0.76	1.00									
Pb(I)	0.79	0.47	0.45	0.64	0.48	0.50	0.66	0.67	0.68	0.60	0.57	0.72	0.72	1.00								
Pb(II)	0.64	0.43	0.32	0.65	0.46	0.72	0.62	0.78	0.67	0.67	0.53	0.62	0.70	0.60	1.00							
Ti	0.72	0.54	0.53	0.63	0.51	0.48	0.74	0.64	0.78	0.78	0.65	0.74	0.72	0.70	0.58	1.00						
Zn(I)	0.67	0.54	0.40	0.70	0.77	0.62	0.80	0.74	0.78	0.79	0.67	0.79	0.78	0.68	0.64	0.74	1.00					
Zn(II)	0.46	0.38	0.30	0.57	0.77	0.56	0.70	0.44	0.61	0.68	0.38	0.62	0.63	0.50	0.52	0.40	0.71	1.00				
Ar	0.82	0.36	0.38	0.68	0.24	0.46	0.58	0.64	0.67	0.53	0.67	0.64	0.75	0.67	0.50	0.64	0.63	0.33	1.00			
Ar	0.85	0.47	0.48	0.67	0.33	0.43	0.65	0.63	0.74	0.60	0.68	0.70	0.79	0.65	0.52	0.69	0.71	0.37	0.94	1.00		
OH	0.41	0.19	0.08	0.31	-0.08	0.33	0.25	0.24	0.28	0.38	0.29	0.46	0.44	0.23	0.28	0.27	0.24	0.02	0.52	0.51	1.00	
O	0.83	0.56	0.59	0.79	0.29	0.57	0.66	0.56	0.68	0.70	0.63	0.72	0.74	0.71	0.58	0.65	0.59	0.49	0.69	0.71	0.49	1.00

The last drift diagnosis set gives a correlation matrix similar to Table 2.7 and Table 2.9. High levels of correlation are observed between all of the analyte lines without exceptions, r > 80%. In terms of the intrinsic plasma lines, the correlation matrix shows an absence of correlation between the analyte lines and the OH line. The argon lines show also very poor correlation, and only the oxygen line presents a similar behaviour to the analyte lines.

TABLE 2.11: CORRELATION MATRIX OF DRIFT DIAGNOSIS 5.

DD 5	Al	Ba	Ca	Cd(I)	Cd(II)	Co	Cr	Cu	Fe	Mg	Mn	Na	Ni	Pb(I)	Pb(II)	Ti	Zn(I)	Zn(II)	Ar	Ar	OH	O
Al	1.00																					
Ba	0.89	1.00																				
Ca	0.93	0.94	1.00																			
Cd(I)	0.91	0.91	0.94	1.00																		
Cd(II)	0.90	0.87	0.90	0.94	1.00																	
Co	0.87	0.87	0.88	0.90	0.94	1.00																
Cr	0.88	0.88	0.91	0.95	0.95	0.90	1.00															
Cu	0.90	0.86	0.87	0.88	0.88	0.88	0.84	1.00														
Fe	0.87	0.89	0.92	0.94	0.93	0.89	0.91	0.84	1.00													
Mg	0.90	0.85	0.91	0.89	0.92	0.87	0.92	0.83	0.92	1.00												
Mn	0.92	0.89	0.91	0.94	0.93	0.91	0.95	0.90	0.92	0.92	1.00											
Na	0.90	0.84	0.89	0.91	0.88	0.80	0.88	0.86	0.86	0.90	0.88	1.00										
Ni	0.93	0.91	0.93	0.95	0.94	0.90	0.96	0.85	0.94	0.93	0.95	0.88	1.00									
Pb(I)	0.90	0.88	0.92	0.93	0.91	0.87	0.90	0.83	0.94	0.94	0.91	0.89	0.93	1.00								
Pb(II)	0.90	0.82	0.91	0.93	0.93	0.87	0.92	0.87	0.94	0.93	0.91	0.89	0.92	0.94	1.00							
Ti	0.94	0.88	0.93	0.94	0.95	0.91	0.95	0.88	0.94	0.94	0.95	0.92	0.97	0.93	0.95	1.00						
Zn(I)	0.92	0.88	0.89	0.94	0.94	0.90	0.93	0.87	0.94	0.93	0.94	0.92	0.94	0.91	0.95	0.96	1.00					
Zn(II)	0.87	0.78	0.83	0.86	0.89	0.89	0.84	0.89	0.88	0.89	0.89	0.81	0.89	0.88	0.92	0.93	0.93	1.00				
Ar	0.48	0.38	0.46	0.49	0.30	0.27	0.34	0.43	0.38	0.38	0.38	0.55	0.36	0.41	0.47	0.42	0.42	0.26	1.00			
Ar	0.50	0.44	0.50	0.53	0.33	0.30	0.37	0.45	0.45	0.43	0.40	0.59	0.40	0.44	0.50	0.45	0.48	0.28	0.96	1.00		
OH	0.41	0.34	0.30	0.25	0.33	0.28	0.23	0.33	0.28	0.26	0.19	0.28	0.28	0.37	0.33	0.31	0.31	0.39	0.21	0.19	1.00	
O	0.78	0.76	0.85	0.86	0.76	0.72	0.75	0.72	0.88	0.79	0.78	0.81	0.80	0.83	0.85	0.81	0.80	0.73	0.63	0.66	0.16	1.00

In order to explain the different correlation matrices shown in Table 2.7 to Table 2.11, the influence of the temperature factor must be considered. As discussed in Section 2.2.2, the room temperature could not be controlled during the early studies and thus, each drift

diagnosis was performed under different temperature conditions (see Table 2.4). Reviewing the results of the correlation matrices, the five drift diagnoses can be separated in two groups. The first group would assemble the drift diagnosis 1, 3 and 5, i.e. the three experiments that produced highly correlated data sets. Drift diagnosis 1 and 3 were obtained at similar temperature conditions, in this cases the experiment was started with a room temperature of 23 C and finished at 25.5 C, $\Delta T = 2.5$. However, the last drift diagnosis, which also shows a quite similar correlation matrix, experiment 5 was performed under warmer conditions, initial temperature 25 Celsius but a similar $\Delta T = 2.0$ C.

The second group would contain the second and the forth drift diagnosis data sets. These diagnoses were performed at very different temperature conditions. The second data set was collected in a cool room, 19 C, but a considerable increase of temperature occurred during the experiment, $\Delta T = 4.5$ C. On the other hand, experiment 4 was obtained at very warm conditions, initial temperature 27 C and $\Delta T = 3.0$ C.

The correlation results can thus be interpreted in terms of temperature. When temperature conditions are too warm or considerably unstable with a high temperature gradient, the long-term behaviour of emission intensities is more erratic, and less correlation is observed between lines and so the drift will be difficult to monitor. On the other hand, when stable temperature conditions are achieved, the system gives high correlation and internal standard correction methods could be considered. The results obtained from the correlation matrices are summarised in Table 2.12.

TABLE 2.12: SUMMARY OF CORRELATION STUDY.

DRIFT DIAGNOSIS	GENERAL CORRELATION	ANALYTE – ANALYTE CORRELATION	ANALYTE - PLASMA CORRELATION
D.D. 1 T(23-25.5 °C)	HIGH r ∈ (0.80-0.98) Except: Zn^{II} & Cd^{II}	HIGH r ∈ (0.80-0.98)	HIGH r ∈ (0.80-0.98)
D.D. 2 T(19-23.5 °C)	LOW r ∈ (0-0.84)	LOW r ∈ (0.5-0.85)	LOW with OH & O VERY LOW With Ar lines
D.D. 3 T(23-25.5 °C)	HIGH r ∈ (0.70-0.94) Except.: OH	HIGH r ∈ (0.80-0.94)	HIGH r ∈ (0.70-0.94) Except: OH
D.D. 4 T(27-30 °C)	VERY LOW r ∈ (0-0.84)	LOW r ∈ (0.25-0.84)	LOW with O VERY LOW With Ar & OH
D.D. 5 T(25-27 °C)	HIGH r ∈ (0.80-0.98)	HIGH r ∈ (0.80-0.98)	VERY LOW r ∈ (0.25-0.60) O Line: r > 0.7

Pattern Classification of the Emission Lines

1) Principal Component Analysis:

In order to better visualise the similarities and differences on the long-term behaviour of emission intensities, a principal component analysis (PCA) was performed on each data set. PCA has been previously used to study errors in ICP-AES determinations. Ramsey *et al.*[180] used PCA to study the correlated variance in ICP-AES fluctuations. Lopez-Molinero[188] applied PCA to classify emission lines using the energetic parameters of the transition causing the emission. Cave[150] applied PCA to improve the short- term precision in

simultaneous ICP-AES determinations. Moreda-Piñeiro et al.[189] applied PCA to study the systematic error in ICP-AES and MS determination.

Special attention was given to the data pre-treatment to be used before the PCA was applied. The success achieved with the application of a certain chemometrics technique to a data set depends on the data pre-treatment previously used. It is common to encounter experimental data set forms by variables of different nature (for instance, temperature, pressure, concentration) which will required some homogenisation before applying a multivariate method. Moreover, even when the data set is homogenous, i.e. same units for all variables, severe differences can be found in the actual magnitudes. PCA works in terms of variation, thus the variables that concentrate the maximum variation will be mainly employed in the construction of the model. This will lead to the variables that offer higher values would be more important in the model, masking the information from the other variables that would have a less weight in the model. Therefore, before using PCA, it is important to prepare the data[115].

In our case, emission intensities vary considerably from one line to another (several orders of magnitude); therefore a mathematic pretreatment is required if the intensity values are to be used. Among the available pretreatments, we discarded those implying mean centred data. This was not convenient because it allows zero values in the middle of the drift trend, rather than at the beginning when the drift is actually zero. Finally, the mathematical pretreatment employed was the use of auto scaling on the first value. This pre-treatment was applied to each data set before running the PCA.

$$I_{A,n}^{AS} = \frac{I_{A,n} - I_{A,1}}{SD_A}$$ EQUATION 2.8

PCA calculations were made using the software package Unscrambler (v7.01, CAMO ASA, Trondheim, Norway). Details of the PCA models are given in Table 2.13.

TABLE 2.13: PCA DETAILS.

Samples:	The 30 replicate determinations.
Variables:	The 23 emission lines monitored.
Pre-treatment:	Auto-scaling on the first value.
	No centred data.
Validation Type:	Full cross validation.

For each data set two PCA models were performed, the first one including of all the emission lines monitored and the second after removing the potential outliers. In every case, the PCA calculation was successful in that most of the variance on the data was explained with just one principal component. Figure 2.4 shows the residual variance after the first PCA model was applied to each data set.

FIGURE 2.4: RESIDUAL VARIANCE PLOTS. BLUE: CALIBRATION RESIDUALS, RED: VALIDATION RESIDUALS.
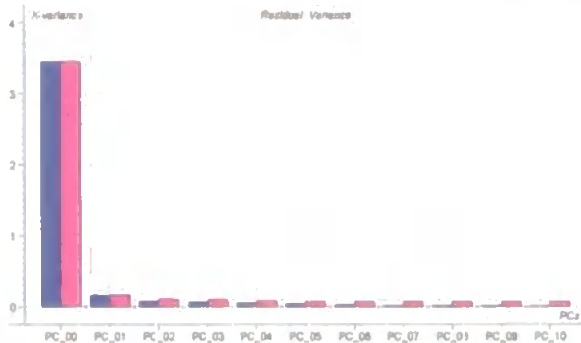
Drift Diagnosis 1: PC1 (95%) PC2 (2%)
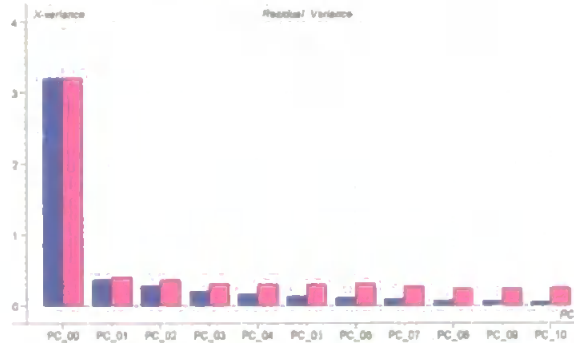
Drift Diagnosis 2: PC1 (89%) PC2 (3%)
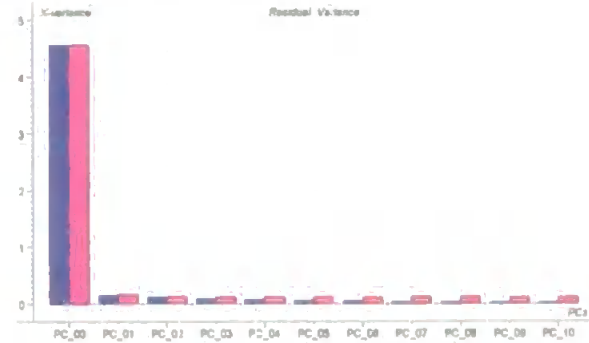
Drift Diagnosis 3: PC1 (97%) PC2 (1%)
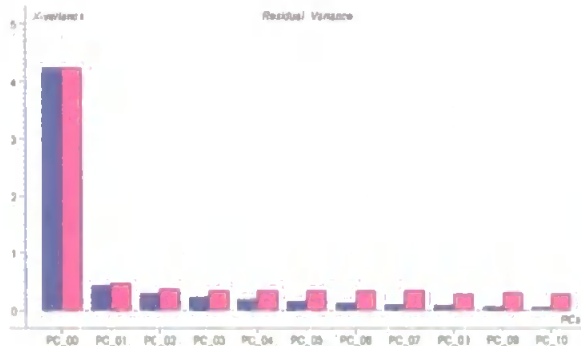
Drift Diagnosis 4: PC1 (90%) PC2 (3%)
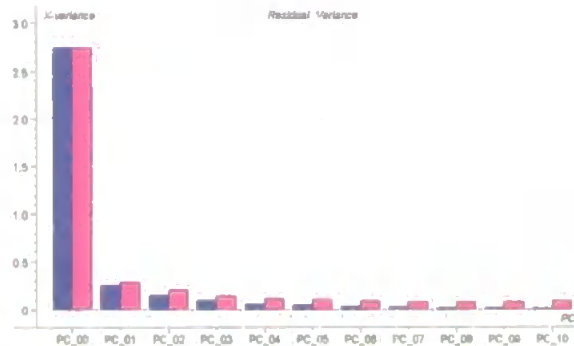
Drift Diagnosis 5: PC1 (91%) PC2 (4%)

Points to note:

In every case, PC 1 accounts for most of variation on the data set.

The calibration and the validation residual variance agreed until PC3.

It can be observed that drift diagnosis 2 and 4 are slightly poorly fitted, probably because the data was initially more noisy.

FIGURE 2.5: SCORES OF THE REPLICATES ON THE FIRST PRINCIPAL COMPONENT.
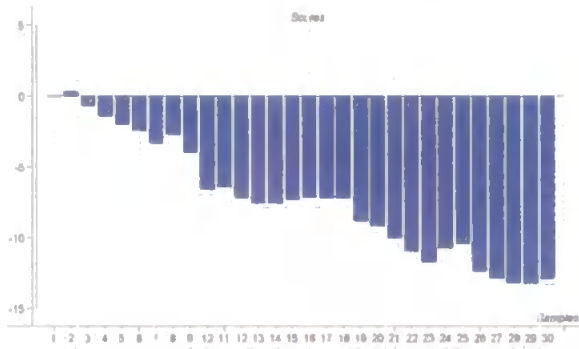
Drift Diagnosis 1: PC1 (95%) PC2 (2%)
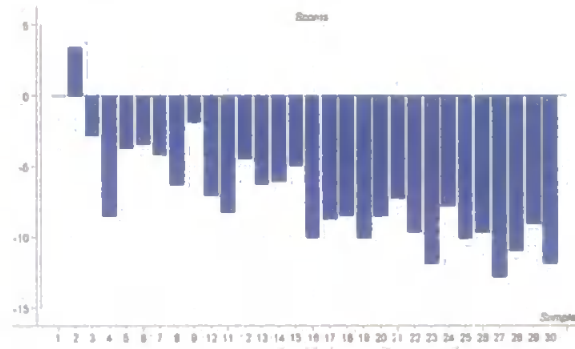
Drift Diagnosis 2: PC1 (89%), PC2 (3%)
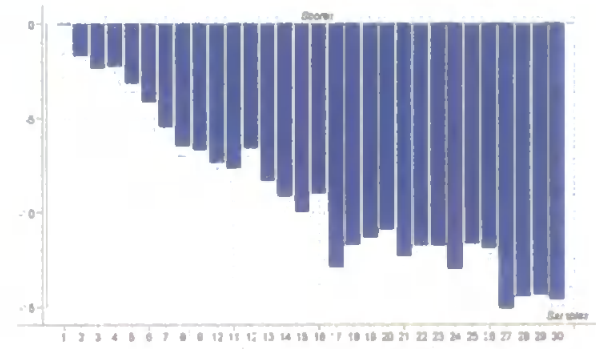
Drift Diagnosis 3: PC1 (97%) PC2 (1%)
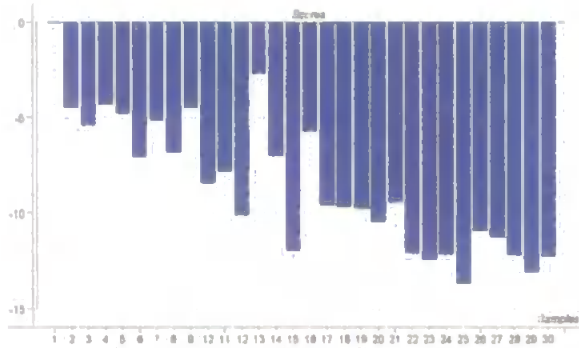
Drift Diagnosis 4: PC1 (90%) PC2 (3%)
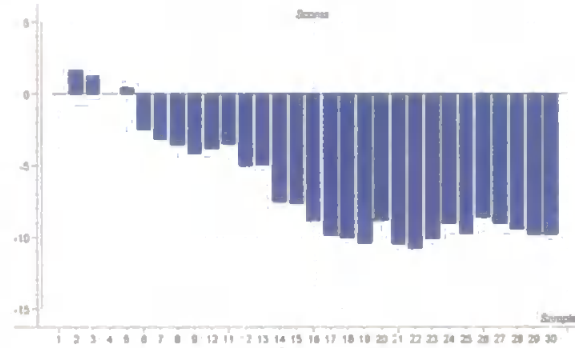
Drift Diagnosis 5: PC1 (91%) PC2 (4%)

The scores of the replicates on the first component mark the average long-term fluctuations on the emission intensities over time. Again, it can be noted a more ordered trend in drift diagnoses 1,3 and 5, when compared to the more chaotic trends in diagnosis 2 and 4.

The loading plots can also provide us with further information about the similarities and differences in long-term behaviour of the studied emission intensities. Such plots for the five drift diagnoses are presented below.

PCA Drift Diagnosis 1:

When a first PCA was performed on this data set, all of the emission lines laid together along a line, except the ionic line of zinc, which appeared well away from the others (Figure 2.6). The different behaviour of this line was already noticed when studying the correlation matrix of this data set. After excluding Zn^{II}, a second model was calculated. Model B fitted all the emission lines along a line. Most of the plasma lines appeared in the top right corner except for OH, which lies in the bottom left corner. Cu, Al and Na, the softer lines of the set, appear between the plasma lines and the rest of the analyte lines. No other significant difference is observed between atomic and ionic lines.

FIGURE 2.6: LOADING PLOTS OF PCA ON DRIFT DIAGNOSIS 1 DATA SET.

Model A: all emission lines included.
PC1 (95%), PC2 (2%).

Model B: Zn^{II} was excluded.
PC1 (97%), PC2 (1%).
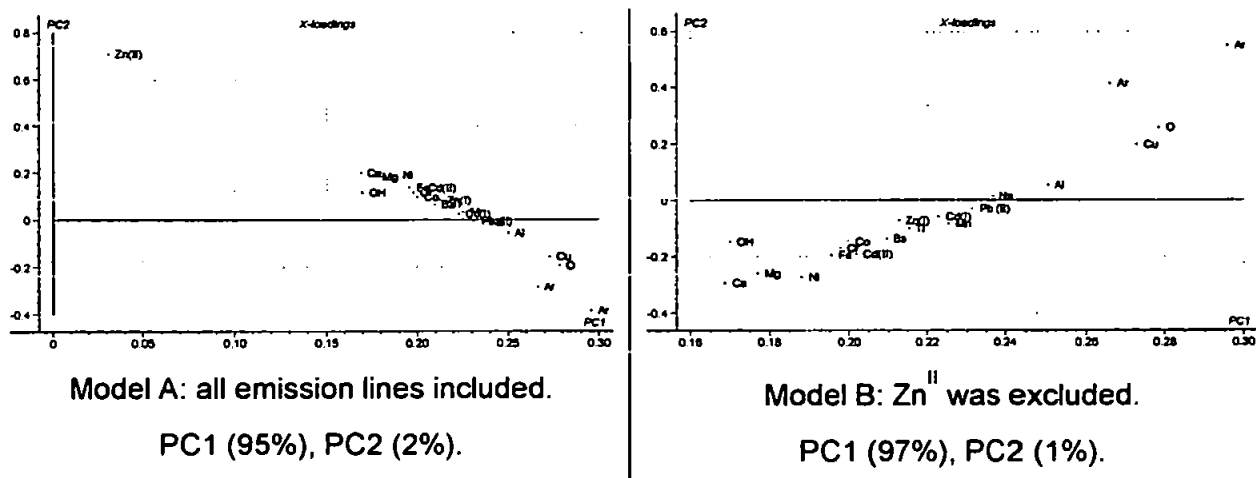
PCA Drift Diagnosis 2:

The loading plot of the first PCA calculated on drift diagnosis 2 enhances the differences between the long-term behaviour of two argon lines studied and the rest of the lines (Figure 2.7). After excluding these two argon lines, a second PCA was fitted to the data and a similar loading plot to that for the first data set was obtained. Again all of the emission lines showed

linear related loadings, although the disposition of the emission lines on the plot is slightly different. The plot seems to be rotated by 180 degrees, but this should not be a problem as PCA has rotation freedom.

In terms of the type of line, some separation is observed between the atomic and ionic lines, for instance, four of the atomic lines appear at the bottom of the plot, Al, Na, Pb[I] and Zn[I].

FIGURE 2.7: LOADING PLOTS OF PCA ON DRIFT DIAGNOSIS 2 DATA SET.

Model A: all emission lines included.
PC1 (89%), PC2 (3%).

Model B: Ar lines excluded.
PC1 (91%), PC2 (2%)
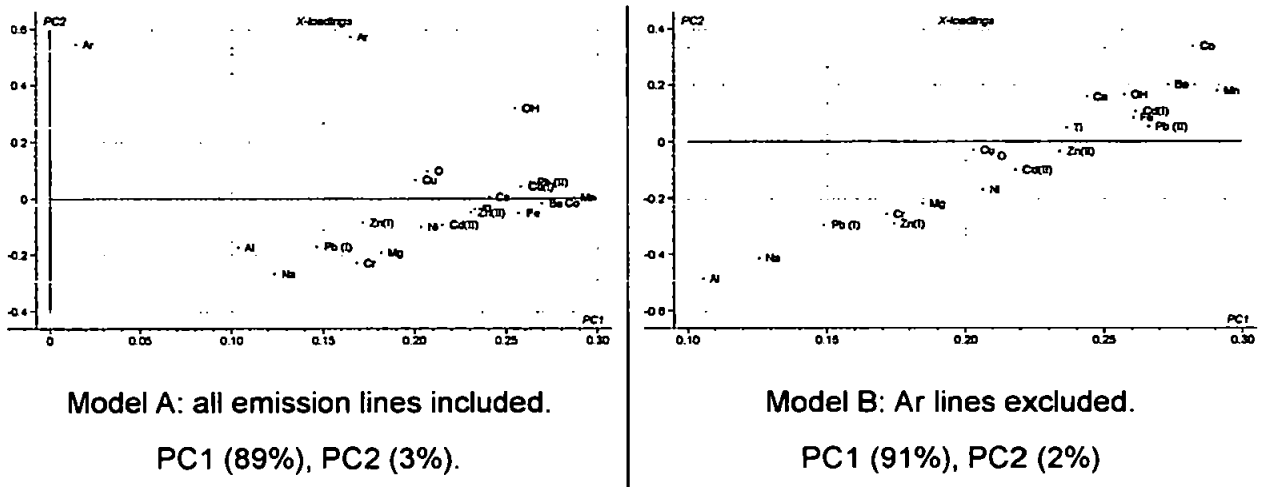
PCA Drift Diagnosis 3:

The PCA on the third data set signalled the OH line as an extreme outlier, but also marked the argon lines different behaviour. The second PCA model calculated after removing the OH data confirmed this. The loading plots of both models are shown in Figure 2.8.

FIGURE 2.8: LOADING PLOTS OF PCA ON DRIFT DIAGNOSIS 3 DATA SET.

Model A: all emission lines included.
PC1 (97%), PC2 (1%).

Model B, after exclusion of OH line.
PC1 (97%), PC2 (1%).
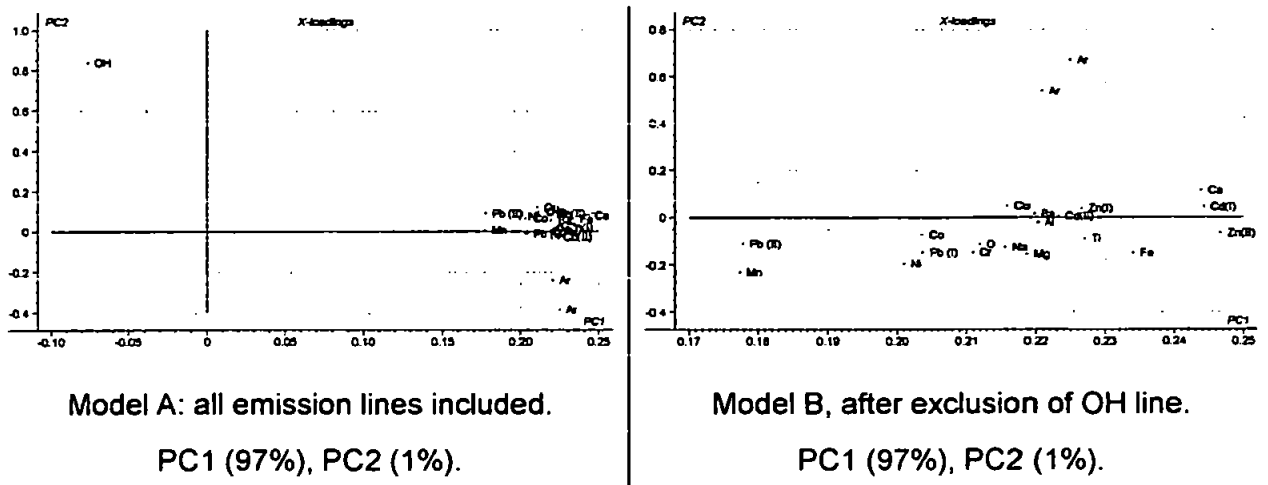
PCA Drift Diagnosis 4:

The first PCA model noted the OH line as an outlier. After its removal, a the second PCA model produces a loading plot with no clear groups formed and no linear trend of the loading disposition.

FIGURE 2.9: LOADING PLOTS OF PCA ON DRIFT DIAGNOSIS 4 DATA SET.

Model A: all emission lines included.
PC1 (90%), PC2 (3%).

Model B: excluding OH line.
PC1 (91%), PC2 (2%).
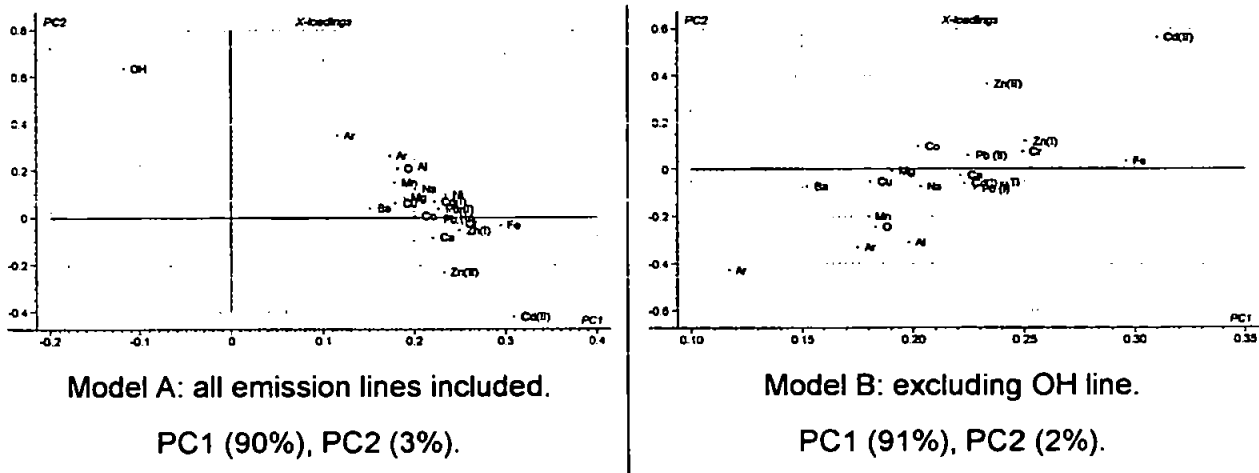
PCA Drift Diagnosis 5

The PCA analysis performed on the fifth data set agreed with the information obtained from the correlation matrix. The first PCA shows a loading plot with most of the lines lying together on linear trend (Figure 2.10). However, the OH line, the argon emissions and the barium line are more remote. A second model was fitted to the data after removing the OH and the Ar lines. All the remaining emission lines lie on the loading plot forming a straight line.

FIGURE 2.10: LOADING PLOTS OF PCA ON DRIFT DIAGNOSIS 5 DATA SET.

D.D. 5:   Model A, all emission lines included.
PC1 (91%), PC2 (4%).

D.D. 5:   Model B, after exclusion of OH & Ar.
PC1 (94%), PC2 (3%).
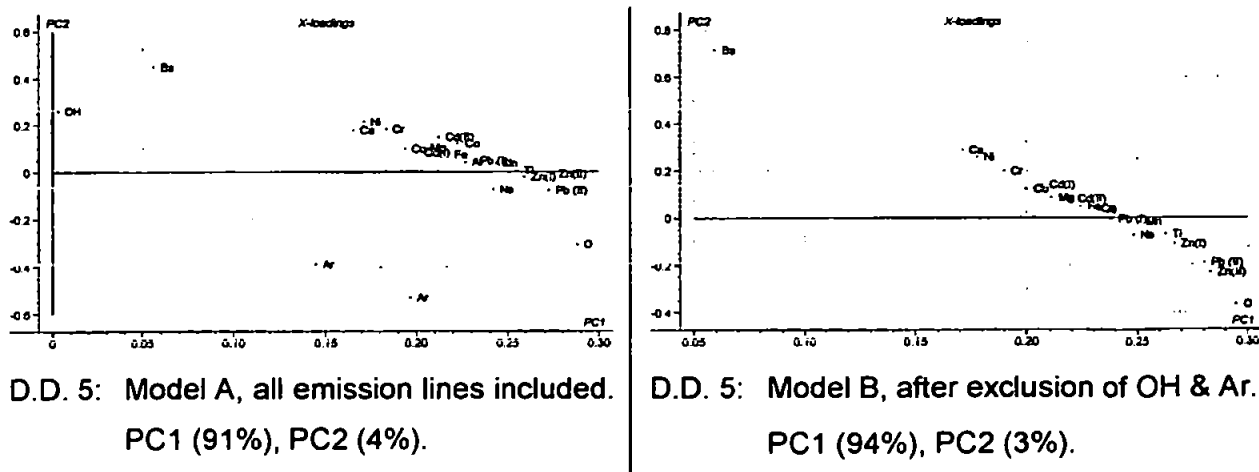
Other pattern recognition methods such LDA and SIMCA were applied to the five data set to attempt line classification according to the nature of the line (i.e. atomic, ionic, intrinsic plasma lines). However, the differences on the long-term drift were not sufficient to allow discrimination. Regression techniques such as PLS and PCR were also tempted using as predicted variable the excitation energy of the lines, however, no successful prediction was obtained. Therefore, even if some differences are observed between the long-term behaviour of emission lines depending on its excitation characteristics, no clear relation can be drawn between the two phenomena.

An example of the results obtained when a PLS was performed on the first data set is presented in Figure 2.11. The Y variable was the excitation energy for the atomic lines and the energy sum, i.e. excitation plus ionisation, for the ionic emissions.

FIGURE 2.11: RESULTS OF A PLS ANALYSIS ON DATA SET 1

Predicted versus Measured according to Component 1 (64%)	Predicted versus Measured according to Component 4 (3%)
No relationship is found (r ~ -0.6)	Some correlation is observed (r ~ -0.9)
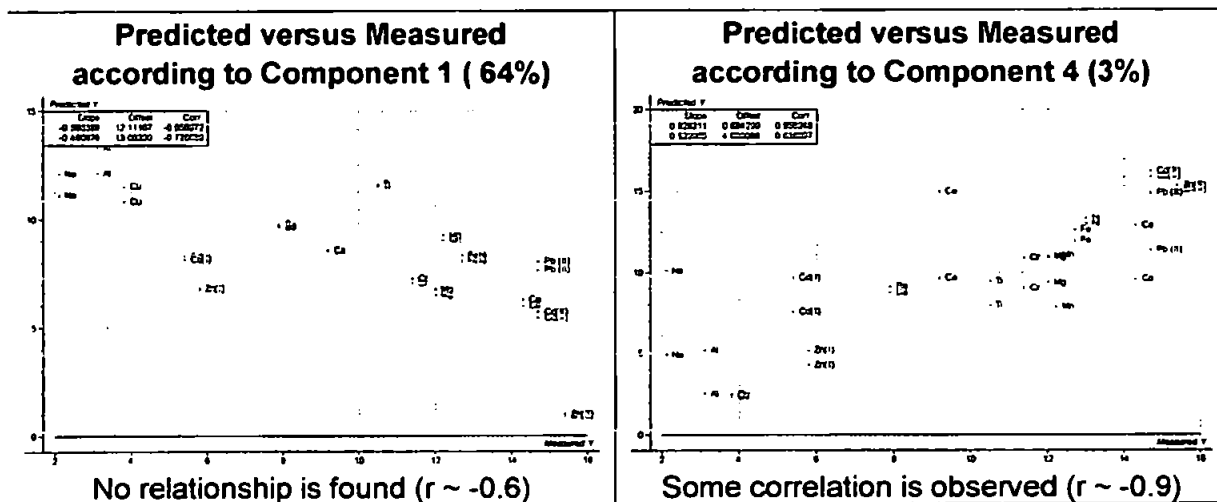
However, even when using the fourth component, the predictions of the model based on the long-term behaviour are very poor. Figure 2.12 plots the predicted values by the model calibration (blue bars), the model validation (pink bars) and actual values (green bars). Severe differences are observed.

FIGURE 2.12: PLS PREDICTED VALUES FOR THE EXCITATION ENERGY

2.3.3 SHORT-TERM PRECISION OVER TIME

Although the objective of this study was to investigate the degradation of accuracy with regard to emission intensities with time, the precision of the instrument could also be affected by drift phenomena. Thus, evolution of change in the short-term precision with time was studied. Each measurement in the drift diagnosis study is quoted as the average of three replicate readings. In order to study the fluctuations on the short-term precision, the relative standard deviation, rsd, of the three replicate measurements has been plotted against time as shown in Figure 2.13.

A slight degradation in the precision of the instrument over the time can be observed. However in every case, most rsd values are less than 3% during all the experiment.

FIGURE 2.13: FLUCTUATIONS OF THE SHORT TERM PRECISION OVER TIME
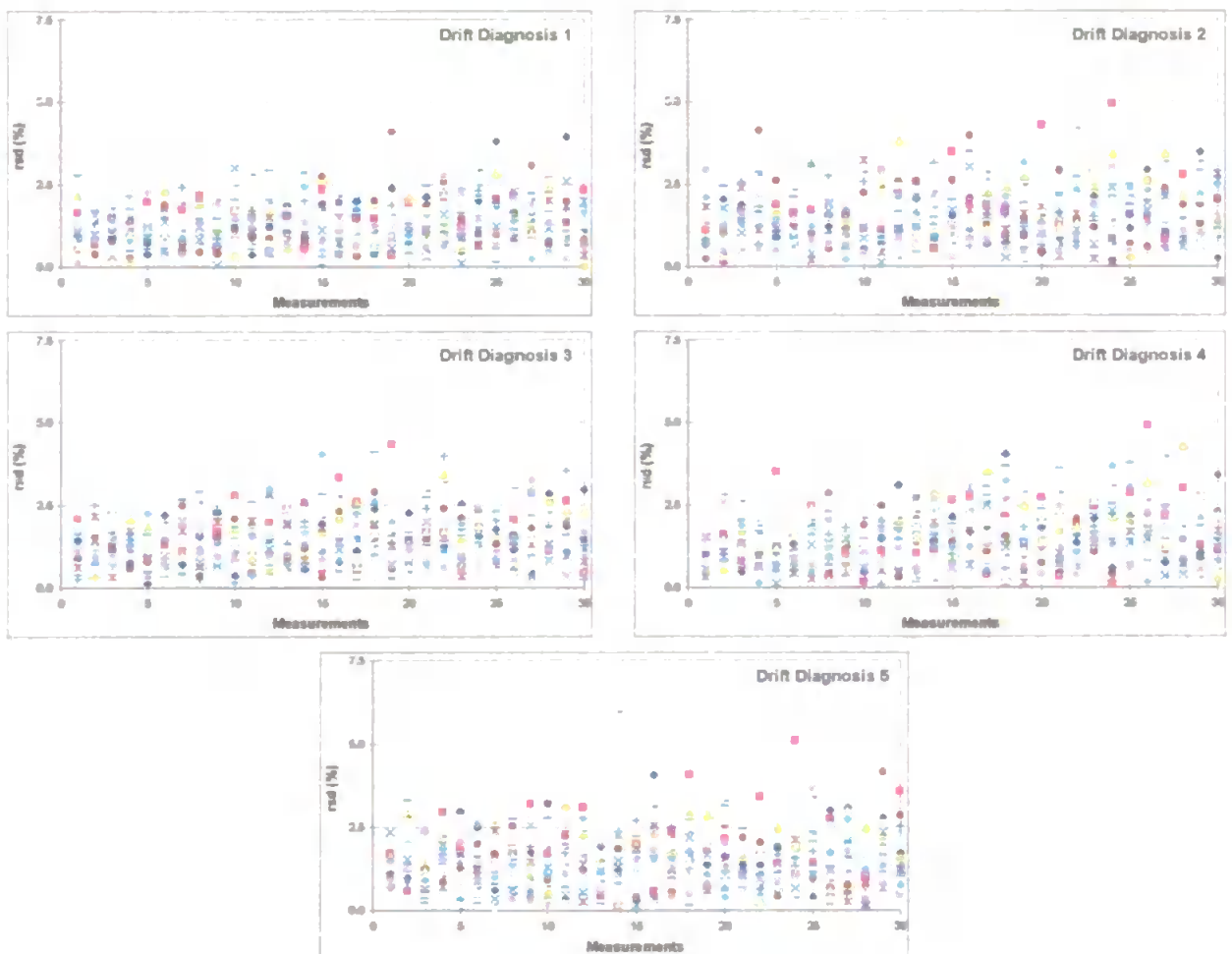
2.3.4 INTRINSIC PLASMA LINES FOR DRIFT CORRECTION

It is well known that internal standard correction methods are usually restricted to systems allowing simultaneous determinations of the analyte and the internal standard element. Simultaneous detection is necessary because the analyte and internal standard signals must be in-phase for effective correction. If internal standardisation is used on a sequential instrument, there will be a time lag between acquisition of the analyte signal and the internal standard signal. During this time short-term fluctuations in the signals (i.e. shot and flicker noise in particular) will render the correction inaccurate, and could lead to precision degradation. However, due to the remarkable correlation observed in the long-term stability of the monitored lines a further investigation was carried to study the potential of intrinsic plasma lines for internal standardisation. Among the data set produced, the first drift diagnosis was retained for this study because it presents a high correlation between most of the lines, including intrinsic plasma emissions. Therefore, in such case, the use of intrinsic plasma lines to correct for drift bias may be possible. Tracy and Myers[65] have shown that two conditions are necessary to obtain a complete correction of flicker noise by internal standardisation:

1) Perfect correlation, $r = 1$

2) The proportional coefficient k must be equal to *unity* for any n:

<div align="right">EQUATION 2.9</div>

$$k = \frac{A_n}{A_1} \times \frac{I_1}{I_n}$$

Where A_1 refers to first measure of analyte intensity (time=0).
             A_n refers to any measure of analyte intensity (time=t).
             I_1 refers to first measure of internal standard intensity (t=0).
             I_n refers to any measure of internal standard intensity (t=t).

The correlation between the emission lines monitored in drift diagnosis 1 was high for most of the lines (as shown in Section 2.3.1). The proportionality between the drift of the analyte lines and the plasma lines has been studied using the first drift diagnosis. The results obtained are shown in Table 2.14 - Table 2.17.

TABLE 2.14: K COEFFICIENT USING AR 763.511 LINE AND DRIFT DIAGNOSIS 1

TIME (nm)	Al 396.152	Ba 493.409	Ca 393.366	Cd(I) 226.502	Cd(II) 214.438	Co 228.616	Cr 267.716	Cu 324.754	Fe 259.940	Mg 279.553	Mn 257.610	Na 589.592	Ni 231.604	Pb(I) 405.783	Pb(II) 220.353	Tl 337.720	Zn(I) 213.856	Zn(II) 206.200
0	1.00	1.00	1.00	1.00	1.00	1.00	1.00	1.00	1.00	1.00	1.00	1.00	1.00	1.00	1.00	1.00	1.00	1.00
10	1.01	1.03	1.04	0.99	0.99	0.99	1.02	1.00	1.00	1.05	1.02	1.02	1.00	1.01	1.00	1.03	1.01	1.06
20	1.00	1.04	1.02	1.03	1.01	1.04	1.03	0.98	1.04	1.04	1.01	1.01	1.04	1.02	1.01	1.01	1.00	1.04
30	0.98	1.00	1.00	1.01	1.00	1.03	1.01	0.98	0.99	1.03	0.98	0.98	0.99	1.01	0.99	1.01	1.00	1.03
40	0.98	0.99	1.06	1.00	1.01	1.04	1.02	0.97	1.01	1.00	1.01	0.98	1.00	1.02	1.00	1.00	1.00	1.04
50	0.96	1.01	1.04	0.99	0.99	1.02	1.01	0.97	1.01	1.03	0.99	1.00	1.04	1.01	0.99	0.99	1.04	1.05
60	0.98	1.01	1.05	1.01	1.01	1.03	1.02	0.98	1.02	1.05	1.02	0.98	0.99	1.02	1.01	1.00	1.01	1.05
70	0.97	1.02	1.04	1.01	1.01	1.04	1.01	0.99	1.01	1.01	1.00	1.01	1.03	1.04	1.00	0.98	1.04	1.06
80	0.98	0.99	1.02	1.00	1.00	1.01	1.02	0.98	1.03	0.97	0.98	0.99	1.02	1.04	0.99	0.99	1.00	1.05
90	0.98	0.97	0.99	1.02	0.99	1.01	1.01	0.97	1.01	1.01	0.99	1.00	1.02	1.08	0.99	0.99	1.00	1.07
100	0.88	0.88	0.98	0.98	0.97	0.99	1.00	0.96	1.00	1.01	0.96	0.95	0.98	1.06	0.96	0.98	1.00	1.04
110	0.92	0.97	1.00	1.02	1.01	1.02	1.02	0.95	0.99	0.99	0.96	0.97	1.00	1.06	0.99	0.98	0.97	1.04
120	0.97	0.98	0.98	0.98	0.97	1.01	1.00	0.97	0.99	0.99	0.98	0.95	0.98	1.06	0.97	0.98	0.98	1.04
130	0.92	0.95	0.99	1.00	1.00	0.97	0.99	0.93	0.97	0.98	0.93	0.91	0.96	1.04	0.94	0.93	0.97	1.04
140	0.83	0.94	0.97	1.01	0.99	0.99	0.98	0.88	0.98	0.99	0.96	0.92	0.98	1.04	0.92	0.97	0.97	1.04
150	0.93	0.87	0.95	1.01	1.00	1.01	0.95	0.86	0.97	1.00	0.93	0.91	0.96	1.11	0.92	0.91	0.98	1.07
160	0.93	0.93	0.96	1.01	0.97	1.00	0.98	0.87	0.97	0.98	0.90	0.93	0.95	1.09	0.86	0.91	0.98	1.07
170	0.86	0.91	0.95	0.99	0.96	0.97	0.98	0.89	0.98	0.99	0.97	0.91	0.96	1.08	0.91	0.92	1.01	1.09
180	0.86	1.00	1.02	1.05	1.01	1.04	1.03	0.87	1.00	1.04	0.98	0.96	1.01	1.08	1.03	0.98	1.01	1.11
190	0.98	1.02	1.00	1.06	1.02	1.05	1.02	0.89	1.01	1.03	0.98	0.97	1.02	1.13	0.95	0.88	1.04	1.10
200	0.97	0.97	0.99	1.01	1.01	1.04	1.01	0.95	0.99	0.99	0.99	0.97	1.03	1.08	0.99	0.94	1.03	1.07
210	0.92	0.97	0.99	1.00	1.01	0.99	1.02	0.86	0.97	0.88	0.87	0.94	0.99	1.04	0.98	0.93	1.00	1.08
220	0.93	1.00	1.00	0.96	0.98	1.02	0.99	0.95	0.97	0.99	0.86	0.95	0.98	1.04	0.92	0.92	0.97	1.04
230	0.93	0.93	1.00	0.97	1.00	0.95	0.97	0.93	0.96	0.98	0.93	0.92	0.95	1.03	0.91	0.94	0.98	1.04
240	0.91	0.92	0.93	0.96	0.99	0.94	0.95	0.86	0.96	1.00	0.85	0.91	0.92	1.00	0.92	0.92	0.98	1.04
250	0.91	0.92	0.96	0.97	1.00	1.01	1.02	0.84	0.97	0.98	0.96	0.83	0.95	1.06	0.94	0.91	0.97	1.05
260	0.91	0.97	0.98	0.97	0.95	0.88	0.98	0.84	0.86	1.00	0.99	0.93	1.00	1.08	0.86	0.91	1.00	1.06
270	0.91	0.96	0.97	0.97	0.96	0.97	0.88	0.86	0.94	0.98	0.88	0.83	0.93	1.05	0.88	0.92	0.96	1.05
280	0.91	0.93	0.99	0.96	0.97	0.88	0.89	0.88	0.92	0.98	0.86	0.93	0.94	1.03	0.86	0.87	0.98	1.04
290	0.88	0.90	0.89	0.95	0.98	0.95	0.88	0.94	0.94	0.96	0.91	0.88	0.92	1.00	0.92	0.91	0.95	1.01
300	0.88	0.84	0.92	0.94	0.99	0.89	0.97	0.92	0.87	0.95	0.94	0.91	0.94	1.01	0.88	0.88	1.01	1.05
310	0.89	0.91	0.93	0.97	1.01	1.02	0.97	0.93	0.95	0.99	1.00	0.98	1.01	1.02	1.03	0.89	1.00	1.08
Maximum	1.01	1.03	1.05	1.03	1.06	1.05	1.03	1.00	1.03	1.05	1.02	1.02	1.04	1.13	1.03	1.04	1.04	1.11
Minimum	0.88	0.80	0.92	0.94	0.96	0.88	0.95	0.88	0.92	0.88	0.91	0.89	0.92	1.00	0.95	0.87	0.86	1.00
Mean	0.95	0.93	0.99	0.99	1.01	1.00	1.00	0.96	0.99	1.00	1.00	0.96	0.99	1.04	0.99	0.96	1.00	1.08

TABLE 2.15: K COEFFICIENT USING AR 811.531 LINE AND DRIFT DIAGNOSIS 1

TIME (nm)	Al 396.152	Ba 493.409	Ca 393.366	Cd(I) 226.502	Cd(II) 214.438	Co 228.616	Cr 267.716	Cu 324.754	Fe 259.940	Mg 279.553	Mn 257.610	Na 589.592	Ni 231.604	Pb(I) 405.783	Pb(II) 220.353	Tl 337.720	Zn(I) 213.856	Zn(II) 206.200
0	1.00	1.00	1.00	1.00	1.00	1.00	1.00	1.00	1.00	1.00	1.00	1.00	1.00	1.00	1.00	1.00	1.00	1.00
10	1.02	1.05	1.06	1.00	1.00	1.00	1.04	1.01	1.01	1.06	1.04	1.04	1.02	1.04	1.02	1.04	1.02	1.07
20	1.00	1.05	1.03	1.05	1.03	1.06	1.04	0.99	1.05	1.05	1.03	1.02	1.06	1.03	1.03	1.02	1.01	1.06
30	0.99	1.01	1.02	1.03	1.01	1.05	1.03	0.99	1.00	1.04	1.00	1.00	1.01	1.02	1.01	1.02	1.01	1.04
40	1.00	1.00	1.08	1.01	1.03	1.05	1.04	0.98	1.03	1.01	1.03	1.00	1.02	1.04	1.01	1.01	1.01	1.06
50	0.97	1.03	1.06	1.00	1.01	1.04	1.02	0.98	1.03	1.05	1.01	1.01	1.06	1.03	1.01	1.00	1.06	1.07
60	1.00	1.03	1.08	1.03	1.03	1.05	1.04	1.00	1.04	1.07	1.04	1.00	1.01	1.04	1.03	1.01	1.03	1.07
70	0.99	1.04	1.06	1.03	1.03	1.07	1.04	1.00	1.04	1.04	1.02	1.03	1.05	1.07	1.02	1.00	1.06	1.08
80	1.00	1.02	1.05	1.02	1.02	1.05	1.04	1.00	1.05	0.99	1.00	1.02	1.04	1.05	1.02	1.02	1.02	1.07
90	1.00	0.99	1.02	1.05	1.02	1.05	1.04	0.99	1.04	1.04	1.01	1.03	1.04	1.11	1.02	1.01	1.02	1.09
100	0.89	0.89	1.00	1.00	0.99	1.02	1.04	0.97	1.03	1.03	0.98	0.97	1.00	1.09	0.99	1.00	1.03	1.07
110	0.94	0.99	1.03	1.04	1.03	1.04	1.04	0.97	1.01	1.02	0.98	0.99	1.04	1.08	1.02	1.00	0.99	1.07
120	0.98	1.00	1.00	1.00	0.99	1.03	1.02	0.99	1.01	1.01	1.00	0.97	1.00	1.08	0.99	1.00	1.00	1.07
130	0.95	0.98	1.02	1.02	1.02	0.99	1.01	0.95	0.99	1.00	0.95	0.94	0.98	1.05	0.97	0.95	0.99	1.07
140	0.86	0.96	1.00	1.03	1.01	1.01	1.00	0.90	1.00	1.01	0.98	0.94	1.00	1.07	0.93	0.99	0.99	1.07
150	0.89	0.89	0.97	1.03	1.02	1.03	0.97	0.88	0.99	1.02	0.96	0.93	0.99	1.12	0.94	0.93	1.00	1.09
160	0.97	0.98	1.00	1.04	1.02	1.02	1.00	0.89	1.00	1.01	0.98	0.96	0.97	1.10	0.88	0.97	1.01	1.09
170	0.87	0.98	0.98	1.01	0.98	1.00	1.00	0.91	1.00	1.01	0.99	0.93	0.98	1.10	0.92	0.94	1.04	1.11
180	0.89	1.01	1.04	1.07	1.03	1.05	1.05	0.89	1.02	1.06	1.00	0.98	1.04	1.11	1.04	1.00	1.04	1.13
190	1.00	1.05	1.02	1.07	1.04	1.07	1.04	0.91	1.05	1.05	1.01	0.99	1.04	1.16	0.98	0.91	1.06	1.12
200	0.98	0.99	1.02	1.03	1.04	1.04	1.05	0.97	1.01	1.02	1.01	0.97	1.04	1.10	1.02	0.97	1.05	1.10
210	0.98	1.00	1.02	1.03	1.04	1.01	1.04	0.88	1.00	0.90	0.90	0.97	1.04	1.11	1.00	0.96	1.03	1.12
220	0.95	1.00	1.03	0.99	1.00	1.04	1.01	0.97	1.00	1.02	0.88	0.97	1.00	1.06	0.94	0.94	1.00	1.07
230	0.95	0.95	1.03	1.00	1.03	0.98	1.00	0.95	0.98	1.00	0.96	0.94	0.98	1.05	0.93	0.96	1.01	1.06
240	0.98	0.97	0.95	0.99	1.01	0.97	0.97	0.87	0.98	1.01	0.88	0.94	0.94	1.02	0.93	0.93	0.99	1.07
250	0.93	0.94	0.98	1.00	1.03	1.03	1.04	0.86	1.00	1.00	0.98	0.84	0.97	1.08	0.96	0.93	1.00	1.06
260	0.98	1.00	0.99	1.00	0.98	0.89	1.00	0.87	0.88	1.03	1.01	0.95	1.00	1.09	0.88	0.93	1.01	1.08
270	0.94	0.98	0.99	1.01	0.98	1.00	0.89	0.88	0.96	1.01	0.89	0.85	0.94	1.05	0.89	0.94	0.98	1.06
280	0.93	0.95	1.01	0.98	1.00	0.89	0.90	0.89	0.94	1.00	0.85	0.95	0.95	1.05	0.87	0.88	1.00	1.05
290	0.90	0.92	0.90	0.98	1.00	0.97	0.89	0.96	0.96	0.98	0.93	0.89	0.94	1.02	0.94	0.93	0.96	1.04
300	0.90	0.86	0.94	0.96	1.01	0.91	1.00	0.94	0.89	0.97	0.96	0.93	0.95	1.03	0.89	0.89	1.02	1.07
310	0.92	0.93	0.94	1.02	1.03	1.03	0.98	0.94	0.96	1.00	1.00	0.98	1.01	1.03	1.00	0.90	1.02	1.10
Maximum	1.02	1.05	1.06	1.04	1.06	1.07	1.05	1.01	1.05	1.07	1.05	1.04	1.06	1.16	1.05	1.04	1.06	1.13
Minimum	0.90	0.82	0.94	0.96	0.98	0.89	0.98	0.90	0.94	0.88	0.93	0.91	0.94	1.00	0.97	0.89	0.88	1.00
Mean	0.97	0.89	1.01	1.01	1.03	1.02	1.02	0.98	1.01	1.00	1.00	0.98	1.01	1.06	0.99	0.96	1.02	1.08

TABLE 2.16: K COEFFICIENT USING OH 309.446 LINE AND DRIFT DIAGNOSIS 1

TIME (min)	Al 398.152	Ba 455.403	Ca 393.366	Cd(I) 228.802	Cd(II) 214.439	Co 228.616	Cr 267.716	Cu 324.754	Fe 259.940	Mg 279.553	Mn 257.610	Na 588.992	Ni 231.604	Pb (I) 405.783	Pb (II) 220.353	Tl 377.290	Zn(I) 213.856	Zn(II) 206.200
0	1.00	1.00	1.00	1.00	1.00	1.00	1.00	1.00	1.00	1.00	1.00	1.00	1.00	1.00	1.00	1.00	1.00	1.00
Maximum	1.01	1.04	1.04	1.07	1.07	1.07	1.04	1.01	1.04	1.06	1.02	1.02	1.05	1.13	1.04	1.02	1.06	1.16
Minimum	0.90	0.93	0.96	0.95	0.92	0.85	0.94	0.91	0.95	0.94	0.92	0.92	0.93	0.95	0.93	0.90	0.94	0.97
Mean	0.96	0.98	1.00	0.99	1.01	1.01	1.00	0.95	1.00	1.01	0.98	1.00	1.00	1.06	0.99	0.97	1.00	1.15

TABLE 2.17: K COEFFICIENT USING O 777.193 LINE AND DRIFT DIAGNOSIS 1

TIME (min)	Al 398.152	Ba 455.403	Ca 393.366	Cd(I) 228.802	Cd(II) 214.439	Co 228.616	Cr 267.716	Cu 324.754	Fe 259.940	Mg 279.553	Mn 257.610	Na 588.992	Ni 231.604	Pb (I) 405.783	Pb (II) 220.353	Tl 377.290	Zn(I) 213.856	Zn(II) 206.200
0	1.00	1.00	1.00	1.00	1.00	1.00	1.00	1.00	1.00	1.00	1.00	1.00	1.00	1.00	1.00	1.00	1.00	1.00
Maximum	1.01	1.03	1.05	1.02	1.03	1.02	1.03	1.00	1.03	1.05	1.02	1.02	1.04	1.10	1.01	1.03	1.03	1.07
Minimum	0.88	0.89	0.90	0.83	0.84	0.85	0.94	0.88	0.92	0.85	0.91	0.89	0.89	0.99	0.93	0.85	0.85	1.00
Mean	0.94	0.96	0.98	0.97	0.99	0.98	0.98	0.95	0.98	0.99	0.96	0.95	0.97	1.03	0.95	0.87	0.89	1.04

From Table 2.14-Table 2.17, it can be observed that the k values differed slightly from unity in every case. This means that the signal ratios are not independent of time. The proportionality coefficients, k, varied from 0.90 to 1.10 will thus give errors of around ten percent when a plasma line is used as internal standard. However, certain compensating effects were identified when comparing the proportionality coefficients of the different plasma lines studied. For instance, when the OH emission had a corrected intensity signal in excess ($k > 1$), the argon signal would have a corrected signals in defect ($k < 1$). It might therefore be possible to improve the results of the internal standard correction using a linear combination of intrinsic plasma emissions as internal standard rather than the individual emissions. The use of a linear combination of signals as reference signal was suggested by Mermet et al.[66].

Thus, two artificial internal standards (AIS) were produced; the first is a linear combination of the plasma emission intensities analysed in this study, X_t:

$$X_t = \frac{1}{p} \times \sum_{i=1}^{p} I_{i,t}$$

EQUATION 2.10

Where:

p is the number of intrinsic plasma lines employed (4).

$I_{i,t}$ is the intensity of the i plasma signal at time t.

The second is an artificial reference standard modified using the results obtained from the principal component analysis. Similarities and differences found by PCA between emission lines could be included on the artificial standard by adding a weight coefficient related to the PCA loadings to each plasma line factor. One could introduce this information to the artificial internal standard by modifying Equation 2.10 as below:

$$X_{A,t}^{PC_j} = \frac{1}{p} \times \sum_{i=1}^{p} \frac{I_{i,t}}{I_i} \left(1 - \left|l_A^j - l_i^j\right|\right)$$

EQUATION 2.11

l_A^j is the loading of analyte line A on principal component j

l_i^j is the loading of plasma line i on principal component j

Here the loadings have been transformed by a maximum minimum transformation[114]. After this kind of treatment, the loading values vary between 0 to 1 for each PC.

$$z = \frac{x_i - x_{min}}{x_{max} - x_{min}}$$

<div style="text-align: right;">**EQUATION 2.12**</div>

If an analyte and a plasma line are found by the PCA to be similar, their loadings on a specific PC will be comparable. This will give that plasma line following Equation 2.11, a bigger weight on the construction of the internal standard. On the contrary, if a plasma line has a completely different behaviour to an analyte line, their loadings will be very different and that plasma signal will have a small effect on the artificial standard. With this *PCA-modified reference standard*, an internal standard, specific for each element was produced. The first principal component, which accounts for most of the data variation, was used in this study

Finally, it needs to be noted, that this method will have no practical application unless the score matrix can be employed from one experiment to another, which is unlikely.

The results obtained when these two reference standards were applied to correct for drift on the first drift diagnosis can be seen in Figure 2.14. The long-term drift is partially corrected by the two artificial standards but the correction is poor in both cases.

FIGURE 2.14: DRIFT PLOTS BEFORE AND AFTER CORRECTION WITH AIS.
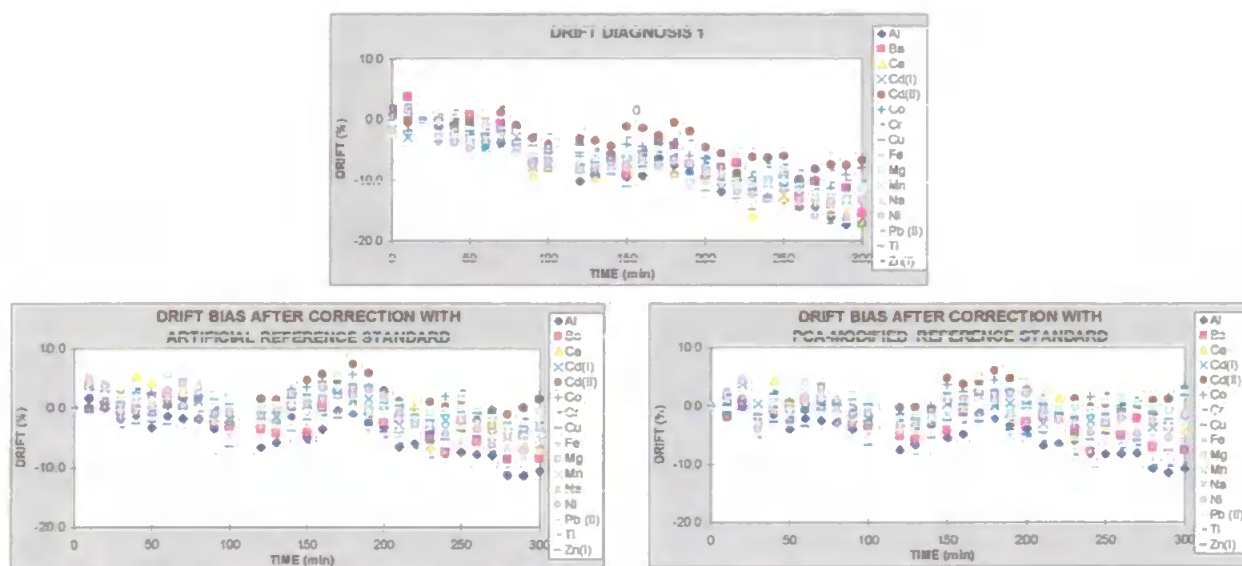
The corrected drift plots show that some of the downward drift is corrected, but not the short-term fluctuation of the data. This could is certainly due to the fact that data has not been acquired simultaneously. Previous studies[64,68] have identified the nebulisation and transport processes as key sources of flicker noise. Accordingly, the ratio of simultaneous acquired emission data will lead to an improvement in precision by compensation of flicker noise. In this study the data was acquired sequentially, with a time delay of up to 8 minutes between two lines were determined. For this reason, the calculated signal does not cancel out the flicker noise, and in fact it may tend to increase it. That said, some of the drift has been removed by internal standardisation and although the data was acquired sequentially, the correlation matrices show high correlation between emission lines. This indicates that in addition to the flicker noise, the system is being degraded by an additional factor operating over several minutes time span.

Three features were employed to quantify the fluctuations and to estimate the possible improvement:

1. The final drift after five hours of analysis.

2. The relative standard deviation of each signal over the whole experiment, (normal RSD).

3. The successive relative standard deviation of each signal over the whole experiment.

TABLE 2.18: VARIOUS PARAMETERS BEFORE AND AFTER DRIFT CORRECTION.

	DRIFT (%)			RSDn (%)			RSDsuc (%)		
	NO CORRECTION	X_{REF}	$X_{REF}{}^{PCA}$	NO CORRECTION	X_{REF}	$X_{REF}{}^{PCA}$	NO CORRECTION	X_{REF}	$X_{REF}{}^{PCA}$
Al	-18.4	-10.6	-10.8	5.9	3.7	3.5	1.3	1.4	1.4
Ba	-16.5	-8.4	-7.6	5.4	3.4	2.9	2.0	2.2	1.9
Ca	-15.2	-7.1	-4.1	5.8	3.6	2.7	1.7	1.8	2.1
Cd(I)	-11.5	-3.0	-2.6	4.2	2.2	1.8	1.0	1.1	1.2
Cd(II)	-7.4	1.5	2.7	3.2	2.3	2.2	1.3	1.3	1.6
Co	-6.9	2.0	3.3	3.6	2.2	2.1	1.4	1.5	1.7
Cr	-11.1	-2.5	-1.2	4.2	2.2	1.8	1.5	1.6	1.7
Cu	-14.8	-6.6	-7.3	4.8	2.7	2.6	1.6	1.7	1.6
Fe	-13.0	-4.6	-3.2	4.9	2.7	2.0	1.1	1.2	1.4
Mg	-9.3	-0.5	2.0	4.3	2.3	2.0	1.3	1.5	2.0
Mn	-14.6	-6.4	-6.0	4.8	2.8	2.4	1.4	1.5	1.4
Na	-13.6	-5.2	-5.2	5.6	3.3	3.0	1.2	1.4	1.4
Ni	-11.7	-3.2	-1.4	5.0	3.2	2.6	1.5	1.6	1.9
Pb (II)	-10.6	-2.0	-1.8	4.0	2.1	1.9	1.5	1.4	1.5
Ti	-18.4	-10.5	-9.9	6.4	4.2	3.7	1.6	1.9	1.7
Zn(I)	-7.9	1.0	1.7	3.6	1.9	1.7	1.3	1.3	1.5

The magnitude of drift bias was reduced for every line with both artificial reference standards. No great improvement was obtained by the use of the pca-modified reference in comparison to the standard reference. In terms of the RSD, the application of the reference standards to the data reduced the relative standard deviation for every line, providing improvement factors of about two. Again, the use of the pca-modified standard improves slightly the precision, so its utility is poor. The successive relative standard deviation is the only level of those studied here, which is degraded by using reference standards to correct the drift. This will mean that some of the trend on the data is being removed, and so, the normal and the successive relative standard deviations tend to similar values.

2.4 SUMMARY

From this initial study, it is possible to reach several conclusions. Firstly, the drift phenomenon is in some way reproducible. The five drift diagnoses employed in the study showed similar drift patterns with a common trend for all the emission lines monitored. This trend has been shown to be linear and negative; i.e. intensities decrease over time. However, a more detailed analysis of the data reveals many differences between the data sets. For instance, the magnitude of drift varied from one set to another, as did the identity of lines showing higher bias. In terms of correlation, differences may separate the five drift diagnoses in two groups, where three data sets present high levels of correlation between most of lines, whilst the other two showed more chaotic patterns with poorer inter-element correlation. The different temperature conditions at which those experiments were performed may explain some of these differences but not all.

Secondly, no clear relationship was found between drift and the physical properties associated to the emission line. In some of the PCA plots, many atomic lines appeared grouped together but no complete separation between atomic and ionic lines was found based on long-term stability. The absence of a clear grouping according to the energy

differences may lead us to suspect that degradation on the energy transfer from the plasma to the aerosol is not the only cause of drift bias. However, high correlation levels were observed, (although the instrument employed had a sequential data acquisition system) indicating that the sample introduction process was not the origin of the drift problem. Therefore, it was necessary to further investigate the problem in order to reach a better understanding of the drift phenomenon and its causes in order to be able to minimise its effects.

Finally, the use of individual plasma lines to correct drift when used as internal standards was shown to be poor. The degree of correlation for such lines with analyte lines was shown to vary considerably from one data set to another. Furthermore, even when high correlation was observed, the signal ratio was not independent of time. The use of a linear combination of plasma lines as internal standards has been shown to partially removes the drift bias. However, the improvements are still poor and the analyst control of the actual correction very low. When the loadings from principal component one were used, the correction was slightly better. None the less, this approach is far from defining a common loading matrix for any experiment, and without this there is limited practical application for the method.

CHAPTER 3

CAUSES OF DRIFT

3.1 INTRODUCTION

The initial results discussed in Chapter 2 facilitated a better characterisation of drift phenomena on a sequential ICP-AES instrument. It can now be established that drift is qualitative reproducible and moreover, a correlation was observed between most of emission lines although no simultaneous determinations were performed. However, little or no information on the causes of long-term fluctuation was obtained.

A short review of the literature reveals that instrumental drift in ICP-AES is related to small uncontrolled variations in the instrumental conditions. Lorber et al.[190] used the generalised internal standard method to characterise the parameters causing drift in ICP-AES signals.

Variations in both, the nebuliser and the cooling gas flow were found to be the origin of long-term stability. Ramsey *et al.*[180,181] reported ten potential instrumental parameters and environmental factors that can induce correlated fluctuations and subsequent lost of long-term precision in the emission signals. These factors are the sample uptake rate, the forward power, the injector gas flow, the spectrometer slit position, the extraction speed, the lens opacity, the air temperature around the spray chamber, the sample solution temperature, its salt content and the ICP warm-up. However, according to the authors, most of these causes of variation can be grouped in to sets. Those parameters causing fluctuation similar to the forward power (injector gas flow, air temperature and lens opacity) and those causing fluctuations similar to the sample uptake rate (solution temperature and salt content). Drift due to warm-up was found to be largely a linear combination of the two grouped-causes.

Carre *et al*[72] agreed on that the origin of drift was related to fluctuations in the instrumental parameters, but divided the causes of drift in three categories:

- Changes in the energy transfer from the plasma to the sample

- Variations in the efficiency of the sample production and transport

- Degradation of the line intensity measurement

Changes in the energy transfer can originate in a variation of the forward power or from variations in any of the gas flow rates. Changes in the sample introduction system can be related to a variation in the carrier gas flow rate or in the solution uptake rate, a partial blocking of the nebuliser or a change in the temperature of the spray chamber and the solution. Degradation of the line intensity measurement may be related to a thermal drift of the instrument optic device or to opacity of the collimating system.

Following these ideas, in this chapter an attempt has been made to study the origin of drift by recording the long-term fluctuations on emission signals at different instrumental conditions. In essence, six parameters need to be set before running an ICP-AES analysis: the three argon flows (plasma, nebuliser and auxiliary flow), the sample uptake rate, the RF power and the viewing height. In addition to these, the size of the entrance slit, the integration time and

the type of background correction employed will determine the nature of the mathematical process used to convert the raw signal into usable data. When trying to identify the effect of small variations in the instrumental parameters on the signals, there is a problem in isolating each function since the working parameters are inter-related. For instance, an increase in the nebuliser flow rate may improve the transport efficiency by creating a finer aerosol, such that more drops will reach the plasma, and thus the intensity of the signal could be enhanced. However, at the same time, a higher nebuliser flow will decrease the residence time of the sample aerosol in the plasma, so that less energy will be transferred to the sample, with the potential loss of some emissions lines. Although the transport of the sample to the plasma will be influenced largely by the sample uptake rate and the nebuliser gas flow rate, other factors will also have an effect on the type of aerosol created. Examples include the viscosity of the sample, type of nebuliser and spray chamber employed or the room temperature. In terms of energy transfer, the instrumental parameters with most influence are the RF power supply, the three argon flows and the sample uptake rate. Since these instrumental parameters are inter-related, a systematic study of the influence of the variation of each parameter on the long-term stability of the emission signal would be required. A full factorial experimental design could be used, however, such approach would lead to a high number of experiments. For example, if the six instrumental parameters mentioned above (i.e. RF power, sample uptake rate, the three argon flows and the viewing high) are considered for just two different settings of each parameter, 64 experiments would be required to study all the interactions. For these reasons, we have limited the number of parameters under study.

According to the work by Carre et al.[72], there are three areas of instability the nebulisation process, the excitation area and optics system. In many modern instruments, software routines control the stability of the optical system and allow this to be monitored during the analysis. However, the operator usually has little or no information about the state of the sample transport system or the stability of the plasma. The nebuliser gas flow rate and the RF power are the two instrumental parameters most likely to have an effect on these parts of

the system. In this work, the effect of these two parameters on the long-term stability of the signals have been studied, although it is recognised that many other instrumental parameters may also have an effect on those processes.

Let's see how these two parameters will affect in general terms the emission intensities:

The power delivered to the plasma will determine its temperature, with higher power resulting in higher temperatures. Higher temperatures enhance emission for all ionic lines. However, the effect on atomic lines depends on the relative excitation and ionisation energies of the emitting atom:

- Short wavelengths atomic lines are enhanced.

- Long wavelength atomic lines are suppressed.

- Moderate wavelength atomic lines remain relatively unaffected.

The nebuliser flow affects the average size of the aerosol droplets, but also the residence time of the sample in the plasma and the plasma temperature. At low nebuliser flow, the average size of the aerosol droplets increases, reducing the transport efficiency of the spray chamber. Thus, every line will partially decrease its emission intensity as less sample reaches the plasma. However, a lower nebuliser flow will also increase the residence time of the aerosol in the plasma and the plasma temperature. This could enhance the emission of any ionic line. For atomic lines, the increased residence time provides energy to promote two competing pathways: the excitation, which leads to emission enhancement and ionisation, which leads to emission suppression. Therefore the net effect will depend on the relative energies of the two processes such that:

- High-energy atomic emission lines emitted by elements that resist ionisation (e.g. Zn) show enhanced emission with increased residence time.

- Low-energy atomic emission lines emitted by easily ionised elements (e.g. Na) show emission suppression with increased residence time.

- Moderate-energy atomic emission lines emitted by atoms of moderate ionisation energy (e.g. Cu) remains unaffected by residence time.

Clearly, even when considering only two factors, an ICP is a complex system, and for this reason a systematic approach to the problem is essential.

To carry out this study, the evolution of emission signals with time at different RF powers and nebuliser gas flow rates was monitored. The long-term stability of the instrument at different operating conditions could then be evaluated using standard parameters: long-term error and drift patterns. In addition, other analytical parameters as sensitivity or robustness were also recorded for each set of conditions. Finally, a correlation study of each data set was performed to identify any linear behaviour and similarities and differences between emission lines i.e. analyte and argon lines, atomic and ionic emission lines. However, for data handling purposes, a multi-way approach was necessary to facilitate the three-dimension nature of the results. The produced data was arranged in a cubic array, indexed: Emission Lines x Replicates x Instrumental Conditions. A multi-way decomposition method, parallel factor analysis, PARAFAC, was then performed on the resulting array. Two PARAFAC-factors were calculated and their physical relevance investigated in terms of energy data, drift patterns and instrumental conditions.

3.2 EXPERIMENTAL

3.2.1 METHODOLOGY

Several drift diagnoses at different experimental conditions were produced following the protocol described in Chapter 2. A test solution containing 15 analytes at 10 μg g^{-1} was repeatedly analysed by a simultaneous ICP-AES over a period of 8 hours without recalibration. The duration of each experimental run has been increased from 5h on the initial studies to 8 hours. The reason is the availability of an auto-sampler device for the OPTIMA instrument, which allows the automation of analysis.

In order to use a common solution throughout the experiment, 10 litres of test solution were produced by diluting the previous prepared multi-element standard (Section 2.2.1). The test solution was matched with 2% nitric acid (Aristar, BDH,UK).

3.2.2 INSTRUMENTATION

The ICP-AES instrument employed for this analysis was an Optima 3000 (Perkin-Elmer Corporation, Norwalk, USA). This instrument combines an echelle polychromator with a solid state detector, which allows simultaneous acquisition of over 5000 lines. The instrumental parameters employed are shown in Table 3.1. The settings for the nebuliser gas flow rate and RF power were defined using an experimental design.

In order to ensure stable starting conditions, two hours were allowed to warm up and stabilise the instrument prior each set of measurements.

TABLE 3.1: INSTRUMENTAL SETTINGS USED IN DRIFT STUDIES.

Generator	40 MHz
RF Power	Designed variable
Plasma Flow	15 Lmin^{-1}
Auxiliary Flow	0.8 Lmin^{-1}
Nebuliser Flow	Designed variable
Sample Uptake Rate	1.0 Lmin^{-1}
Viewing Height	12 mm
Read Time	10 – 20 sec
Number of Replicates	3 readings
Nebuliser Type	Cross Flow Pneumatic Nebuliser
Injector Diameter	2 mm

The intensities from 29 emission lines, one atomic and one ionic line for most elements, were then followed over time. Table 3.2.

TABLE 3.2: EMISSION LINES USED IN THIS STUDY.

ELEMENT	λ (nm)	INTENSITY I_n/I_b	EE = λ (eV)	IP (eV)	EP + IP (eV)
Al (I)	396.152	10.5	3.13	—	3.1
Ba (II)	230.424	73.0	5.38	5.21	≥ 10.6
Ba (II)	233.527	75.0	5.31	5.21	11.2
Ca (I)	422.673	1.5	2.99	—	2.9
Ca (II)	317.933	1.5	3.90	6.11	13.1
Cd (I)	228.802	110	5.42	—	5.4
Cd (II)	226.502	120	5.47	8.99	14.4
Co (I)	340.512	NO DATA	3.64	—	4.0
Co (II)	228.616	43.0	5.42	7.88	14.3
Cr (I)	357.869	13.0	3.46	—	≥ 3.46
Cr (II)	267.716	42.0	4.63	6.77	≥ 11.4
Cu (I)	324.754	56.0	3.82	—	3.8
Cu (II)	224.700	39.0	5.52	7.73	15.9
Fe (II)	259.940	48.0	4.77	7.90	≥ 12.7
Mg (I)	285.213	NO DATA	4.35	—	4.3
Mg (II)	279.079	1.0	4.44	7.65	≥ 12.1
Mn (I)	403.076	6.8	3.08	—	3.1
Mn (II)	257.610	220	4.81	7.43	12.2
Na (I)	589.592	43.0	2.10	—	2.1
Ni (I)	232.003	20.0	5.34	—	≥ 5.34
Ni (II)	231.604	15.0	5.35	7.64	≥ 13.0
Pb (II)	220.353	70.0	5.62	7.42	14.7
Ti (II)	379.280	NO DATA	3.27	6.83	≥ 10.1
Zn (I)	213.856	170	5.80	—	5.8
Zn (II)	202.548	75.0	6.12	9.39	15.5

The optical grating system of the instrument used in this study prevents access to some parts of the spectrum. This problem made the inclusion of intrinsic plasma lines more difficult than when using the sequential spectrometer in Chapter 2. Thus only argon lines were used

since the hydroxyl, oxygen or hydrogen emissions could not be monitored. Four argon lines were selected because of their peak quality as shown in Table 3.3.

TABLE 3.3: INTRINSIC PLASMA LINES STUDIED.

ELEMENT	λ (nm)	INTENSITY I_n/I_b	EE = λ (eV)	EP + IP (eV)
Ar (I)	357.229	2.3	3.47	≥ 3.47
Ar (I)	404.597	2.5	3.06	≥ 3.06
Ar (I)	420.068	50	2.95	≥ 2.95
Ar (I)	451.074	21	2.75	≥ 2.75

3.2.3 EXPERIMENTAL DESIGN SETTINGS

Settings for the RF power and the nebuliser gas flow rate were selected following an experimental design. A combination of two full-factorial designs was employed:

- A full-factorial experiment of two factors at three levels (Table 3.4) $\Rightarrow$ *9 Experiments*

TABLE 3.4: EXPERIMENTAL DESIGNED LEVELS, BLOCK 1.

Factor 1 RF Power			Factor 2 Nebuliser Flow Rate		
-1	0	+1	-1	0	+1
1000 W	1250 W	1500 W	0.6 Lmin^{-1}	0.9 Lmin^{-1}	1.2 Lmin^{-1}

- A full-factorial experiment of two factors at two levels (Table 3.5) $\Rightarrow$ *4 Experiments*

TABLE 3.5: EXPERIMENTAL DESIGNED LEVELS, BLOCK 2.

Factor 1 RF Power		Factor 2 Nebuliser Flow Rate	
-0.5	+0.5	-0.5	+0.5
1125 W	1375 W	0.75 Lmin^{-1}	1.05 Lmin^{-1}

The centre conditions, *Point (0,0) i.e. RF power 1250W and nebuliser flow rate 0.9Lmin^{-1}* were replicated three times.

A graphical representation of the experimental points is shown in Figure 3.1.

FIGURE 3.1: GRAPHICAL REPRESENTATION OF THE EXPERIMENTAL DESIGN.
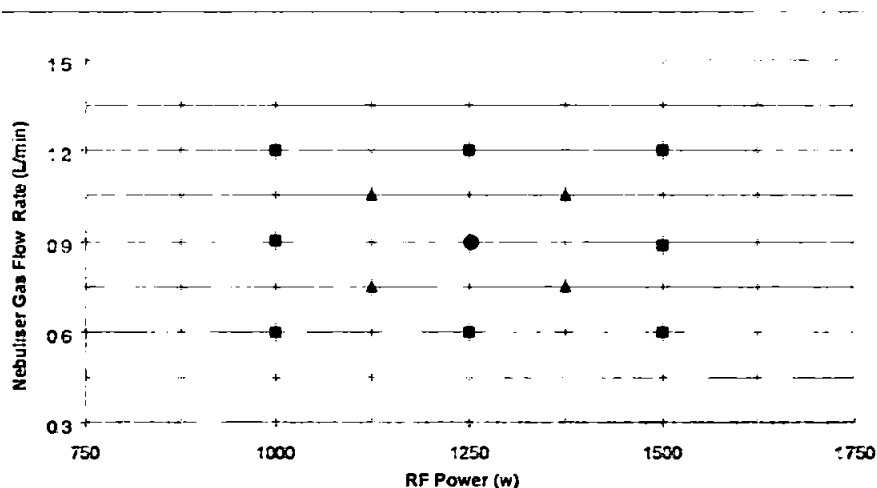
In total, 15 experiments were planned, and for each experiment point, a drift diagnosis was produced, i.e. the intensity of the selected emission lines was repeatedly measured 99 times (approx. 8h). An overview of the final experimental protocol is presented in Table 3.6.

TABLE 3.6: EXPERIMENT PLAN

Experiment	RF Power (W)	Nebuliser Flow Rate (Lmin^{-1})	Room Temperature (°C)	Magnesium Ratio (Mg^{II} / Mg^{I})
Central Conditions (A)	1250	0.90	26-27	10.5
Experiment 1	1125	1.05	27.5-28.5	8.9
Experiment 2	1125	0.75	28	8.4
Experiment 3	1375	1.05	29.5-29	10.9
Experiment 4	1375	0.75	28.5-29.5	11.1
Central Conditions (B)	1250	0.90	28.5-27	10.5
Experiment 5	1000	0.90	26	6.7
Experiment 6	1250	1.2	26-26.5	8.6
Experiment 7	1250	0.6	26-25	10.1
Experiment 8	1500	0.9	25-25.5	12.5
Central Conditions (C)	1250	0.90	24.5-24	10.5
Experiment 9	1000	1.2	23-26	5.8
Experiment 10	*1000*	*0.6*	*Unstable Conditions*	
Experiment 11	1500	1.2	25-26.5	10.3
Experiment 12	1500	0.6	26-28	11.6

3.2.4 N-WAY DATA HANDING

The data obtained on the twelve experiments was arranged on a cubic array as shows Figure 3.2.

FIGURE 3.2: 3-WAY ARRANGEMENT OF THE DATA SETS.
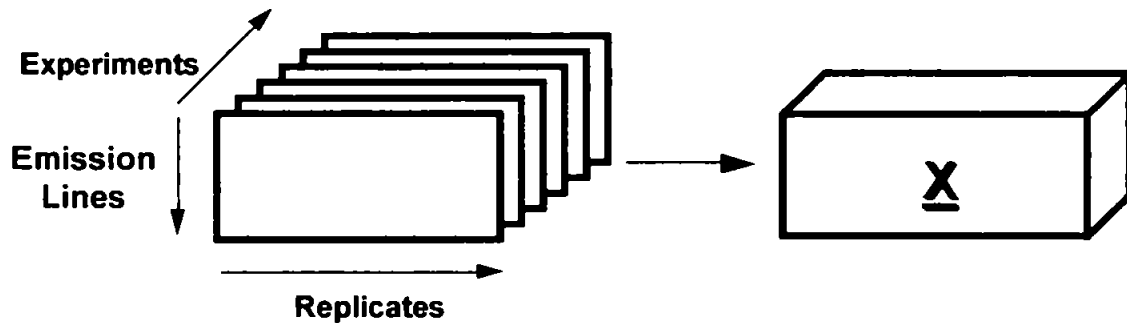
Matlab software (Mathworks, Inc., Version 5.1, Natick, MA) and the N-Way Toolbox for Matlab[191] were employed to perform the 3-way analysis. Before running a PARAFAC analysis, data was scaled to unit squared variation. Scaling in multi-way analysis has to be done taking the trilinear model into account. If variable i of the first mode is to be scaled (compared to the rest of the variables in the first mode), it is necessary to scale all rows where variable i occurs by the same scalar. This means that whole matrices are scaled. Mathematically scaling within the first mode can be described as:

$$x_{ijk}^{scal} = \frac{x_{ijk}}{s_i}$$

EQUATION 3.3.1

Where S_i will scale to unit squared variation:

$$s_i = \sqrt{\left(\sum_{j=1}^{J}\sum_{k=1}^{K} x_{ijk}^2\right)}$$

EQUATION 3.3.2

The core consistency[192] and the explained variance were the two parameters employed to optimise the number of component to use in the PARAFAC model. The core consistence diagnosis is a percentage below or equal to 100%. A value of 80-100% means that the model is valid, while a value below 40% means that the model is not valid. A core consistency between 40 and 80% means that the model is probably valid but somehow difficult to estimate, e.g., due to slight miss-specification or high correlation. The core

consistency may decrease with number of components but very sharply where the correct number of components is exceeded. Hence, the appropriate number of components is the model with the highest number of components, highest explained variation and a valid core consistency. Four PARAFAC models were calculated using one, two, three and four components. The explained variance increased continuously with the number of components, see Figure 3.3A. The core consistency fell to values around 10%, when more than two components were calculated, Figure 3.3B. Therefore, a two components PARAFAC model was employed in this analysis.

FIGURE 3.3: OPTIMISATION OF THE NUMBER OF PARAFAC COMPONENTS.

A) Explained Variation
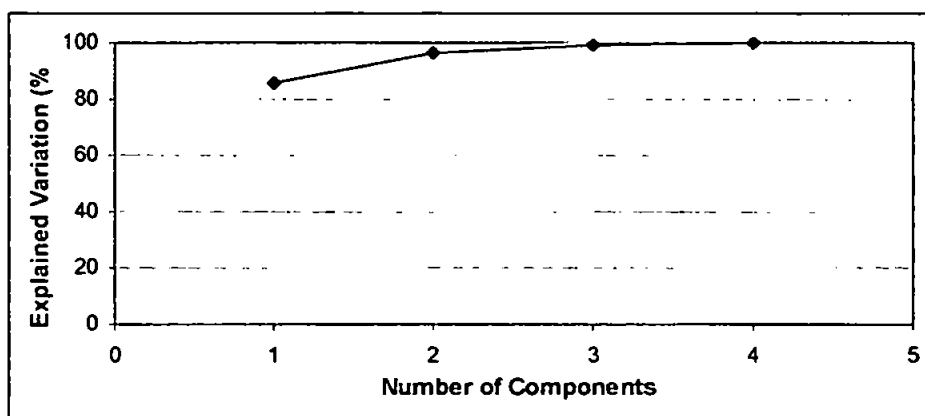
B) Core consistencies of the different models.
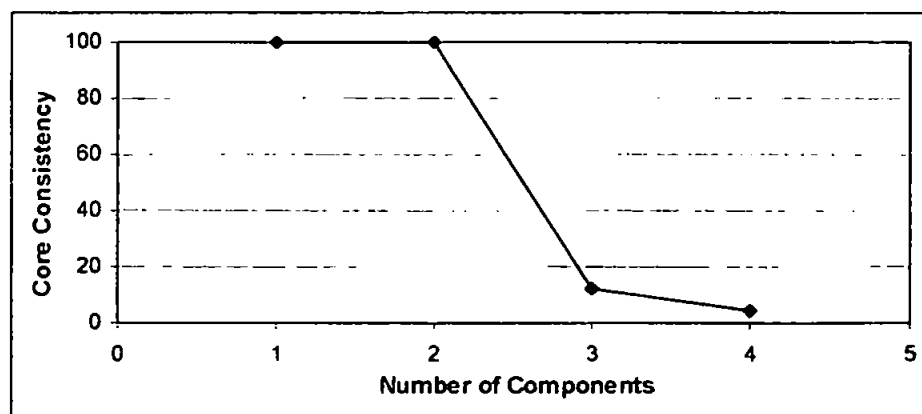
To perform a PARAFAC analysis in Matlab, the following commands are used:

» [Factors]=parafac(X,DimX,Fac);

    Where

    X   the input array. If the dimensions of the array is I x J x K , and X is input as an I x JK. In our case X (29 x 1188)

    DimX   A vector of the dimensions of the different orders. DimX was [29 99 12].

    Fac   No of factors/components sought.

The command *fac2let* converts the PARAFAC results in the three loading matrices:

»[A,B,C]=fac2let(Factors,DimX,Fac);

Finally, the core consistence of the model is calculated using the *corcond* function:

» cf = corcond(X,DimX,f,Factorsf);

3.3 RESULTS AND DISCUSSIONS

3.3.1 CLASSICAL DATA ANALYSIS

One data set was obtained for each drift diagnosis with the exception of where the experimental conditions were such that the plasma could not be sustained, i.e. RF power 1000W and nebuliser gas flow rate 0.6Lmin^{-1}.

As expected, the intensity levels of every line changed from one set of experimental conditions to another, and so the sensitivity. Table 3.7 shows the limits of detection for every line at the different operating condition selected for this study. A number of important variations may be observed. For example, the data in Table 3.7 reflects a degradation in the sensitivity when robust conditions are employed, and more precisely when low nebuliser flows are set. One of the questions to be answered from this work is therefore whether this lost of sensitivity is worthy for a more robust instrument.

In order to check the stability of the instrument from one day to another, an intensity check using the central conditions (RF: 1250W; nebuliser gas flow: 0.9 Lmin^{-1}) was performed prior to each experiment. Table 3.8 compiles the results obtained on the intensity checks. Very similar intensity values were obtained over the whole period of experimental work (rsd≤6%). The reproducibility of the experimental protocol was also checked at the above conditions, by replicating the procedure three times. The three data sets obtained are comparable, particularly in terms of their characteristic drift patterns and the magnitude of the drift, as shown in Figure 3.4.

FIGURE 3.4: DRIFT PATTERNS AT CENTRAL CONDITIONS, THREE REPLICATES.

RF POWER = 1250 W AND NEBULISER GAS FLOW RATE = 0.9 L/MIN
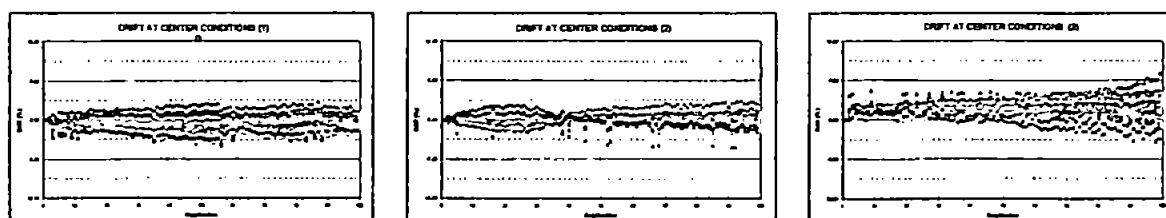
TABLE 3.7: LIMIT OF DETECTION OF STUDIED LINES AT DIFFERENT OPERATING CONDITIONS, (μg L^{-1}).

Experiment No.	CC	Ex 1	Ex 2	Ex 3	Ex 4	Ex 5	Ex 6	Ex 7	Ex 8	Ex 9	Ex 11	Ex 12
RF (W)	1250	1125	1125	1375	1375	1000	1250	1250	1500	1000	1500	1500
Nebuliser Gas Flow (Lmin^{-1})	0.9	1.05	0.75	1.05	0.75	0.9	1.2	0.6	0.9	1.2	1.2	0.6
Al - 396.152 - (I)	57	11	43	19	48	14	19	170	59	3	15	140
Ba - 230.424 - (II)	4	3	8	3	7	3	3	22	2	5	2	20
Ba - 233.527 - (II)	3	1	4	2	4	3	2	13	2	3	2	23
Ca - 317.933 - (II)	6	4	6	3	6	5	4	35	5	3	2	60
Ca - 422.673 - (I)	17	3	15	4	9	7	5	35	8	1	3	120
Cd - 226.502 - (II)	3	2	3	2	3	3	2	10	2	4	2	14
Cd - 228.802 - (I)	6	5	8	4	9	5	5	20	6	7	4	31
Co - 228.616 - (II)	11	9	25	7	15	15	7	52	8	6	4	69
Co - 340.512 - (I)	75	23	63	24	110	29	21	190	33	12	21	840
Cr - 267.716 - (II)	6	2	6	2	2	4	3	9	2	4	2	33
Cr - 357.869 - (I)	15	4	21	7	41	5	6	100	11	2	7	240
Cu - 224.700 - (II)	10	6	12	4	16	4	3	45	7	1	6	65
Cu - 324.754 - (I)	3	1	5	1	8	1	1	26	3	0.5	1	45
Fe - 259.940 - (II)	3	1	3	2	5	3	2	13	1	1	1	19
Mg - 279.079 - (II)	30	11	25	9	21	14	14	82	18	8	13	260
Mg - 280.270 - (II)	1	0.2	0.5	1	1	4	0.5	2	1	0.2	1	1
Mg - 285.213 - (I)	1	1	2	1	2	5	1	6	1	0.5	1	13
Mg 279.553 - (II)	1	0.3	0.4	0.5	1	4	0.5	1	0.5	0.2	1	2
Mn - 257.610 - (II)	1	0.3	1	0.3	1	0	0.3	3	1	0.3	0.3	3
Mn - 403.076 - (I)	120	14	56	44	55	19	23	430	130	4	20	520
Na - 589.592 - (I)	40	7	31	8	30	15	14	110	32	3	11	360
Ni - 231.604 - (II)	6	3	11	2	13	8	6	32	5	6	7	64
Ni - 232.003 - (I)	16	11	34	13	26	11	9	69	12	9	11	77
Pb - 216.999 - (I)	160	72	250	87	220	81	77	520	110	41	46	690
Pb - 220.353 - (II)	36	32	55	25	52	45	37	88	34	20	36	230
Ti - 337.280 - (II)	3	1	4	1	5	1	1	5	2	1	1	17
Zn - 202.548 - (II)	4	3	5	2	3	6	4	12	2	8	2	16
Zn - 213.856 - (I)	2	1	3	2	3	2	1	6	1	2	1	6

TABLE 3.8: INTENSITY CHECK AT CENTRE CONDITIONS BEFORE EACH EXPERIMENT.

	CC1	EX1	EX2	EX3	EX4	CC2	EX5	EX6	EX7	EX8	CC3	EX9	EX11	EX12	RSD%
Al (I)	14124	14791	14136	14299	14073	14124	14209	14263	14413	14443	14492	14847	14176	14853	1.9
Ba 232	4555	4768	4517	4839	4548	4512	4663	4620	4578	4810	5032	5332	4574	4861	4.9
Ba 230	4637	4885	4634	4982	4699	4691	4878	4838	4804	5092	5361	5683	4897	5270	6.1
Ca (I)	129192	135818	130596	130049	126792	130738	128657	130296	135243	130287	127041	128853	131431	134181	2.1
Ca (II)	20497	21591	20406	21706	20518	20341	21081	20943	20837	21786	22665	24171	21389	22879	5.1
Cd (I)	1879	1967	1867	1976	1888	1888	1966	1951	1935	2045	2146	2266	1966	2095	5.7
Cd (II)	9785	10400	9895	10424	10020	9996	10102	10120	10171	10476	10780	11329	10073	10847	4.1
Co (I)	2940	3079	2949	3047	2938	2943	3003	2975	2942	3051	3127	3230	2910	3197	3.4
Co (II)	1405	1487	1415	1495	1430	1431	1461	1453	1450	1507	1562	1642	1446	1568	4.5
Cr (I)	24419	25799	24769	24216	24534	24763	24034	24342	25192	24132	23596	23596	24211	24949	2.5
Cr (II)	13686	14399	13587	14325	13620	13547	13892	13744	13673	14145	14631	15311	13638	14559	3.7
Cu (I)	100119	106535	100387	101441	99657	100304	97298	98698	101177	98097	97364	98016	96178	101700	2.6
Cu (II)	4234	4462	4255	4313	4262	4299	4291	4304	4381	4390	4430	4553	4288	4495	2.3
Fe (I)	60688	64059	60303	63431	60255	59752	60445	60195	60270	61528	63338	66024	59165	62855	3.3
Fe (II)	21968	23385	21973	22877	21955	21789	21955	21919	22111	22356	22820	23779	21642	22873	2.9
Mg (I)	89271	93181	88742	90503	88443	88861	88133	88838	89956	89432	90059	91789	87556	92162	1.8
Mg (II)	3938	4098	3948	3984	3875	3971	3963	3966	4030	4002	4005	4074	3946	4125	1.7
Mn (I)	13995	14769	14164	13844	14237	14416	13806	14035	14576	13935	13567	13566	14051	14483	2.6
Mn (II)	60496	63858	60112	63239	60061	59557	60248	59987	60044	61312	63127	65801	58932	62652	3.3
Na (I)	68328	72893	70215	69098	70149	70877	67503	70107	75788	69253	65888	65799	72782	72705	4.0
Ni (I)	1582	1677	1588	1647	1595	1592	1619	1619	1615	1661	1699	1773	1600	1714	3.5
Ni (II)	3132	3319	3117	3262	3136	3161	3199	3150	3159	3236	3341	3474	3121	3347	3.4
Pb (II)	368	390	370	386	374	376	379	377	380	390	402	419	376	403	3.7
Ti (II)	199214	210003	200513	205867	200638	201121	203677	203842	205874	208050	210071	217484	203142	216410	2.8
Zn (I)	8152	8862	8085	8455	8186	8163	8373	8346	8203	8654	8963	9429	8024	8805	4.8
Zn (II)	2151	2332	2151	2306	2176	2168	2234	2206	2176	2305	2439	2589	2192	2400	5.7
Ar 357	1948	1891	1894	1892	1902	1895	2008	2007	1917	2051	2126	2192	2053	1992	4.8
Ar 404	10852	10996	10704	10811	10720	10697	11128	11106	10917	11387	11657	11990	11222	11366	3.5
Ar 420	374176	365164	364818	380662	365776	362524	388340	384227	365733	393925	409164	423350	393445	382989	5.0
Ar 451	28701	27971	28035	27868	28172	27941	29617	29713	28688	30316	31325	32289	30746	29519	4.8

On the following pages, the drift plots obtained at different experimental conditions and their corresponding correlation matrices are presented and discussed.

At the centre conditions, the instrument showed very stable signals with time, Figure 3.5. Absolute drift values were below 3% over the whole experiment for all atomic or ionic, analyte or argon emission lines. Under such conditions, a drift correction would not be necessary.

FIGURE 3.5: DRIFT PLOT AT CENTRE CONDITIONS (A)
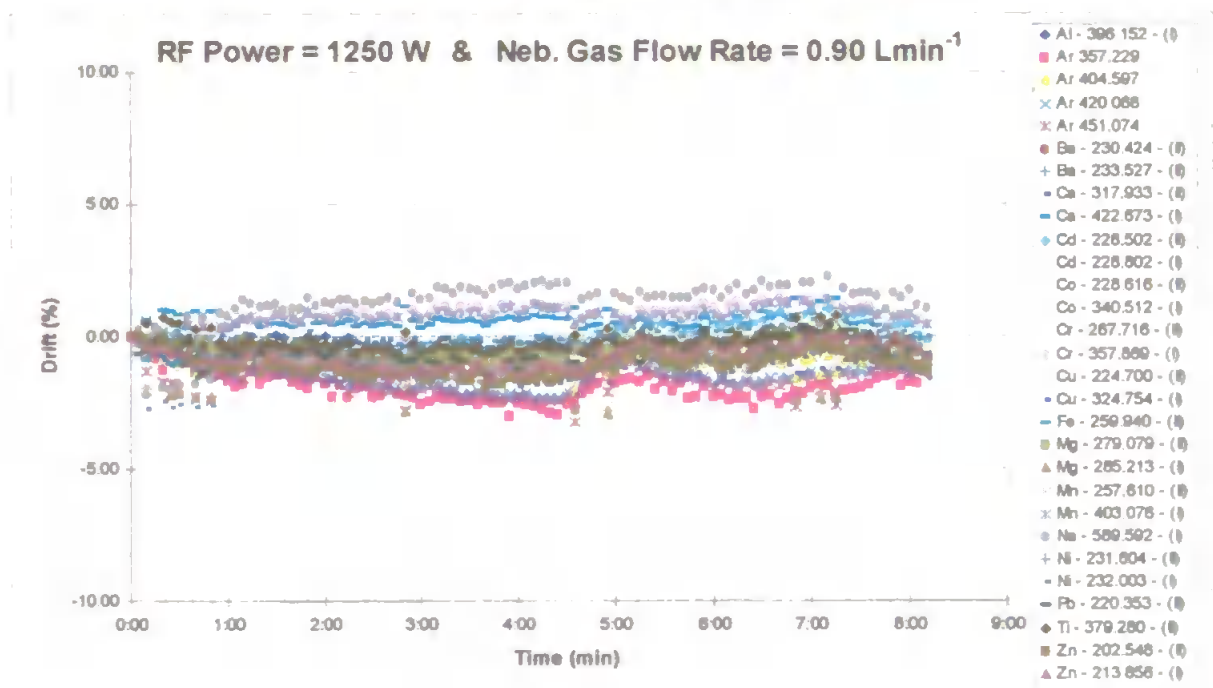
In terms of correlation, differences between the lines can be noticed. Table 3.9 shows the correlation matrix of the first data set obtained at centre conditions. It can be observed that some atomic lines present moderate correlation (Cr^I, Cu^I, Mn^I, Na^I), meanwhile others, i.e. Al^I, Cd^I, Co^I, Zn^I, have better correlation with several ionic lines (Ba^{II}, Ca^{II}, Co^{II}, Cr^{II}, Mg^{II}, Zn^{II}). The energetic characteristics of the emissions may explain these groupings. Argon lines show poor correlation with most of the analyte emissions.

RF Power 1250 W   &   Nebuliser Gas Flow Rate 0.9 Lmin^{-1}

	Al (I)	Ba^{230}	Ba^{232}	Ca (II)	Ca (I)	Cd (II)	Cd (I)	Co (II)	Co (I)	Cr (II)	Cr (I)	Cu (II)	Cu (I)	Fe (II)	Mg (II)	Mg (I)	Mn (II)	Mn (I)	Na (I)	Ni (II)	Ni (I)	Pb (II)	Tl (II)	Zn (II)	Zn (I)	Ar^{357}	Ar^{404}	Ar^{420}	Ar^{451}
Al (I)	1.00																												
Ba (230)	0.70	1.00																											
Ba (232)	0.88	0.97	1.00																										
Ca (II)	0.61	0.84	0.83	1.00																									
Ca (I)	0.47	0.07	0.06	-0.23	1.00																								
Cd (II)	0.59	0.48	0.53	0.35	0.15	1.00																							
Cd (I)	0.69	0.92	0.93	0.76	0.09	0.59	1.00																						
Co (II)	0.69	0.82	0.85	0.67	0.13	0.74	0.86	1.00																					
Co (I)	0.77	0.84	0.86	0.70	0.24	0.65	0.86	0.84	1.00																				
Cr (II)	0.69	0.88	0.88	0.95	-0.08	0.42	0.81	0.73	0.79	1.00																			
Cr (I)	0.17	-0.32	-0.32	-0.13	0.01	0.46	-0.21	0.02	-0.07	-0.16	1.00																		
Cu (II)	0.65	0.60	0.63	0.42	0.20	0.92	0.72	0.80	0.76	0.52	0.33	1.00																	
Cu (I)	-0.01	-0.20	-0.22	0.23	-0.54	0.12	-0.20	-0.10	-0.17	0.09	0.72	0.02	1.00																
Fe (II)	0.56	0.48	0.49	0.68	-0.25	0.73	0.51	0.60	0.56	0.64	0.58	0.67	0.63	1.00															
Mg (II)	0.74	0.79	0.81	0.71	0.28	0.45	0.75	0.72	0.81	0.80	-0.10	0.60	-0.10	0.47	1.00														
Mg (I)	0.12	0.04	0.01	0.48	-0.57	0.10	-0.01	0.03	0.00	0.34	0.54	0.05	0.95	0.69	0.10	1.00													
Mn (II)	0.28	0.28	0.27	0.66	-0.57	0.36	0.26	0.30	0.25	0.54	0.51	0.30	0.87	0.86	0.26	0.94	1.00												
Mn (I)	0.28	-0.25	-0.26	-0.12	0.12	0.48	-0.14	0.05	-0.01	-0.14	0.96	0.38	0.64	0.54	-0.03	0.48	0.45	1.00											
Na (I)	-0.05	-0.38	-0.38	-0.08	-0.34	0.30	-0.29	-0.11	-0.23	-0.18	0.91	0.17	0.89	0.57	-0.24	0.73	0.67	0.85	1.00										
Ni (II)	0.59	0.82	0.79	0.80	0.09	0.09	0.69	0.57	0.63	0.83	-0.43	0.24	-0.15	0.26	0.76	0.12	0.23	-0.39	-0.46	1.00									
Ni (I)	0.56	0.51	0.57	0.35	0.19	0.90	0.63	0.76	0.70	0.41	0.35	0.89	-0.02	0.63	0.47	-0.02	0.25	0.35	0.17	0.12	1.00								
Pb (II)	0.48	0.47	0.45	0.38	0.17	0.51	0.54	0.50	0.53	0.42	0.13	0.53	-0.03	0.41	0.45	0.04	0.19	0.13	0.00	0.32	0.51	1.00							
Tl (II)	0.71	0.70	0.70	0.39	0.70	0.37	0.67	0.61	0.73	0.55	-0.37	0.48	-0.64	0.06	0.69	-0.49	-0.30	-0.26	-0.64	0.62	0.43	0.40	1.00						
Zn (II)	0.69	0.92	0.94	0.81	0.09	0.51	0.86	0.82	0.84	0.88	-0.27	0.62	-0.19	0.49	0.80	0.03	0.28	-0.24	-0.35	0.78	0.55	0.49	0.71	1.00					
Zn (I)	0.71	0.84	0.87	0.77	0.01	0.77	0.89	0.87	0.85	0.82	0.05	0.83	0.03	0.73	0.74	0.19	0.46	0.10	-0.02	0.57	0.73	0.56	0.55	0.84	1.00				
Ar (357)	0.19	0.68	0.67	0.69	-0.27	-0.13	0.56	0.35	0.38	0.67	-0.70	-0.02	-0.24	0.06	0.38	0.02	0.14	-0.69	-0.57	0.71	-0.06	0.11	0.35	0.62	0.41	1.00			
Ar (404)	0.40	0.72	0.71	0.92	-0.48	0.23	0.64	0.52	0.53	0.83	-0.15	0.31	0.32	0.63	0.55	0.55	0.70	-0.16	0.00	0.67	0.21	0.29	0.15	0.68	0.67	0.70	1.00		
Ar (420)	0.34	0.78	0.79	0.54	0.11	0.07	0.71	0.52	0.59	0.60	-0.79	0.22	-0.65	-0.07	0.53	-0.42	-0.22	-0.73	-0.82	0.70	0.19	0.23	0.71	0.73	0.50	0.82	0.48	1.00	
Ar (451)	0.19	0.62	0.62	0.83	-0.67	0.15	0.55	0.42	0.38	0.72	-0.19	0.20	0.36	0.56	0.36	0.57	0.71	-0.22	0.05	0.54	0.14	0.17	-0.05	0.56	0.57	0.72	0.93	0.43	1.00

At RF power 1125 W and nebuliser gas flow rate 1.05 Lmin⁻¹, a very unusual drift plot was obtained (Figure 3.6). However at similar but more drastic conditions, the same type of plot was found. During the first hour of analysis, a marked degradation of many emission intensities was noticed. The emission signals then recovered to near to the original values. This "down and up" effect on the emission intensities might be interpret as an initial cooling effect, maybe due to the moderately high nebuliser flow employed. Finally, during the last two hours of analysis, the instrument became more unstable and drift values increased.

FIGURE 3.6: DRIFT PLOT AT EXPERIMENT 1 CONDITIONS
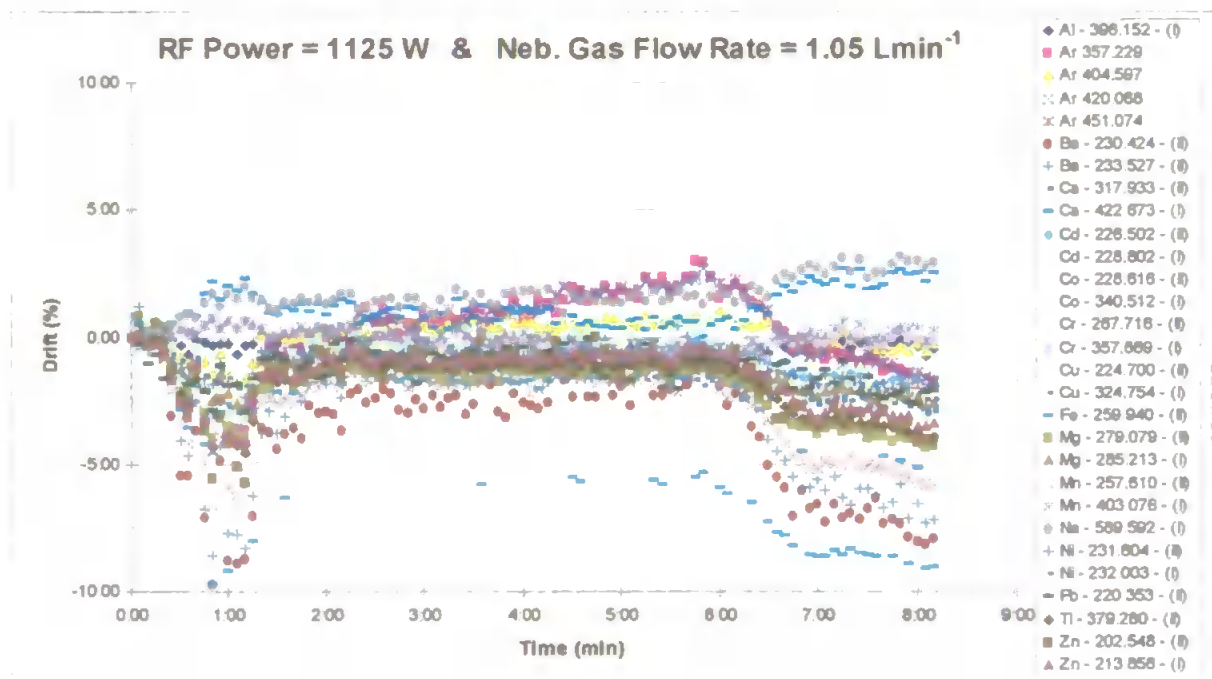
The correlation matrix for this data set (Table 3.10) shows high levels of correlation between the ionic lines and some of the hardest atomic lines (Cd^I, Mg^I, Ni^I, Zn^I), and also with the argon lines. The remaining atomic lines gave low levels of correlation.

Ionic lines, more affected by drift at these conditions, showed higher correlation. This can be due to their drift behaviour is induced by the instrumental conditions employed.

TABLE 3.10: CORRELATION MATRIX OF DATA SET OBTAINED AT EXPERIMENT 1 CONDITIONS

RF Power 1125 W & Nebuliser Gas Flow Rate 1.05 Lmin^{-1}

	Al (l)	Ba 230	Ba 232	Ca (II)	Ca (l)	Cd (II)	Cd (l)	Co (II)	Co (l)	Cr (II)	Cr (l)	Cu (II)	Cu (l)	Fe (II)	Mg (II)	Mg (l)	Mn (II)	Mn (l)	Na (l)	Ni (II)	Ni (l)	Pb (II)	Tl (II)	Zn (II)	Zn (l)	Ar 357	Ar 404	Ar 420	Ar 451
Al (l)	1.00																												
Ba (230)	0.16	1.00																											
Ba (232)	0.14	0.98	1.00																										
Ca (II)	0.24	0.97	0.96	1.00																									
Ca (l)	0.08	-0.89	-0.88	-0.83	1.00																								
Cd (II)	0.17	0.95	0.94	0.97	-0.80	1.00																							
Cd (l)	0.26	0.94	0.94	0.95	-0.84	0.93	1.00																						
Co (II)	0.39	0.81	0.79	0.84	-0.65	0.81	0.81	1.00																					
Co (l)	0.29	-0.82	-0.85	-0.76	0.78	-0.80	-0.74	-0.53	1.00																				
Cr (II)	0.26	0.98	0.97	0.98	-0.88	0.95	0.96	0.83	-0.77	1.00																			
Cr (l)	0.69	-0.44	-0.47	-0.41	0.50	-0.51	-0.38	-0.17	0.78	-0.36	1.00																		
Cu (II)	0.35	0.95	0.93	0.93	-0.88	0.87	0.93	0.83	-0.66	0.97	-0.20	1.00																	
Cu (l)	0.68	0.67	0.64	0.66	-0.62	0.54	0.69	0.69	-0.21	0.73	0.32	0.85	1.00																
Fe (II)	0.31	0.78	0.77	0.77	-0.74	0.69	0.78	0.68	-0.49	0.81	-0.11	0.84	0.76	1.00															
Mg (II)	0.31	0.95	0.94	0.94	-0.89	0.89	0.93	0.83	-0.68	0.97	-0.23	0.99	0.83	0.83	1.00														
Mg (l)	0.49	0.91	0.90	0.93	-0.79	0.87	0.92	0.86	-0.57	0.95	-0.10	0.97	0.88	0.82	0.96	1.00													
Mn (II)	0.25	0.98	0.97	0.98	-0.90	0.94	0.96	0.84	-0.75	0.99	-0.37	0.97	0.74	0.81	0.97	0.96	1.00												
Mn (l)	0.63	-0.58	-0.59	-0.53	0.69	-0.59	-0.48	-0.26	0.82	-0.51	0.94	-0.38	0.11	-0.29	-0.41	-0.25	-0.51	1.00											
Na (l)	-0.19	-0.68	-0.65	-0.61	0.85	-0.50	-0.64	-0.54	0.37	-0.70	0.03	-0.80	-0.82	-0.72	-0.79	-0.74	-0.73	0.28	1.00										
Ni (II)	0.45	0.87	0.85	0.87	-0.79	0.83	0.86	0.80	-0.53	0.91	-0.11	0.94	0.85	0.79	0.93	0.95	0.92	-0.27	-0.76	1.00									
Ni (l)	0.42	0.90	0.88	0.92	-0.78	0.87	0.91	0.83	-0.61	0.94	-0.18	0.93	0.79	0.79	0.93	0.94	0.94	-0.33	-0.68	0.88	1.00								
Pb (II)	0.17	0.71	0.68	0.75	-0.62	0.74	0.71	0.73	-0.49	0.73	-0.31	0.71	0.49	0.57	0.70	0.71	0.74	-0.40	-0.47	0.67	0.69	1.00							
Tl (II)	0.26	0.98	0.97	0.98	-0.89	0.95	0.96	0.84	-0.76	1.00	-0.37	0.97	0.73	0.80	0.97	0.96	1.00	-0.51	-0.71	0.92	0.93	0.73	1.00						
Zn (II)	0.25	0.94	0.93	0.94	-0.83	0.92	0.92	0.80	-0.74	0.95	-0.39	0.91	0.67	0.75	0.92	0.91	0.95	-0.52	-0.64	0.86	0.90	0.69	0.95	1.00					
Zn (l)	0.19	0.98	0.97	0.98	-0.86	0.97	0.95	0.82	-0.81	0.98	-0.46	0.93	0.64	0.75	0.94	0.91	0.98	-0.58	-0.62	0.87	0.91	0.74	0.98	0.95	1.00				
Ar (357)	-0.19	0.78	0.80	0.79	-0.64	0.86	0.74	0.58	-0.91	0.75	-0.78	0.60	0.12	0.41	0.62	0.57	0.73	-0.77	-0.19	0.51	0.61	0.58	0.74	0.74	0.82	1.00			
Ar (404)	0.05	0.81	0.83	0.66	-0.62	0.90	0.80	0.69	-0.79	0.60	-0.61	0.68	0.29	0.52	0.70	0.69	0.79	-0.61	-0.24	0.64	0.71	0.64	0.81	0.80	0.86	0.90	1.00		
Ar (420)	-0.19	0.82	0.84	0.83	-0.69	0.89	0.77	0.61	-0.91	0.78	-0.80	0.64	0.16	0.47	0.66	0.60	0.77	-0.80	-0.24	0.56	0.65	0.63	0.78	0.78	0.85	0.98	0.92	1.00	
Ar (451)	-0.21	0.80	0.82	0.81	-0.68	0.88	0.76	0.59	-0.91	0.76	-0.81	0.62	0.13	0.45	0.64	0.58	0.75	-0.80	-0.21	0.53	0.63	0.61	0.76	0.76	0.83	0.98	0.92	1.00	1.00

The drift diagnosis performed at 1125 W of power and with a nebuliser gas flow rate of 0.75Lmin^{-1}, gave reasonably stable signals over time, see Figure 3.7. The emission intensities fluctuated, but the overall drift values were below 3%.

FIGURE 3.7: DRIFT PLOT AT EXPERIMENT 2 CONDITIONS

In terms of correlation (Table 3.11), a similar situation than under Experiment 1 conditions (Table 3.10) was found i.e. a high correlation between ionic and some hard atomic lines (Cd^I, Co^I, Ni^I, Zn^I), and the argon lines. However, lack of correlation between the other atomic lines is observed. Probably, the low power employed on these two experiments (1125 W) is inducing the long-term behaviour of the hardest lines, and thus, they showed high correlation. Meanwhile the softest lines, less affected by the drift phenomena under such conditions, fluctuated more freely.

TABLE 3.11: CORRELATION MATRIX OF DATA SET OBTAINED AT EXPERIMENT 2 CONDITIONS

RF Power 1125 W & Nebuliser Gas Flow Rate 0.75 Lmin^{-1}

	Al (I)	Ba^{230}	Ba^{232}	Ca (II)	Ca (I)	Cd (II)	Cd (I)	Co (II)	Co (I)	Cr (II)	Cr (I)	Cu (II)	Cu (I)	Fo (II)	Mg (II)	Mg (I)	Mn (II)	Mn (I)	Na (I)	Ni (II)	Ni (I)	Pb (II)	Tl (II)	Zn (II)	Zn (I)	Ar^{357}	Ar^{404}	Ar^{420}	Ar^{451}
Al (I)	1.00																												
Ba (230)	0.33	1.00																											
Ba (232)	0.38	0.99	1.00																										
Ca (II)	0.45	0.96	0.97	1.00																									
Ca (I)	0.64	-0.48	-0.43	-0.37	1.00																								
Cd (II)	0.45	0.96	0.97	0.99	-0.36	1.00																							
Cd (I)	0.29	0.98	0.98	0.95	-0.51	0.95	1.00																						
Co (II)	0.40	0.98	0.98	0.97	-0.40	0.97	0.96	1.00																					
Co (I)	0.59	0.82	0.83	0.83	-0.07	0.83	0.82	0.84	1.00																				
Cr (II)	0.57	0.93	0.95	0.98	-0.24	0.98	0.91	0.95	0.86	1.00																			
Cr (I)	0.60	-0.50	-0.45	-0.37	0.97	-0.37	-0.53	-0.42	-0.09	-0.24	1.00																		
Cu (II)	0.82	0.64	0.68	0.69	0.29	0.68	0.62	0.68	0.83	0.76	0.25	1.00																	
Cu (I)	0.69	0.00	0.04	0.15	0.63	0.13	-0.04	0.07	0.31	0.26	0.75	0.50	1.00																
Fo (II)	0.66	0.87	0.89	0.94	-0.09	0.94	0.85	0.90	0.87	0.97	-0.08	0.82	0.43	1.00															
Mg (II)	0.91	0.30	0.35	0.39	0.64	0.38	0.28	0.37	0.62	0.50	0.60	0.85	0.68	0.60	1.00														
Mg (I)	0.79	0.51	0.55	0.64	0.30	0.62	0.48	0.56	0.70	0.72	0.39	0.78	0.84	0.83	0.76	1.00													
Mn (II)	0.54	0.89	0.90	0.96	-0.23	0.94	0.87	0.90	0.83	0.96	-0.19	0.73	0.40	0.98	0.49	0.82	1.00												
Mn (I)	0.50	-0.59	-0.55	-0.48	0.95	-0.47	-0.63	-0.52	-0.20	-0.35	0.98	0.13	0.70	-0.19	0.50	0.28	-0.29	1.00											
Na (I)	0.74	-0.18	-0.13	-0.03	0.84	-0.04	-0.23	-0.09	0.14	0.10	0.89	0.47	0.91	0.26	0.72	0.67	0.18	0.86	1.00										
Ni (II)	0.48	0.97	0.98	0.97	-0.32	0.97	0.95	0.98	0.86	0.97	-0.34	0.73	0.15	0.93	0.44	0.63	0.93	-0.44	0.00	1.00									
Ni (I)	0.51	0.92	0.93	0.92	-0.25	0.91	0.91	0.93	0.88	0.92	-0.27	0.79	0.18	0.90	0.50	0.64	0.89	-0.38	0.01	0.93	1.00								
Pb (II)	0.32	0.91	0.92	0.89	-0.42	0.89	0.93	0.90	0.78	0.86	-0.46	0.63	0.00	0.81	0.31	0.48	0.83	-0.54	-0.17	0.88	0.87	1.00							
Tl (II)	0.89	0.67	0.71	0.76	0.28	0.77	0.63	0.72	0.76	0.84	0.23	0.88	0.46	0.87	0.79	0.76	0.77	0.11	0.47	0.78	0.76	0.62	1.00						
Zn (II)	0.24	0.99	0.98	0.95	-0.56	0.95	0.98	0.97	0.77	0.91	-0.58	0.56	-0.07	0.83	0.20	0.44	0.86	-0.66	-0.25	0.95	0.88	0.90	0.61	1.00					
Zn (I)	0.47	0.96	0.97	0.99	-0.36	0.99	0.95	0.97	0.83	0.98	-0.37	0.69	0.14	0.94	0.40	0.63	0.94	-0.47	-0.03	0.97	0.92	0.89	0.77	0.95	1.00				
Ar (357)	0.14	0.94	0.92	0.90	-0.64	0.88	0.95	0.90	0.67	0.84	-0.65	0.45	-0.19	0.74	0.10	0.34	0.78	-0.74	-0.38	0.87	0.82	0.87	0.50	0.95	0.89	1.00			
Ar (404)	0.33	0.96	0.96	0.98	-0.49	0.96	0.96	0.95	0.77	0.94	-0.49	0.60	0.02	0.88	0.28	0.54	0.91	-0.60	-0.16	0.94	0.89	0.89	0.66	0.96	0.97	0.94	1.00		
Ar (420)	0.21	0.94	0.93	0.93	-0.59	0.92	0.95	0.92	0.69	0.88	-0.63	0.50	-0.20	0.77	0.15	0.35	0.80	-0.72	-0.34	0.90	0.84	0.88	0.58	0.95	0.93	0.97	0.97	1.00	
Ar (451)	0.26	0.95	0.95	0.96	-0.56	0.94	0.95	0.94	0.72	0.92	-0.55	0.54	-0.04	0.84	0.21	0.49	0.88	-0.65	-0.22	0.93	0.88	0.88	0.61	0.96	0.95	0.96	0.99	0.98	1.00

A higher RF power, 1375 W, in conjunction with a moderately high nebuliser gas flow, produced very unstable conditions for long-term analysis, see Figure 3.8. As found with the Experiment 1 conditions, Figure 3.6, an initial degradation of the emission signals during the first couple of hours of analysis is followed by a partial recovery to need the original values. This phenomenon may be related to the nebuliser flow of 1.05 Lmin^{-1}. With such high flow rates, the residence time of excited species in the plasma is considerably reduced, and therefore so is the energy transfer from the plasma to the sample. Another important observation under these instrumental conditions is the different behaviour followed by some atomic lines, i.e. Al^I, Ca^I, Co^I, Cr^I, Mn^I and Na^I (top of Figure 3.8).

FIGURE 3.8: DRIFT PLOT AT EXPERIMENT 3 CONDITIONS
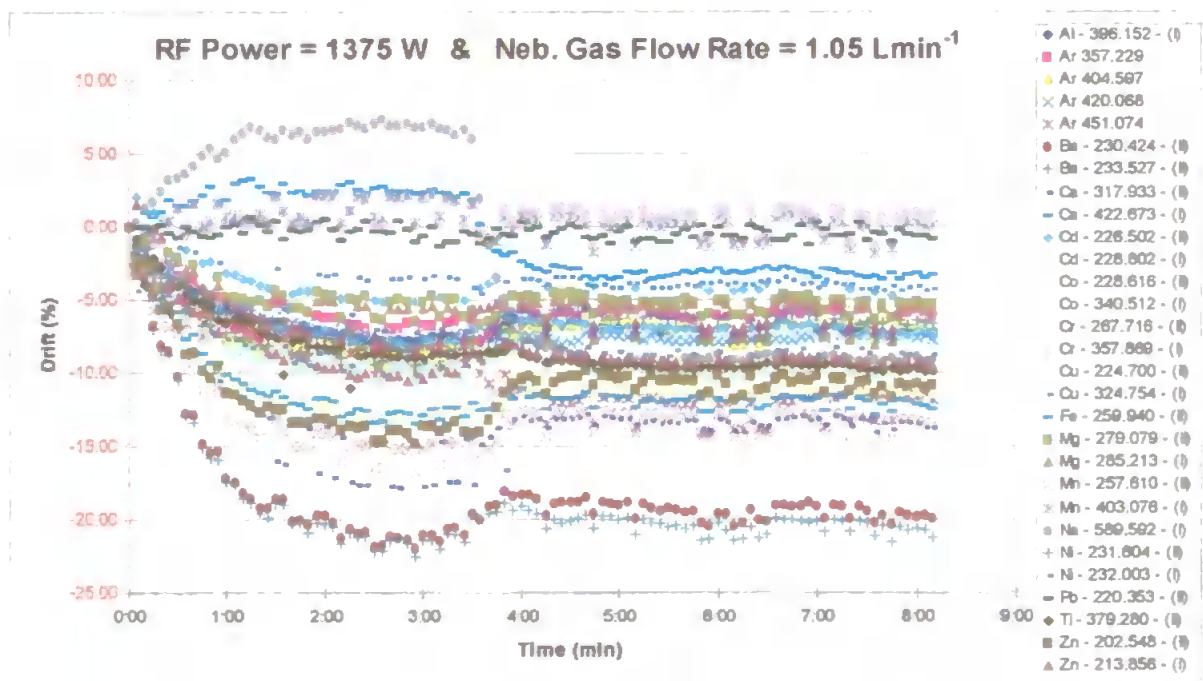
The correlation matrix for Experiment 3, Table 3.12, reflects numerically the trend observed in Figure 3.8. A high correlation was found between most of the lines, including the argon lines, r~0.8. Exceptions are for Ca^I, Cr^I, Cu^I, Mn^I, Pb^{II} and for Ar 451.074, which showed poorer values than the other argon lines.

TABLE 3.12: CORRELATION MATRIX OF DATA SET OBTAINED AT EXPERIMENT 3 CONDITIONS

RF Power 1375 W & Nebuliser Gas Flow Rate 1.05 Lmin^{-1}

	Al (I)	Ba230	Ba232	Ca (II)	Ca (I)	Cd (II)	Cd (I)	Co (II)	Co (I)	Cr (II)	Cr (I)	Cu (II)	Cu (I)	Fe (II)	Mg (II)	Mg (I)	Mn (II)	Mn (I)	Na (I)	Ni (II)	Ni (I)	Pb (II)	Tl (II)	Zn (II)	Zn (I)	Ar357	Ar404	Ar420	Ar451
Al (I)	1.00																												
Ba (230)	0.99	1.00																											
Ba (232)	0.98	1.00	1.00																										
Ca (II)	0.93	0.92	0.90	1.00																									
Ca (I)	0.15	0.12	0.20	-0.04	1.00																								
Cd (II)	0.74	0.71	0.72	0.75	0.23	1.00																							
Cd (I)	0.97	0.98	0.99	0.87	0.23	0.66	1.00																						
Co (II)	0.98	0.99	0.98	0.94	0.02	0.69	0.96	1.00																					
Co (I)	0.84	0.86	0.82	0.82	-0.23	0.35	0.82	0.89	1.00																				
Cr (II)	0.91	0.89	0.89	0.89	0.23	0.95	0.85	0.87	0.60	1.00																			
Cr (I)	-0.31	-0.30	-0.28	-0.48	0.19	-0.77	-0.20	-0.32	-0.05	-0.62	1.00																		
Cu (II)	0.93	0.95	0.93	0.87	-0.05	0.55	0.93	0.98	0.91	0.76	-0.18	1.00																	
Cu (I)	0.28	0.31	0.28	0.20	-0.32	-0.19	0.31	0.36	0.59	0.01	0.37	0.40	1.00																
Fe (II)	0.99	0.99	1.00	0.91	0.18	0.69	0.99	0.98	0.85	0.88	-0.25	0.94	0.32	1.00															
Mg (II)	0.89	0.89	0.89	0.75	0.20	0.38	0.91	0.88	0.89	0.64	0.13	0.89	0.51	0.91	1.00														
Mg (I)	0.68	0.69	0.67	0.56	-0.02	0.03	0.71	0.70	0.86	0.33	0.41	0.77	0.70	0.72	0.89	1.00													
Mn (II)	0.96	0.97	0.95	0.91	-0.05	0.57	0.94	0.98	0.95	0.79	-0.19	0.97	0.47	0.97	0.92	0.80	1.00												
Mn (I)	-0.17	-0.17	-0.13	-0.36	0.58	-0.53	-0.05	-0.23	-0.11	-0.39	0.91	-0.14	0.17	-0.10	0.21	0.36	-0.15	1.00											
Na (I)	0.13	0.11	0.19	-0.07	1.00	0.21	0.22	0.00	-0.26	0.21	0.20	-0.08	-0.32	0.16	0.18	-0.03	-0.06	0.58	1.00										
Ni (II)	0.84	0.86	0.82	0.83	-0.32	0.40	0.82	0.90	0.97	0.62	-0.14	0.93	0.55	0.84	0.83	0.80	0.94	-0.23	-0.34	1.00									
Ni (I)	0.97	0.98	0.98	0.86	0.21	0.62	0.99	0.96	0.84	0.82	-0.14	0.93	0.36	0.98	0.94	0.76	0.95	-0.01	0.20	0.83	1.00								
Pb (II)	0.21	0.18	0.20	0.13	0.23	0.11	0.23	0.16	0.16	0.17	0.15	0.19	0.10	0.21	0.27	0.24	0.18	0.22	0.21	0.14	0.24	1.00							
Tl (II)	0.89	0.88	0.90	0.80	0.47	0.79	0.89	0.83	0.58	0.90	-0.27	0.76	0.11	0.90	0.76	0.52	0.78	0.00	0.46	0.57	0.88	0.27	1.00						
Zn (II)	0.90	0.91	0.87	0.91	-0.27	0.55	0.85	0.94	0.96	0.74	-0.30	0.93	0.47	0.89	0.82	0.72	0.96	-0.34	-0.30	0.97	0.86	0.11	0.65	1.00					
Zn (I)	0.83	0.81	0.82	0.82	0.22	0.98	0.78	0.79	0.47	0.98	-0.71	0.68	-0.09	0.80	0.51	0.17	0.69	-0.47	0.20	0.53	0.74	0.13	0.85	0.65	1.00				
Ar (357)	0.82	0.86	0.84	0.73	-0.06	0.26	0.86	0.88	0.93	0.54	0.11	0.90	0.56	0.86	0.92	0.90	0.92	0.08	-0.07	0.91	0.88	0.15	0.62	0.87	0.42	1.00			
Ar (404)	0.87	0.90	0.87	0.85	-0.20	0.42	0.86	0.93	0.97	0.66	-0.11	0.94	0.56	0.89	0.88	0.85	0.97	-0.14	-0.21	0.97	0.88	0.15	0.66	0.96	0.55	0.95	1.00		
Ar (420)	0.94	0.94	0.96	0.84	0.38	0.77	0.94	0.90	0.67	0.91	-0.34	0.82	0.09	0.94	0.80	0.52	0.85	-0.11	0.38	0.85	0.92	0.19	0.92	0.74	0.73	0.92	0.74	1.00	
Ar (451)	0.67	0.68	0.73	0.47	0.74	0.40	0.77	0.60	0.41	0.57	0.17	0.57	0.12	0.72	0.75	0.57	0.58	0.47	0.75	0.34	0.76	0.27	0.82	0.36	0.49	0.60	0.48	0.79	1.00
	Al (I)	Ba^{230}	Ba^{232}	Ca (II)	Ca (I)	Cd (II)	Cd (I)	Co (II)	Co (I)	Cr (II)	Cr (I)	Cu (II)	Cu (I)	Fe (II)	Mg (II)	Mg (I)	Mn (II)	Mn (I)	Na (I)	Ni (II)	Ni (I)	Pb (II)	Tl (II)	Zn (II)	Zn (I)	Ar^{357}	Ar^{404}	Ar^{420}	Ar^{451}

Figure 3.9 shows the drift plot obtained under conditions close to the so called "robust conditions", 1375W of power and a slight low nebuliser gas flow rate 0.75Lmin⁻¹. Two groups of lines were identified. At the top of the plot in Figure 3.9 all the analyte lines followed the same drift pattern. On the bottom of the plot, the four argon lines appear, fluctuating in a similar way. This clear distinction between the two sets of signals indicates that the transport process may be the cause of fluctuation of the analyte lines since all analytes will be affected in a similar way whilst the argon species are not. The low nebuliser flow employed will have an effect on the sample introduction system.

FIGURE 3.9: DRIFT PLOT AT EXPERIMENT 4 CONDITIONS

As expected from the drift plot (Figure 3.9) a high correlation is observed between all the analyte lines, r ~0.9 (Table 3.13). Of particular interest is the high "negative" correlation observed between analyte lines and the argon lines.

RF Power 1375 W & Nebuliser Gas Flow Rate 0.75 Lmin^{-1}

	Al (I)	Ba 230	Ba 232	Ca (II)	Ca (I)	Cd (II)	Cd (I)	Co (II)	Co (I)	Cr (II)	Cr (I)	Cu (II)	Cu (I)	Fe (II)	Mg (II)	Mg (I)	Mn (II)	Mn (I)	Na (I)	Ni (II)	Ni (I)	Pb (II)	Tl (II)	Zn (II)	Zn (I)	Ar 357	Ar 404	Ar 420	Ar 451
Al (I)	1.00																												
Ba (230)	0.98	1.00																											
Ba (232)	0.98	1.00	1.00																										
Ca (II)	0.99	0.98	0.98	1.00																									
Ca (I)	0.99	0.97	0.97	0.96	1.00																								
Cd (II)	0.99	0.99	0.98	0.99	0.98	1.00																							
Cd (I)	0.98	0.99	0.99	0.98	0.95	0.98	1.00																						
Co (II)	0.98	0.99	0.99	0.97	0.97	0.98	0.99	1.00																					
Co (I)	0.98	0.99	0.99	0.98	0.96	0.98	0.99	0.89	1.00																				
Cr (II)	0.99	0.98	0.98	1.00	0.98	0.99	0.98	0.98	0.98	1.00																			
Cr (I)	1.00	0.98	0.98	0.98	1.00	0.99	0.97	0.98	0.97	0.99	1.00																		
Cu (II)	0.98	0.99	0.99	0.97	0.98	0.98	0.99	0.99	0.99	0.88	0.98	1.00																	
Cu (I)	1.00	0.98	0.98	0.99	0.99	0.99	0.97	0.98	0.98	0.99	1.00	0.98	1.00																
Fe (II)	1.00	0.98	0.98	0.99	0.98	0.99	0.98	0.98	0.98	0.99	0.99	0.98	1.00	1.00															
Mg (II)	0.98	0.99	0.99	0.98	0.96	0.98	0.99	0.99	0.99	0.88	0.97	0.99	0.97	0.97	1.00														
Mg (I)	0.99	0.97	0.98	0.99	0.97	0.99	0.97	0.97	0.98	0.99	0.98	0.97	0.99	1.00	0.97	1.00													
Mn (II)	0.99	0.98	0.98	1.00	0.98	0.99	0.98	0.97	0.98	1.00	0.99	0.98	0.99	1.00	0.98	1.00	1.00												
Mn (I)	0.99	0.98	0.97	0.96	1.00	0.98	0.96	0.98	0.97	0.98	1.00	0.98	0.99	0.98	0.96	0.97	0.97	1.00											
Na (I)	0.95	0.94	0.93	0.90	0.98	0.94	0.90	0.94	0.91	0.92	0.97	0.95	0.95	0.93	0.91	0.91	0.92	0.98	1.00										
Ni (II)	0.98	0.99	0.99	0.98	0.96	0.98	0.99	0.88	0.99	0.98	0.97	0.98	0.98	0.98	0.99	0.98	0.98	0.96	0.91	1.00									
Ni (I)	0.98	0.99	0.99	0.97	0.97	0.98	0.98	0.99	0.98	0.98	0.98	0.99	0.98	0.97	0.98	0.97	0.97	0.98	0.94	0.97	1.00								
Pb (II)	0.96	0.98	0.97	0.96	0.95	0.97	0.97	0.97	0.97	0.96	0.95	0.97	0.96	0.96	0.97	0.95	0.96	0.95	0.91	0.97	0.97	1.00							
Tl (II)	1.00	0.98	0.98	0.99	0.99	0.99	0.97	0.98	0.98	0.99	1.00	0.98	1.00	1.00	0.98	0.99	0.99	0.99	0.95	0.98	0.98	0.96	1.00						
Zn (II)	0.96	0.98	0.98	0.97	0.93	0.97	0.99	0.98	0.98	0.97	0.94	0.97	0.96	0.96	0.98	0.96	0.97	0.93	0.86	0.98	0.96	0.97	0.96	1.00					
Zn (I)	0.99	0.98	0.98	0.99	0.98	0.99	0.98	0.98	0.98	1.00	0.99	0.98	0.99	0.99	0.98	0.99	0.99	0.98	0.94	0.97	0.98	0.96	0.99	0.97	1.00				
Ar (357)	-0.91	-0.91	-0.90	-0.85	-0.95	-0.90	-0.87	-0.91	-0.89	-0.88	-0.93	-0.92	-0.91	-0.89	-0.88	-0.87	-0.87	-0.95	-0.98	-0.88	-0.91	-0.88	-0.92	-0.83	-0.89	1.00			
Ar (404)	-0.81	-0.79	-0.79	-0.72	-0.87	-0.79	-0.74	-0.80	-0.76	-0.76	-0.84	-0.81	-0.81	-0.78	-0.76	-0.75	-0.75	-0.87	-0.94	-0.76	-0.81	-0.77	-0.82	-0.68	-0.78	0.96	1.00		
Ar (420)	-0.90	-0.90	-0.89	-0.84	-0.95	-0.89	-0.85	-0.90	-0.87	-0.87	-0.93	-0.91	-0.90	-0.88	-0.87	-0.85	-0.86	-0.95	-0.99	-0.87	-0.90	-0.87	-0.91	-0.81	-0.88	0.99	0.97	1.00	
Ar (451)	-0.94	-0.92	-0.92	-0.89	-0.97	-0.93	-0.89	-0.93	-0.91	-0.91	-0.96	-0.94	-0.94	-0.92	-0.90	-0.90	-0.90	-0.97	-0.99	-0.90	-0.93	-0.90	-0.94	-0.85	-0.92	0.99	0.95	0.99	1.00

The data set produced when using a RF power of 1000 W and a nebuliser gas flow rate of 0.9 Lmin^{-1} is shown in Figure 3.10. This instrumental setting is very close to the so called standard conditions of RF power 1000 W and nebuliser gas flow rate 1.0 Lmin^{-1}, and thus to the conditions employed for the initial studies.

The drift plot obtained is similar to those found using the sequential instrument at standard conditions (see Figure 2.1). All of the emission lines monitored follow a similar drift pattern. However, this time, the emission intensities continuously increased with time, such like an extended warming up effect. The atomic lines provide more stable trends than the ionic lines. This could be explained by the low power setting since the hardest lines are more vulnerable to drift. The argon emission lines also demonstrated a marked positive drift.

FIGURE 3.10: DRIFT PLOT AT EXPERIMENT 5 CONDITIONS
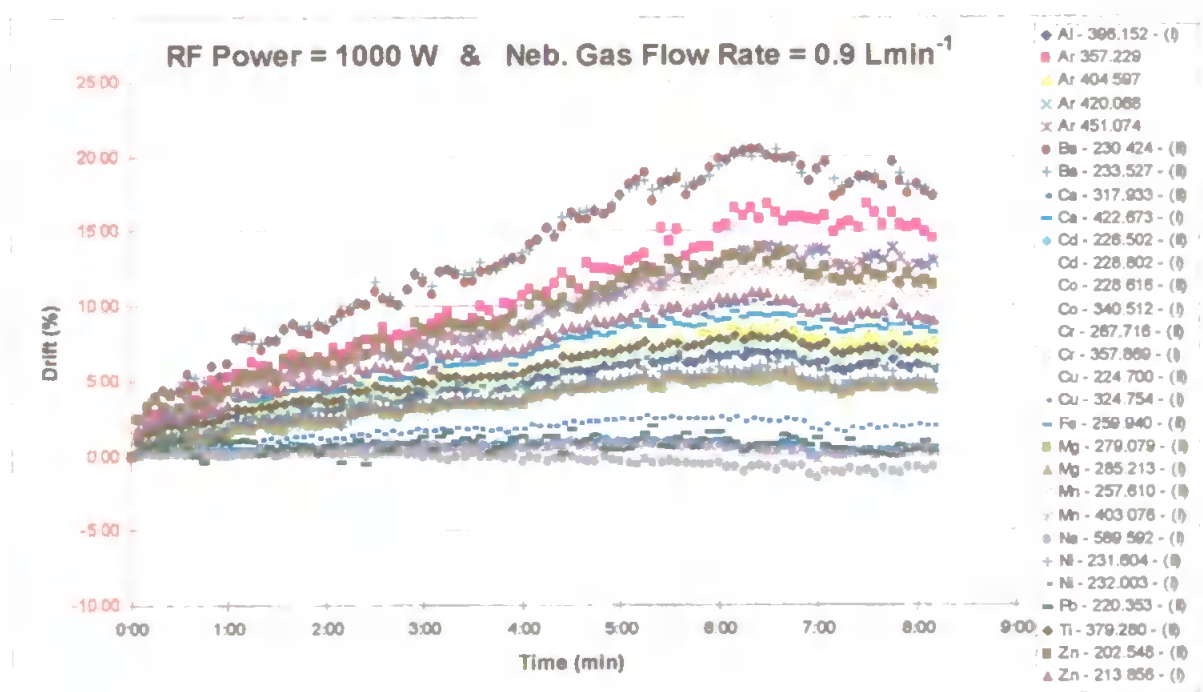
The correlation matrix at these conditions (Table 3.14) shows high correlation between most of the lines. Exceptions are the atomic lines Ca^I, Cr^I, Mn^I, (which correlate well), Na^I and the ionic line Pb^{II}. The latter is probably due to the low sensitivity of this emission line. However, the rest of the lines, including the argon lines present a very high correlation, r > 0.95.

TABLE 3.14: CORRELATION MATRIX OF DATA SET OBTAINED AT EXPERIMENT 5 CONDITIONS

RF Power 1000 W & Nebuliser Gas Flow Rate 0.9 Lmin^{-1}

	Al (I)	Ba^{230}	Ba^{232}	Ca (II)	Ca (I)	Cd (II)	Cd (I)	Co (II)	Co (I)	Cr (II)	Cr (I)	Cu (II)	Cu (I)	Fo (II)	Mg (II)	Mg (I)	Mn (II)	Mn (I)	Na (I)	NI (II)	NI (I)	Pb (II)	TI (II)	Zn (II)	Zn (I)	Ar^{357}	Ar^{404}	Ar^{420}	Ar^{451}
Al (I)	1.00																												
Ba (230)	0.99	1.00																											
Ba (232)	0.99	1.00	1.00																										
Ca (II)	1.00	1.00	1.00	1.00																									
Ca (I)	0.48	0.40	0.40	0.44	1.00																								
Cd (II)	1.00	0.99	0.99	0.99	0.50	1.00																							
Cd (I)	0.99	0.99	0.99	0.99	0.45	0.99	1.00																						
Co (II)	0.99	0.99	0.99	0.99	0.45	0.99	0.98	1.00																					
Co (I)	0.98	0.97	0.97	0.98	0.52	0.99	0.98	0.97	1.00																				
Cr (II)	1.00	1.00	1.00	1.00	0.42	0.99	0.99	0.99	0.98	1.00																			
Cr (I)	0.38	0.30	0.30	0.34	0.96	0.40	0.35	0.35	0.44	0.32	1.00																		
Cu (II)	1.00	0.99	0.99	1.00	0.47	0.99	0.99	0.99	0.99	1.00	0.37	1.00																	
Cu (I)	0.95	0.92	0.92	0.94	0.71	0.96	0.94	0.93	0.96	0.93	0.63	0.95	1.00																
Fo (II)	1.00	0.99	1.00	1.00	0.45	0.99	0.99	0.99	0.98	1.00	0.36	1.00	0.94	1.00															
Mg (II)	0.99	0.98	0.98	0.99	0.51	0.99	0.99	0.98	0.99	0.99	0.42	0.99	0.96	0.99	1.00														
Mg (I)	1.00	0.99	0.99	0.99	0.52	1.00	0.99	0.99	0.99	0.99	0.42	1.00	0.97	0.99	0.99	1.00													
Mn (II)	1.00	1.00	1.00	1.00	0.42	0.99	0.99	0.99	0.98	1.00	0.33	1.00	0.93	1.00	0.99	0.99	1.00												
Mn (I)	0.45	0.37	0.37	0.41	0.97	0.47	0.42	0.42	0.50	0.39	0.97	0.44	0.69	0.42	0.48	0.49	0.39	1.00											
Na (I)	-0.79	-0.83	-0.84	-0.81	0.15	-0.77	-0.80	-0.80	-0.75	-0.83	0.21	-0.79	-0.59	-0.80	-0.76	-0.76	-0.82	0.14	1.00										
NI (II)	0.99	0.99	0.99	0.99	0.49	0.99	0.99	0.99	0.99	0.99	0.39	0.99	0.96	0.99	0.99	0.99	0.99	0.46	-0.77	1.00									
NI (I)	0.99	0.99	0.99	0.99	0.48	0.99	0.99	0.98	0.98	0.99	0.39	0.99	0.95	0.99	0.99	0.99	0.99	0.45	-0.78	0.99	1.00								
Pb (II)	0.23	0.21	0.20	0.22	0.36	0.25	0.23	0.23	0.25	0.20	0.35	0.22	0.32	0.22	0.23	0.25	0.21	0.37	-0.04	0.24	0.22	1.00							
TI (II)	1.00	1.00	1.00	1.00	0.48	1.00	0.99	0.99	0.98	1.00	0.37	1.00	0.95	1.00	0.99	1.00	1.00	0.43	-0.80	0.99	0.99	0.22	1.00						
Zn (II)	0.99	0.99	0.99	0.99	0.45	0.99	0.99	0.98	0.98	0.99	0.35	0.99	0.94	0.99	0.99	0.99	0.99	0.42	-0.80	0.99	0.99	0.24	0.99	1.00					
Zn (I)	1.00	1.00	1.00	1.00	0.44	0.99	0.99	0.99	0.98	1.00	0.34	1.00	0.94	1.00	0.99	0.99	1.00	0.41	-0.81	0.99	0.99	0.21	1.00	0.99	1.00				
Ar (357)	0.97	0.99	0.99	0.98	0.29	0.96	0.97	0.97	0.94	0.98	0.20	0.97	0.87	0.98	0.96	0.96	0.98	0.27	-0.88	0.96	0.97	0.14	0.98	0.98	0.98	1.00			
Ar (404)	0.99	0.99	0.99	0.99	0.40	0.99	0.99	0.99	0.97	0.99	0.30	0.99	0.92	0.99	0.98	0.99	1.00	0.37	-0.83	0.99	0.98	0.20	0.99	0.99	0.99	0.98	1.00		
Ar (420)	0.98	0.89	0.98	0.99	0.31	0.97	0.98	0.98	0.95	0.99	0.20	0.98	0.88	0.98	0.97	0.97	0.99	0.28	-0.88	0.97	0.97	0.16	0.98	0.98	0.99	0.99	0.99	1.00	
Ar (451)	0.98	0.99	0.99	0.99	0.30	0.97	0.98	0.98	0.95	0.99	0.20	0.98	0.88	0.98	0.97	0.97	0.99	0.27	-0.88	0.97	0.97	0.15	0.98	0.98	0.99	0.99	0.99	1.00	1.00

Experiment 6 conditions, RF power = 1250 W and nebuliser flow = 1.2 Lmin^{-1}, provided a moderately stable data set, Figure 3.11. The emission lines fluctuated chaotically with time to lower values. Again, the atomic lines showed more stability than ionic lines. The drift pattern observed at this instrumental setting has similarities with the long-term behaviour at centre conditions (Figure 3.5), but with a higher drift bias.
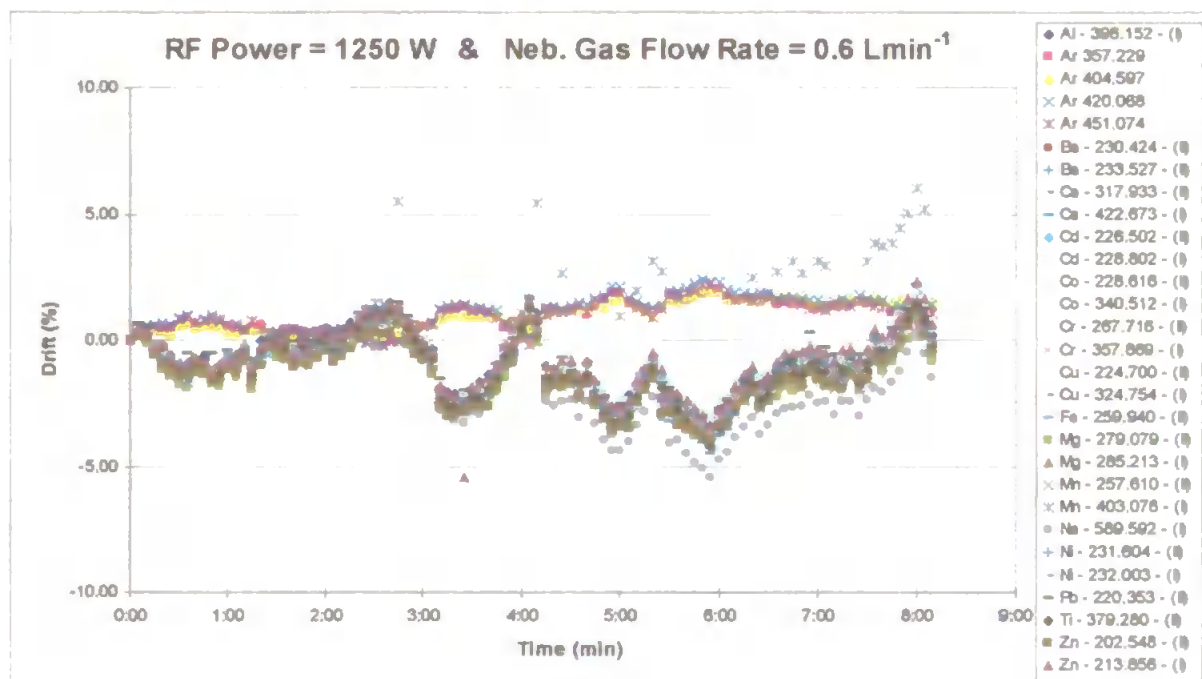
FIGURE 3.11: DRIFT PLOT AT EXPERIMENT 6 CONDITIONS

In terms of correlation, see Table 3.15, clear differences between the types of line can be observed. Ionic lines showed a high correlation between them and also with the argon lines. The atomic lines showed a more complex behaviour. Al, Ca and Na are the lines with lowest levels of correlation.

TABLE 3.15: CORRELATION MATRIX OF DATA SET OBTAINED AT EXPERIMENT 6 CONDITIONS

RF Power 1250 W & Nebuliser Gas Flow Rate 1.2 Lmin^{-1}

	Al (I)	Ba (230)	Ba (232)	Ca (II)	Ca (I)	Cd (II)	Cd (I)	Co (II)	Co (I)	Cr (II)	Cr (I)	Cu (II)	Cu (I)	Fo (II)	Mg (II)	Mg (I)	Mn (II)	Mn (I)	Na (I)	Ni (II)	Ni (I)	Pb (II)	Tl (II)	Zn (II)	Zn (I)	Ar (357)	Ar (404)	Ar (420)	Ar (451)
Al (I)	1.00																												
Ba (230)	-0.10	1.00																											
Ba (232)	-0.03	0.62	1.00																										
Ca (II)	-0.02	0.77	0.79	1.00																									
Ca (I)	0.45	-0.41	-0.40	-0.46	1.00																								
Cd (II)	0.09	0.79	0.80	0.95	-0.42	1.00																							
Cd (I)	0.12	0.74	0.71	0.85	-0.32	0.88	1.00																						
Co (II)	0.08	0.72	0.70	0.85	-0.37	0.88	0.82	1.00																					
Co (I)	0.44	0.62	0.64	0.76	-0.11	0.88	0.82	0.74	1.00																				
Cr (II)	0.02	0.79	0.81	0.94	-0.45	0.96	0.86	0.87	0.80	1.00																			
Cr (I)	0.65	0.54	0.60	0.71	-0.07	0.79	0.74	0.70	0.90	0.74	1.00																		
Cu (II)	0.10	0.76	0.78	0.93	-0.38	0.96	0.87	0.87	0.86	0.95	0.79	1.00																	
Cu (I)	0.35	0.73	0.76	0.88	-0.27	0.94	0.88	0.85	0.92	0.91	0.93	0.93	1.00																
Fo (II)	0.02	0.80	0.82	0.93	-0.47	0.95	0.87	0.89	0.81	0.96	0.75	0.95	0.93	1.00															
Mg (II)	0.10	0.78	0.80	0.91	-0.40	0.95	0.88	0.85	0.86	0.93	0.78	0.94	0.94	0.96	1.00														
Mg (I)	0.43	0.69	0.72	0.84	-0.22	0.90	0.85	0.82	0.92	0.87	0.95	0.90	0.99	0.90	0.91	1.00													
Mn (II)	0.04	0.81	0.82	0.95	-0.44	0.97	0.89	0.88	0.83	0.97	0.77	0.96	0.95	0.99	0.97	0.91	1.00												
Mn (I)	0.76	0.44	0.49	0.59	0.03	0.68	0.65	0.61	0.83	0.62	0.97	0.68	0.86	0.64	0.69	0.90	0.68	1.00											
Na (I)	0.35	-0.59	-0.59	-0.66	0.91	-0.64	-0.58	-0.59	-0.35	-0.67	-0.29	-0.62	-0.53	-0.71	-0.64	-0.49	-0.69	-0.18	1.00										
Ni (II)	0.08	0.79	0.78	0.93	-0.36	0.95	0.89	0.85	0.83	0.93	0.77	0.94	0.93	0.95	0.95	0.90	0.96	0.67	-0.60	1.00									
Ni (I)	0.25	0.67	0.67	0.82	-0.20	0.88	0.79	0.75	0.85	0.84	0.80	0.86	0.88	0.85	0.85	0.87	0.88	0.72	-0.45	0.84	1.00								
Pb (II)	-0.07	0.69	0.60	0.76	-0.40	0.80	0.71	0.70	0.65	0.76	0.54	0.76	0.71	0.75	0.77	0.67	0.77	0.44	-0.56	0.74	0.67	1.00							
Tl (II)	-0.08	0.82	0.82	0.95	-0.50	0.96	0.87	0.88	0.78	0.96	0.71	0.95	0.91	0.98	0.95	0.87	0.99	0.59	-0.73	0.95	0.83	0.79	1.00						
Zn (II)	0.17	0.58	0.65	0.80	-0.29	0.81	0.74	0.74	0.76	0.81	0.71	0.78	0.80	0.79	0.78	0.80	0.80	0.62	-0.48	0.78	0.76	0.60	0.78	1.00					
Zn (I)	0.19	0.76	0.78	0.92	-0.32	0.96	0.88	0.87	0.90	0.94	0.83	0.94	0.96	0.95	0.95	0.94	0.96	0.74	-0.57	0.95	0.88	0.75	0.94	0.83	1.00				
Ar (357)	-0.22	0.73	0.73	0.91	-0.60	0.85	0.73	0.79	0.58	0.87	0.52	0.84	0.73	0.87	0.82	0.70	0.87	0.39	-0.75	0.82	0.69	0.68	0.89	0.71	0.79	1.00			
Ar (404)	-0.06	0.78	0.77	0.95	-0.50	0.94	0.82	0.85	0.74	0.95	0.68	0.92	0.87	0.93	0.90	0.83	0.95	0.55	-0.70	0.92	0.81	0.78	0.95	0.77	0.91	0.89	1.00		
Ar (420)	-0.09	0.68	0.69	0.86	-0.25	0.82	0.77	0.77	0.60	0.82	0.58	0.81	0.74	0.81	0.78	0.72	0.83	0.45	-0.55	0.83	0.73	0.64	0.83	0.69	0.79	0.82	0.84	1.00	
Ar (451)	-0.40	0.70	0.70	0.87	-0.55	0.80	0.68	0.72	0.50	0.82	0.36	0.78	0.62	0.79	0.75	0.56	0.80	0.20	-0.68	0.77	0.63	0.68	0.84	0.66	0.73	0.90	0.87	0.83	1.00

For Experiment 7, the nebuliser gas was again set at lower flow rates, 0.6 Lmin^{-1}, and again separation of the lines tell into two groups, see Figure 3.12. The analyte lines intensities clearly fluctuated over time, whist the argon lines showed a progressive increase in their intensities. However, it should be noted that the overall drift values are below 5% for the whole experiment.

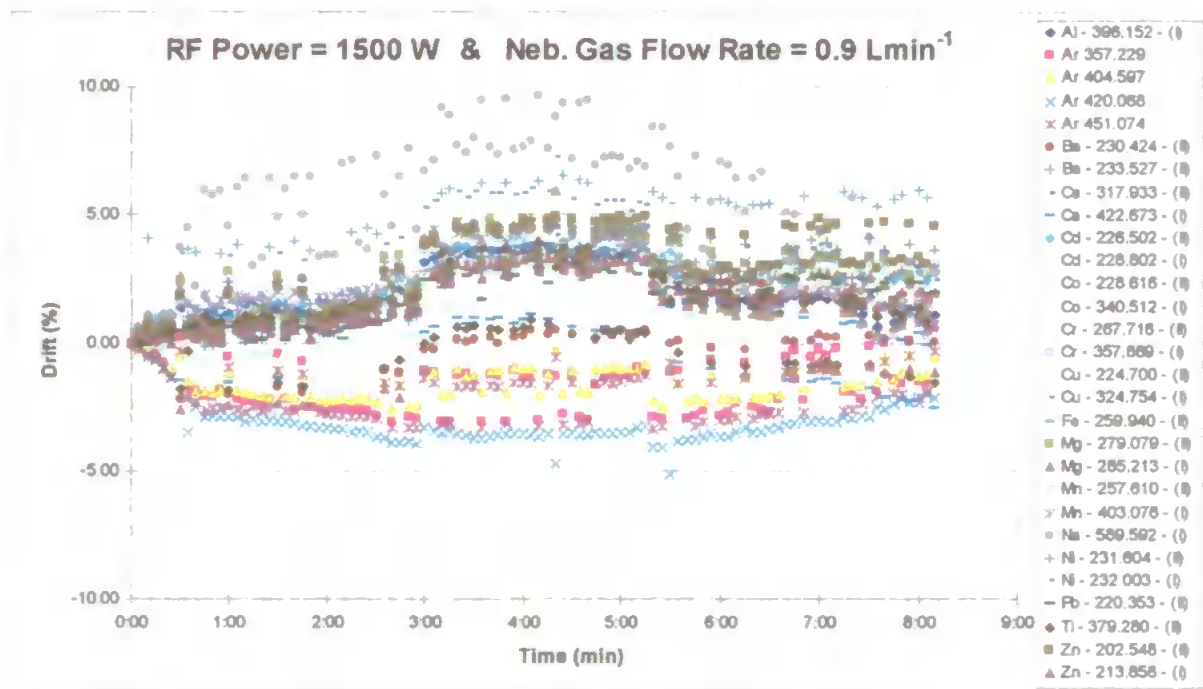**FIGURE 3.12:** DRIFT PLOT AT EXPERIMENT 7 CONDITIONS

The correlation matrix for data set Experiment 7 is shown in Table 3.16. A very high correlation is observed between all the analyte lines, whilst the argon lines showed negative correlation with most analyte emissions.

TABLE 3.16: CORRELATION MATRIX OF DATA SET OBTAINED AT EXPERIMENT 7 CONDITIONS

RF Power 1250 W & Nebuliser Gas Flow Rate 0.6 Lmin^{-1}

	Al (I)	Ba 230	Ba 232	Ca (II)	Ca (I)	Cd (II)	Cd (I)	Co (II)	Co (I)	Cr (II)	Cr (I)	Cu (II)	Cu (I)	Fe (II)	Mg (II)	Mg (I)	Mn (II)	Mn (I)	Na (I)	Ni (II)	Ni (I)	Pb (II)	Tl (II)	Zn (II)	Zn (I)	Ar 357	Ar 404	Ar 420	Ar 451
Al (I)	1.00																												
Ba (230)	0.98	1.00																											
Ba (232)	0.98	0.99	1.00																										
Ca (II)	0.99	0.98	0.99	1.00																									
Ca (I)	0.99	0.97	0.98	0.89	1.00																								
Cd (II)	0.99	0.98	0.97	0.99	0.97	1.00																							
Cd (I)	0.97	0.99	0.97	0.96	0.94	0.98	1.00																						
Co (II)	0.98	0.99	0.99	0.98	0.97	0.97	0.98	1.00																					
Co (I)	0.97	0.97	0.99	0.98	0.98	0.95	0.94	0.98	1.00																				
Cr (II)	0.88	0.96	0.98	0.99	1.00	0.97	0.93	0.97	0.98	1.00																			
Cr (I)	0.99	0.99	1.00	0.99	0.98	0.97	0.97	0.99	0.98	0.98	1.00																		
Cu (II)	0.97	1.00	0.98	0.97	0.95	0.98	0.99	0.98	0.95	0.94	0.98	1.00																	
Cu (I)	0.99	0.96	0.98	0.99	1.00	0.97	0.94	0.97	0.98	1.00	0.98	0.95	1.00																
Fe (II)	0.98	0.96	0.98	0.99	1.00	0.97	0.93	0.97	0.98	1.00	0.98	0.94	1.00	1.00															
Mg (II)	0.98	0.98	0.99	0.98	0.98	0.96	0.95	0.98	0.89	0.98	0.99	0.96	0.98	0.98	1.00														
Mg (I)	0.99	0.97	0.99	1.00	1.00	0.98	0.96	0.98	0.98	0.99	0.99	0.96	1.00	0.99	0.98	1.00													
Mn (II)	0.98	0.96	0.98	0.99	1.00	0.97	0.93	0.97	0.98	1.00	0.98	0.94	1.00	1.00	0.98	1.00	1.00												
Mn (I)	0.67	0.69	0.64	0.66	0.62	0.70	0.72	0.64	0.58	0.60	0.63	0.71	0.62	0.60	0.61	0.64	0.61	1.00											
Na (I)	0.92	0.88	0.93	0.94	0.96	0.88	0.83	0.90	0.95	0.97	0.92	0.85	0.96	0.97	0.94	0.95	0.97	0.46	1.00										
Ni (II)	0.98	1.00	0.99	0.98	0.97	0.98	0.99	0.99	0.97	0.96	0.99	0.99	0.97	0.96	0.98	0.98	0.96	0.66	0.89	1.00									
Ni (I)	0.98	0.99	1.00	0.98	0.98	0.97	0.97	0.99	0.98	0.98	0.89	0.98	0.98	0.98	0.99	0.98	0.98	0.63	0.93	0.99	1.00								
Pb (II)	0.97	0.97	0.98	0.97	0.96	0.97	0.97	0.97	0.96	0.86	0.97	0.97	0.96	0.96	0.96	0.97	0.96	0.66	0.89	0.97	0.97	1.00							
Tl (II)	0.99	0.97	0.99	1.00	1.00	0.98	0.95	0.98	0.98	1.00	0.99	0.96	1.00	1.00	0.98	1.00	1.00	0.63	0.95	0.97	0.98	0.97	1.00						
Zn (II)	0.98	0.98	0.99	0.99	0.98	0.97	0.97	0.99	0.98	0.98	0.99	0.97	0.98	0.98	0.99	0.98	0.98	0.63	0.93	0.99	0.99	0.97	0.98	1.00					
Zn (I)	0.96	0.85	0.94	0.95	0.94	0.96	0.95	0.94	0.92	0.93	0.94	0.95	0.94	0.92	0.92	0.95	0.93	0.70	0.84	0.95	0.93	0.93	0.94	0.93	1.00				
Ar (357)	-0.74	-0.68	-0.76	-0.76	-0.81	-0.67	-0.62	-0.72	-0.82	-0.83	-0.76	-0.64	-0.81	-0.83	-0.78	-0.78	-0.82	-0.21	-0.92	-0.70	-0.76	-0.71	-0.80	-0.75	-0.63	1.00			
Ar (404)	-0.59	-0.52	-0.62	-0.62	-0.68	-0.51	-0.44	-0.57	-0.69	-0.71	-0.62	-0.48	-0.68	-0.71	-0.65	-0.65	-0.70	-0.06	-0.84	-0.53	-0.62	-0.56	-0.68	-0.61	-0.46	0.96	1.00		
Ar (420)	-0.80	-0.74	-0.81	-0.81	-0.86	-0.73	-0.68	-0.78	-0.86	-0.87	-0.81	-0.70	-0.86	-0.87	-0.83	-0.83	-0.87	-0.29	-0.95	-0.75	-0.81	-0.76	-0.85	-0.80	-0.68	0.98	0.95	1.00	
Ar (451)	-0.84	-0.78	-0.85	-0.85	-0.90	-0.78	-0.73	-0.82	-0.89	-0.90	-0.86	-0.75	-0.90	-0.90	-0.87	-0.87	-0.90	-0.34	-0.96	-0.79	-0.85	-0.80	-0.88	-0.84	-0.74	0.96	0.92	0.99	1.00
	Al (I)	Ba^{230}	Ba^{232}	Ca (II)	Ca (I)	Cd (II)	Cd (I)	Co (II)	Co (I)	Cr (II)	Cr (I)	Cu (II)	Cu (I)	Fe (II)	Mg (II)	Mg (I)	Mn (II)	Mn (I)	Na (I)	Ni (II)	Ni (I)	Pb (II)	Tl (II)	Zn (II)	Zn (I)	Ar^{357}	Ar^{404}	Ar^{420}	Ar^{451}

The drift plot obtained with instrument settings of 1500W and 0.9 Lmin^{-1}, is shown in Figure 3.13. The analyte emission lines are partially separated from the argon lines, but this separation is much less distinct than at lower nebuliser flow rates.

The overall drift bias is around 5%. Na was the most unstable line, reaching intensities of up to 10% higher than the initial value. The high power employed is probably affecting more severely this line because it is the softest of the set.

FIGURE 3.13: DRIFT PLOT AT EXPERIMENT 8 CONDITIONS

The correlation matrix of data set Experiment 8 is complex, Table 3.17, and it is difficult to generalise any trends since the correlation levels vary from line to line. No correlation is detected between the analyte lines and the argon lines.

TABLE 3.17: CORRELATION MATRIX OF DATA SET OBTAINED AT EXPERIMENT 8 CONDITIONS

RF Power 1500 W & Nebuliser Gas Flow Rate 0.9 Lmin^{-1}

	Al (I)	Ba^{230}	Ba^{232}	Ca (II)	Ca (I)	Cd (II)	Cd (I)	Co (II)	Co (I)	Cr (II)	Cr (I)	Cu (II)	Cu (I)	Fe (II)	Mg (II)	Mg (I)	Mn (II)	Mn (I)	Na (I)	Ni (II)	Ni (I)	Pb (II)	Tl (II)	Zn (II)	Zn (I)	Ar^{357}	Ar^{404}	Ar^{420}	Ar^{451}
Al (I)	1.00																												
Ba (230)	-0.01	1.00																											
Ba (232)	0.32	0.63	1.00																										
Ca (II)	0.87	-0.04	0.40	1.00																									
Ca (I)	0.28	0.68	0.35	-0.05	1.00																								
Cd (II)	0.88	0.17	0.51	0.97	0.13	1.00																							
Cd (I)	0.74	-0.10	0.38	0.97	-0.24	0.91	1.00																						
Co (II)	0.81	0.01	0.44	0.97	-0.09	0.98	0.96	1.00																					
Co (I)	0.83	-0.29	0.23	0.95	-0.22	0.88	0.93	0.94	1.00																				
Cr (II)	0.94	0.03	0.42	0.98	0.13	0.97	0.90	0.93	0.90	1.00																			
Cr (I)	0.97	-0.13	0.18	0.76	0.33	0.75	0.60	0.68	0.76	0.85	1.00																		
Cu (II)	0.92	-0.11	0.35	0.97	-0.01	0.94	0.92	0.96	0.97	0.96	0.84	1.00																	
Cu (I)	0.90	-0.36	0.13	0.89	-0.04	0.82	0.81	0.84	0.94	0.90	0.91	0.94	1.00																
Fe (II)	0.94	-0.08	0.35	0.98	0.06	0.95	0.91	0.93	0.93	0.99	0.87	0.98	0.94	1.00															
Mg (II)	0.90	-0.27	0.20	0.93	-0.09	0.87	0.88	0.91	0.98	0.92	0.85	0.97	0.97	0.94	1.00														
Mg (I)	0.93	-0.29	0.17	0.91	0.01	0.85	0.83	0.85	0.93	0.93	0.92	0.94	0.99	0.96	0.96	1.00													
Mn (II)	0.87	-0.21	0.28	0.98	-0.10	0.92	0.94	0.95	0.98	0.95	0.80	0.98	0.96	0.98	0.96	0.96	1.00												
Mn (I)	0.96	-0.08	0.21	0.75	0.36	0.76	0.59	0.68	0.76	0.84	0.99	0.84	0.89	0.85	0.85	0.89	0.79	1.00											
Na (I)	0.73	0.11	0.35	0.50	0.51	0.57	0.33	0.48	0.50	0.60	0.77	0.60	0.62	0.59	0.60	0.62	0.53	0.81	1.00										
Ni (II)	0.84	-0.06	0.39	0.96	-0.09	0.94	0.94	0.99	0.96	0.93	0.73	0.98	0.88	0.94	0.94	0.88	0.96	0.74	0.53	1.00									
Ni (I)	0.86	-0.11	0.34	0.98	-0.10	0.95	0.96	0.97	0.97	0.95	0.77	0.97	0.91	0.96	0.96	0.92	0.98	0.76	0.52	0.97	1.00								
Pb (II)	0.81	0.15	0.54	0.93	0.06	0.95	0.90	0.94	0.86	0.92	0.68	0.91	0.77	0.90	0.84	0.80	0.88	0.68	0.51	0.92	0.92	1.00							
Tl (II)	0.20	0.85	0.50	-0.01	0.95	0.18	-0.17	-0.03	-0.23	0.13	0.18	-0.02	-0.14	0.04	-0.14	-0.07	-0.12	0.23	0.42	-0.05	-0.08	0.12	1.00						
Zn (II)	0.73	-0.02	0.42	0.96	-0.21	0.93	0.98	0.98	0.93	0.89	0.58	0.92	0.79	0.89	0.87	0.80	0.92	0.58	0.37	0.96	0.96	0.92	-0.12	1.00					
Zn (I)	0.63	0.53	0.46	0.47	0.62	0.58	0.34	0.43	0.29	0.58	0.56	0.46	0.35	0.51	0.35	0.41	0.38	0.57	0.45	0.42	0.41	0.53	0.62	0.35	1.00				
Ar (357)	-0.01	-0.72	-0.30	0.28	-0.84	0.07	0.44	0.23	0.38	0.15	-0.04	0.21	0.31	0.22	0.28	0.29	0.35	-0.11	-0.38	0.23	0.29	0.12	-0.85	0.34	-0.43	1.00			
Ar (404)	0.18	-0.55	-0.14	0.43	-0.58	0.24	0.54	0.34	0.44	0.34	0.14	0.34	0.42	0.40	0.35	0.44	0.47	0.05	-0.27	0.31	0.39	0.28	-0.60	0.41	-0.15	0.90	1.00		
Ar (420)	-0.54	-0.15	-0.27	-0.43	-0.38	-0.52	-0.30	-0.50	-0.48	-0.47	-0.56	-0.53	-0.50	-0.47	-0.55	-0.47	-0.47	-0.64	-0.75	-0.55	-0.49	-0.47	-0.34	-0.41	-0.32	0.47	0.48	1.00	
Ar (451)	0.03	-0.73	-0.32	0.31	-0.74	0.09	0.43	0.23	0.39	0.19	0.03	0.24	0.35	0.26	0.30	0.35	0.38	-0.06	-0.35	0.22	0.30	0.14	-0.77	0.32	-0.37	0.97	0.95	0.46	1.00

The data set obtained at 1000W and a nebuliser gas flow rate of 1.2 Lmin^{-1}, Experiment 9, produced a drift plot (Figure 3.14) similar to the Experiment 1 (rf power 1125 W and nebuliser gas flow rate of 1.05 Lmin^{-1}, Figure 3.6). During the first three hours of diagnosis, the "down and up" effect is observed, after which most of the emission lines remained stable over the remainder of the experiment. Some lines show particularly chaotic behaviour: Na, Pb and both barium lines. The high nebuliser flow rate in conjunction the low power setting, could be causing variations on the plasma temperature, and thus on the emission intensities.

FIGURE 3.14: DRIFT PLOT AT EXPERIMENT 9 CONDITIONS

The correlation matrix of data set Experiment 9 is shown in Table 3.18. The correlation levels vary from one emission line to another. The ionic lines of Pb, Zn and Ba show low correlation, as do the atomic lines of Na and Co. The rest of the emission lines monitored present a high degree of correlation.

RF Power 1000 W & Nebuliser Gas Flow Rate 1.2 Lmin^{-1}

	Al (I)	Ba^{230}	Ba^{232}	Ca (II)	Ca (I)	Cd (II)	Cd (I)	Co (II)	Co (I)	Cr (II)	Cr (I)	Cu (II)	Cu (I)	Fe (II)	Mg (II)	Mg (I)	Mn (II)	Mn (I)	Na (I)	Ni (II)	Ni (I)	Pb (II)	Tl (II)	Zn (II)	Zn (I)	Ar^{357}	Ar^{404}	Ar^{420}	Ar^{451}
Al (I)	1.00																												
Ba (230)	0.26	1.00																											
Ba (232)	0.58	0.26	1.00																										
Ca (II)	0.84	0.27	0.64	1.00																									
Ca (I)	0.30	-0.14	-0.13	0.02	1.00																								
Cd (II)	0.88	0.30	0.63	0.94	-0.01	1.00																							
Cd (I)	0.65	0.21	0.53	0.81	-0.11	0.80	1.00																						
Co (II)	0.62	0.28	0.58	0.75	-0.08	0.75	0.61	1.00																					
Co (I)	0.49	0.24	0.33	0.36	-0.26	0.58	0.47	0.45	1.00																				
Cr (II)	0.79	0.27	0.62	0.92	-0.05	0.91	0.75	0.78	0.49	1.00																			
Cr (I)	0.97	0.27	0.62	0.94	0.21	0.93	0.74	0.71	0.45	0.87	1.00																		
Cu (II)	0.83	0.30	0.61	0.90	-0.07	0.94	0.80	0.77	0.65	0.90	0.89	1.00																	
Cu (I)	0.90	0.31	0.61	0.84	-0.01	0.93	0.74	0.72	0.76	0.85	0.90	0.93	1.00																
Fe (II)	0.87	0.33	0.67	0.92	-0.08	0.96	0.80	0.74	0.62	0.90	0.92	0.95	0.94	1.00															
Mg (II)	0.86	0.25	0.62	0.93	0.00	0.93	0.74	0.75	0.50	0.90	0.92	0.92	0.89	0.92	1.00														
Mg (I)	0.91	0.31	0.63	0.91	0.01	0.95	0.78	0.75	0.65	0.89	0.94	0.95	0.97	0.95	0.93	1.00													
Mn (II)	0.86	0.30	0.66	0.95	-0.09	0.96	0.83	0.77	0.60	0.92	0.93	0.96	0.94	0.97	0.94	0.97	1.00												
Mn (I)	0.98	0.27	0.61	0.92	0.24	0.92	0.71	0.69	0.46	0.85	0.99	0.88	0.91	0.90	0.91	0.94	0.91	1.00											
Na (I)	0.24	-0.13	-0.05	0.11	0.80	-0.05	-0.12	-0.09	-0.62	-0.05	0.21	-0.16	-0.17	-0.11	0.00	-0.08	-0.11	0.22	1.00										
Ni (II)	0.80	0.27	0.62	0.86	-0.03	0.88	0.70	0.70	0.57	0.85	0.85	0.86	0.87	0.88	0.84	0.88	0.89	0.84	-0.08	1.00									
Ni (I)	0.71	0.22	0.48	0.74	0.01	0.80	0.69	0.63	0.59	0.73	0.75	0.80	0.80	0.77	0.78	0.80	0.81	0.74	-0.11	0.72	1.00								
Pb (II)	0.50	0.25	0.43	0.50	-0.02	0.61	0.50	0.41	0.40	0.55	0.52	0.56	0.54	0.56	0.51	0.54	0.55	0.50	-0.09	0.55	0.47	1.00							
Tl (II)	0.88	0.27	0.65	0.99	0.02	0.96	0.81	0.76	0.44	0.92	0.96	0.92	0.88	0.95	0.95	0.93	0.97	0.94	0.09	0.88	0.76	0.53	1.00						
Zn (II)	0.37	0.16	0.29	0.51	-0.13	0.50	0.46	0.39	0.36	0.47	0.43	0.55	0.48	0.49	0.52	0.53	0.53	0.42	-0.18	0.44	0.45	0.23	0.50	1.00					
Zn (I)	0.72	0.27	0.62	0.91	-0.14	0.91	0.81	0.77	0.53	0.88	0.82	0.90	0.85	0.90	0.87	0.89	0.93	0.80	-0.18	0.83	0.77	0.51	0.89	0.57	1.00				
Ar (357)	0.67	0.26	0.63	0.92	-0.21	0.85	0.76	0.71	0.34	0.86	0.80	0.84	0.75	0.85	0.86	0.83	0.89	0.77	-0.09	0.80	0.69	0.46	0.90	0.54	0.90	1.00			
Ar (404)	0.82	0.26	0.64	0.97	-0.09	0.95	0.82	0.77	0.48	0.93	0.90	0.93	0.88	0.94	0.93	0.92	0.96	0.89	-0.05	0.87	0.77	0.53	0.97	0.55	0.94	0.92	1.00		
Ar (420)	0.67	0.26	0.62	0.94	-0.20	0.87	0.80	0.74	0.32	0.88	0.80	0.85	0.74	0.86	0.87	0.83	0.91	0.77	-0.07	0.79	0.70	0.44	0.92	0.56	0.92	0.97	0.84	1.00	
Ar (451)	0.69	0.24	0.60	0.96	-0.08	0.87	0.79	0.73	0.24	0.88	0.83	0.83	0.71	0.85	0.87	0.81	0.89	0.80	0.07	0.78	0.69	0.45	0.93	0.53	0.90	0.95	0.84	0.89	1.00

The drift plot obtained when using a high RF power (1500 W) and a high nebuliser flow rate (1.2Lmin⁻¹), Figure 3.15, resembles the plot obtained at moderate high RF power and nebuliser flow rate (1375 W, 1.05Lmin⁻¹), Figure 3.8.

Again high drift bias is observed and most of atomic lines appear towards the top of the plot, showing lower drift errors than most of ionic lines. The high nebuliser flow employed is probably influencing the drift pattern due to the reduction in the residence time. Atomic lines, which are less energetic, are less sensitive to this effect than hard lines.

FIGURE 3.15: DRIFT PLOT AT EXPERIMENT 11 CONDITIONS
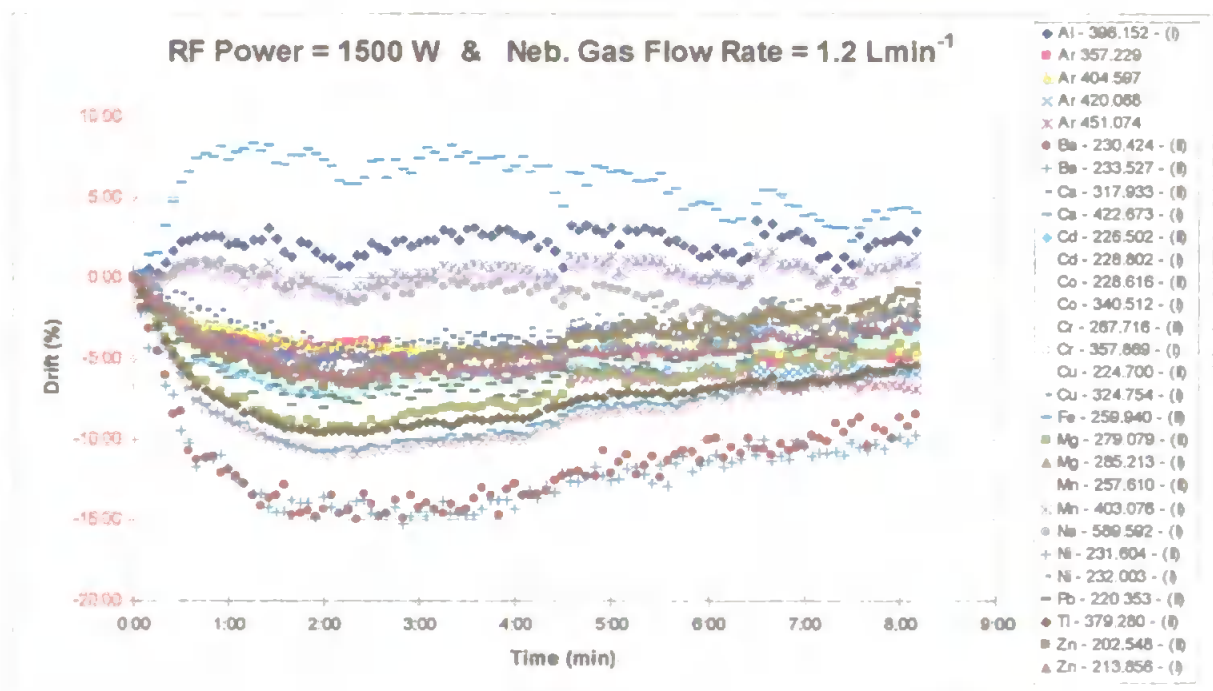
The correlation matrix for data set 11 (Table 3.19) shows a high level of correlation between all the ionic lines, some atomic emissions (Cd^I, Cu^I, Ni^I, Zn^I), and the argon lines. The remaining atomic lines present a distinctive behaviour. Al^I, Co^I, Cr^I, and Mg^I are highly correlated while, Na and Ca show a different behaviour and a less correlated trend.

TABLE 3.19: CORRELATION MATRIX OF DATA SET OBTAINED AT EXPERIMENT 11 CONDITIONS

RF Power 1500 W & Nebuliser Gas Flow Rate 1.2 Lmin^{-1}

	Al (I)	Ba 230	Ba 232	Ca (II)	Ca (I)	Cd (II)	Cd (I)	Co (II)	Co (I)	Cr (II)	Cr (I)	Cu (II)	Cu (I)	Fe (II)	Mg (II)	Mg (I)	Mn (II)	Mn (I)	Na (I)	Ni (II)	Ni (I)	Pb (II)	Tl (II)	Zn (II)	Zn (I)	Ar 357	Ar 404	Ar 420	Ar 451
Al (I)	1.00																												
Ba (230)	-0.39	1.00																											
Ba (232)	-0.41	0.97	1.00																										
Ca (II)	-0.05	0.70	0.78	1.00																									
Ca (I)	0.54	-0.84	-0.80	-0.30	1.00																								
Cd (II)	-0.12	0.91	0.89	0.60	-0.79	1.00																							
Cd (I)	-0.22	0.95	0.95	0.78	-0.74	0.93	1.00																						
Co (II)	-0.12	0.89	0.86	0.58	-0.78	0.96	0.93	1.00																					
Co (I)	0.81	-0.17	-0.22	-0.16	0.25	0.15	-0.01	0.18	1.00																				
Cr (II)	-0.37	0.98	0.98	0.75	-0.81	0.93	0.97	0.90	-0.16	1.00																			
Cr (I)	0.71	0.33	0.31	0.44	-0.10	0.59	0.49	0.57	0.71	0.37	1.00																		
Cu (II)	-0.19	0.93	0.90	0.60	-0.82	0.96	0.95	0.97	0.11	0.93	0.52	1.00																	
Cu (I)	0.01	0.89	0.86	0.67	-0.72	0.97	0.94	0.96	0.23	0.90	0.68	0.97	1.00																
Fe (II)	-0.30	0.97	0.96	0.68	-0.85	0.97	0.97	0.95	-0.06	0.98	0.43	0.97	0.94	1.00															
Mg (II)	-0.20	0.94	0.92	0.64	-0.82	0.98	0.96	0.97	0.07	0.95	0.53	0.98	0.97	0.99	1.00														
Mg (I)	0.00	0.90	0.88	0.70	-0.72	0.96	0.95	0.95	0.20	0.91	0.67	0.97	1.00	0.95	0.97	1.00													
Mn (II)	-0.31	0.97	0.96	0.69	-0.84	0.95	0.97	0.94	-0.07	0.98	0.42	0.97	0.95	1.00	0.98	0.95	1.00												
Mn (I)	0.85	0.12	0.11	0.38	0.14	0.38	0.30	0.38	0.77	0.16	0.96	0.30	0.50	0.21	0.31	0.49	0.21	1.00											
Na (I)	0.18	-0.23	-0.13	0.45	0.65	-0.33	-0.13	-0.35	-0.15	-0.16	-0.02	-0.38	-0.28	-0.28	-0.32	-0.25	-0.28	0.14	1.00										
Ni (II)	-0.05	0.88	0.85	0.59	-0.75	0.99	0.91	0.95	0.22	0.89	0.83	0.95	0.96	0.94	0.97	0.96	0.93	0.43	-0.31	1.00									
Ni (I)	-0.04	0.86	0.82	0.58	-0.71	0.93	0.91	0.94	0.27	0.88	0.61	0.96	0.96	0.91	0.94	0.95	0.91	0.43	-0.33	0.92	1.00								
Pb (II)	-0.18	0.92	0.89	0.61	-0.80	0.94	0.93	0.95	0.09	0.92	0.51	0.96	0.95	0.95	0.96	0.94	0.95	0.31	-0.35	0.92	0.93	1.00							
Tl (II)	-0.32	0.98	0.97	0.73	-0.82	0.95	0.98	0.93	-0.10	0.99	0.42	0.96	0.93	0.99	0.97	0.94	0.99	0.21	-0.21	0.92	0.89	0.94	1.00						
Zn (II)	-0.09	0.85	0.80	0.45	-0.80	0.95	0.87	0.94	0.23	0.85	0.57	0.96	0.95	0.92	0.94	0.93	0.91	0.36	-0.49	0.94	0.93	0.93	0.89	1.00					
Zn (I)	-0.22	0.95	0.95	0.78	-0.73	0.92	0.98	0.92	0.01	0.97	0.49	0.95	0.95	0.97	0.95	0.95	0.97	0.31	-0.13	0.90	0.92	0.94	0.97	0.87	1.00				
Ar (357)	-0.59	0.63	0.70	0.78	-0.38	0.38	0.58	0.34	-0.68	0.65	-0.16	0.38	0.34	0.54	0.43	0.37	0.55	-0.25	0.41	0.31	0.28	0.40	0.60	0.19	0.58	1.00			
Ar (404)	-0.48	0.65	0.72	0.85	-0.33	0.42	0.64	0.39	-0.55	0.68	-0.03	0.42	0.41	0.57	0.48	0.44	0.58	-0.11	0.48	0.38	0.36	0.45	0.63	0.24	0.64	0.97	1.00		
Ar (420)	-0.56	0.59	0.67	0.79	-0.33	0.33	0.56	0.30	-0.68	0.62	-0.15	0.34	0.31	0.50	0.40	0.35	0.51	-0.22	0.46	0.29	0.26	0.37	0.56	0.15	0.55	0.98	0.88	1.00	
Ar (451)	-0.53	0.41	0.50	0.71	-0.11	0.13	0.38	0.11	-0.68	0.44	-0.27	0.14	0.11	0.31	0.20	0.15	0.32	-0.29	0.62	0.09	0.06	0.17	0.38	-0.06	0.38	0.95	0.95	0.97	1.00

The last drift diagnosis confirmed the separation between analyte and plasma lines when low nebuliser flow rates are employed. Using conditions of a power setting of 1500W and nebuliser gas flow rate of 0.6Lmin^{-1}, two groups of lines are observed, Figure 3.16.

In terms of drift, it can be seen that the analyte emission intensities fluctuate over the time, but drift bias remained low (< 5%). The argon lines however show a very stable trend over the 8 hour experiment.

FIGURE 3.16: DRIFT PLOT AT EXPERIMENT 12 CONDITIONS

The correlation matrix of this data set, Table 3.20, shows high levels of correlation between all the analyte lines. This would allow drift correction by use of an internal standard. Moreover, the argon lines also showed good correlation.

TABLE 3.20: CORRELATION MATRIX OF DATA SET OBTAINED AT EXPERIMENT 12 CONDITIONS

RF Power 1500 W & Nebuliser Gas Flow Rate 0.6 Lmin⁻¹

	Al (I)	Ba²³⁰	Ba²³²	Ca (II)	Ca (I)	Cd (II)	Cd (I)	Co (II)	Co (I)	Cr (II)	Cr (I)	Cu (II)	Cu (I)	Fe (II)	Mg (II)	Mg (I)	Mn (II)	Mn (I)	Na (I)	Ni (II)	Ni (I)	Pb (II)	Tl (II)	Zn (II)	Zn (I)	Ar³⁵⁷	Ar⁴⁰⁴	Ar⁴²⁰	Ar⁴⁵¹
Al (I)	1.00																												
Ba (230)	0.97	1.00																											
Ba (232)	0.98	1.00	1.00																										
Ca (II)	0.98	0.96	0.98	1.00																									
Ca (I)	0.97	0.98	0.98	0.99	1.00																								
Cd (II)	0.94	0.99	0.98	0.94	0.96	1.00																							
Cd (I)	0.97	1.00	1.00	0.97	0.98	0.99	1.00																						
Co (II)	0.96	0.99	0.99	0.96	0.97	0.99	0.99	1.00																					
Co (I)	0.99	0.97	0.98	0.97	0.97	0.95	0.97	0.96	1.00																				
Cr (II)	0.99	0.98	0.99	0.98	0.97	0.95	0.98	0.97	0.98	1.00																			
Cr (I)	0.99	0.96	0.98	0.98	0.96	0.93	0.97	0.95	0.98	0.99	1.00																		
Cu (II)	0.95	0.99	0.99	0.95	0.97	0.99	0.99	0.99	0.96	0.96	0.95	1.00																	
Cu (I)	0.98	0.96	0.97	0.99	0.98	0.93	0.96	0.95	0.97	0.98	0.98	0.94	1.00																
Fe (II)	0.98	0.97	0.98	0.99	0.99	0.95	0.98	0.97	0.97	0.98	0.97	0.97	0.99	1.00															
Mg (II)	0.98	0.96	0.97	0.97	0.95	0.94	0.96	0.95	0.97	0.98	0.98	0.94	0.96	0.96	1.00														
Mg (I)	0.98	0.94	0.96	0.99	0.98	0.92	0.95	0.94	0.97	0.98	0.98	0.93	0.99	0.99	0.96	1.00													
Mn (II)	0.98	0.97	0.98	0.99	0.99	0.94	0.97	0.97	0.97	0.99	0.97	0.96	1.00	1.00	0.96	0.99	1.00												
Mn (I)	0.99	0.97	0.98	0.97	0.97	0.94	0.97	0.96	0.98	0.98	0.98	0.96	0.97	0.97	0.97	0.97	0.97	1.00											
Na (I)	0.89	0.94	0.94	0.90	0.94	0.94	0.94	0.96	0.89	0.92	0.87	0.95	0.92	0.94	0.86	0.89	0.93	0.90	1.00										
Ni (II)	0.98	0.99	0.99	0.97	0.97	0.88	0.99	0.98	0.98	0.98	0.98	0.97	0.96	0.97	0.98	0.96	0.97	0.98	0.90	1.00									
Ni (I)	0.97	0.99	0.99	0.96	0.98	0.98	0.99	0.99	0.97	0.98	0.86	0.99	0.96	0.98	0.95	0.95	0.97	0.97	0.95	0.97	1.00								
Pb (II)	0.94	0.98	0.98	0.94	0.96	0.97	0.98	0.99	0.94	0.96	0.92	0.97	0.94	0.96	0.93	0.92	0.95	0.94	0.96	0.95	0.98	1.00							
Tl (II)	0.98	0.96	0.98	1.00	0.99	0.94	0.97	0.96	0.97	0.98	0.98	0.95	1.00	0.99	0.97	1.00	1.00	0.97	0.91	0.97	0.96	0.94	1.00						
Zn (II)	0.95	1.00	0.99	0.95	0.97	0.99	0.99	0.99	0.95	0.96	0.94	0.99	0.94	0.96	0.94	0.92	0.95	0.95	0.95	0.98	0.98	0.98	0.94	1.00					
Zn (I)	0.97	0.99	0.99	0.96	0.98	0.99	0.99	0.99	0.97	0.97	0.96	0.99	0.95	0.97	0.96	0.95	0.96	0.97	0.93	0.99	0.99	0.96	0.96	0.99	1.00				
Ar (357)	-0.80	-0.87	-0.86	-0.79	-0.85	-0.87	-0.88	-0.89	-0.80	-0.83	-0.77	-0.88	-0.82	-0.85	-0.76	-0.77	-0.83	-0.82	-0.95	-0.81	-0.89	-0.89	-0.80	-0.88	-0.86	1.00			
Ar (404)	-0.72	-0.76	-0.78	-0.70	-0.77	-0.78	-0.77	-0.81	-0.71	-0.75	-0.69	-0.79	-0.74	-0.77	-0.67	-0.69	-0.76	-0.74	-0.91	-0.71	-0.81	-0.83	-0.72	-0.80	-0.76	0.93	1.00		
Ar (420)	-0.83	-0.89	-0.88	-0.82	-0.88	-0.89	-0.88	-0.91	-0.83	-0.86	-0.81	-0.91	-0.85	-0.88	-0.79	-0.81	-0.86	-0.85	-0.97	-0.84	-0.91	-0.91	-0.83	-0.90	-0.88	0.97	0.86	1.00	
Ar (451)	-0.80	-0.65	-0.70	-0.76	-0.72	-0.59	-0.67	-0.65	-0.76	-0.78	-0.79	-0.63	-0.81	-0.76	-0.75	-0.82	-0.79	-0.78	-0.62	-0.69	-0.69	-0.65	-0.79	-0.61	-0.68	0.53	0.56	0.61	1.00

3.3.2 THE DRIFT PATTERN EVOLUTION

Table 3.21 resumes the information obtained from the drift plots and correlation matrices.

As expected, the study identified different drift patterns depending on the instrumental parameters. The magnitude of the drift error also varied with the instrumental settings as can be observed in Figure 3.5 to Figure 3.16. Some of the instrumental settings produced very stable signals with drift values below 3% over the entire experiment, as was the case when using the central conditions, i.e. RF power of 1250 W and nebuliser flow rate of 0.9 Lmin^{-1}, and the moderate conditions, RF power of 1125 W, and nebuliser flow rate of 0.75 Lmin^{-1}. In other cases, the magnitude of the drift can reach values over 20%, i.e. experimental conditions: RF power of 1375 W, nebuliser flow rate of 1.05Lmin^{-1}.

However, one of the most interesting observation from the results is the evolution of the type of drift patterns with the changes in the instrumental parameters. Some similarities were found between drift plots at experimental conditions 1 and 9, (Figure 3.6 and Figure 3.14, respectively). The same for Experiments 3 and 11, Figure 3.8 and Figure 3.15, respectively.

To better visualise the trends, the results are summarised in Figure 3.17. A number of points may be noted. For instance, in the right-bottom corner, the plots show two trends, one grouping all the analyte lines and the other containing the four argon lines. This separation into two groups was found every time the instrument was set at robust or at least moderately robust conditions (e.g. 1500W, 0.60Lmin^{-1}; 1375W, 0.75Lmin^{-1}; 1250W, 0.60Lmin^{-1} for the RF power and the nebuliser gas flow rate respectively). A deficiency in the transport system due to a low nebuliser flow may cause this effect, since such conditions may lead to a partial blocking of the nebuliser tip, thus deteriorating its performance. This problem will only affect the analyte lines, since the argon line characteristics do not necessarily rise from the nebulisation process.

TABLE 3.21: SUMMARY OF RESULTS.

INSTRUMENTAL	RF Power (W)	1000			1125		1250			1375		1500		
CONDITIONS	Nebuliser Flow Rate (L/min)	0.60	0.90	1.20	0.75	1.05	0.60	0.90	1.20	0.75	1.05	0.60	0.90	1.20
DRIFT	Average	—	7.32	1.14	1.08	3.20	0.53	0.87	2.89	3.17	8.89	3.47	2.18	3.75
After 8 hours	Minimum	—	0.24	0.02	0.02	0.12	0.07	0.01	0.49	1.98	0.11	0.35	0.01	0.36
(%)	Maximum	—	17.46	5.59	2.59	9.01	1.48	1.61	5.79	6.45	21.17	8.83	4.56	9.79
CORRELATION	Average	—	0.71	0.62	0.54	0.40	0.95	0.41	0.61	0.98	0.53	0.97	0.64	0.55
	Atomic-Atomic	—	0.58	0.58	0.44	0.18	0.91	0.35	0.50	0.98	0.39	0.97	0.68	0.36
Analyte- Analyte	Ionic-Ionic	—	0.89	0.69	0.83	0.88	0.98	0.61	0.86	0.98	0.77	0.97	0.66	0.91
	Atomic-Ionic	—	0.66	0.59	0.42	0.21	0.94	0.32	0.52	0.97	0.46	0.97	0.61	0.42
CORRELATION	Average	—	0.79	0.70	0.54	0.40	-0.74	0.28	0.62	-0.87	0.63	-0.80	-0.05	0.28
	Argon-Atomic	—	0.64	0.62	0.23	0.04	-0.73	0.08	0.40	-0.89	0.52	-0.79	-0.06	0.09
Argon- Analyte	Argon-Ionic	—	0.92	0.76	0.80	0.71	-0.75	0.46	0.81	-0.86	0.72	-0.80	-0.04	0.44
REMARKS	Trends	—	YES	?	NO	?	YES	NO	NO	YES	YES	YES	YES	YES

FIGURE 3.17: DRIFT PATTERNS AT DIFFERENT EXPERIMENTAL CONDITIONS
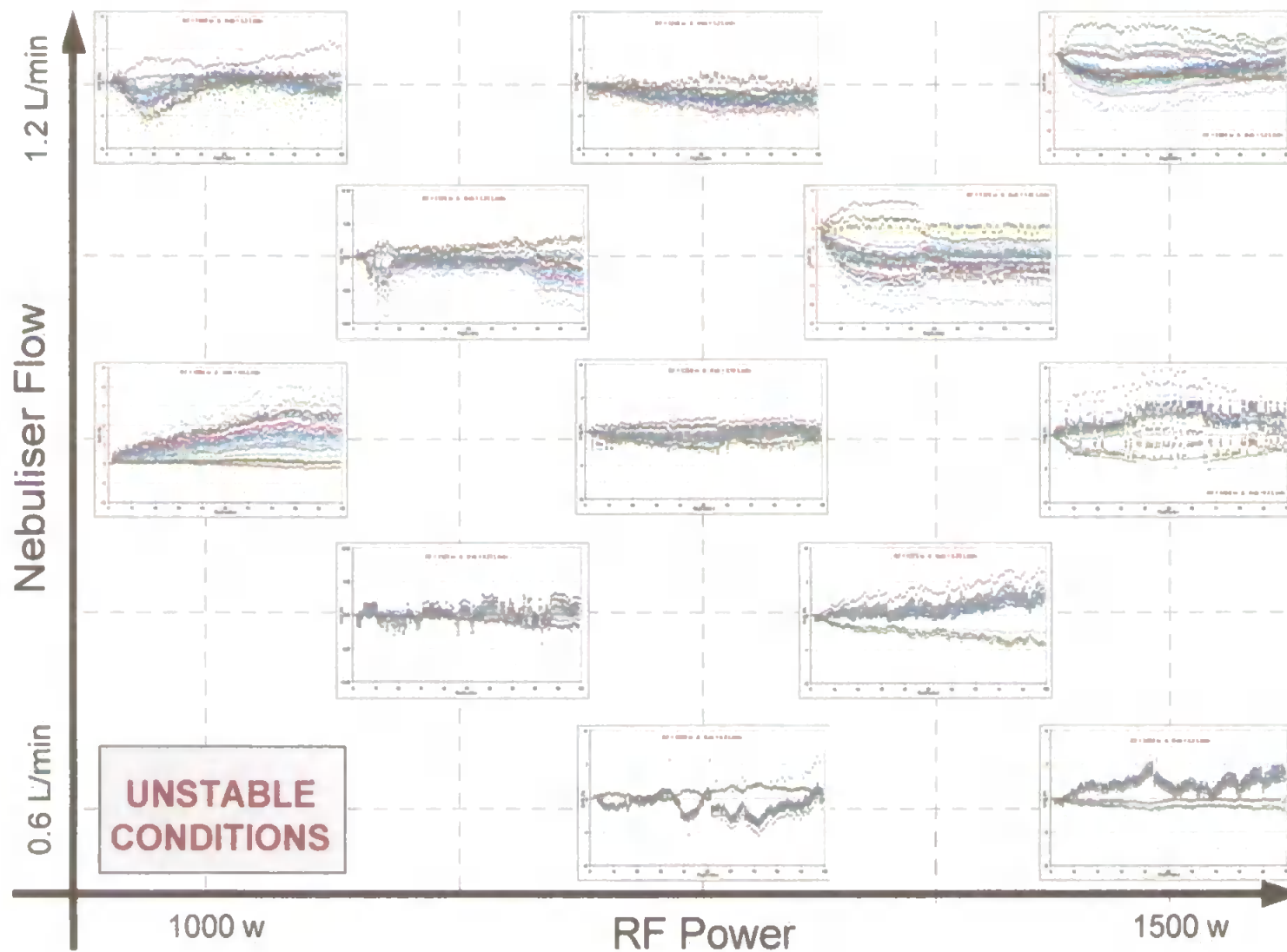
Another set of similar patterns can be found in the right-top area of Figure 3.17. This zone corresponds to unusual instrumental conditions, i.e. both high RF power and nebuliser gas flow, and is therefore not of great practical interest. However, in a similar way to the results in the right-bottom area discussed above, a couple of the plots show similar trends. The experiments run at RF power setting of 1375 W and nebuliser flow rate of 1.05Lmin^{-1} and at RF power 1500 W with a nebuliser flow rate of 1.20Lmin^{-1} present similar patterns, with very unstable signals during half of the experiment prior to a stabilising of the signals.

In the middle area of Figure 3.17, near the central conditions, various plots show more stable data sets, with low drift values but relatively noisy signals (i.e. the experimental settings 1250W, 0.9 Lmin^{-1}; 1250 W, 1.2 Lmin^{-1} and 1125 W, 0.75 Lmin^{-1}). Under such conditions, no trends are observed and the evolution in the signal is quite chaotic.

A final group of plots can be recognised at the top left corner of Figure 3.17. When using a low RF power and a high nebuliser gas flow rate (i.e. 1000 W, 1.2 Lmin^{-1} or 1125 W, 1.05 Lmin^{-1}) a warming up effect is observed. At such conditions, the plasma is slightly cooler due to the low power employed and the high setting for the nebuliser gas, which also contributes to the cooling effect.

Finally, when setting the instrument at 1000W and 0.9L/min, i.e. operating conditions which are very similar to the so-called 'standard conditions', (1000W and 1.0L/min), high values of drift were observed. Under such setting, the emission signals tended to drift to progressively higher values.

3.3.3 CORRELATION AND INTERNAL STANDARDISATION

The correlation coefficient is a measure of the linear relationship between fluctuations in the analyte and internal standard signals. Thus, to achieve good drift correction by internal standardisation, a high correlation between the analyte and internal standards is necessary. The correlation matrices of each data set (Table 3.9 -Table 3.20) have shown how the

correlation between emission lines changes from one set of experimental conditions to another, as well as the type (i.e. atomic, ionic, argon) of the line. These results indicate that only when working at robust or moderately robust conditions, do we observe very high inter-analyte correlation independent of the nature of the emission line, i.e. atomic or ionic line. This implies a limitation to the use of internal standardisation to correct for drift. The results indicate that whilst internal standardisation may be an option when working at robust conditions, the approach is of very little value when softer settings are employed. This is in agreement with the work by Romero et al.[69] where they found that the use of non-robust conditions made the use of internal standardization complex. This problem will be studied in more detail in Chapter 4.

3.3.4 MULTI-WAY ANALYSIS

As discussed in Section 3.3.2, the variation in the drift patterns from one set of conditions to another is not random. Groups of settings with similar drift patterns are observed, reflecting a progressive change in drift patterns as the instrumental conditions vary. For this reason, a multi-way analysis allowing the complete array of data to be analysed at once was performed.

Parallel factor analysis was applied to the data array. PARAFAC found that the best model resulted when only two factors were calculated see Section 3.2.4 (96.8% of the total variance was explained). Clearly, this was expected since we are altering just two instrumental parameters in this study, although it may additionally indicate that the model is working well. The PARAFAC results are presented in three data matrices, one for each mode, which compile the scores of each sample on each new PARAFAC factor. The first mode corresponding to emission lines, the score matrix-A has been plotted in Figure 3.18. A partial separation can be observed between atomic and ionic lines and more specifically between soft and hard lines.

FIGURE 3.18: PARAFAC SCORE PLOT ALONG THE FIRST MODE.
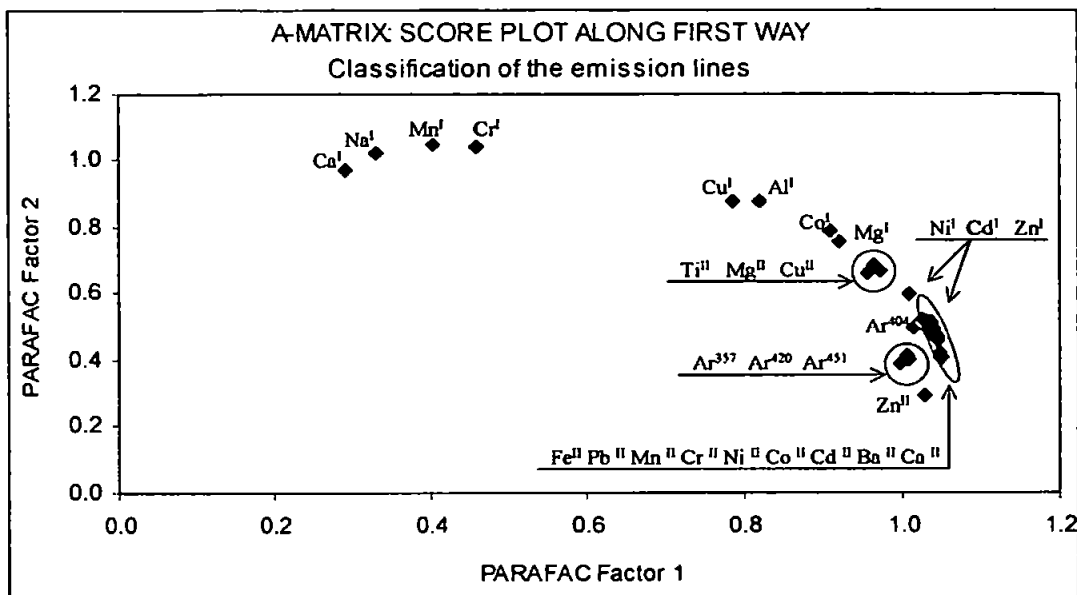
The closer to the right hand side bottom corner of the plot, i.e. high score on PARAFAC factor 1 and low on PARAFAC factor 2, the harder is the emission line.

In a similar way, Figure 3.19 represents the scores of factor 1 and 2 along the second dimension versus replicates, i.e. time. The drift patterns of some specific instrumental conditions have clearly conditioned the formation of these factors.

FIGURE 3.19: PARAFAC FACTORS ALONG THE SECOND MODE.
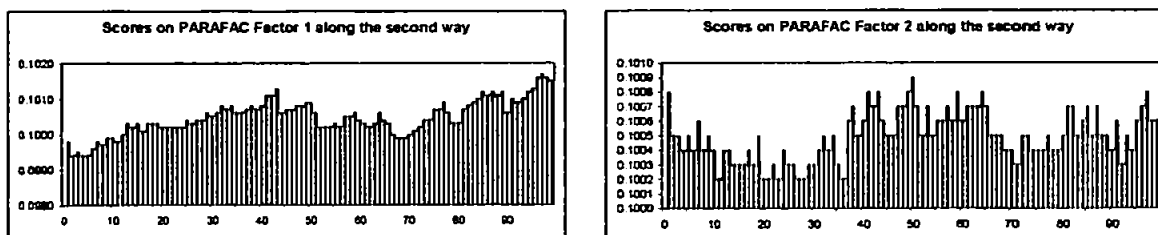
Finally, Figure 3.20 shows the PARAFAC score plot along the third mode. The distribution of the experiment points on the new axes is nearly linear, with a remarkable trend to robust conditions, i.e. high RF power and low nebuliser gas flow rate.

FIGURE 3.20: PARAFAC SCORE PLOT ALONG THE THIRD MODE.

In order to quantify these graphic observations, the degree of correlation, *r*, between the loadings of the new PARAFAC factors and several physical parameters of our data has been calculated. Thus, the scores of the new components in the first mode (A-Matrix) were correlated to the energy data of the lines studied: excitation energy, ionisation energy and emission energy of the monitored lines. The B-loading matrix was compared to the shape of the drift patterns, and the C-loadings were correlated to the levels of the RF power and the nebuliser flow rate set in each experiment.

Importantly, the correlation levels found in this exercise, enables the interpretation of the physical significance of the PARAFAC factors. The results are summarised below:

⇒ Within the 1st Mode: **Emission Lines**

- Factor 1: Some correlation was found with the emission energy of the emission lines (r = 0.58).

- Factor 2: The scores of the second factor are highly correlated to the inverse of the excitation energy of the emission lines (r = 0.90).

⇒ Within the 2nd Mode: **Replicates/Time**

- Factor 1: The loadings of this factor are highly correlated to the general (average) analyte drift patterns at robust and moderately robust conditions (r = 0.92).

- Factor 2: Some correlation was found (r~0.6) between this factor and the average drift pattern when using 1500W+0.9Lmin^{-1}, (Figure 3.21).

FIGURE 3.21: SIMILARITIES BETWEEN THE PARAFAC FACTORS AND THE DRIFT PATTERNS.

Drift Pattern at Robust Conditions

Drift Pattern when using 1500 W & 0.9 Lmin^{-1}
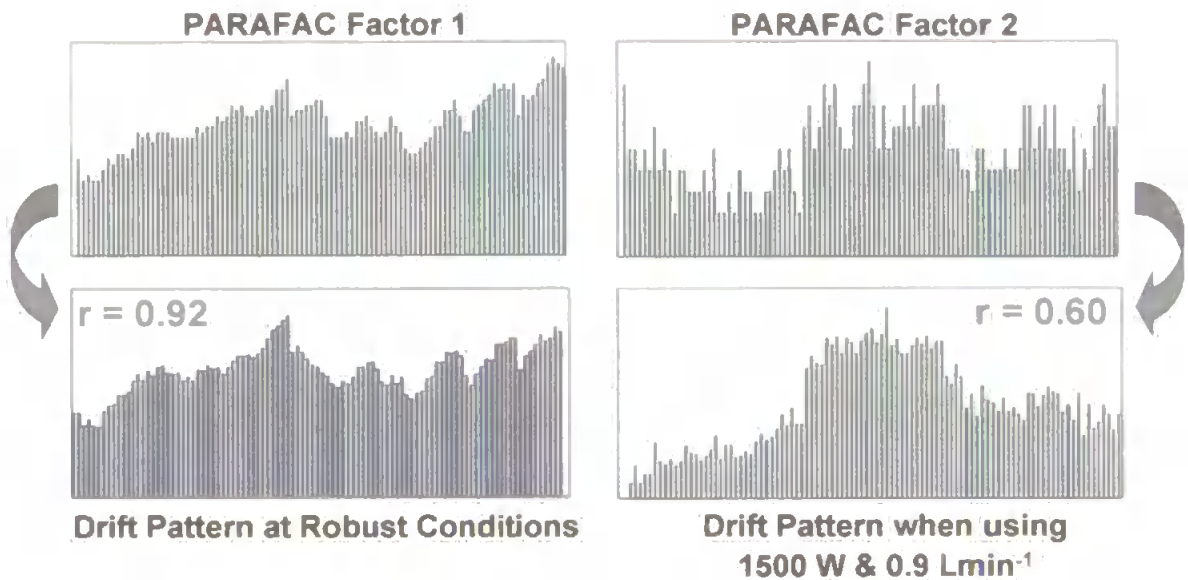
⇒ Within the 3rd Mode: **Experimental Conditions**

- Factor 1: Highly correlated to the nebuliser flow setting (r = 0.93), see Figure 3.22.

- Factor 2: Very highly correlated (r = 0.97) to the ratio: "(RF power) / (Nebuliser flow rate)"

FIGURE 3.22: PHYSICAL INTERPRETATION OF THE MODEL FACTORS ON THE THIRD MODE
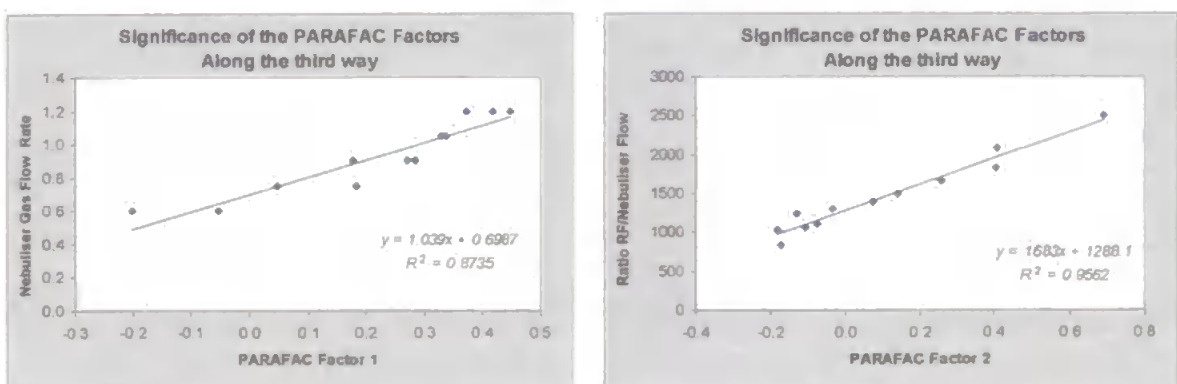
It seems important to notice that even though most of the variance in the data array is concentrated along the third mode, the drift patterns and the physical characteristics of the lines are also conditioning the formation of the PARAFAC factors.

The PARAFAC model therefore successfully fits most of the variation in the data using only two 3-dimensional factors. Although, no analytical information was incorporated into the matrix when performing the PARAFAC analysis, the new factors are highly correlated to some of the physical knowledge we have for the data, thus the new PARAFAC factors are easy to interpret. The results so far suggests that the two instrumental parameters modified in our study are indeed the cause of most of the variation in the data set and so, are directly implicated in the drift phenomena.

3.4 SUMMARY

The results presented here are in agreement with and complementary to previous work indicating that the RF power and the nebuliser gas flow rate settings have a fundamental effect on the robustness of the data.

The results shown in Figure 3.17 can provide the analyst with a quick reference to better optimise their instruments for long-term stability. In addition, this study facilitates the appropriate use of internal standards for drift correction:

- Soft conditions, low power (RF~1000 W) with medium to high nebuliser flow (>1.0 Lmin^{-1}), give very unstable signals over time and complex drift patterns. At these conditions, the use of an internal standard to compensate for instrument drift will not lead to an improvement on the quality of the data.

- At medium power (RF=1250W), the data obtained indicates that the instrument is generally quite stable, showing drift values below 5%. However, the drift patterns are very complex, and internal standardisation methods would not be appropriated.

- At robust conditions, the instability is highly correlated between all the analyte lines and any line can be employed to correct for drift.

The use of the multi-way approach, PARAFAC, has also been shown to be a powerful tool to describe the system:

- The results are easier to interpret than those obtained using PCA due to the smaller number of parameter implied in the formation of the PARAFAC factors.

- A mathematical interpretation of the tri-dimensional factors has been achieved by using physical parameters related to the system.

CHAPTER 4

DRIFT CORRECTION

4.1 INTRODUCTION

The study of the drift obtained at different instrumental conditions in Chapter 3, revealed the difficulties of finding a generic methodology for drift correction. In particular, the limitation of using an internal standard based method to correct for long-term bias was apparent.

Many internal standard methods are reported in the literature to correct for drift and to minimise matrix effects. The criteria considered important in the selection of the internal standard element[193] are listed below:

- The concentration of the internal standard element in the sample should be negligible.

- In order to avoid contamination, the IS element need to be available at high purity.

- The internal standard element and the analyte should have similar volatilisation rates.

- The ionisation energies should be comparable.

- The atomic weights should be roughly the same.

- Similar excitation energies.

- Similar wavelengths.

- Similar intensity.

In addition, the use of internal standard methods is usually restricted to simultaneous detectors. It seems clear that fulfilment of these conditions is usually not possible and particularly when multi-element determinations are attempted; therefore compromises are a necessity.

The work of Fassel *et al.* was the first to report the application of internal standardisation to improve the accuracy and precision of ICP-AES determinations[193,194]. However, later studies identified the limitations of using a single standard element to correct for drift[69] and several authors suggested more complicated correction procedures often involving the use of several internal standards. One such multi-internal standard method described in the literature is the generalised internal reference method, GIRM proposed by Lorber[195]. This approach uses several internal standards, ideally between four and six, and may be used to correct for drift[196], to improve sensitivity[197] or to compensate for background noise[198]. Applications of the GIRM are reported for improving the accuracy in metallurgical sample analysis[199] and to eliminate interferences and effects from drift[200]. The parameter related internal standard method, PRISM by Ramsey *et al.*[180,181] used two internal standard elements. PRISM is based on the observation that the majority of the correlated fluctuations in the instrumental signal for a given element with respect to time can be traced by two parameters: the forward power and the introduction efficiency. Since each of these parameters affect atomic and ionic lines

differently, using one internal standard for each of these parameters can correct for drift on both atomic and ionic lines. More recently, Mermet and Ivaldi[66] suggested another multi-element internal standard method. In this case, an artificial reference standard was produced by linear combination of multiple signals.

However, internal standard methods, even when appropriate, have several disadvantages in practical analysis. Matching samples and standards with one or several internal standards is time consuming, may be expensive and is often a potential source of contamination. For these reasons, research has investigated alternative solutions where the internal standard matching step can be avoided. Several papers have been published by Barnes group using an additional spectral line of the analyte under analysis as the internal standard. This approach known as the common analyte internal standard method (C.A.I.S.) has been applied to correct for drift[109], matrix effects [110,201] and solvent volatility variations[202,203]. The CAIS procedure avoids the internal standardisation step, however it does require a control solution to be measured regularly.

The use of chemometrics techniques such as Kalman filters and neural networks have also been utilised for drift correction in ICP-AES analysis. Kalman filters have been applied to correct for low frequency random drift and flicker noise based drift[158,159]. Catasus *et al.* have developed a specific neural network, the generalised regression neural network for ICP-AES calibration which is reported to minimise matrix effects and drift error[204].

In this chapter, a number of different correction procedures are evaluated for a range of instrumental conditions. The data sets obtained previously, (Section 3.3), were employed for this study and special attention was given to working conditions that are commonly used for analytical determinations, i.e. standard and robust conditions. In both cases, the potential of using intrinsic plasma lines to correct for drift in order to avoid the internal standard matching step is discussed.

4.2 DRIFT CORRECTION AT STANDARD CONDITIONS

Previous work on ICP-AES systems has demonstrated the convenience of working at robust conditions, i.e. low nebuliser gas flow rate and high RF power. At such conditions, the emission intensities are more stable and the drift patterns are highly correlated between all the analyte lines. Under these conditions, internal standardisation methods may correct for long-term drift error. However, many ICP-AES users employ soft conditions to perform their analysis, i.e. the so-called "standard conditions", which implies low RF power (~1000W) and a medium nebuliser flow rate (~1.0Lmin^{-1}). These values facilitate the use of both soft and hard emission lines with reasonable detection limits, and thus in practice are more versatile. In addition, standard conditions are often promoted by manufacturers[205]. However, when using such working parameters, the ICP-AES technique can give very unstable signals over time and complex drift patterns as shown in Chapter 3, Figure 3.10. This chapter describes work to develop a correction method for drift correction when the instrument is operated under standard conditions:

Low RF power ~ 1000 W and moderate nebuliser gas flow rate ~ 1.0 Lmin^{-1}

The procedure avoids re-calibration and sample matching with an internal standard element by using an intrinsic argon emission line. The approach thus requires the analyst to monitor only the drift on one argon line. A polynomial regression trendline is then fitted to the argon drift, and the long-term drift on the other lines is estimated using the trendline of the argon emission once modified by a correction factor, f_i, which is specific for each emission line. To date, this correction factor has been estimated by employing the results of a principal component analysis performed on the data set. However, the ideal case would be to estimate f_i using only the physical properties of the emission lines. Section 4.2.6 will further discuss this possibility.

The correction procedure described here has been developed using the data set obtained from "Experiment 5", i.e. 1000 W and a nebuliser gas flow rate of 0.9 Lmin^{-1}. Further details are given in Section 3.2.

4.2.1 THE CORRECTION PROCEDURE

In order to explain how the correction procedure works, the different steps employed in the process are described below:

1. The trendline of the argon line is calculated by employing a polynomial model up to the 5th order:

$y = \beta_0 + \beta_1 n + \beta_2 n^2 + \beta_3 n^3 + \beta_4 n^4 + \beta_5 n^5$
 Where:
      y refers to the measured drift error
      n refers to the replicate number
	EQUATION 4.1

2. A correction factor, f_i, specific for each emission line is determined using the results of a principal component analysis, PCA, performed on the data:

$$f_i = \frac{Lod_{Anal_i}}{Lod_{Ar}}$$
 Where
     $Lod_{Anal\,i}$ refers to the loading of analyte line i on PC1
     Lod_{Ar} refers to the loading of argon line on PC1
	EQUATION 4.2

3. The drift on each emission line is then estimated using the trendline of the argon, and the correction factor specific for the line, f_i. All the parameters, β, of the argon trendline in n, (i.e. β_1, β_2 β_3 β_4 β_5, not β_0) are multiplied by f_i.

$$y_{Anal_i} = \beta_0^{Ar_{404}} + f_i \cdot \beta_1^{Ar_{404}} \cdot n + f_i \cdot \beta_2^{Ar_{404}} \cdot n^2 + f_i \cdot \beta_3^{Ar_{404}} \cdot n^3 + f_i \cdot \beta_4^{Ar_{404}} \cdot n^4 + f_i \cdot \beta_5^{Ar_{404}} \cdot n^5$$

EQUATION 4.3

4. The estimated drift is removed from the measured data to create the "corrected data set".

5. The long-term drift on the corrected data set is calculated and compared to the drift on the data before correction.

4.2.2 CALCULATION OF THE TRENDLINES

Most curves can be fitted using a polynomial regression to the nth order. Increasing the order has the effect of improving the fit, i.e. the regression coefficient, r, will tend to one. In this study, the drift patterns have been regressed to polynomial curves up to the 5th order, which give an improved regression coefficient using a practical number of parameters: six (Equation 4.1).

The polynomial equations were calculated using the software "CurveExpert, version 1.3" (Daniel Hyams & Microsoft Corporation, USA). Of the argon emission lines monitored previously (Table 3.3), three were retained for this study, Ar^{404nm}, Ar^{420nm}, Ar^{451nm}. These were selected due to their higher intensity and slightly better correlation with most of the analyte lines of the set, as shown in Table 3.14. However, the Ar 404 nm line was later rejected due to an interference with iron when this metal is present at high concentrations.

Although, only the trendline of argon were used in the correction procedure, the polynomial regressions of all the other lines studied were also calculated. This facilitated a comparison of the polynomial parameters of every line to those of the argon trendline, and thus allowed the determination of where the specific correction factor should be applied. The parameters of the polynomial regressions of the emission lines studied are reported in Table 4.1.

TABLE 4.1: POLYNOMIAL REGRESSIONS OF THE EMISSION LINES STUDIED.

	POLYNOMIAL PARAMETERS						STATISTICS	
	β_0	β_1	β_2	β_3	β_4	β_5	s	r
Al (I)	0.107	0.313	-0.014	3.5E-04	-3.7E-06	1.4E-08	0.23	0.992
Ca (I)	0.033	0.071	-0.0038	1.1E-04	-1.3E-06	5.5E-09	0.13	0.886
Cd (I)	-0.048	0.316	-0.0133	3.2E-04	-3.4E-06	1.2E-08	0.31	0.989
Co (I)	-0.074	0.196	-0.0095	0.00026	-3.0E-06	1.2E-08	0.25	0.981
Cr (I)	0.016	0.045	-0.0027	8.9E-05	-1.2E-06	5.4E-09	0.13	0.865
Cu (I)	0.011	0.124	-0.0062	1.7E-04	-2.0E-06	8.2E-09	0.16	0.973
Mg (I)	0.047	0.257	-0.0116	2.9E-04	-3.1E-06	1.1E-08	0.20	0.990
Mn (I)	-0.026	0.047	-0.0029	9.2E-05	-1.2E-06	5.4E-09	0.13	0.859
Na (I)	0.070	0.039	-0.0026	6.8E-05	-8.4E-07	3.7E-09	0.14	0.958
Ni (I)	0.047	0.319	-0.0145	3.6E-04	-3.8E-06	1.4E-08	0.30	0.986
Zn (I)	0.254	0.462	-0.02	4.7E-04	-4.8E-06	1.7E-08	0.35	0.992
Ba (II)	-0.012	0.885	-0.0382	9.0E-04	-9.0E-06	3.1E-08	0.66	0.993
Ba (II)	0.321	0.832	-0.0348	8.1E-04	-8.1E-06	2.8E-08	0.58	0.994
Ca (II)	0.075	0.447	-0.0194	4.7E-04	-4.9E-06	1.8E-08	0.31	0.994
Cd (II)	0.122	0.238	-0.0108	2.7E-04	-2.9E-06	1.1E-08	0.22	0.988
Co (II)	-0.003	0.404	-0.0171	4.1E-04	-4.3E-06	1.6E-08	0.44	0.985
Cr (II)	-0.068	0.606	-0.0267	6.4E-04	-6.5E-06	2.3E-08	0.41	0.994
Cu (II)	0.053	0.381	-0.0169	4.1E-04	-4.4E-06	1.6E-08	0.25	0.993
Fe (II)	0.271	0.423	-0.0188	4.6E-04	-4.8E-06	1.8E-08	0.29	0.993
Mg (II)	-0.204	0.233	-0.01	2.5E-04	-2.8E-06	1.1E-08	0.23	0.988
Mn (II)	0.334	0.540	-0.0234	5.5E-04	-5.7E-06	2.0E-08	0.36	0.994
Ni (II)	-0.206	0.282	-0.0126	3.1E-04	-3.3E-06	1.2E-08	0.28	0.984
Pb (II)	0.534	0.016	-0.0016	5.8E-05	-7.6E-07	3.2E-09	0.43	0.442
Ti (II)	0.193	0.353	-0.0154	3.7E-04	-3.9E-06	1.4E-08	0.23	0.994
Zn (II)	1.031	0.503	-0.0215	5.2E-04	-5.5E-06	2.0E-08	0.53	0.988
Ar 357nm	0.048	0.617	-0.0239	5.1E-04	-4.6E-06	1.4E-08	0.56	0.993
Ar 404nm	-0.011	0.415	-0.0187	4.4E-04	-4.4E-06	1.6E-08	0.32	0.991
Ar 420nm	0.033	0.593	-0.0249	5.5E-04	-5.2E-06	1.7E-08	0.34	0.996
Ar 451nm	0.004	0.588	-0.0242	5.3E-04	-4.9E-06	1.6E-08	0.36	0.996

4.2.3 THE CORRECTION FACTOR

The specific correction factors, f_i, were calculated using the loadings of a principal component analysis performed on the Experiment 5 data set, as shown in Figure 4.1. The loading in the first principal component of every emission line is compared to the loading of the argon line (Equation 4.2).

FIGURE 4.1: DETAILS OF THE PRINCIPAL COMPONENT ANALYSIS PERFORMED TO THE DATA

Model:	PCA
Data Employed:	Drift values of Experiment 5
Samples:	The 100 replicates
Variables:	The 30 emission lines monitored
Pretreatment:	None
Results:	PC1 accounts for ~ 100% of the variation
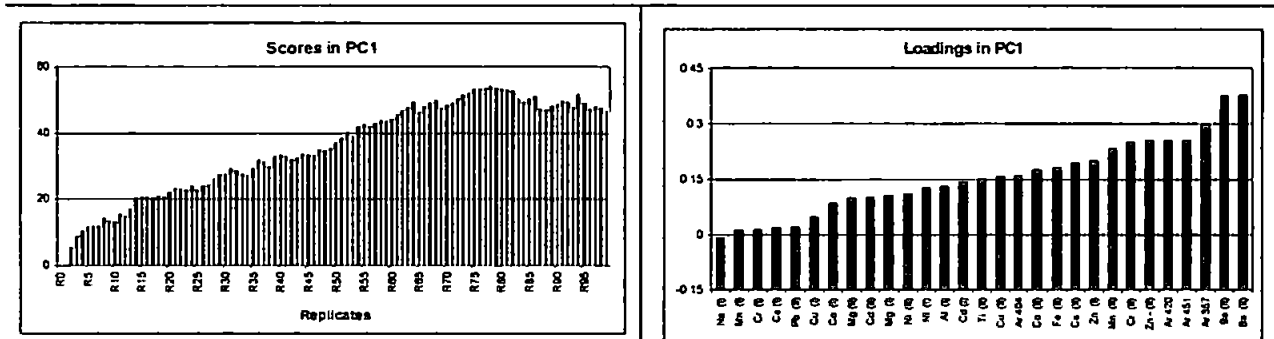
The "loading ratios" have been employed as specific correction factors, as shows Equation 4.2. In order to investigate where to apply the specific correction factor, the polynomial parameters of all the fitted curves are compared. It was observed that the ratio of all parameters of the analyte line multiplying n, to those of the argon line were relatively constant, and this ratio was similar to the ratio of the PCA loadings, (Table 4.2 -Table 4.4). Thus, the correction factors were calculated using the PCA loading ratios and applied to the argon trendline by multiplying every parameter by f_i, except the intercept, β_0. The drift on each analyte line was then estimated using the procedure shown in Equation 4.3.

TABLE 4.2: COMPARISON OF THE POLYNOMIAL PARAMETERS OF THE ANALYTE LINES TO THOSE OF AR 404NM.

	Ratio (Parameters of the analyte trendline/parameters of the Ar 404)						FROM THE PCA	
	β_0	β_1	β_2	β_3	β_4	β_5	LOADINGS RATIO (anal/Ar)	LOADINGS in PC 1
Al (I)	-9.47	0.76	0.75	0.79	0.84	0.89	0.82	0.13
Ca (I)	-2.91	0.17	0.20	0.24	0.29	0.35	0.11	0.02
Cd (I)	4.25	0.76	0.71	0.74	0.77	0.79	0.89	0.14
Co (I)	6.51	0.47	0.50	0.59	0.68	0.76	0.53	0.08
Cr (I)	-1.40	0.11	0.15	0.20	0.27	0.35	0.08	0.01
Cu (I)	-0.97	0.30	0.33	0.39	0.46	0.52	0.30	0.05
Mg (I)	-4.13	0.62	0.62	0.65	0.69	0.73	0.65	0.10
Mn (I)	2.34	0.11	0.15	0.21	0.27	0.34	0.07	0.01
Na (I)	-6.19	0.09	0.14	0.15	0.19	0.24	-0.06	-0.01
Ni (I)	-4.13	0.77	0.77	0.82	0.87	0.92	0.80	0.12
Zn (I)	-22.48	1.11	1.07	1.08	1.10	1.10	1.26	0.19
Ba (II)	1.05	2.13	2.04	2.04	2.03	2.01	2.37	0.37
Ba (II)	-28.44	2.01	1.86	1.84	1.83	1.81	2.38	0.37
Ca (II)	-6.64	1.08	1.03	1.06	1.10	1.13	1.21	0.19
Cd (II)	-10.84	0.57	0.58	0.62	0.66	0.71	0.63	0.10
Co (II)	0.31	0.97	0.91	0.93	0.96	0.99	1.10	0.17
Cr (II)	6.05	1.46	1.43	1.45	1.47	1.47	1.57	0.24
Cu (II)	-4.71	0.92	0.90	0.94	1.00	1.05	0.98	0.15
Fe (II)	-23.95	1.02	1.00	1.05	1.10	1.14	1.13	0.18
Mg (II)	18.09	0.56	0.53	0.58	0.64	0.70	0.62	0.10
Mn (II)	-29.53	1.30	1.25	1.26	1.28	1.29	1.46	0.23
Ni (II)	18.24	0.68	0.67	0.70	0.74	0.77	0.68	0.11
Pb (II)	-47.21	0.04	0.08	0.13	0.17	0.20	0.12	0.02
Ti (II)	-17.11	0.85	0.82	0.85	0.88	0.91	0.95	0.15
Zn (II)	-91.23	1.21	1.14	1.19	1.24	1.27	1.60	0.25
Ar 357nm	-4.22	1.49	1.27	1.16	1.03	0.89	1.87	0.29
Ar 404nm	1.00	1.00	1.00	1.00	1.00	1.00	1.00	0.15
Ar 420nm	-2.91	1.43	1.33	1.25	1.17	1.09	1.60	0.25
Ar 451nm	-0.32	1.42	1.29	1.20	1.10	1.00	1.60	0.25

TABLE 4.3: COMPARISON OF THE POLYNOMIAL PARAMETERS OF THE ANALYTE LINES TO THOSE OF AR 420NM.

Ratio (Parameters of the analyte trendline/parameters of the Ar 404)						FROM THE PCA	
β_0	β_1	β_2	β_3	β_4	β_5	LOADINGS RATIO (anal/Ar)	LOADINGS in PC 1
Al (I) 3.25	0.53	0.56	0.63	0.71	0.81	0.51	0.13
Ca (I) 1.00	0.12	0.15	0.19	0.25	0.32	0.07	0.02
Cd (I) -1.46	0.53	0.53	0.59	0.65	0.73	0.56	0.14
Co (I) -2.24	0.33	0.38	0.47	0.58	0.70	0.33	0.08
Cr (I) 0.48	0.08	0.11	0.16	0.23	0.32	0.05	0.01
Cu (I) 0.33	0.21	0.25	0.31	0.39	0.48	0.18	0.05
Mg (I) 1.42	0.43	0.47	0.52	0.59	0.67	0.41	0.10
Mn (I) -0.80	0.08	0.12	0.17	0.23	0.31	0.05	0.01
Na (I) 2.13	0.07	0.10	0.12	0.16	0.22	-0.04	-0.01
Ni (I) 1.42	0.54	0.58	0.65	0.74	0.84	0.50	0.12
Zn (I) 7.72	0.78	0.80	0.86	0.93	1.01	0.79	0.19
Ba (II) -0.36	1.49	1.54	1.63	1.73	1.84	1.48	0.37
Ba (II) 9.77	1.40	1.40	1.47	1.56	1.66	1.49	0.37
Ca (II) 2.28	0.75	0.78	0.85	0.94	1.03	0.76	0.19
Cd (II) 3.72	0.40	0.44	0.49	0.57	0.65	0.40	0.10
Co (II) -0.11	0.68	0.69	0.74	0.82	0.91	0.69	0.17
Cr (II) -2.08	1.02	1.07	1.16	1.25	1.35	0.99	0.24
Cu (II) 1.62	0.64	0.68	0.75	0.85	0.97	0.62	0.15
Fe (II) 8.22	0.71	0.76	0.83	0.93	1.05	0.71	0.18
Mg (II) -6.21	0.39	0.40	0.46	0.54	0.64	0.39	0.10
Mn (II) 10.14	0.91	0.94	1.01	1.09	1.19	0.92	0.23
Ni (II) -6.26	0.47	0.51	0.56	0.63	0.71	0.43	0.11
Pb (II) 16.21	0.03	0.06	0.11	0.15	0.19	0.07	0.02
Ti (II) 5.88	0.60	0.62	0.68	0.75	0.84	0.60	0.15
Zn (II) 31.33	0.85	0.86	0.95	1.05	1.16	1.00	0.25
Ar 357nm 1.45	1.04	0.96	0.92	0.88	0.82	1.17	0.29
Ar 404nm -0.34	0.70	0.75	0.80	0.85	0.92	0.63	0.15
Ar 420nm 1.00	1.00	1.00	1.00	1.00	1.00	1.00	0.25
Ar 451nm 0.11	0.99	0.97	0.96	0.94	0.91	1.00	0.25

TABLE 4.4: COMPARISON OF THE POLYNOMIAL PARAMETERS

OF THE ANALYTE LINES TO THOSE OF AR 451NM.

| | Ratio (Parameters of the analyte trendline/parameters of the Ar 404) | | | | | | FROM THE PCA | |
| | | | | | | | LOADINGS RATIO (anal/Ar) | LOADINGS in PC 1 |
	β_0	β_1	β_2	β_3	β_4	β_5		
Al (I)	29.89	0.53	0.58	0.66	0.76	0.89	0.51	0.13
Ca (I)	9.19	0.12	0.16	0.20	0.27	0.35	0.07	0.02
Cd (I)	-13.41	0.54	0.55	0.61	0.70	0.80	0.56	0.14
Co (I)	-20.56	0.33	0.39	0.49	0.61	0.76	0.33	0.08
Cr (I)	4.42	0.08	0.11	0.17	0.25	0.35	0.05	0.01
Cu (I)	3.06	0.21	0.26	0.33	0.41	0.53	0.18	0.05
Mg (I)	13.04	0.44	0.48	0.54	0.63	0.74	0.41	0.10
Mn (I)	-7.40	0.08	0.12	0.17	0.25	0.34	0.05	0.01
Na (I)	19.54	0.07	0.11	0.13	0.17	0.24	-0.04	-0.01
Ni (I)	13.04	0.54	0.60	0.68	0.79	0.92	0.50	0.12
Zn (I)	70.96	0.79	0.83	0.90	1.00	1.10	0.79	0.19
Ba (II)	-3.33	1.51	1.58	1.70	1.85	2.01	1.48	0.37
Ba (II)	89.79	1.42	1.44	1.54	1.67	1.81	1.49	0.37
Ca (II)	20.96	0.76	0.80	0.89	1.00	1.13	0.76	0.19
Cd (II)	34.21	0.40	0.45	0.52	0.60	0.71	0.40	0.10
Co (II)	-0.97	0.69	0.71	0.78	0.88	1.00	0.69	0.17
Cr (II)	-19.10	1.03	1.10	1.21	1.33	1.48	0.98	0.24
Cu (II)	14.86	0.65	0.70	0.79	0.90	1.06	0.62	0.15
Fe (II)	75.62	0.72	0.78	0.87	1.00	1.15	0.71	0.18
Mg (II)	-57.11	0.40	0.41	0.48	0.58	0.70	0.39	0.10
Mn (II)	93.23	0.92	0.97	1.05	1.16	1.30	0.91	0.23
Ni (II)	-57.57	0.48	0.52	0.59	0.67	0.78	0.43	0.11
Pb (II)	149.03	0.03	0.06	0.11	0.16	0.20	0.07	0.02
Ti (II)	54.02	0.60	0.64	0.71	0.80	0.92	0.60	0.15
Zn (II)	287.99	0.86	0.89	0.99	1.12	1.27	1.00	0.25
Ar 357nm	13.31	1.05	0.99	0.97	0.94	0.89	1.17	0.29
Ar 404nm	-3.16	0.71	0.77	0.83	0.91	1.00	0.63	0.15
Ar 420nm	9.19	1.01	1.03	1.05	1.07	1.09	1.00	0.25
Ar 451nm	1.00	1.00	1.00	1.00	1.00	1.00	1.00	0.25

4.2.4 DRIFT ESTIMATION AND CORRECTION

The developed correction procedure has been applied to the data set obtained in Chapter 3 when using "standard" experimental conditions, i.e. Experiment 5. It was noted that the drift patterns were similar for all the lines, but with a different gradient at the beginning of the analysis. Figure 4.2 re-plots the drift plot obtained from this data set.

FIGURE 4.2: DRIFT PLOT OBTAINED AT 1000 W & 0.9 $LMIN^{-1}$ CONDITIONS
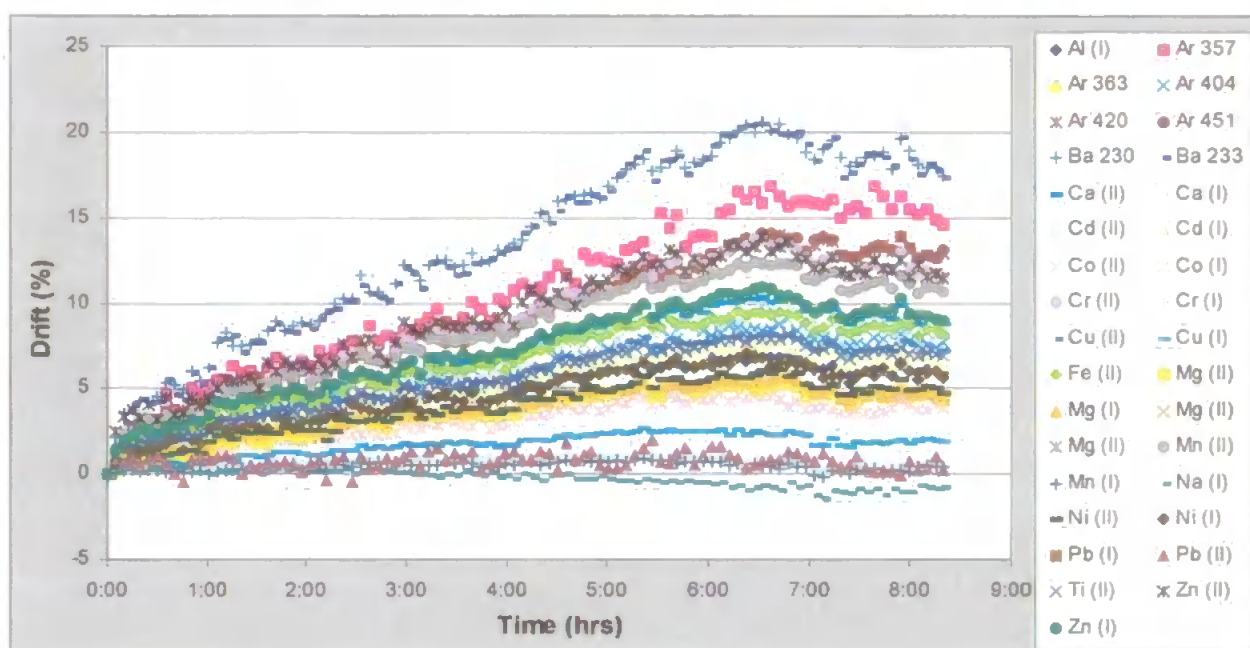
The "estimated drift" for each emission line when using Ar 404nm, Ar 420nm and Ar 451nm drift patterns are shown in Figure 4.3. The remaining drift error after correction has been also plotted as shown in Figure 4.4. It can be observed that the long-term drift drops from around 20% in the original data set, Figure 4.2, to better than 2% after applying the correction procedure. The factors of improvement reached with this correction procedure have been calculated for each argon line employed and are show in Table 4.5. It can be seen that all of the results are very similar regardless of the argon emission line employed.

FIGURE 4.3: DRIFT ESTIMATED USING THE CORRECTION PROCEDURE WITH VARIOUS AR EMISSION LINES

Axes titles common for all the plots: x-axes Time (hrs), y-axes Drift (%)

Ar 404.597 nm

Ar 420.068 nm

Ar 451.074 nm
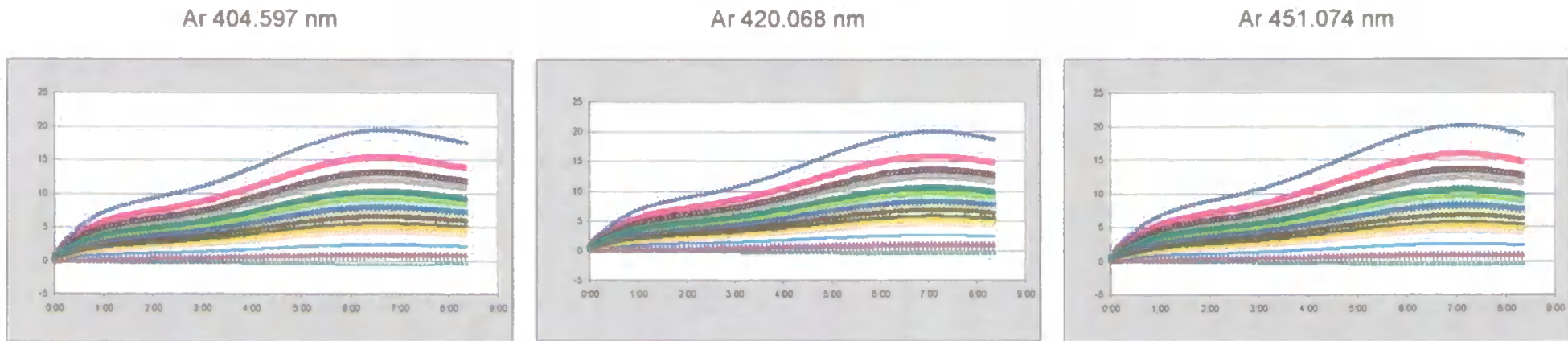
FIGURE 4.4: DRIFT AFTER CORRECTION

Axes titles common for all the plots: x-axes Time (hrs), y-axes Drift (%)

Ar 404.597 nm

Ar 420.068 nm

Ar 451.074 nm
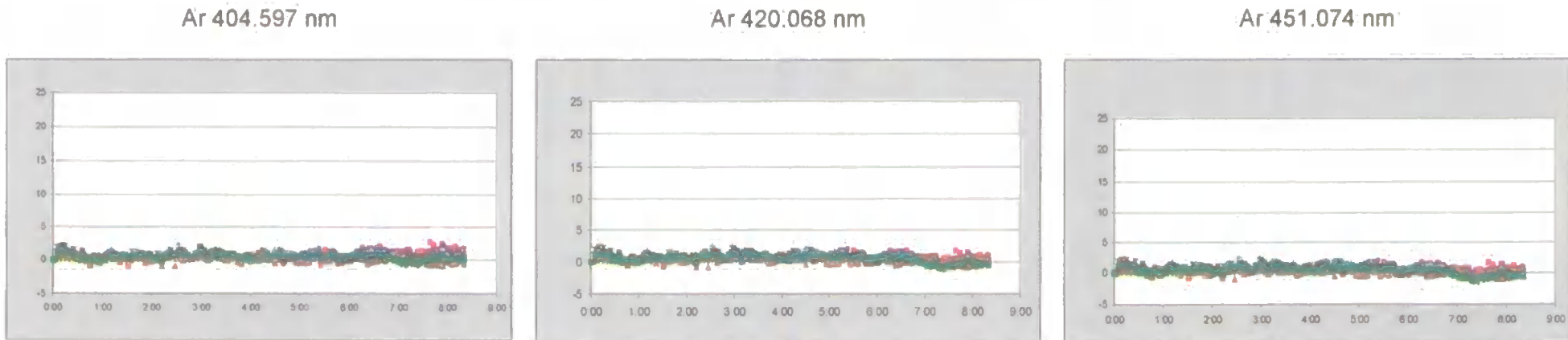
TABLE 4.5: IMPROVEMENT FACTOR AFTER USING THE DRIFT CORRECTION PROCEDURE

	Final Drift Measured	Drift After Correction by			Improvement Factor		
		Ar 404 nm	Ar 420 nm	Ar 451 nm	Ar 404 nm	Ar 420 nm	Ar 451 nm
Al (I)	6.0	0.2	-0.2	-0.2	30	32	31
Ca (I)	0.5	-0.2	-0.3	-0.3	2	2	2
Cd (I)	6.3	0.0	-0.4	-0.4	176	16	16
Co (I)	3.9	0.2	-0.1	-0.1	25	39	39
Cr (I)	0.3	-0.2	-0.3	-0.3	2	1	1
Cu (I)	1.9	-0.1	-0.3	-0.3	13	7	7
Mg (I)	4.6	0.0	-0.3	-0.3	174	13	13
Mn (I)	0.4	-0.1	-0.2	-0.2	3	2	2
Na (I)	-0.8	-0.3	-0.3	-0.3	2	2	2
Ni (I)	5.6	0.0	-0.4	-0.4	725	15	15
Zn (I)	9.0	0.2	-0.4	-0.4	58	21	21
Ba 230	17.5	0.8	-0.2	-0.2	21	99	94
Ba 233	17.4	0.7	-0.3	-0.3	24	56	54
Ca (II)	8.8	0.3	-0.3	-0.3	34	29	29
Cd (II)	4.4	0.0	-0.3	-0.3	102	13	13
Co (II)	8.2	0.4	-0.1	-0.1	19	102	97
Cr (II)	11.5	0.5	-0.2	-0.2	25	48	47
Cu (II)	7.2	0.3	-0.2	-0.2	26	38	38
Fe (II)	8.2	0.2	-0.3	-0.3	34	29	28
Mg (II)	4.4	0.0	-0.3	-0.3	412	15	15
Mn (II)	10.6	0.4	-0.3	-0.3	28	37	36
Ni (II)	4.8	0.0	-0.3	-0.3	957	14	14
Pb (II)	0.2	-0.6	-0.7	-0.7	0	0	0
Ti (II)	6.9	0.2	-0.2	-0.2	29	34	33
Zn (II)	11.4	0.2	-0.5	-0.5	50	23	23

4.2.5 VALIDATION OF THE CORRECTION PROCEDURE

The application of the new correction procedure to other data sets has also been checked. Two additional data sets were produced at standard conditions. The only difference in terms of experimental procedure in this study was the control of the room temperature during the analysis. For this work a temperature control system (i.e. full air conditioning) was available in our laboratory, and therefore data was obtained under cooler and fixed conditions.

FIGURE 4.5: DRIFT PLOT OF SECOND DATA SET OBTAINED AT STANDARD CONDITIONS
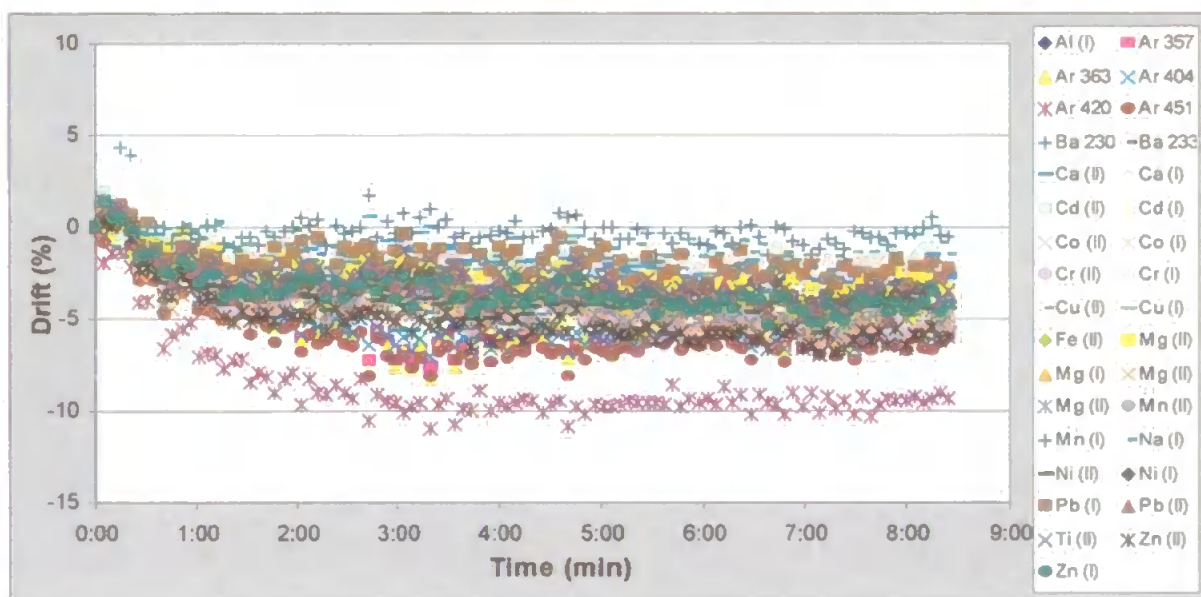
Figure 4.5 shows the drift plot obtained when the standard conditions were replicated. The drift plot is considerably different from that obtained in the previous study using similar instrumental conditions. First of all, the instrument shows a much more stable behaviour, with drift values of around 5 to 10% over the experimental run. A downward trend in the drift is also observed in contrast with the "continuous warm up" recorded previously. The cooler laboratory temperature for this work (T = 20C) is the most probable cause for the higher stability. However despite these differences between data sets, some pattern characteristics are reproduced such us the high inter-element correlation between emission lines and a similar effect in the slope or gradient.

The third data set obtained using standard conditions is plotted in Figure 4.6. In this case, the instrument showed a more unstable behaviour with drift values up to 15%. Drift patterns resemble to those recorded on the first data set performed using these conditions (Figure 4.2).

FIGURE 4.6: THIRD DATA SET OBTAINED AT STANDARD CONDITIONS
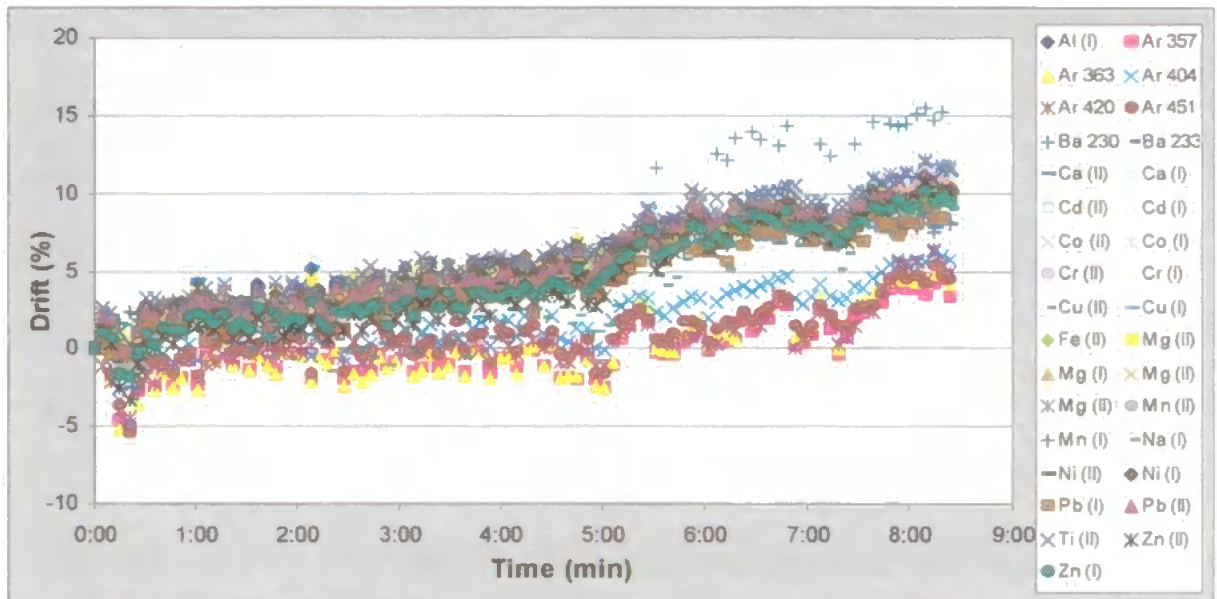
The correction procedure has again been applied to these data sets. Drift estimation and drift after correction plots are shown in Figure 4.7 and Figure 4.8 respectively for the second data set and Figure 4.9 and Figure 4.10 for the third data set. It is important to note that the correction procedure improves the accuracy even when correcting lower levels of errors. Difficulties were encountered when using the third data set and the argon line at 420 nm due to a poor fit of the polynomial, which leads to errors in correction.

The improvement factors obtained when using the correction procedure are detailed in Table 4.6 and Table 4.7 for the second and the third data set, respectively.

FIGURE 4.7: SECOND DATA SET. DRIFT ESTIMATED USING THE CORRECTION PROCEDURE WITH VARIOUS AR EMISSION LINES

Axes titles common for all the plots: x-axes Time (hrs), y-axes Drift (%)

Ar 404.597 nm

Ar 420.068 nm

Ar 451.074 nm
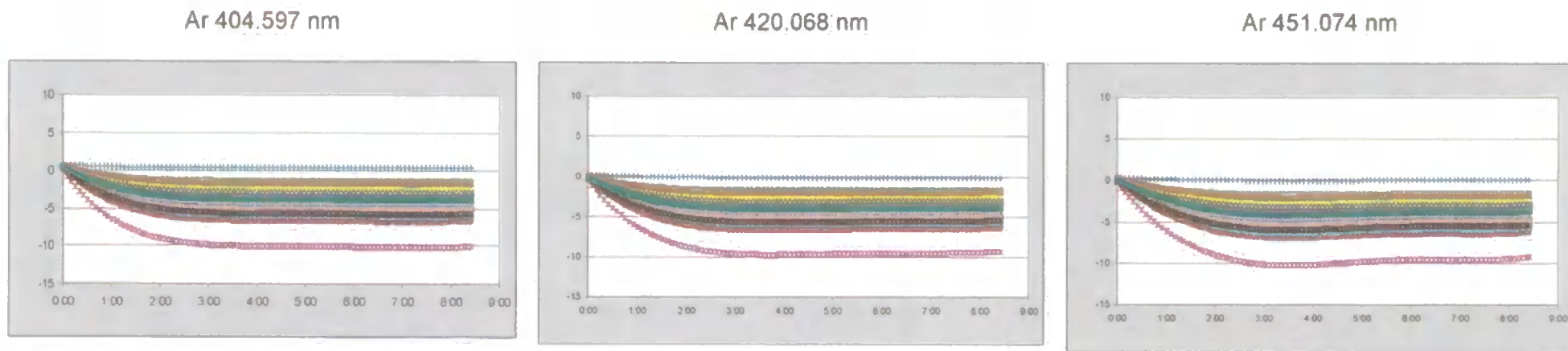
FIGURE 4.8: SECOND DATA SET. DRIFT AFTER CORRECTION

Axes titles common for all the plots: x-axes Time (hrs), y-axes Drift (%)

Ar 404.597 nm

Ar 420.068 nm

Ar 451.074 nm
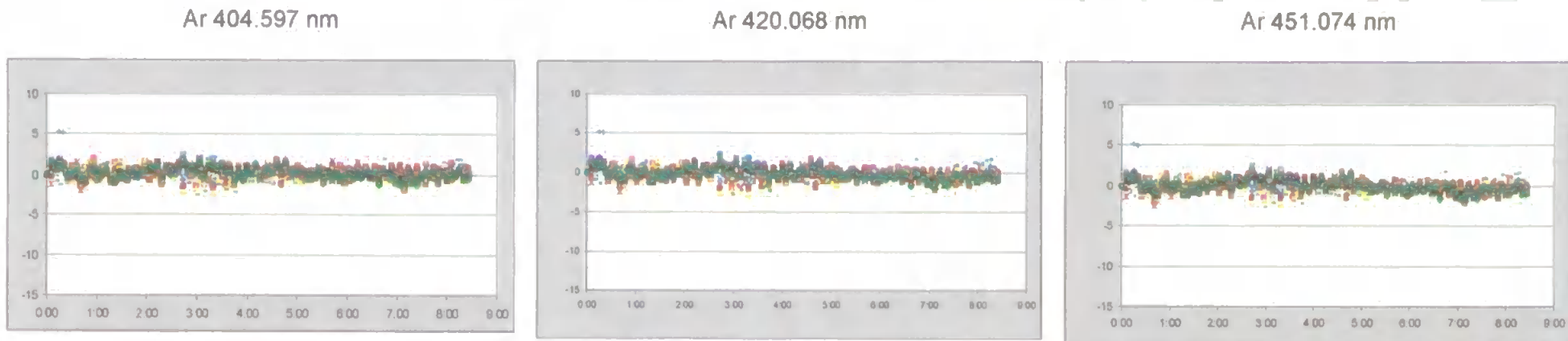
FIGURE 4.9: THIRD DATA SET. DRIFT ESTIMATED USING THE CORRECTION PROCEDURE WITH VARIOUS AR EMISSION LINES

Axes titles common for all the plots: x-axes Time (hrs), y-axes Drift (%)

Ar 404.597 nm

Ar 420.068 nm

Ar 451.074 nm
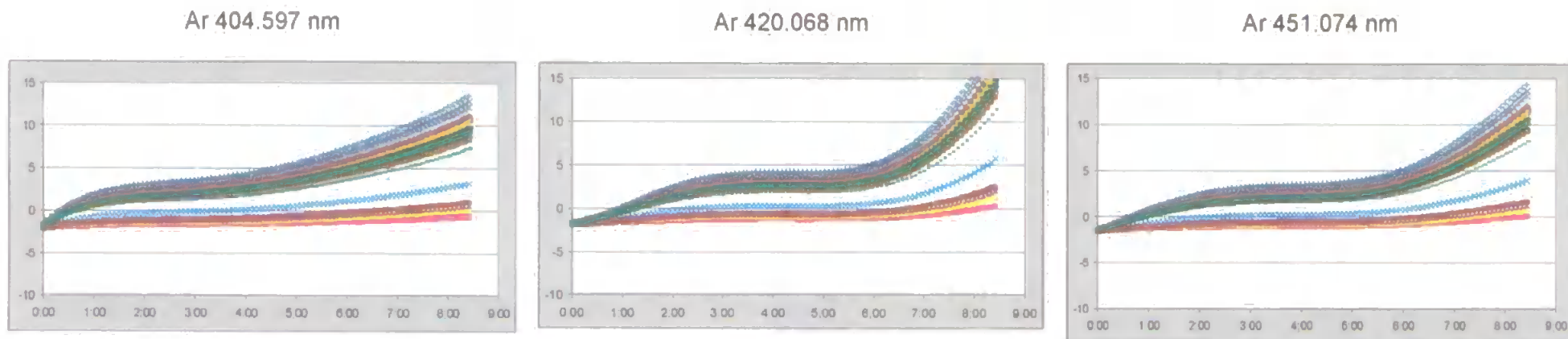
FIGURE 4.10: THIRD DATA SET. DRIFT AFTER CORRECTION.

Axes titles common for all the plots: x-axes Time (hrs), y-axes Drift (%)

Ar 404.597 nm

Ar 420.068 nm

Ar 451.074 nm
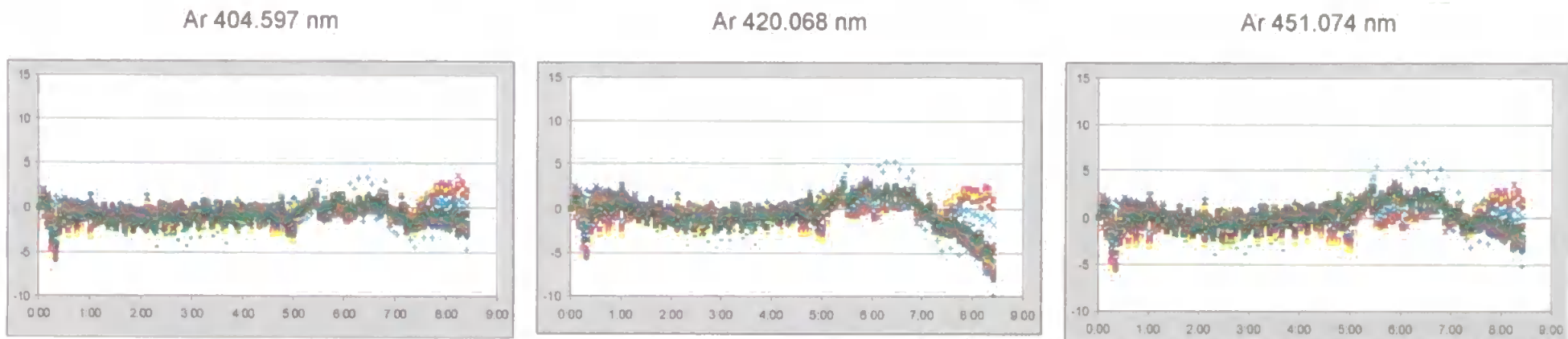
TABLE 4.6: SECOND DATA SET.

IMPROVEMENT FACTORS AFTER USING THE CORRECTION PROCEDURE

	Final Drift Measured	Drift After Correction with			Improvement Factor		
		Ar 404 nm	Ar 420 nm	Ar 451 nm	Ar 404 nm	Ar 420 nm	Ar 451 nm
Al (I)	-3.4	0.0	-0.4	-0.4	114	8	9
Ca (I)	-1.9	0.1	-0.1	-0.1	22	14	16
Cd (I)	-4.7	0.1	-0.4	-0.4	44	11	12
Co (I)	-2.3	-0.3	-0.5	-0.5	8	4	5
Cr (I)	-2.2	-0.5	-0.7	-0.7	4	3	3
Cu (I)	-2.9	-0.8	-1.0	-1.0	4	3	3
Mg (I)	-4.6	-0.4	-0.9	-0.9	11	5	5
Mn (I)	-0.6	-0.2	-0.2	-0.2	3	2	2
Na (I)	-1.5	0.3	0.1	0.1	5	15	13
Ni (I)	-3.9	-0.2	-0.6	-0.6	18	6	6
Zn (I)	-4.3	-0.1	-0.5	-0.5	58	8	8
Ba 230	-4.2	-0.1	-0.5	-0.5	53	8	8
Ba 233	-4.1	-0.3	-0.7	-0.7	16	6	6
Ca (II)	-5.5	-0.1	-0.7	-0.7	48	7	8
Cd (II)	-4.1	-0.4	-0.8	-0.8	10	5	5
Co (II)	-4.5	0.0	-0.5	-0.5	271	9	9
Cr (II)	-5.5	-0.3	-0.9	-0.8	20	6	7
Cu (II)	-2.7	0.0	-0.3	-0.3	404	9	9
Fe (II)	-4.6	-0.7	-1.1	-1.1	7	4	4
Mg (II)	-3.3	-0.3	-0.6	-0.6	12	5	6
Mn (II)	-4.6	-0.5	-0.9	-0.9	9	5	5
Ni (II)	-4.5	0.0	-0.5	-0.5	246	9	9
Pb (II)	-3.7	0.1	-0.3	-0.3	34	11	13
Ti (II)	-3.5	-0.1	-0.5	-0.5	28	7	7
Zn (II)	-6.0	-0.1	-0.8	-0.7	67	8	8

TABLE 4.7: THIRD DATA SET.

IMPROVEMENT FACTORS AFTER USING THE CORRECTION PROCEDURE.

	Final Drift Measured	Drift After Correction with			Improvement Factor		
		Ar 404 nm	Ar 420 nm	Ar 451 nm	Ar 404 nm	Ar 420 nm	Ar 451 nm
Al (I)	10.2	-3.1	-8.0	-3.5	3	1	3
Ca (I)	11.1	-2.3	-7.2	-2.7	5	2	4
Cd (I)	10.5	-1.5	-5.9	-1.9	7	2	6
Co (I)	8.3	-2.2	-6.1	-2.5	4	1	3
Cr (I)	9.1	-3.1	-7.6	-3.4	3	1	3
Cu (I)	8.0	-3.0	-7.1	-3.3	3	1	2
Mg (I)	9.9	-2.3	-6.8	-2.7	4	1	4
Mn (I)	8.0	-3.2	-7.4	-3.5	2	1	2
Na (I)	9.0	-0.4	-3.9	-0.6	25	2	14
Ni (I)	10.3	-2.5	-7.2	-2.9	4	1	4
Zn (I)	9.4	-1.7	-5.9	-2.0	5	2	5
Ba 230	10.1	-4.7	-9.9	-5.1	2	1	2
Ba 233	10.1	-2.2	-6.7	-2.5	5	2	4
Ca (II)	11.1	-1.6	-6.2	-1.9	7	2	6
Cd (II)	9.9	-1.8	-6.1	-2.1	5	2	5
Co (II)	10.0	-2.0	-6.4	-2.4	5	2	4
Cr (II)	10.3	-1.9	-6.4	-2.2	5	2	5
Cu (II)	8.9	-2.5	-6.8	-2.9	4	1	3
Fe (II)	9.9	-2.1	-6.6	-2.5	5	2	4
Mg (II)	10.1	-2.3	-6.8	-2.6	4	1	4
Mn (II)	9.3	-2.0	-6.2	-2.3	5	1	4
Ni (II)	10.0	-1.6	-5.9	-1.9	6	2	5
Pb (II)	10.4	-2.5	-7.2	-2.8	4	1	4
Ti (II)	11.5	-2.9	-8.0	-3.3	4	1	3
Zn (II)	10.1	-0.8	-4.9	-1.2	12	2	9

4.2.6 FURTHER STUDY OF THE CORRECTION FACTOR

Although the developed correction procedure successfully corrects most of the drift, it will not have any practical utility unless the correction factors are exportable for one data set to another. Unfortunately, this is not the case. Table 4.8 shows the correction factor calculated on the three data sets obtained at standard conditions for the three argon lines employed in the correction procedure. Severe differences between the three data sets are observed.

TABLE 4.8: COMPARISON OF THE SPECIFIC CORRECTION FACTORS ON THE THREE DATA SETS

	1st Data Set Correction Factor using			2nd Data Set Correction Factor using			3rd Data Set Correction Factor using		
	Ar 404 nm	Ar 420 nm	Ar 451 nm	Ar 404 nm	Ar 420 nm	Ar 451 nm	Ar 404 nm	Ar 420 nm	Ar 451 nm
Al (I)	0.82	0.51	0.51	0.53	0.34	0.49	2.58	5.07	4.39
Ca (I)	0.11	0.07	0.07	0.32	0.20	0.29	2.57	5.05	4.38
Cd (I)	0.89	0.56	0.56	0.76	0.48	0.69	2.28	4.49	3.89
Co (I)	0.53	0.33	0.33	0.32	0.20	0.29	2.01	3.95	3.42
Cr (I)	0.08	0.05	0.05	0.26	0.16	0.24	2.36	4.63	4.02
Cu (I)	0.30	0.18	0.18	0.33	0.21	0.31	2.12	4.17	3.62
Mg (I)	0.65	0.41	0.41	0.66	0.42	0.60	2.34	4.61	4.00
Mn (I)	0.07	0.05	0.05	0.06	0.04	0.05	2.16	4.25	3.69
Na (I)	-0.06	-0.04	-0.04	0.28	0.18	0.26	1.76	3.46	3.00
Ni (I)	0.80	0.50	0.50	0.59	0.37	0.54	2.46	4.84	4.20
Zn (I)	1.26	0.79	0.79	0.66	0.42	0.60	2.12	4.16	3.61
Ba 230	2.37	1.48	1.48	0.64	0.41	0.59	2.90	5.70	4.94
Ba 233	2.38	1.49	1.49	0.61	0.39	0.56	2.34	4.60	3.99
Ca (II)	1.21	0.76	0.76	0.85	0.54	0.78	2.40	4.72	4.09
Cd (II)	0.63	0.40	0.40	0.58	0.37	0.53	2.23	4.38	3.80
Co (II)	1.10	0.69	0.69	0.70	0.44	0.64	2.30	4.52	3.92
Cr (II)	1.57	0.99	0.98	0.83	0.52	0.76	2.33	4.58	3.97
Cu (II)	0.98	0.62	0.62	0.42	0.26	0.38	2.20	4.33	3.76
Fe (II)	1.13	0.71	0.71	0.62	0.39	0.57	2.30	4.52	3.92
Mg (II)	0.62	0.39	0.39	0.49	0.31	0.44	2.37	4.65	4.03
Mn (II)	1.46	0.92	0.91	0.64	0.41	0.59	2.15	4.23	3.67
Ni (II)	0.68	0.43	0.43	0.71	0.45	0.65	2.21	4.35	3.77
Pb (II)	0.12	0.07	0.07	0.60	0.38	0.55	2.46	4.84	4.20
Ti (II)	0.95	0.60	0.60	0.53	0.34	0.48	2.77	5.44	4.72
Zn (II)	1.60	1.00	1.00	0.94	0.59	0.86	2.07	4.07	3.53
Ar 357 nm	1.87	1.17	1.17	0.95	0.60	0.87	0.28	0.55	0.48
Ar 404 nm	1.00	0.63	0.63	1.00	0.63	0.91	1.00	1.97	1.70
Ar 420 nm	1.60	1.00	1.00	1.58	1.00	1.44	0.51	1.00	0.87
Ar 451 nm	1.60	1.00	1.00	1.09	0.69	1.00	0.59	1.15	1.00

Despite these differences, an attempt was made to estimate specific correction factors using physical characteristics of the emission lines.

Using the first data set obtained under standard conditions, different patterns were observed for atomic and ionic emission lines in terms of drift bias. If the range of variation for each emission line is plotted, Figure 4.11, it can be seen that the atomic lines are more stable than the ionic lines. This feature is almost certainly due to the low RF power employed (1000 W), which tends to make hard lines more vulnerable to drift. As can be seen in Figure 4.11, the variation in the sequence of lines is not random, and so some physical characteristic of the emission lines probably accounts for these differences.

FIGURE 4.11: RANGES OF VARIATION FOR EACH MONITORED EMISSION LINE
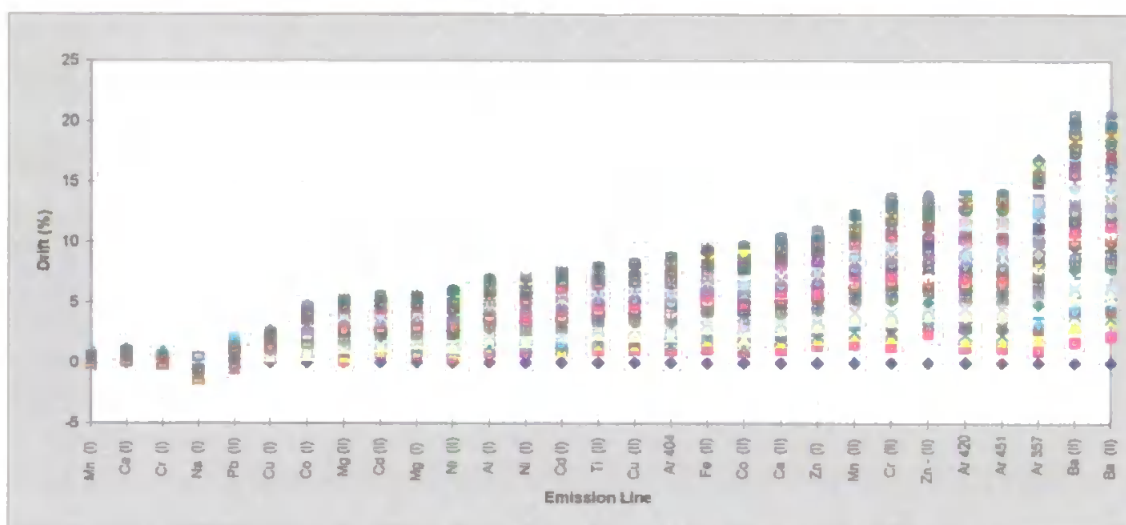
A number of fundamental properties related to the emission lines under study were therefore correlated to the variation sequence, e.g. emission energy, excitation energy, ionisation potentials and intensity of the lines, in order to estimate the correction factor. Figure 4.12 plots the calculated correction factor against the energy associated with each emission line. The excitation energy (E_{exc}) was used for the atomic lines, and the energy sum, E_{sum}, excitation energy plus the ionisation potential (IP) for the ionic emission lines.

FIGURE 4.12: CORRECTION FACTOR VERSUS ENERGY SUM (E_{EXC} + IP)
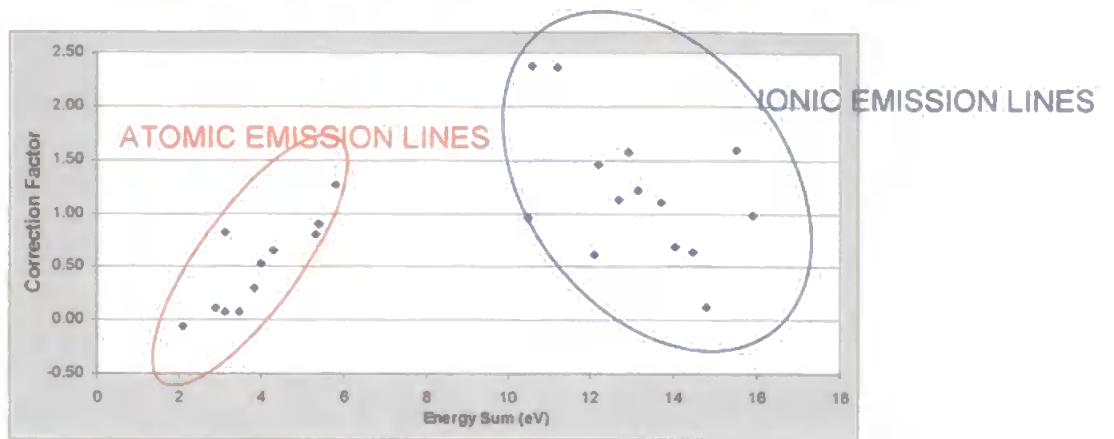
Lines may be separated according to their excitation energy in two groups, atomic and ionic. Some correlation is observed within each group between the experimentally calculated correction factor and the excitation energy associated with each transition. Figure 4.13 shows the linear regression between this two factors.

FIGURE 4.13: LINEAR REGRESSION BETWEEN F_I AND E_{SUM} OF THE EMISSION LINES.

A) ATOMIC LINES
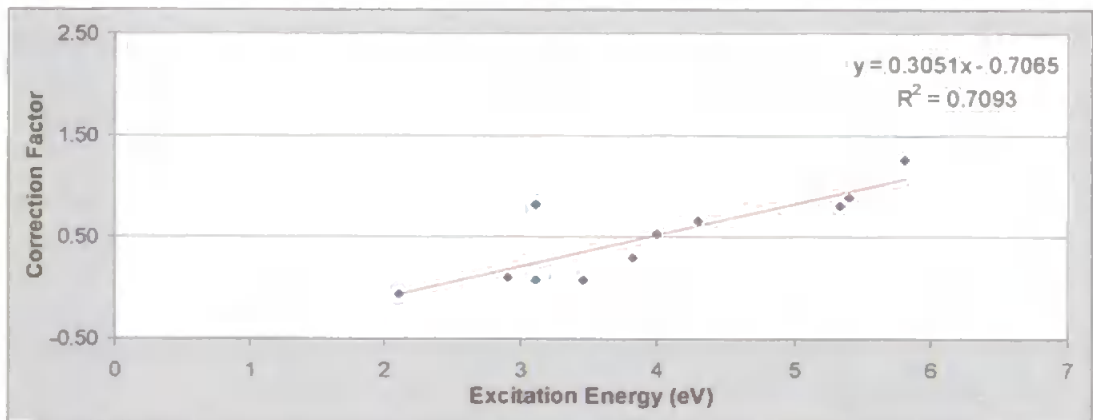
B) IONIC LINES
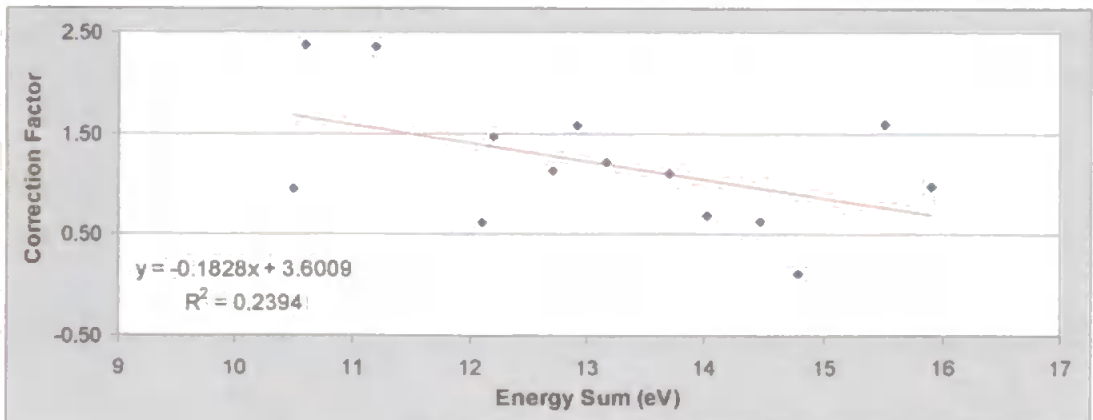
The relationships are far from linear, however, the regression may be improved by the exclusion of the five emission lines, one atomic and four ionic.

FIGURE 4.14: LINEAR REGRESSION BETWEEN F_i AND E_{SUM} OF THE EMISSION LINES AFTER EXCLUSION OF OUTLIERS.

A) ATOMIC LINES EXCEPT AL(I)   B) IONIC LINES EXCEPT CU, MG, TI, ZN
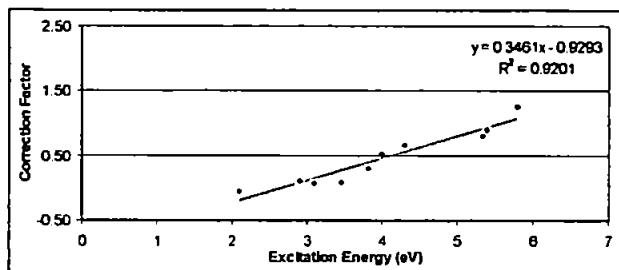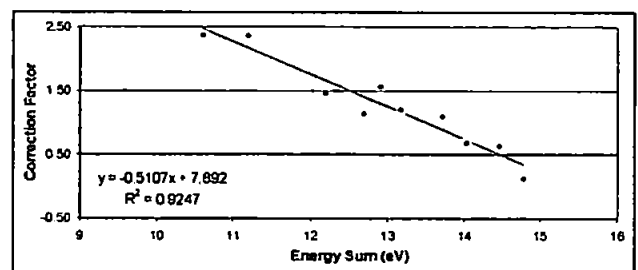
Although, some correlation is observed, the sequence of lines according to their variation range is not reproducible, i.e. differences are observed from one experiment to another. For this reason a theoretical calculation of f_i will not be possible, even if some similarities between long-term stability and the energetic characteristic of the emission lines can be found for the data set obtained at standard conditions.

Therefore from this study we can conclude the following:

➢ f_i is directly proportional to the drift of the line

➢ f_i is indirectly proportional to the drift of an argon correcting line

➢ and in terms of energy:

  • For atomic lines, f_i increases with the excitation energy

  • For ionic lines, f_i slightly decreases with the energy sum (E_{exc} + IP)

4.3 DRIFT CORRECTION AT ROBUST CONDITIONS

The three data sets obtained at robust or moderately robust conditions presented similar drift patterns. In every case, the emission lines were split into two groups according to their drift patterns. The first group contained all of the analyte lines (independent of atom or ion lines), and the second group the four argon emissions. Moreover, very high correlation was observed between all of the lines in a group. Figure 4.15 re-plots the three data sets obtained at robust conditions (taken from Figure 3.17).

FIGURE 4.15: DRIFT PATTERNS OBSERVED WHEN WORKING AT ROBUST CONDITIONS.

| RF 1375 W | RF 1250 W | RF 1500 W |
| Neb. Gas Flow 0.75 Lmin^{-1} | Neb. Gas Flow 0.60 Lmin^{-1} | Neb. Gas Flow 0.60 Lmin^{-1} |
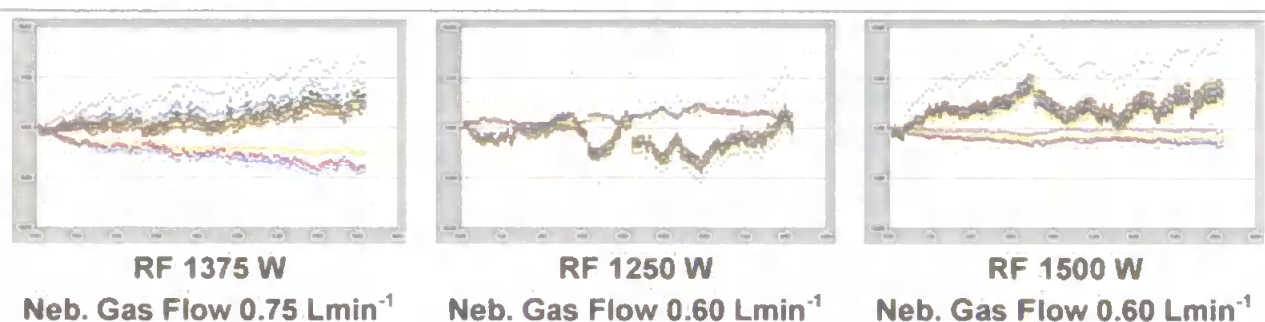
The low nebuliser flow rate employed in these experiments probably explains this separation since argon lines are not necessarily involved in the nebulisation process. Clearly, this kind of drift pattern would allow for a single internal standard to be used to correct for drift. None of the lines used in this study would fulfil the analytical conditions to be used as internal standard, i.e. all the elements studied may be present in real samples and thus not suitable as internal standards. However, in order to quantify the improvement when correcting for long-term drift by internal standardisation, one of the emission lines monitored has been used as an internal standard. A purist criterion for selection of an appropriate internal standard would include the same type of line[206] (either atom or ion). Considering the drift plots shown in Figure 4.15 however, this consideration may not be necessary because of the high correlation observed between all lines, independently of their nature. This is in agreement with the work of Mermet *et al.*[69], which reports the advantages of working at robust conditions to achieve effective internal standardisation.

Of the emission lines studied, Mg II was selected as internal standard. In addition, the potential of using argon lines to correct for drift was also estimated by employing the Ar 420.068 nm line as an internal standard. This approach could be of special interest for the data set obtained at moderately robust conditions (RF power: 1375W, nebuliser flow rate: 1.05Lmin^{-1}), where a high negative correlation was observed between the analyte and the argon emission lines (see Table 3.13).

4.3.1 INTERNAL STANDARDISATION USING A MG ION LINE

Figure 4.16 to Figure 4.18 show the improvements obtained when correcting drift at robust or moderately robust conditions using Mg (II) as internal standard. Drift trends are completely removed with the exception of the sodium line in data sets from Experiments 4 and 12, where some error remains after correction. A poor correction is also obtained for emission line Mn (I) on data set 7.

FIGURE 4.16: DRIFT ON ANALYTE LINES (EXPERIMENT 4) BEFORE AND AFTER CORRECTION BY INTERNAL STANDARDISATION USING MG(II).

Axes titles: x-axes Time (hrs), y-axes Drift (%)
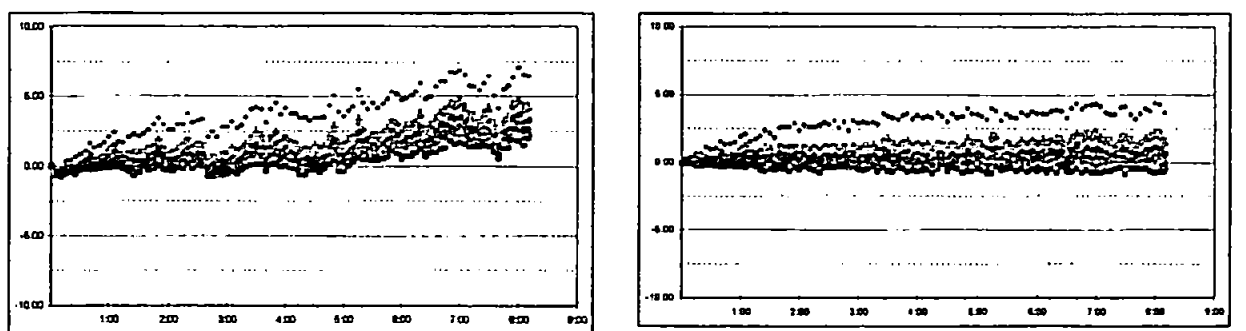
FIGURE 4.17: DRIFT ON ANALYTE LINES (EXPERIMENT 7) BEFORE AND AFTER CORRECTION BY INTERNAL STANDARDISATION USING MG(II).

Axes titles: x-axes Time (hrs), y-axes Drift (%)
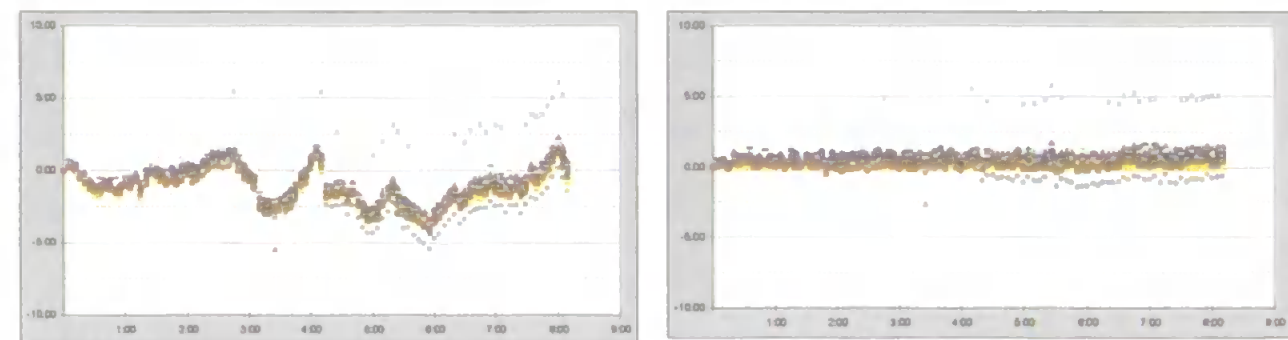
FIGURE 4.18: DRIFT ON ANALYTE LINES (EXPERIMENT 12) BEFORE AND AFTER CORRECTION BY INTERNAL STANDARDISATION USING MG(II).

Axes titles: x-axes Time (hrs), y-axes Drift (%)
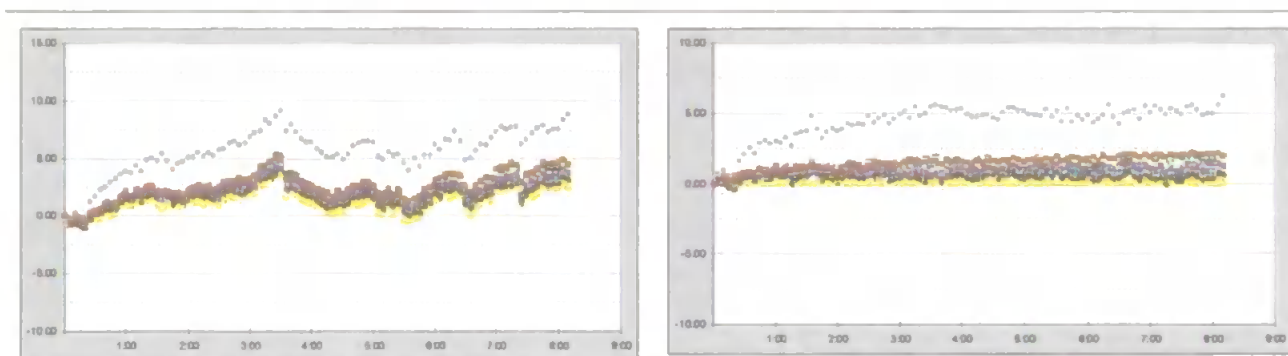
4.3.2 INTERNAL STANDARDISATION USING THE AR 420 NM LINE

When an argon line was employed as an internal standard, no successful correction was achieved except in the case of Experiment 4. Here the use of the inverse of argon intensity as an internal standard partially removes some of the drift. However, the correction is less effective than when using an analyte emission line as the internal standard.

FIGURE 4.19: COMPARISON OF DRIFT CORRECTION BY MG LINE AND (1/AR) INTENSITY.

Axes titles: x-axes Time (hrs), y-axes Drift (%)

A) DRIFT CORRECTED BY MG^{II}
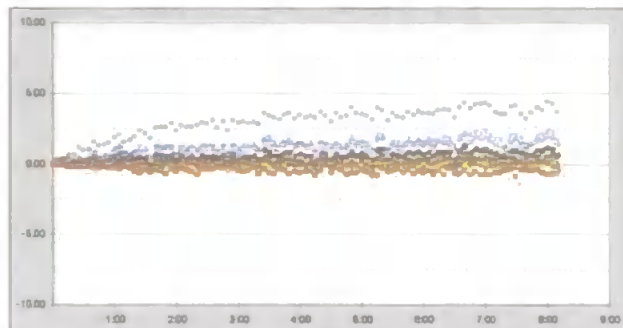
B) DRIFT CORRECTED BY 1/AR^{420}
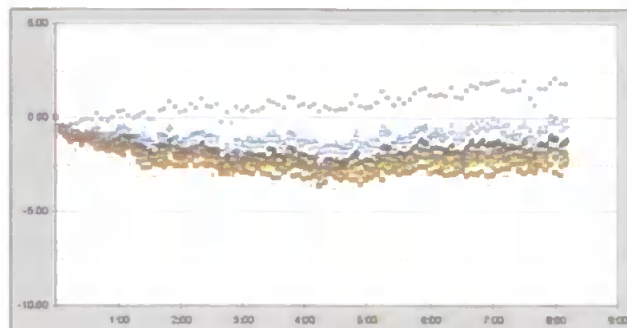
4.4 DRIFT CORRECTION AT OTHER CONDITIONS

In Sections 4.2 and 4.3 drift correction was attempted for data sets obtained at standard and robust conditions. However from the drift mapping at different instrumental conditions plotted in Figure 3.17, it is clear that other instrumental conditions may also require a drift correction. Among the data sets obtained, some operating conditions give rise to stable data sets which do not necessitate drift correction. This was the case for drift diagnoses experiments at Central Conditions (RF power 1250 W and nebuliser gas flow rate 0.9 Lmin^{-1}). In addition, data sets from Experiments 2 and 6, obtained at 1125 W, 0.75 Lmin^{-1} and 1250 W, 1.2 Lmin^{-1} respectively presented quite stable drift patterns. Figure 4.20 re-plots the drift patterns obtained at these operating conditions.

FIGURE 4.20: THE MOST STABLE DATA SETS

Central Conditions (A)	Experiment 2 Data Set	Experiment 6 Data Set
RF 1250 W	RF 1125 W	RF 1250 W
Neb. Gas Flow 0.9 Lmin^{-1}	Neb. Gas Flow 0.75 Lmin^{-1}	Neb. Gas Flow 1.2 Lmin^{-1}
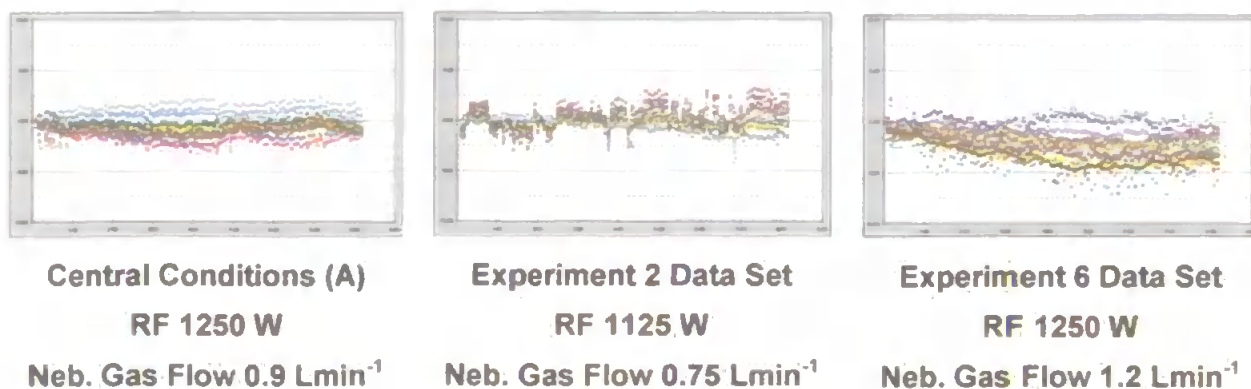
However, sets of instrumental conditions produced signals where drift bias can not be neglected and drift correction will be required if the re-calibration step is to be avoided. This was the case when working at high RF power and nebuliser gas flow rate, as in Experiment 3 & 8 (Figure 4.21).

FIGURE 4.21: DRIFT PATTERNS WHEN WORKING UNDER HIGH RF AND HIGH NEBULISER FLOW.

Axes titles: x-axes Time (hrs), y-axes Drift (%)
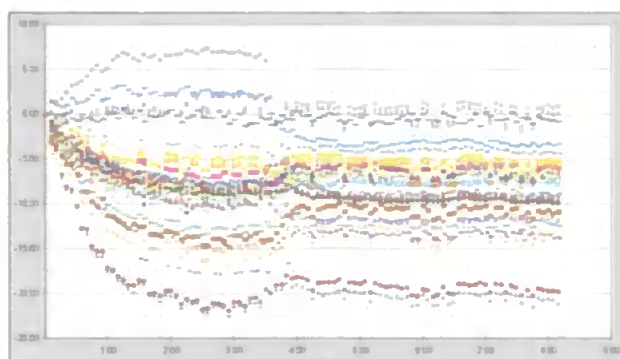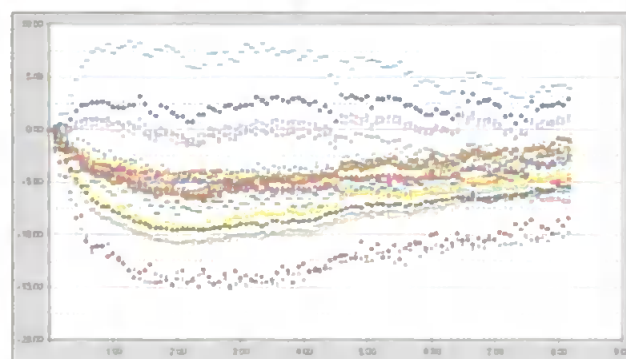
Experiment 3 Data Set	Experiment 11 Data Set
RF 1375 W	RF 1500 W
Neb. Gas Flow 1.05 Lmin^{-1}	Neb. Gas Flow 1.2 Lmin^{-1}

The mathematical procedure developed for drift correction at standard conditions (Section 4.2.1) has been applied to these two data sets.

Figure 4.22 to Figure 4.25 show the estimated and the drift after correction when using the correction procedure. Although removal of some of the drift is achieved, the correction is not as good as when using the standard condition data sets.

FIGURE 4.22: EXPERIMENT 3 DATA SET. (RF 1375 W & NEBULISER GAS FLOW 1.05LMIN^{-1})

DRIFT ESTIMATED USING THE CORRECTION PROCEDURE WITH VARIOUS AR EMISSION LINES

Axes titles: x-axes Time (hrs), y-axes Drift (%)

Ar 404.597 nm   Ar 420.068 nm   Ar 451.074 nm
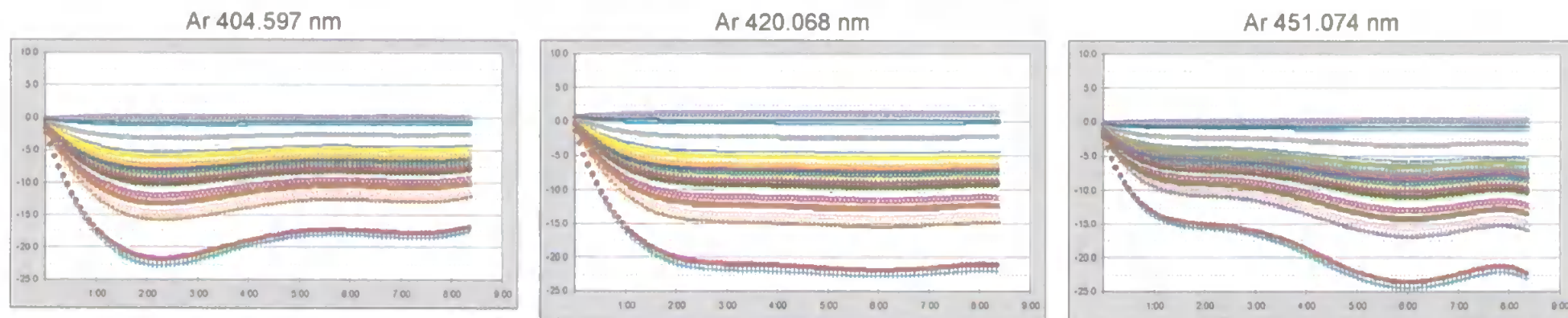
FIGURE 4.23: EXPERIMENT 3 DATA SET. (RF 1375 W & NEBULISER GAS FLOW 1.05LMIN^{-1} DRIFT AFTER CORRECTION.

Axes titles: x-axes Time (hrs), y-axes Drift (%)

Ar 404.597 nm   Ar 420.068 nm   Ar 451.074 nm
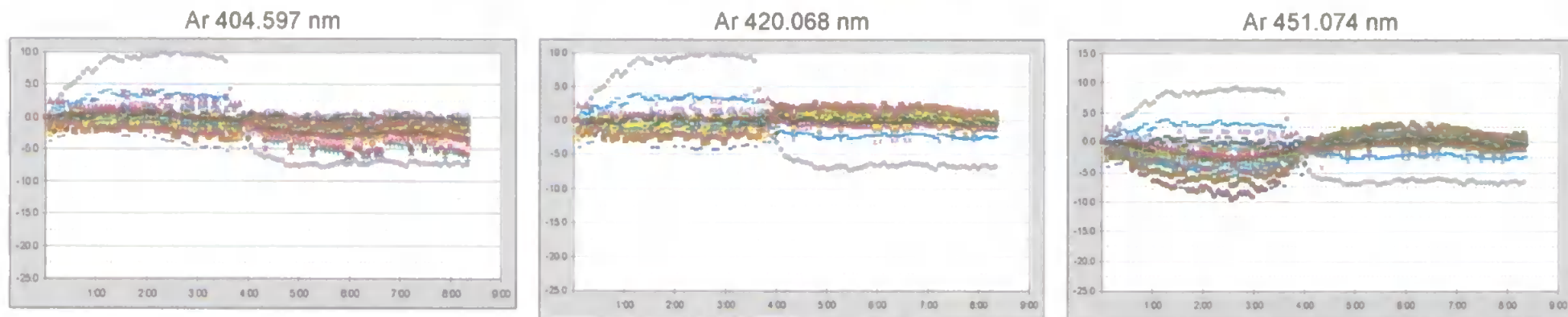
FIGURE 4.24: EXPERIMENT 11 DATA SET. (RF 1500 W & NEBULISER GAS FLOW 1.2 LMIN^{-1}) DRIFT ESTIMATED USING THE CORRECTION PROCEDURE WITH VARIOUS AR EMISSION LINES

Axes titles: x-axes Time (hrs), y-axes Drift (%)
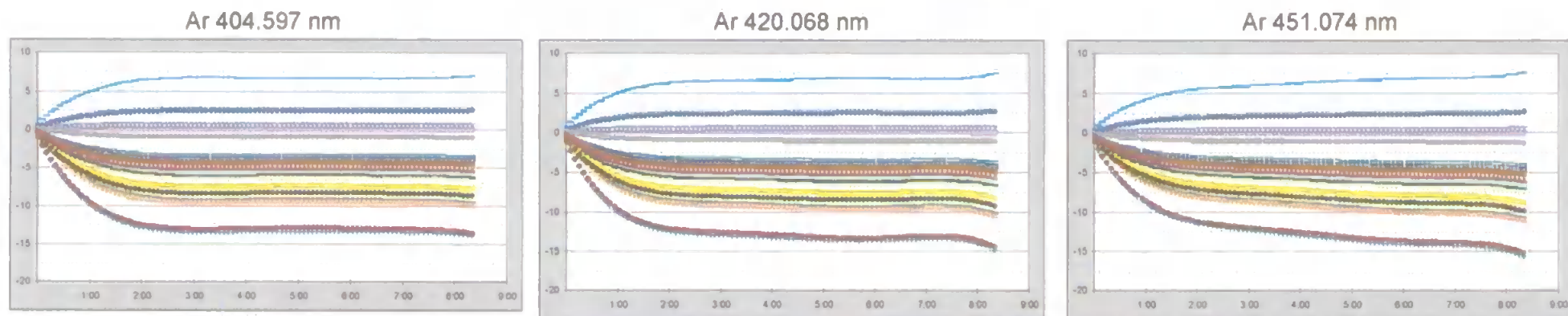
FIGURE 4.25: EXPERIMENT 11 DATA SET. (RF 1500 W & NEBULISER GAS FLOW 1.2LMIN^{-1} DRIFT AFTER CORRECTION.

Axes titles: x-axes Time (hrs), y-axes Drift (%)
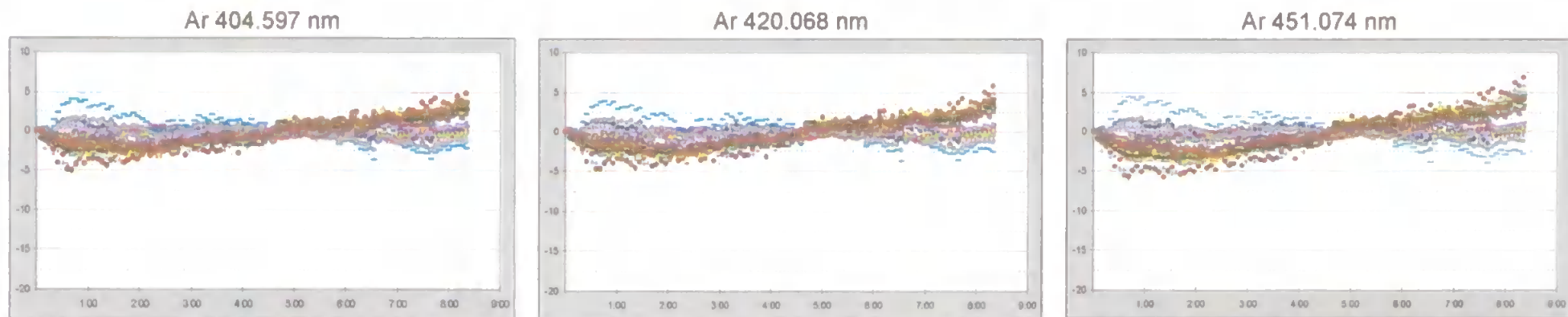
Finally, the data sets obtained from Experiments 1, 8 and 9 present a more complicated situation. At these instrumental conditions, complex drift patterns were recorded with drift values around 5%. At such conditions, drift correction may be convenient but difficult to achieve. Regular recalibration is probably the best option when these conditions are required for ICP-AES analysis.

FIGURE 4.26: EXAMPLES OF COMPLEX DRIFT PATTERNS
WHICH MAY REQUIRED RE-CALIBRATION

Experiment 1 Data Set	**Experiment 8 Data Set**	**Experiment 9 Data Set**
RF 1125 W	**RF 1500 W**	**RF 1000 W**
Neb. Gas Flow 1.05 Lmin^{-1}	**Neb. Gas Flow 0.9 Lmin^{-1}**	**Neb. Gas Flow 1.2 Lmin^{-1}**
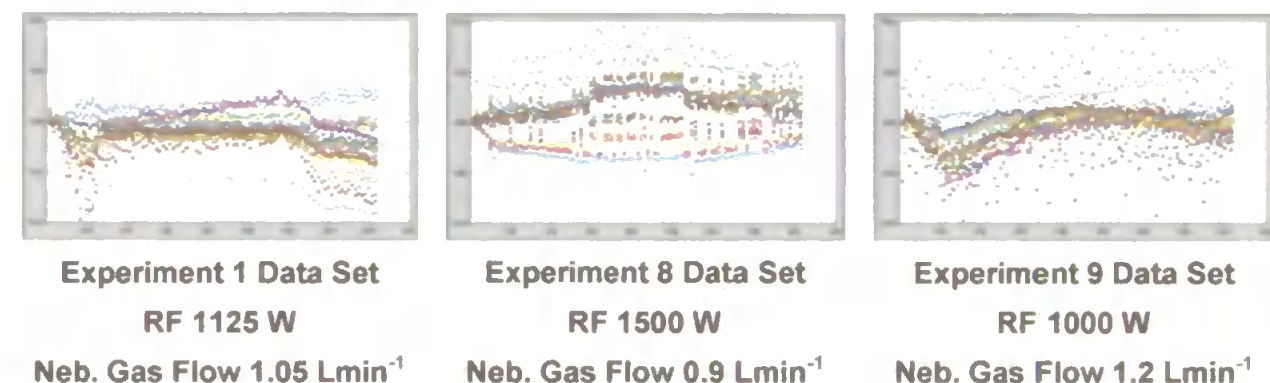
4.5 SUMMARY

The operating parameters selected for elemental analysis by ICP-AES will condition not only the long-term stability of the instrument but also the applicability of a drift correction method. The suggested correction procedure has been shown to successfully remove most of the drift from the data when using standard instrumental conditions. The procedure, which employs the drift pattern of an intrinsic plasma line, can also be applied to those conditions were moderate to high nebuliser flows are employed.

CHAPTER 5

MATRIX EFFECTS

5.1 INTRODUCTION

Matrix effects refer to induced changes in the determination of an analyte due to the sample major species. Acids and easily ionised elements are commonly found in the sample matrix during elemental analysis. Acids are often involved in the sample preparation step, i.e. acid digestions, sample stabilisation and acid extractions, whilst easily ionised elements are commonly present in environmental samples. Both give rise to well known matrix effects. Matrix effects in ICP-AES have been extensively studied and reported in the literature (see Section1.2.6). In this study, work focussed on how the presence of a chemical matrix may degrade the long-term stability in ICP-AES analysis. Various drift diagnosis experiments have been performed using three synthetic chemical matrices. The influence of the operating conditions on the magnitude of the matrix effects was taken in account, together with the concentration level of the analytes. Finally, the potential for using intrinsic plasma lines to correct for drift is discussed when complex matrices are present in the solution.

5.2 EXPERIMENTAL

5.2.1 SAMPLE PREPARATION

In order to evaluate typical geo-chemical matrices, two matrices simulating water and soil samples were synthesised. The composition of these matrices is described in Table 5.1. In addition, a 2% nitric acid matrix was also prepared for use as a reference point.

TABLE 5.1: SYNTHETIC MATRIX COMPOSITION (mgl^{-1})

	Nitric Acid Matrix	Water Matrix	Soil Matrix	From Reagent
HNO_3	2%	2%	2%	HNO_3 (69%) Aristar
Al	---	—	2000	$Al (NO_3)_3$ $9H_2O$ GPR
Ca	---	40	1000	$CaCO_3$ AnalaR
Fe	---	—	1000	$Fe(NO_3)_3$ $9H_2O$ AnalaR
K	—	40	150	KNO_3 AnalaR
Mg	—	100	50	$MgCl_2$ $6H_2O$ AnalaR
Mn	—	---	150	$MnSO_4$ $4H_2O$ GPR
Na	---	1000	20	NaCl AnalaR

The composition of the matrix used reflected the finding from extensive studies at the laboratories of British Geological Survey. Two test multi-element solutions (0.1 and 10 mgL^{-1}) were prepared for each synthesised matrix, using the previously prepared multi-element standard (Section 2.2.1). Thus in total, six test solutions were employed for this study: three matrices, each at two concentration levels.

5.2.2 METHODOLOGY

The influence of matrix effects on long-term stability was investigated by performing drift diagnosis experiments for each matrix over approximately 4 hours (100 determinations) without re-calibration. The diagnosis duration was reduced due to the faster determination capabilities of the instrument employed in this study. However for the nitric matrix, diagnoses over eight hours of analysis were used in order to compare these results with those

previously obtained in the Optima instrument (see Section 3.2.1). Solutions at two different concentrations were randomly distributed during each analysis in order to better simulate the data acquisition in real sample analysis. The influence of the operating parameters was considered by repeating each diagnosis at two instrumental settings, i.e. at standard and at robust conditions. In summary, six drift diagnosis experiments were performed, one per matrix type at each set of instrumental conditions.

5.2.3 INSTRUMENTATION

A VISTA AX (Varian) ICP-AES was employed for this study. This instrument utilises an axially viewed plasma and a simultaneous acquisition detector. The dispersive system of this instrument is based on an echelle grating (94 g mm^{-1}) in conjunction with a CaF_2 prism-grooves based cross dispersion element. A 2-D spectrum is then obtained which displays the orders 19-88. The Vista detector described by Zander[207] is a segmented CDD, with each segment covering one of the 70 orders of the 2D spectrum. The total number of pixels is about 70 000 with a pixel width of 12.5μm.

The instrumental parameters adopted when working at robust and at standard conditions are described in Table 5.2.

TABLE 5.2: INSTRUMENTAL CONDITIONS

	At Standard Conditions	At Robust Conditions
Power (W)	1000	1350
Plasma Flow (Lmin^{-1})	15	18
Auxiliary Flow (Lmin^{-1})	1.5	1.5
Nebuliser Flow (Lmin^{-1})	1.0	0.75
Sample Uptake Rate (mLmin^{-1})	1.0	1.0
Read Time (s)	10	10
Nebuliser Type	Pneumatic Nebuliser	
Injector Diameter (mm)	2	2
Warming-Up Time (min)	0	0

A large number of emission lines were monitored in this study utilising the rapid performance of the VISTA AX. In addition, the instrument also allows a wide range of intrinsic plasma lines to be monitored. The lines selected for the drift diagnosis experiments are listed in Table 5.4. and Table 5.3

TABLE 5.3: ANALYTE LINES MONITORED

Atomic Lines (nm)		Ionic Lines (nm)	
Al 396.152	(I)	Al 172.438	(II)
Ba 705.994	(I)	Ba 230.424	(II)
Ca 422.673	(I)	Ba 233.527	(II)
Cd 228.802	(I)	Ba 455.403	(II)
Co 240.725	(I)	Ca 317.933	(II)
Co 340.511	(I)	Ca 396.847	(II)
Cr 357.868	(I)	Cd 214.439	(II)
Cu 324.754	(I)	Cd 226.502	(II)
Cu 327.395	(I)	Co 228.615	(II)
Mg 285.213	(I)	Co 238.892	(II)
Mn 279.482	(I)	Cr 267.716	(II)
Na 588.995	(I)	Cu 213.598	(II)
Na 589.592	(I)	Cu 224.700	(II)
Ni 232.003	(I)	Fe 238.204	(II)
Ni 232.138	(I)	Fe 259.940	(II)
Pb 217.000	(I)	Mg 279.078	(II)
Pb 283.305	(I)	Mg 279.553	(II)
Zn 213.857	(I)	Mg 280.270	(II)
Zn 334.502	(I)	Mn 257.610	(II)
		Ni 231.604	(II)
		Pb 220.353	(II)
		Ti 336.122	(II)
		Ti 337.280	(II)
		Zn 202.548	(II)
		Zn 206.200	(II)

TABLE 5.4: INTRINSIC PLASMA LINES SELECTED

Argon Emission Lines (nm)				Other Plasma Lines (nm)	
Ar 415.859	Ar 451.073	Ar 614.544	Ar 702.108	H 434.047	O 436.824
Ar 419.832	Ar 549.587	Ar 641.631	Ar 703.025	H 486.133	O 615.820
Ar 420.067	Ar 560.673	Ar 645.918	Ar 735.328	N 174.213	O 645.607
Ar 430.010	Ar 565.070	Ar 675.283	Ar 737.212	N 174.465	—

Many of the elements monitored were present in the matrix composition (Ca, Mg and Na) in the water matrix and (Al, Ca, Fe, Mg, Mn, and Na) in the soil matrix. These emission lines were excluded when analysing the synthetic matrices.

The magnesium ratios were calculated for each set of instrumental parameters when working with the different matrices (Table 5.5). Values are lower than on the Optima instrument (see Section 3.2.2, Table 3.6) due to the axial disposition of the Vista AX, as noticed by previous authors[87]. However, clear differences are still observed with respect to the working conditions.

TABLE 5.5: MAGNESIUM RATIOS

		Mg (II) 280.270 nm	Mg (I) 285.213 nm	Magnesium Ratio
USING STANDARD CONDITIONS	NITRIC	307668	149597	2.1
	WATER	1429343	882781	1.6
	SOIL	142254	161781	0.9
USING ROBUST CONDITIONS	NITRIC	2090044	393664	5.3
	WATER	9133955	3061957	3.0
	SOIL	5083538	1498597	3.4

5.3 RESULTS AND DISCUSSION

5.3.1 MATRIX EFFECTS ON EMISSION INTENSITIES

Although the main objective of this study was to evaluate the effects of chemical matrices on long-term stability, the matrix effects on the emission intensities have also been studied. Many authors have previously recorded signal enhancements and suppressions on emission intensities due to the presence chemical matrices. In order to quantify these effects, the relative emission intensities of every line monitored have been calculated using as reference the emission intensity of the line on the 2% nitric matrix. This approach has been previously used by Masson et. al.[49,208].

Figure 5.1 and Figure 5.2 shows the variations in intensities found for the atomic lines when working at standard and at robust conditions respectively. Intensity suppressions were recorded for nearly every line, and were more marked when using the synthetic soil matrix. Within each matrix set, the suppression was slightly worse when operating at standard conditions. The same type of plot was produced for the ionic lines monitored in

Figure 5.3 and Figure 5.4 for standard and robust conditions, respectively. Intensity suppression are marked for the soil matrix when working at standard conditions and around 50% when the more robust conditions were employed. The water matrix had a slight effect on the ionic line intensities at standard conditions, although this was amplified when working at robust conditions. Finally, in the case of the intrinsic plasma lines, Figure 5.5 and Figure 5.6 show the relative intensities on the different matrices employed. Although argon lines originate in a different way, i.e. they are not involved in the nebulisation process, intensity suppressions and enhancement are still recorded. Using standard conditions (Figure 5.5) the situation is complex. Many argon lines are completely suppressed on the soil matrix, while some other intrinsic plasma lines such as nitrogen are enhanced. At robust conditions, the emission intensities remain much more stable independently of the type of matrix.

FIGURE 5.1: MATRIX EFFECTS ON ATOMIC EMISSION LINES USING STANDARD CONDITIONS
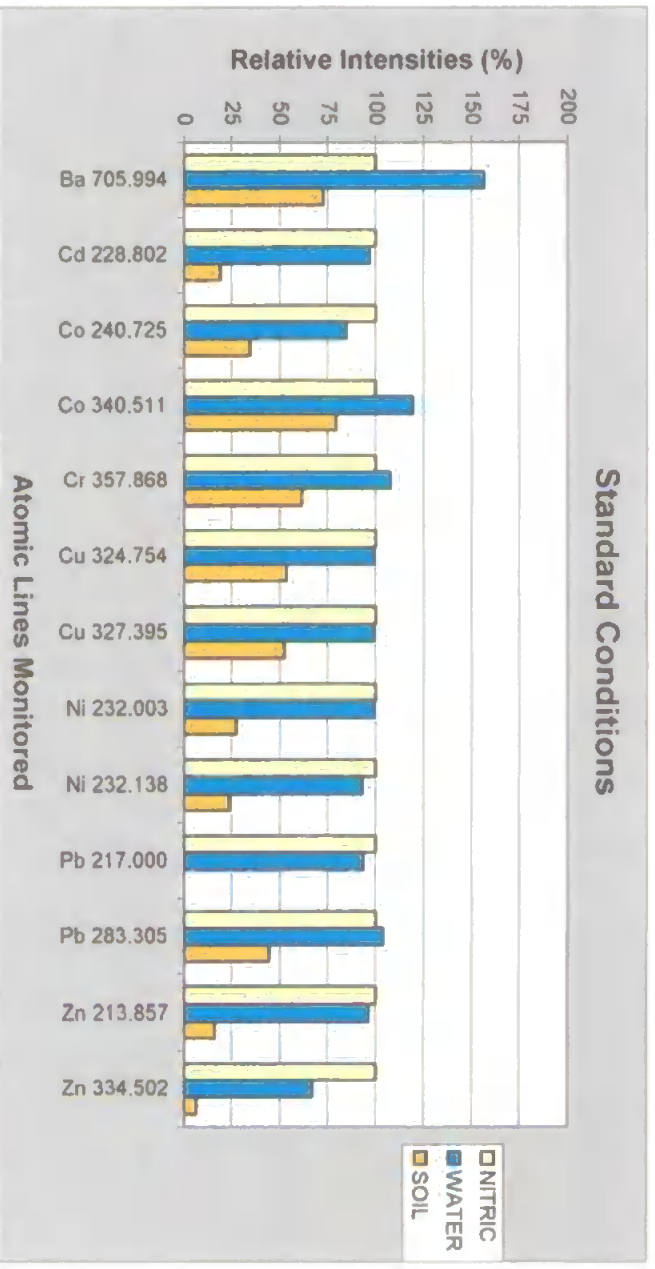
FIGURE 5.2: MATRIX EFFECTS ON ATOMIC LINES USING ROBUST CONDITIONS.
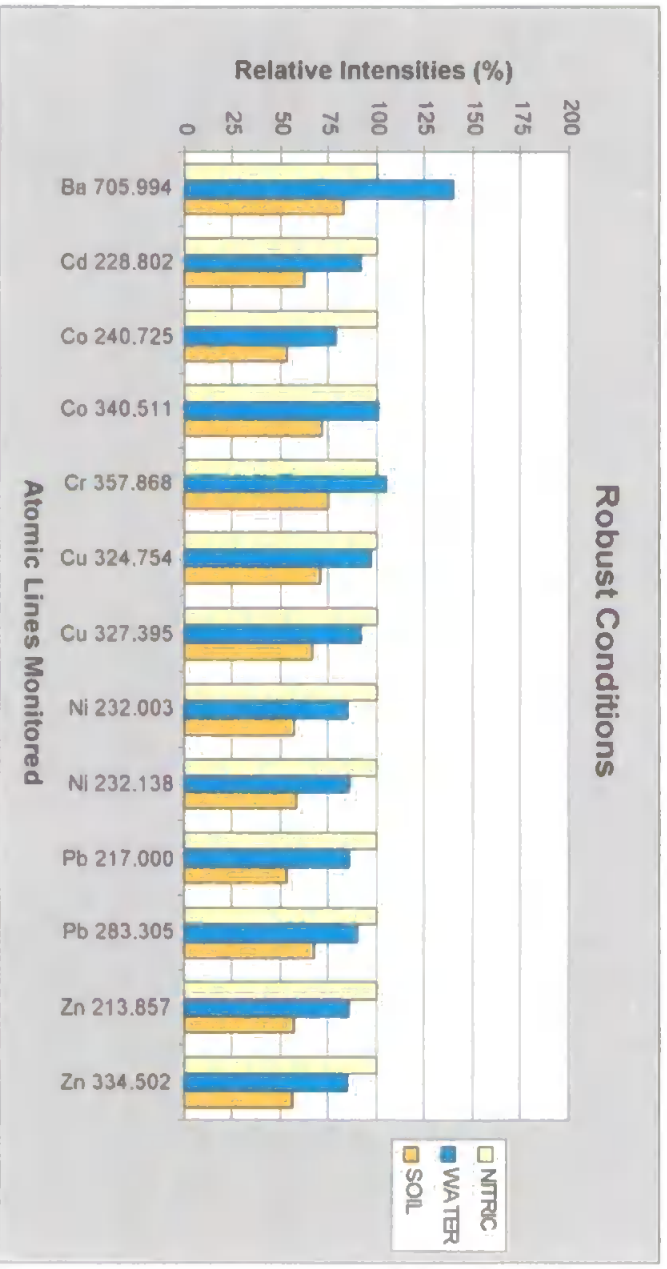
FIGURE 5.3: MATRIX EFFECTS ON IONIC EMISSION LINES USING STANDARD CONDITIONS.
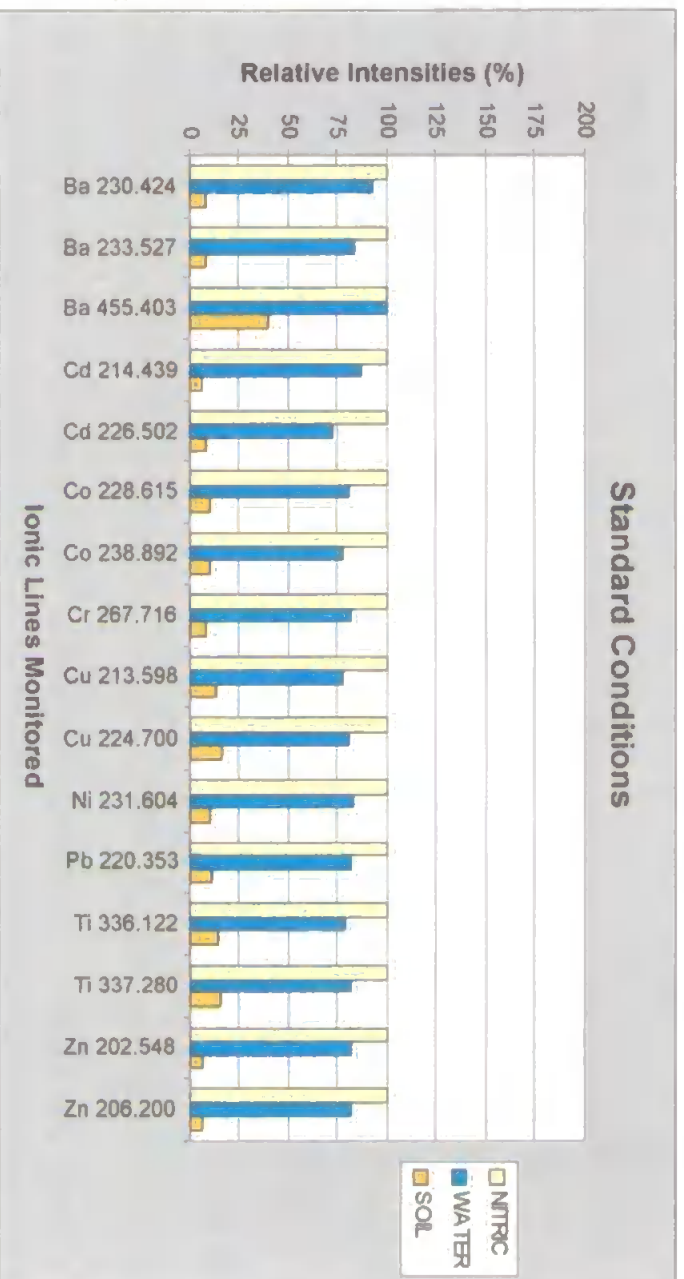
FIGURE 5.4: MATRIX EFFECTS ON IONIC LINES USING ROBUST CONDITIONS
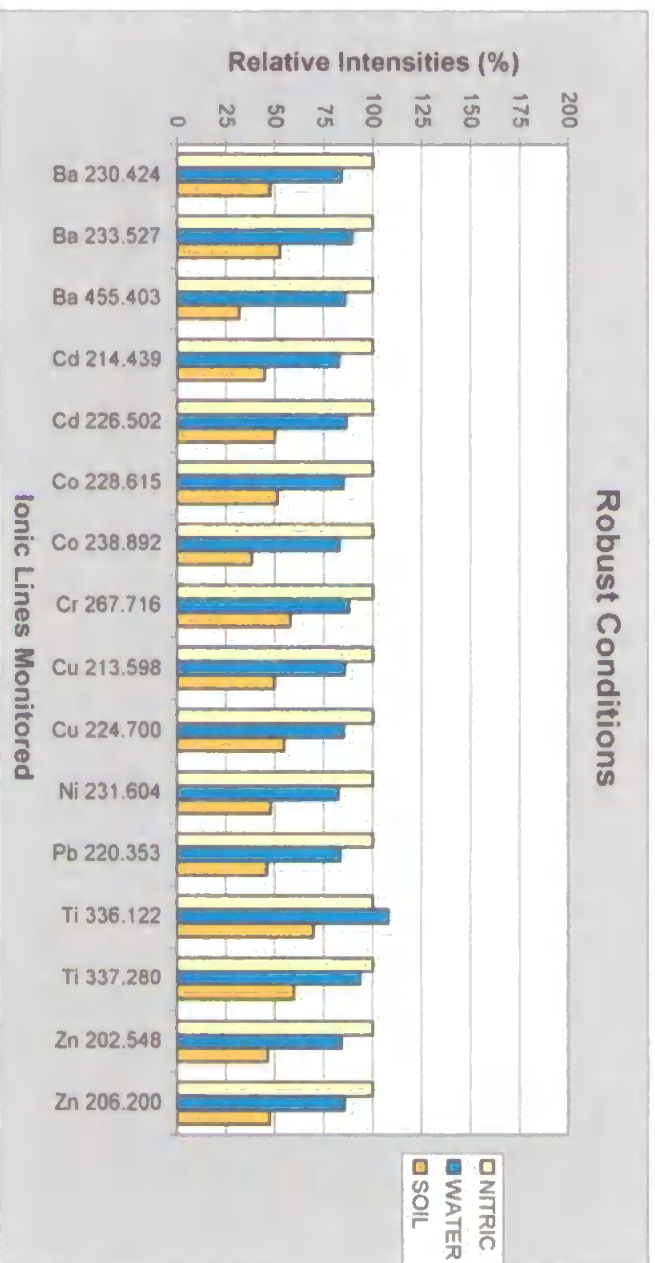
FIGURE 5.5: MATRIX EFFECTS ON INTRINSIC PLASMA LINES USING STANDARD COND.
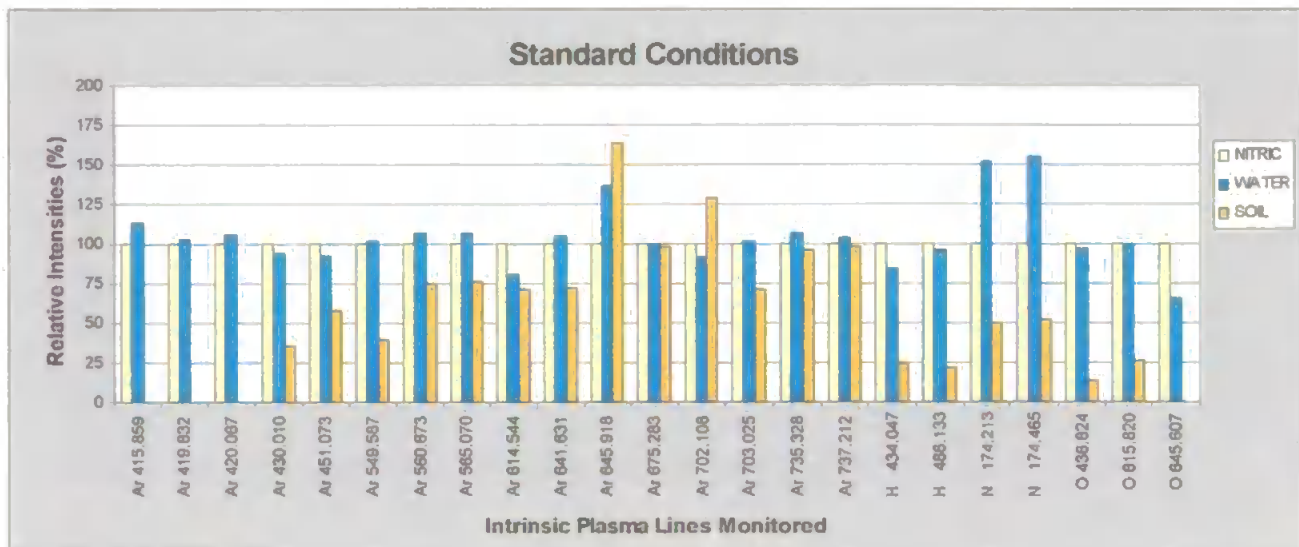
FIGURE 5.6: MATRIX EFFECTS ON INTRINSIC PLASMA LINES USING ROBUST CONDITIONS
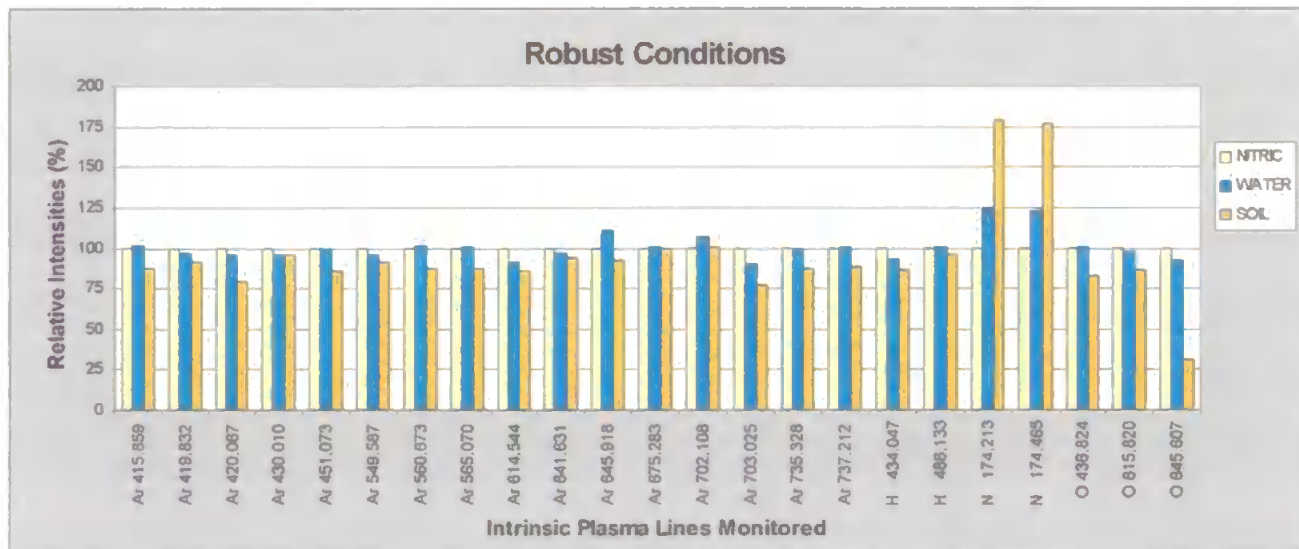
5.3.2 MATRIX EFFECTS ON THE LONG-TERM STABILITY OF ICP-AES

The intensity fluctuations with time were recorded using the three synthetic matrices. The following section presents the results obtained for each matrix at both concentrations levels when the determinations were done at both standard and robust conditions. For each case, four drift plots are presented, each one grouping together emission lines, i.e. atomic and ionic analyte emissions, argon emission lines and other intrinsic plasma lines. For all of the plots, the x-axes corresponds to the experiment time (in hours), while the y-axis represents the drift magnitude (as a percentage). In order to allow a comparison, an attempt has been made to use the same y-scale for all of the plots. However, as great differences in long-term stability were observed, the same scale could only be employed when the same matrix and the same operating conditions were used. In many cases, some emission lines were excluded from the plots due to extreme variability in their intensities, which impeded the observation of the drift patterns for the other emission lines.

FIGURE 5.7: DRIFT PLOTS OBTAINED FROM THE HIGH CONCENTRATION SOLUTION ON THE NITRIC ACID MATRIX WORKING AT STANDARD CONDITIONS

A) ATOMIC LINES DRIFT PATTERNS
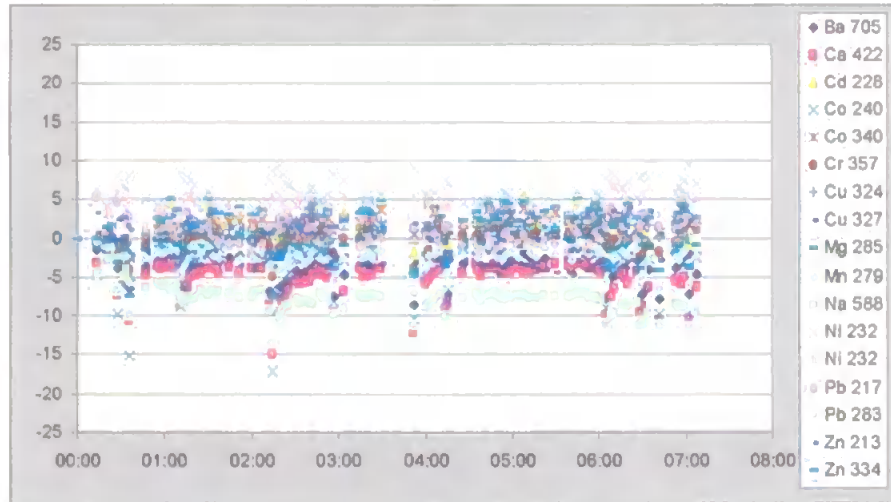
B) ARGON LINES DRIFT PATTERNS
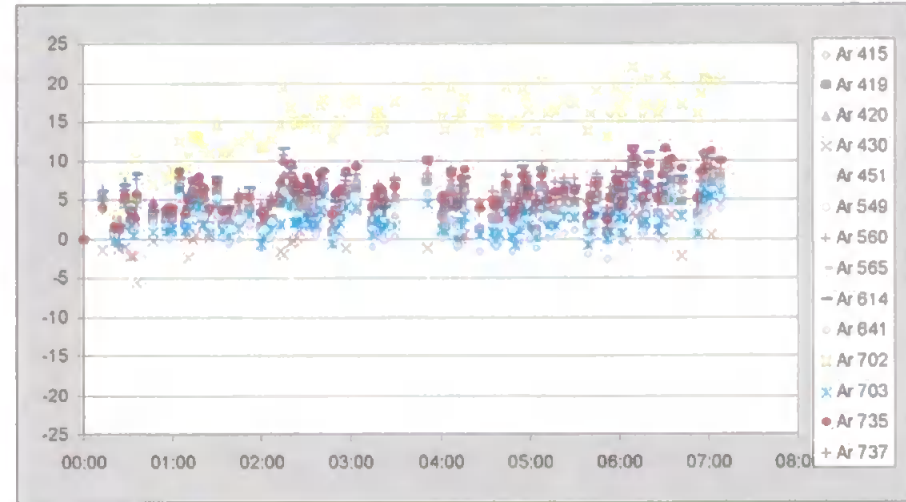
C) IONIC LINES DRIFT PATTERNS
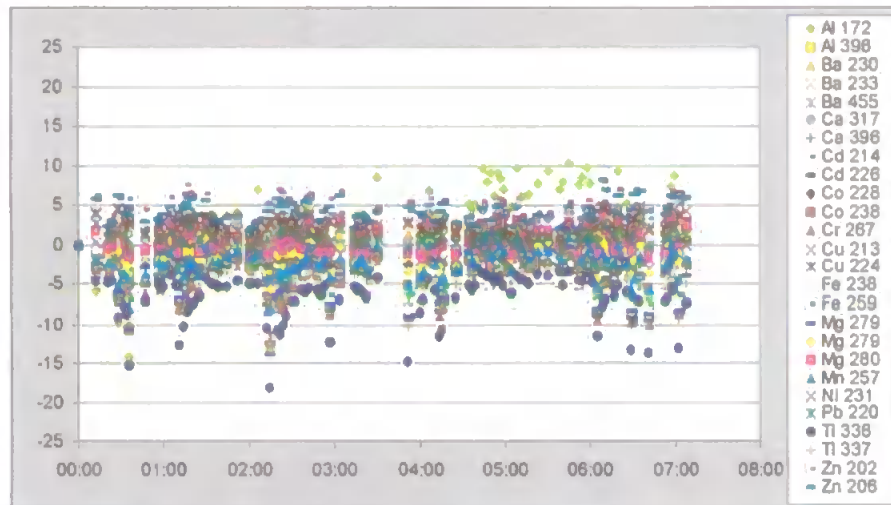
D) OTHER INTRINSIC PLASMA LINES DRIFT PATTERNS
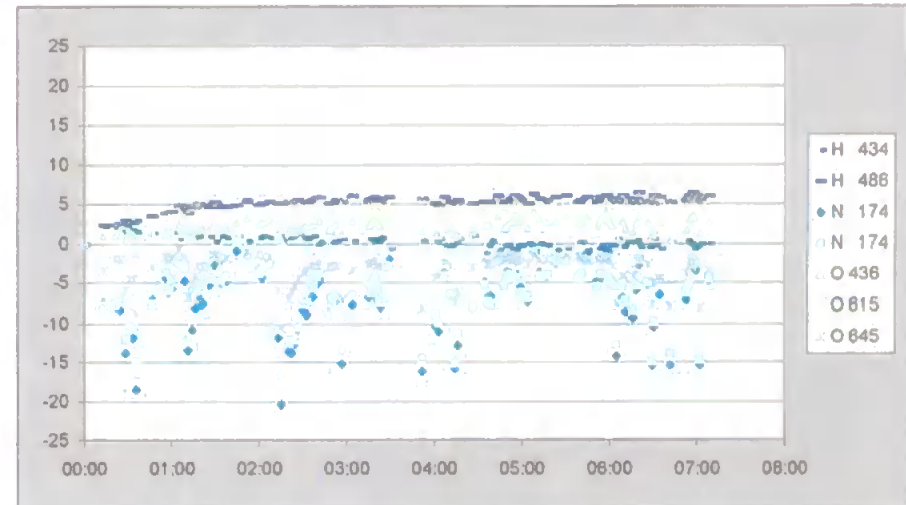
Lines excluded: Ar[645] Ar[675] Na[589]

FIGURE 5.8: DRIFT PLOTS OBTAINED FROM THE LOW CONCENTRATION SOLUTION ON THE NITRIC ACID MATRIX WORKING AT STANDARD CONDITIONS

A) ATOMIC LINES DRIFT PATTERNS
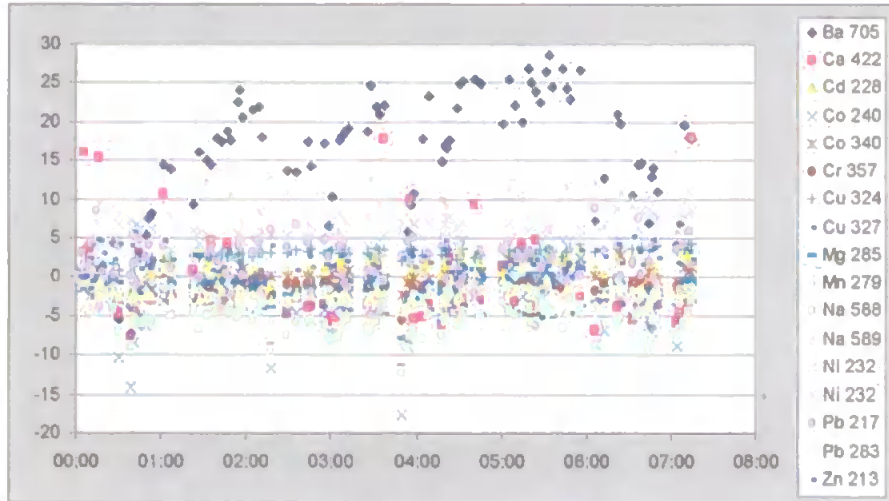
B) ARGON LINES DRIFT PATTERNS
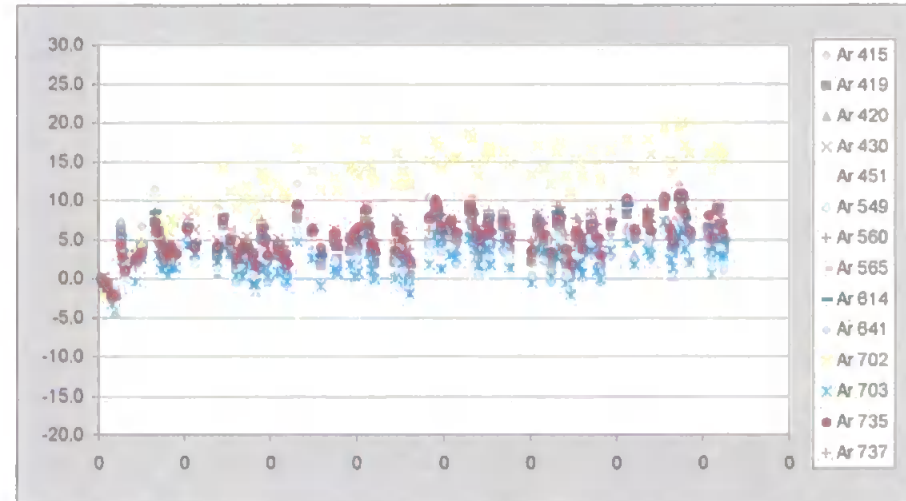
C) IONIC LINES DRIFT PATTERNS
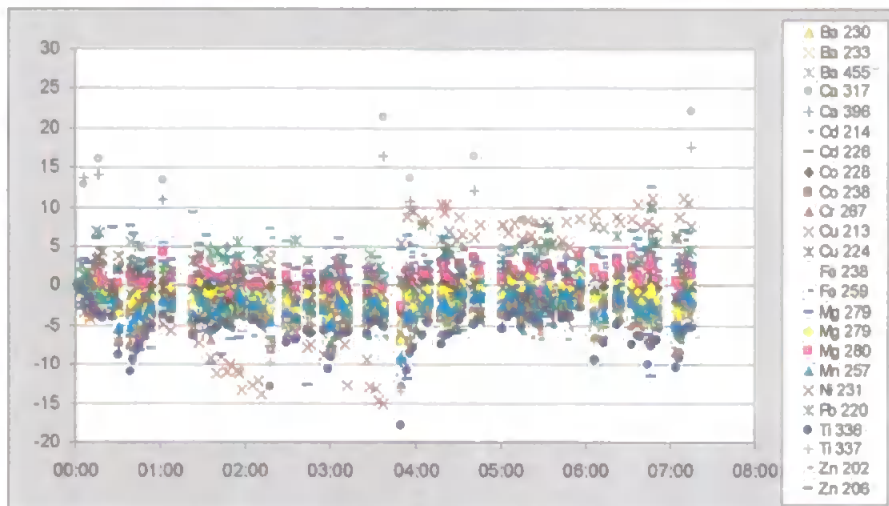
D) OTHER INTRINSIC PLASMA LINES DRIFT PATTERNS
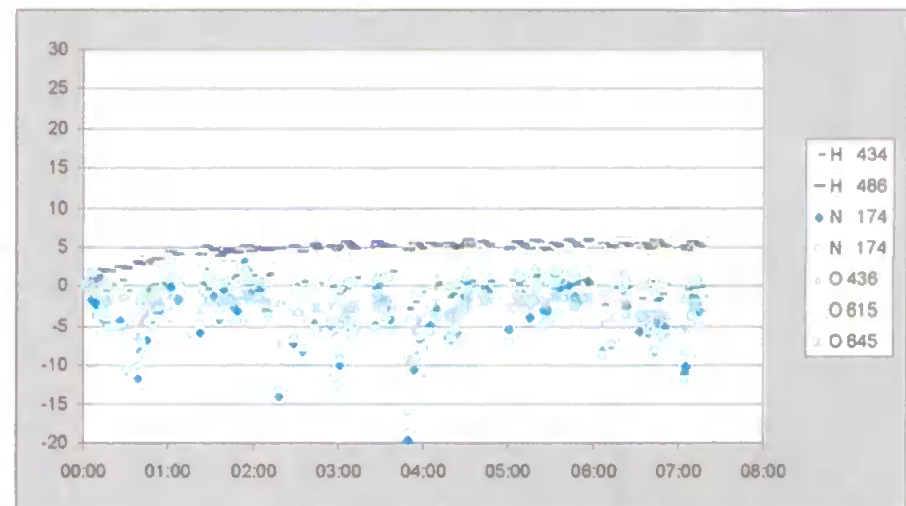
Lines excluded: Al^{172} Al^{396} Ar^{645} Ar^{675} Zn^{334}

FIGURE 5.9: DRIFT PLOTS OBTAINED FROM THE HIGH CONCENTRATION SOLUTION ON THE NITRIC ACID MATRIX WORKING AT ROBUST CONDITIONS

A) ATOMIC LINES DRIFT PATTERNS
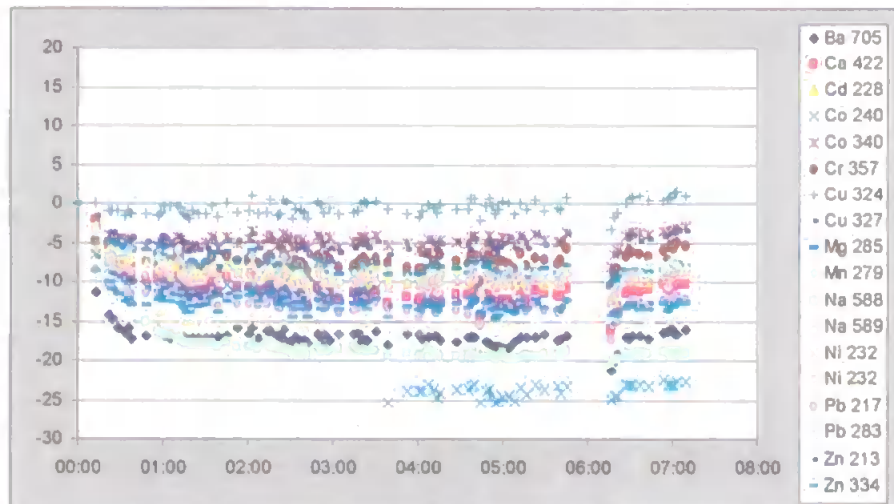
B) ARGON LINES DRIFT PATTERNS
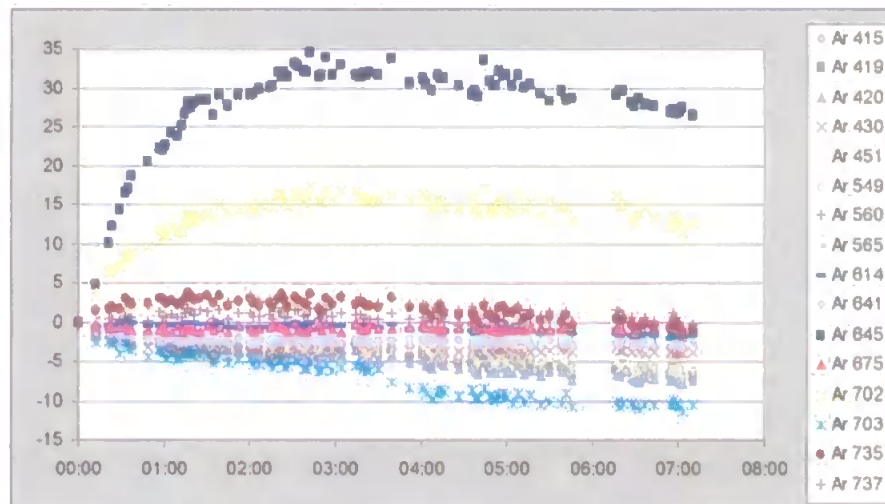
C) IONIC LINES DRIFT PATTERNS
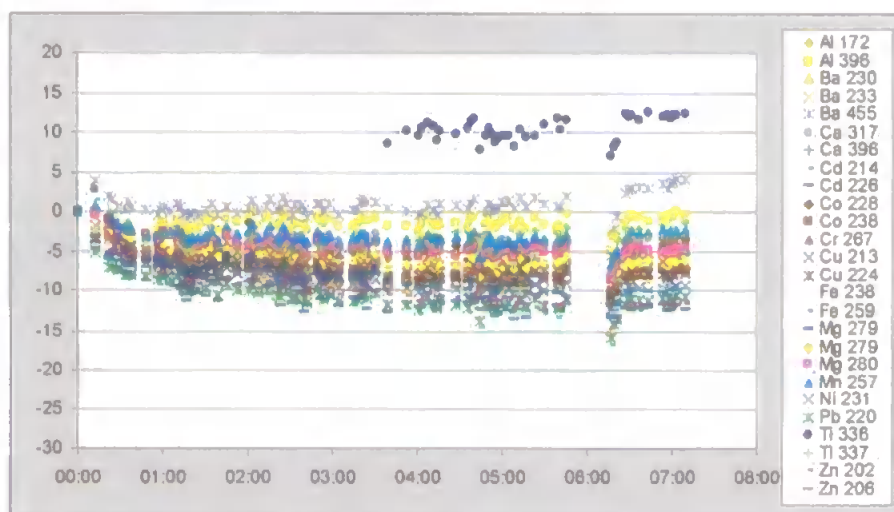
D) OTHER INTRINSIC PLASMA LINES DRIFT PATTERNS
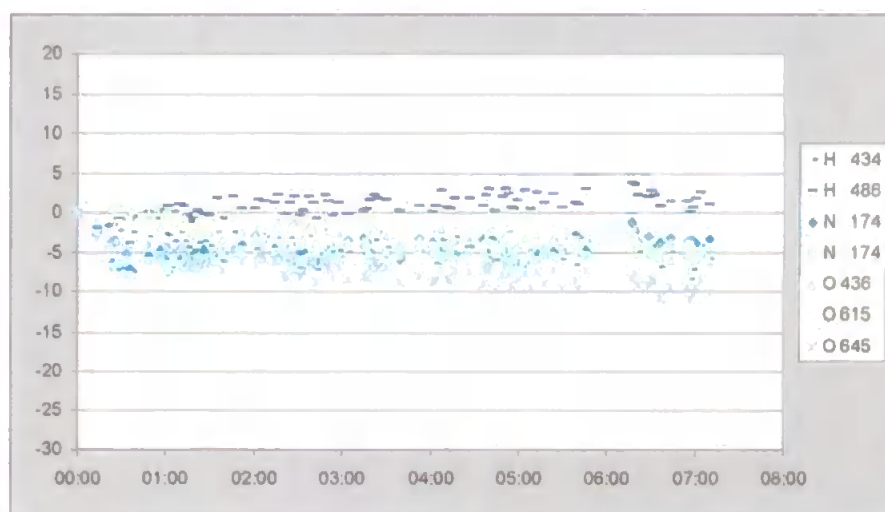
No lines excluded

FIGURE 5.10: DRIFT PLOTS OBTAINED FROM THE LOW CONCENTRATION SOLUTION
ON THE NITRIC ACID MATRIX WORKING AT ROBUST CONDITIONS

A) ATOMIC LINES DRIFT PATTERNS
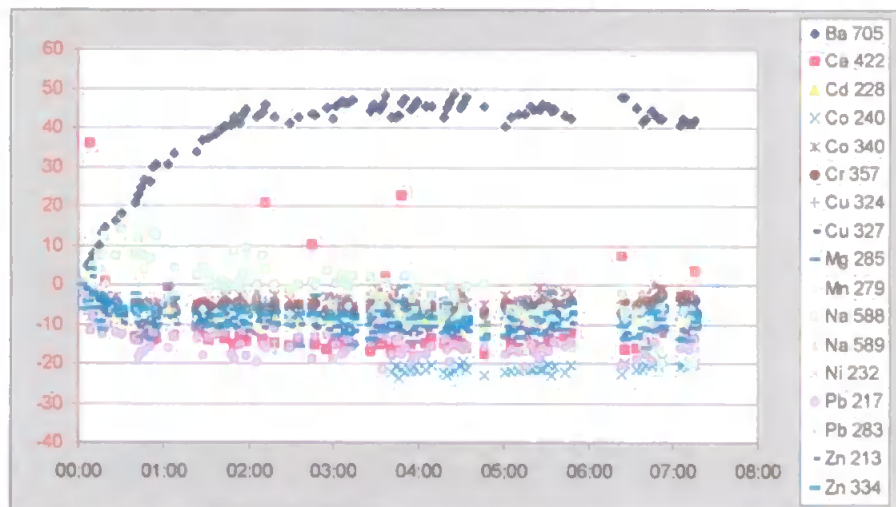
B) ARGON LINES DRIFT PATTERNS
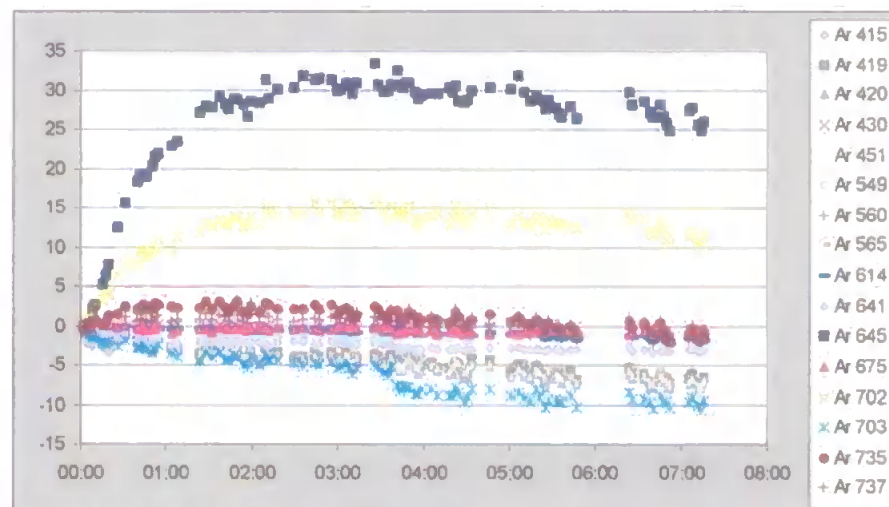
C) IONIC LINES DRIFT PATTERNS
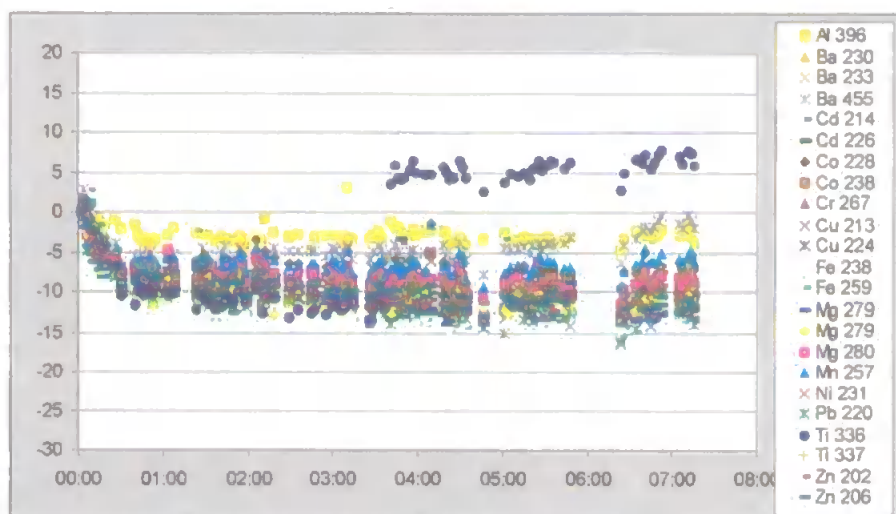
D) OTHER INTRINSIC PLASMA LINES DRIFT PATTERNS
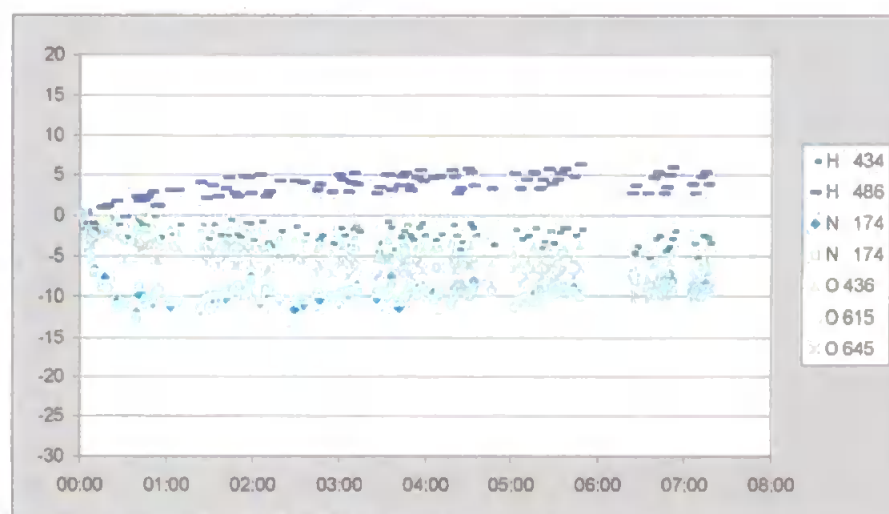
Lines excluded: Al ^{172} Ca ^{317} Ca ^{398} Ni $^{232.138}$

FIGURE 5.11: DRIFT PLOTS OBTAINED FROM THE HIGH CONCENTRATION SOLUTION ON THE WATER MATRIX WORKING AT STANDARD CONDITIONS

A) ATOMIC LINES DRIFT PATTERNS
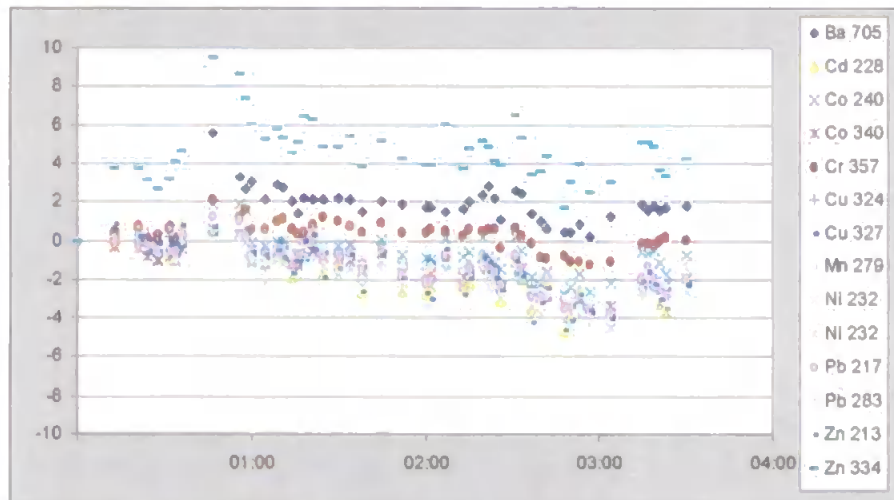
B) ARGON LINES DRIFT PATTERNS
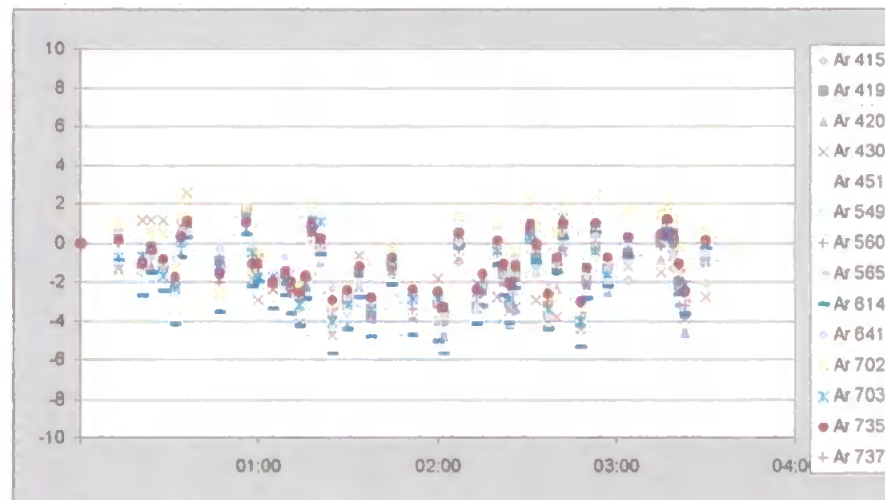
C) IONIC LINES DRIFT PATTERNS
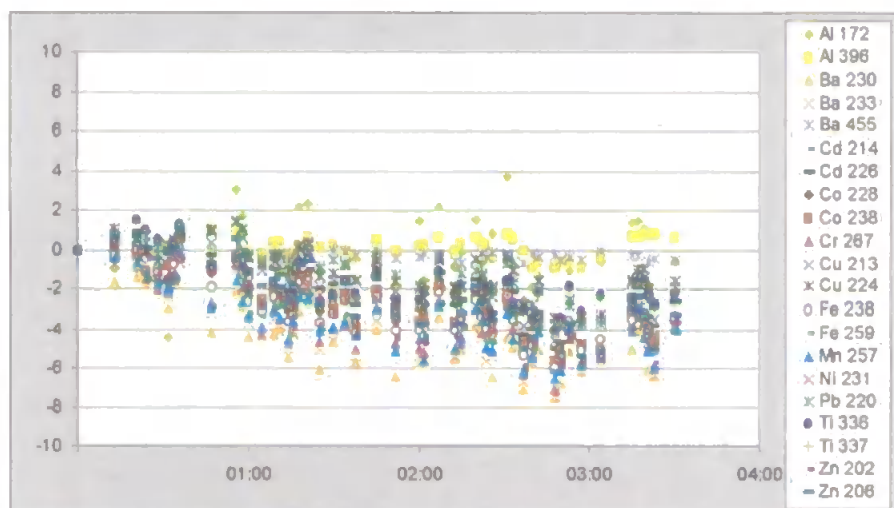
D) OTHER INTRINSIC PLASMA LINES DRIFT PATTERNS
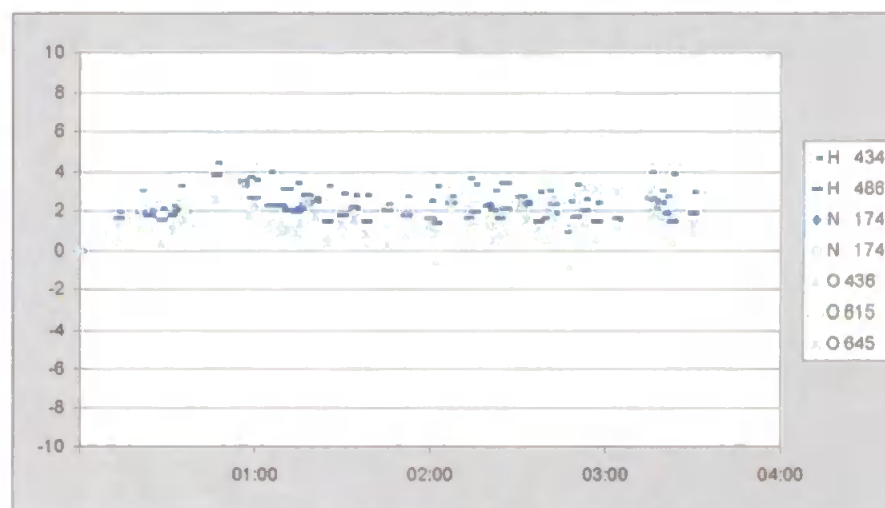
Lines excluded: Ar [645] Ar [675] Na [589]

FIGURE 5.12: DRIFT PLOTS OBTAINED FROM THE LOW CONCENTRATION SOLUTION ON THE WATER MATRIX WORKING AT STANDARD CONDITIONS

A) ATOMIC LINES DRIFT PATTERNS
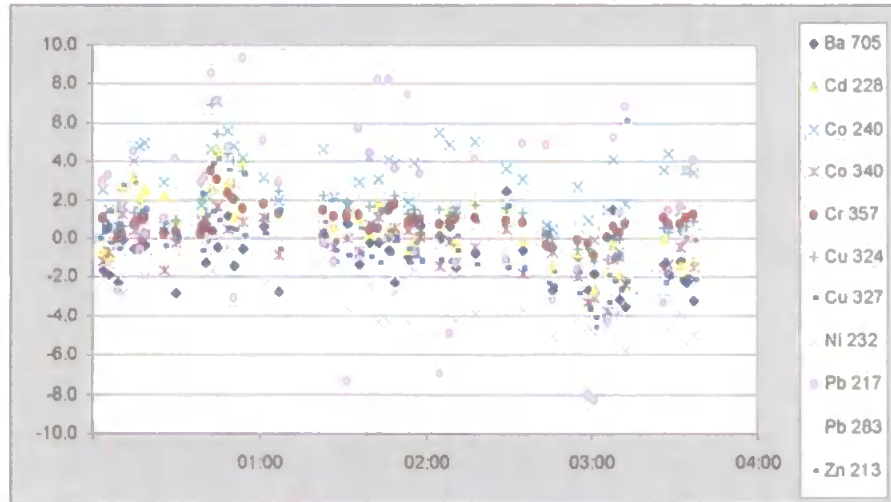
B) ARGON LINES DRIFT PATTERNS
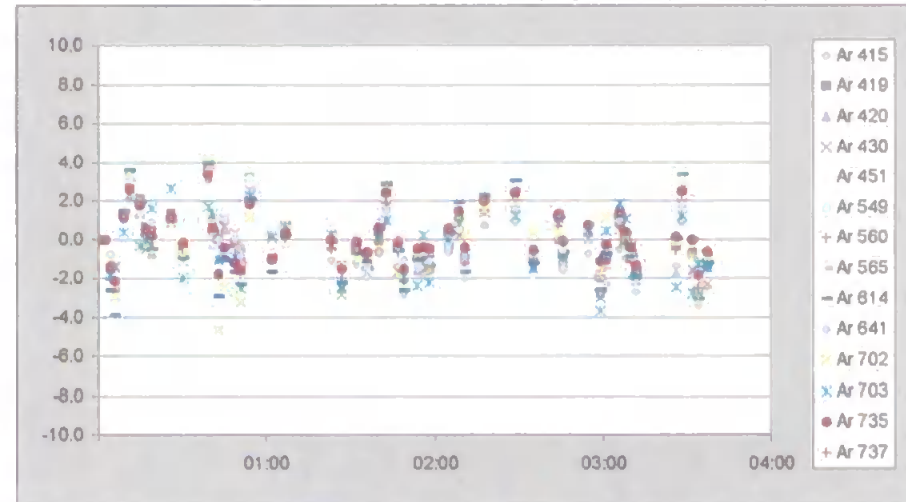
C) IONIC LINES DRIFT PATTERNS
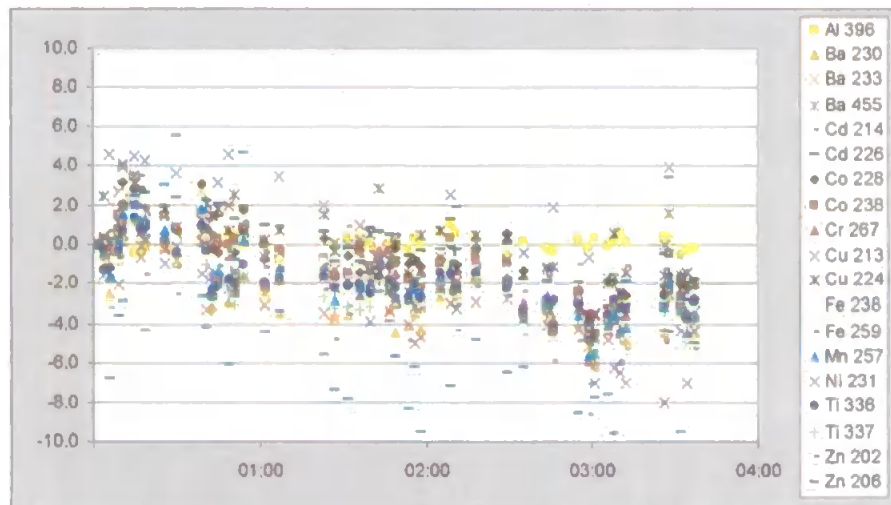
D) OTHER INTRINSIC PLASMA LINES DRIFT PATTERNS
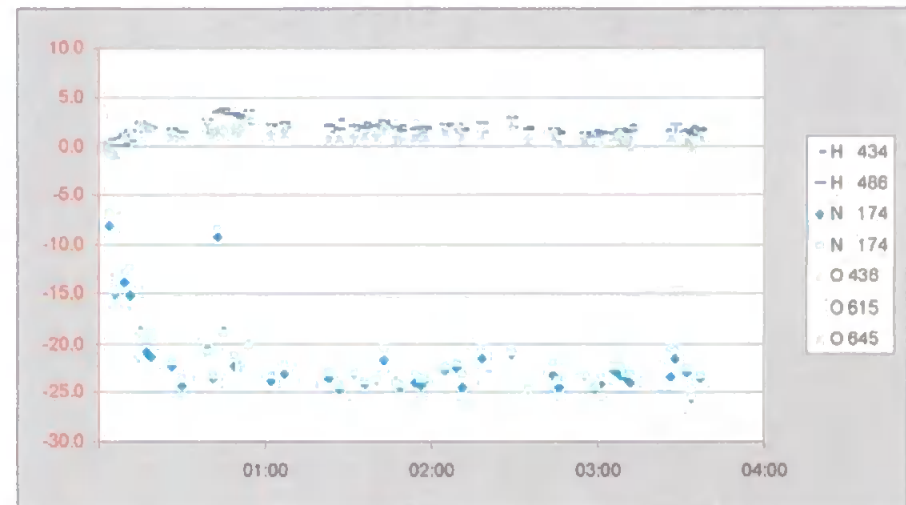
Lines excluded: Mn ^{279} Ni $^{232.138}$ Pb ^{220}

FIGURE 5.13: DRIFT PLOTS OBTAINED FROM THE HIGH CONCENTRATION SOLUTION ON THE WATER MATRIX WORKING AT ROBUST CONDITIONS.

A) ATOMIC LINES DRIFT PATTERNS
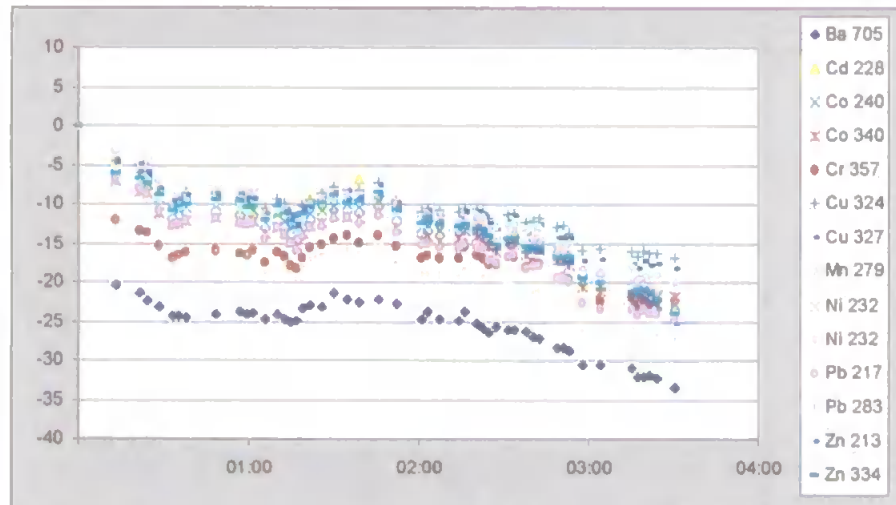
B) ARGON LINES DRIFT PATTERNS
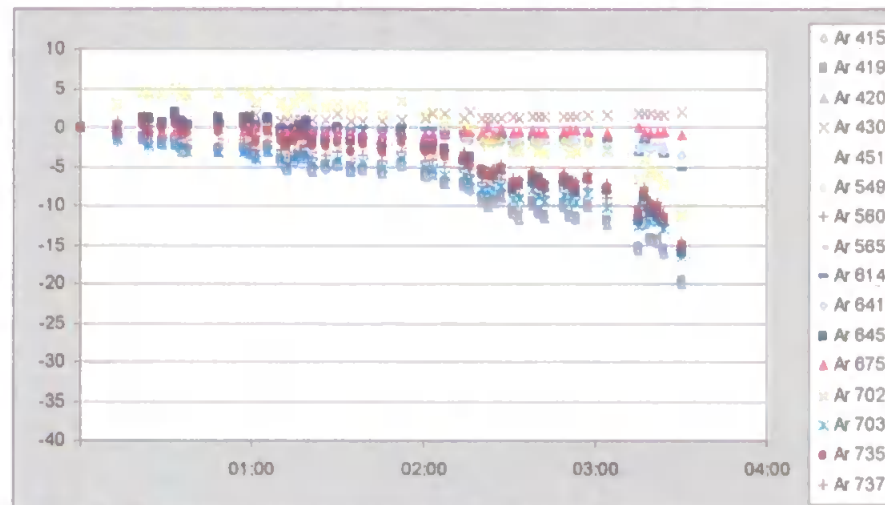
C) IONIC LINES DRIFT PATTERNS
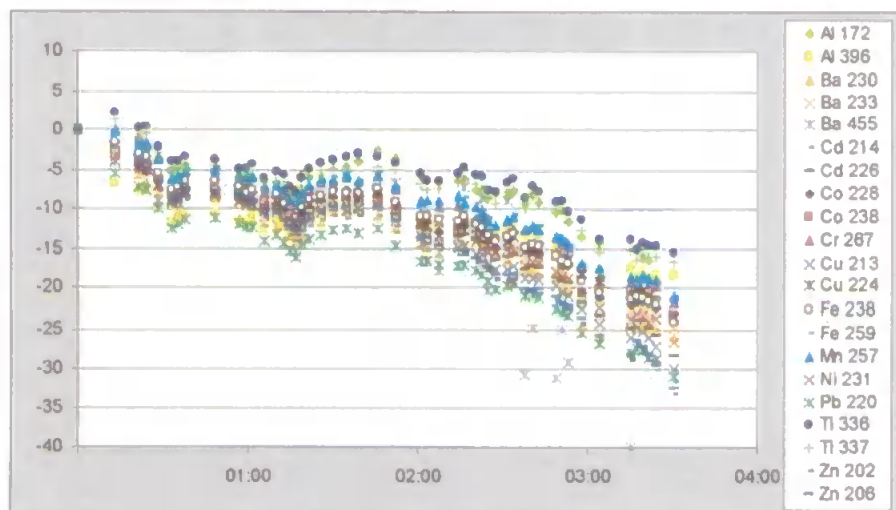
D) OTHER INTRINSIC PLASMA LINES DRIFT PATTERNS
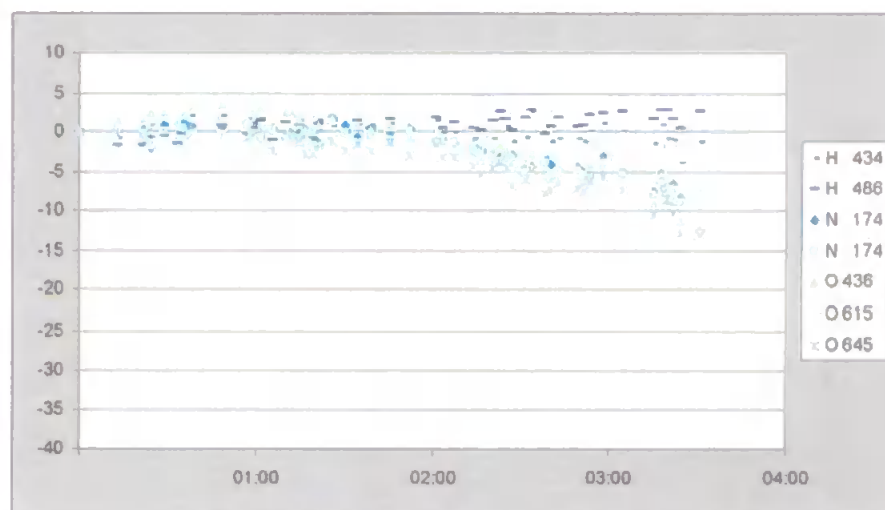
No lines excluded

FIGURE 5.14: DRIFT PLOTS OBTAINED FROM THE LOW CONCENTRATION SOLUTION ON THE WATER MATRIX WORKING AT ROBUST CONDITIONS

A) ATOMIC LINES DRIFT PATTERNS
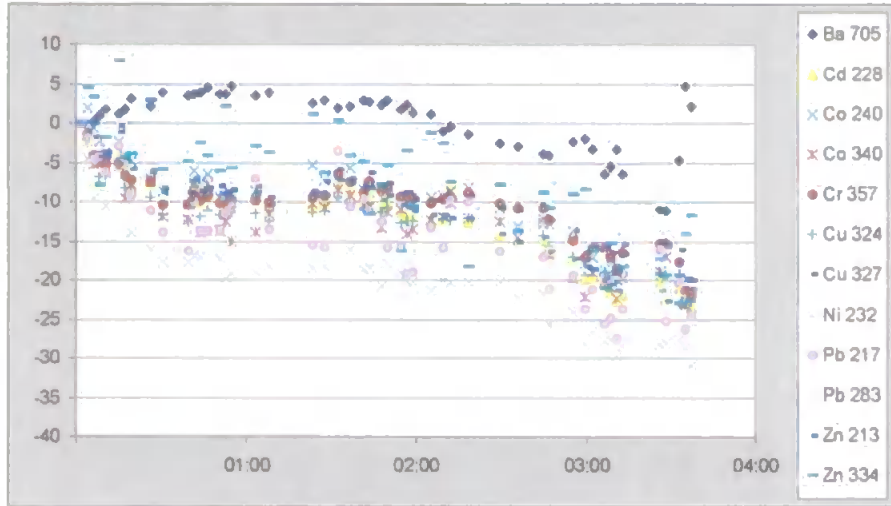
B) ARGON LINES DRIFT PATTERNS
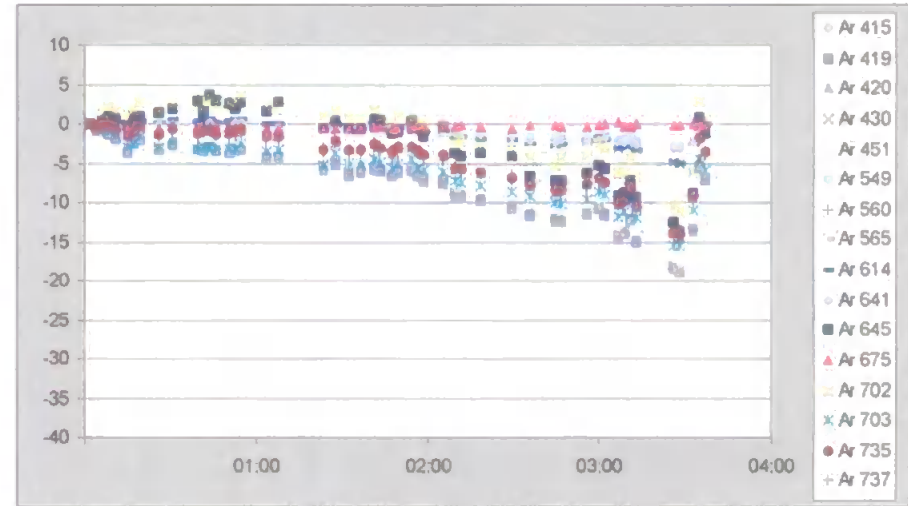
C) IONIC LINES DRIFT PATTERNS
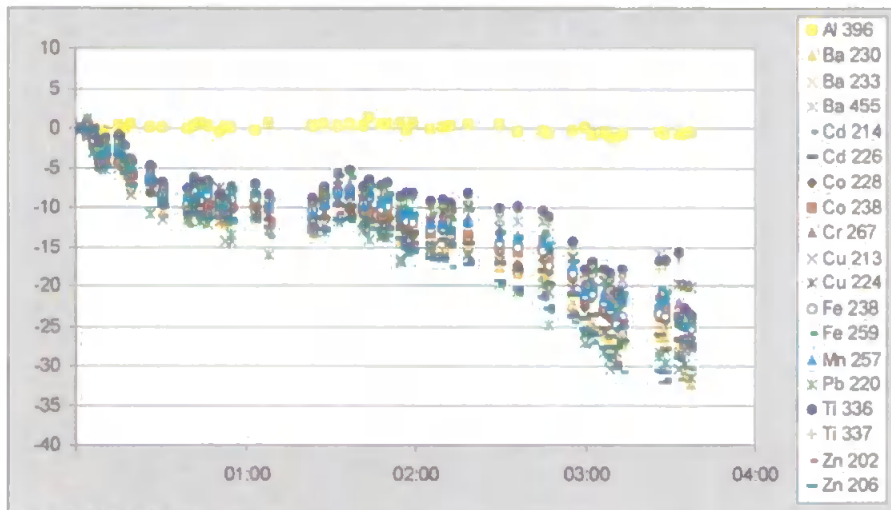
D) OTHER INTRINSIC PLASMA LINES DRIFT PATTERNS
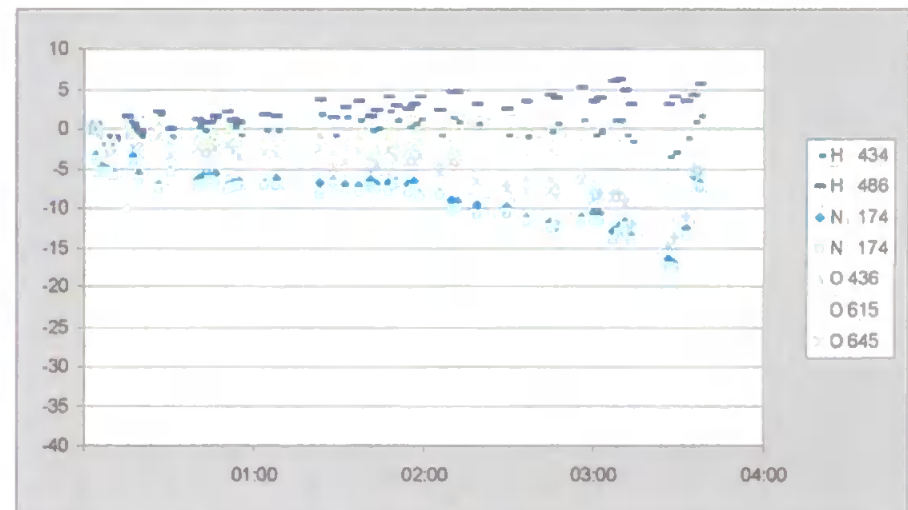
Lines excluded: Al [172] Ni [231] Ni [232.138] Mn [279]

FIGURE 5.15: DRIFT PLOTS OBTAINED FROM THE HIGH CONCENTRATION SOLUTION ON THE SOIL MATRIX WORKING AT STANDARD CONDITIONS

A) ATOMIC LINES DRIFT PATTERNS
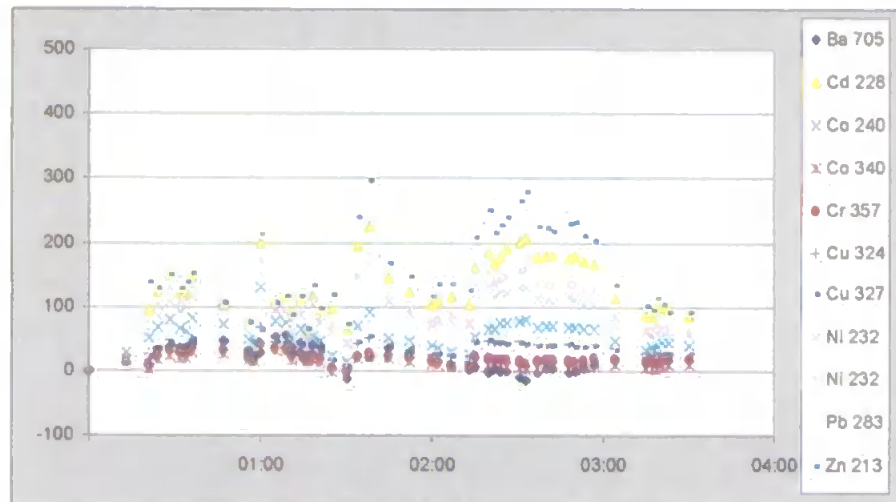
B) ARGON LINES DRIFT PATTERNS
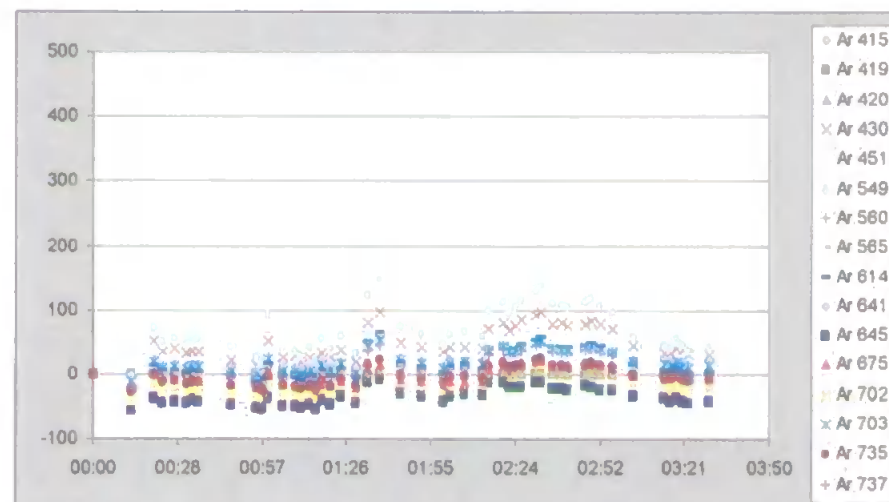
C) IONIC LINES DRIFT PATTERNS
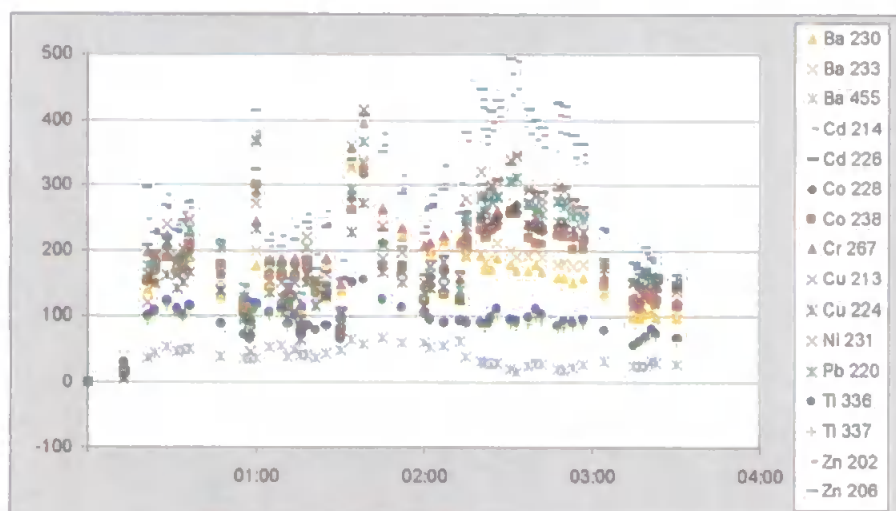
D) OTHER INTRINSIC PLASMA LINES DRIFT PATTERNS
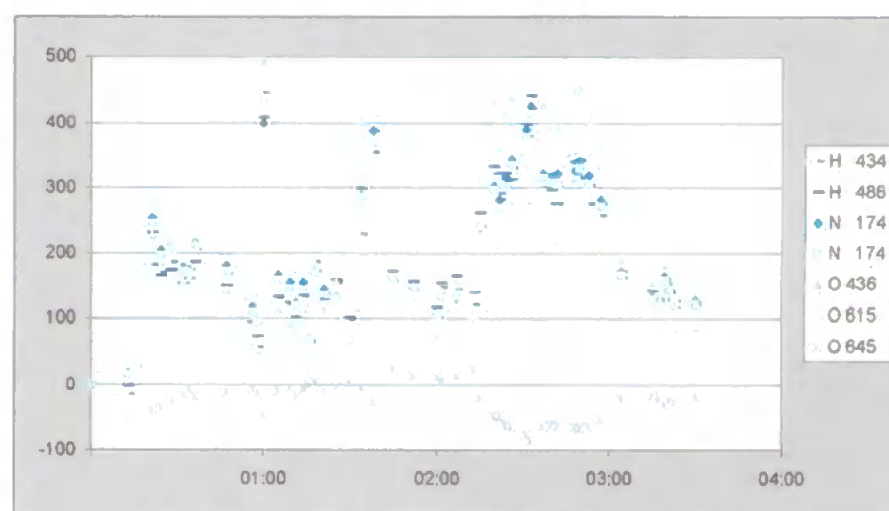
Lines excluded: Pb ^{217} Zn ^{334}

FIGURE 5.16: DRIFT PLOTS OBTAINED FROM THE LOW CONCENTRATION SOLUTION ON THE SOIL MATRIX WORKING AT STANDARD CONDITIONS

A) ATOMIC LINES DRIFT PATTERNS
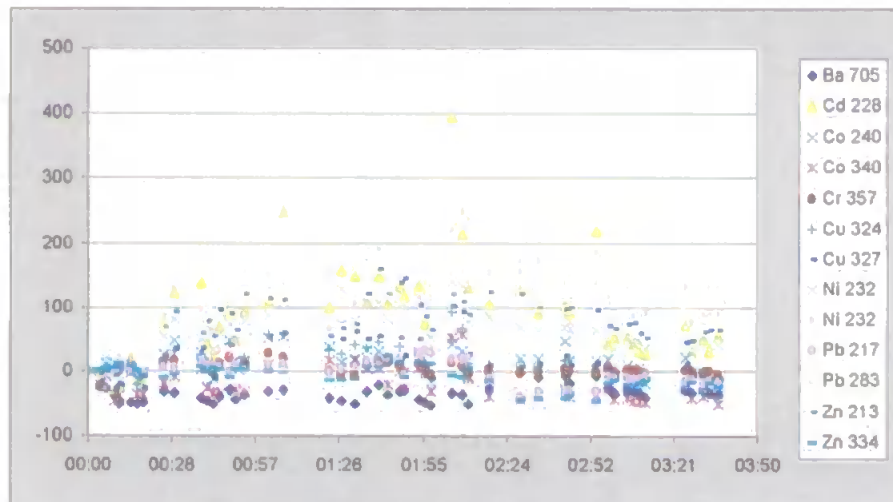
B) ARGON LINES DRIFT PATTERNS
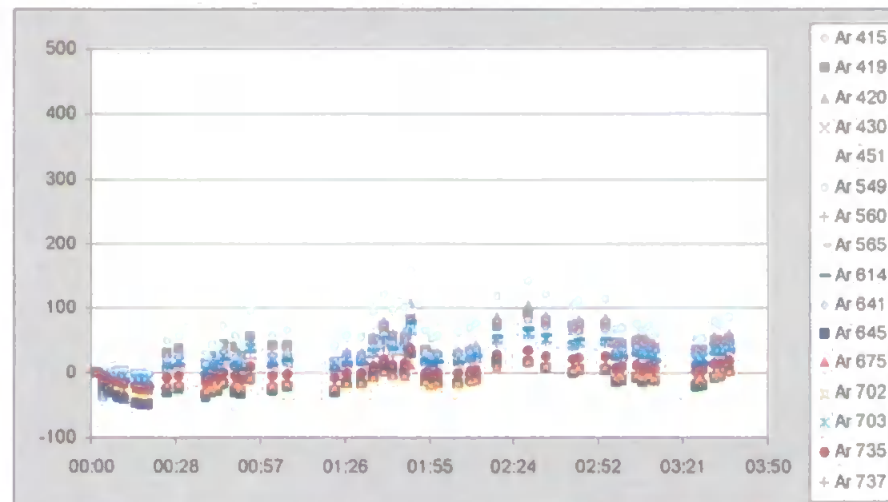
C) IONIC LINES DRIFT PATTERNS
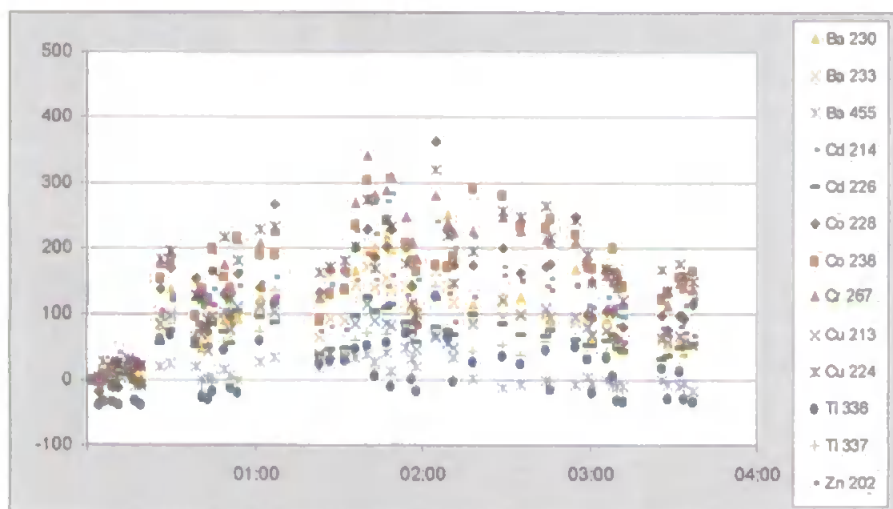
D) OTHER INTRINSIC PLASMA LINES DRIFT PATTERNS
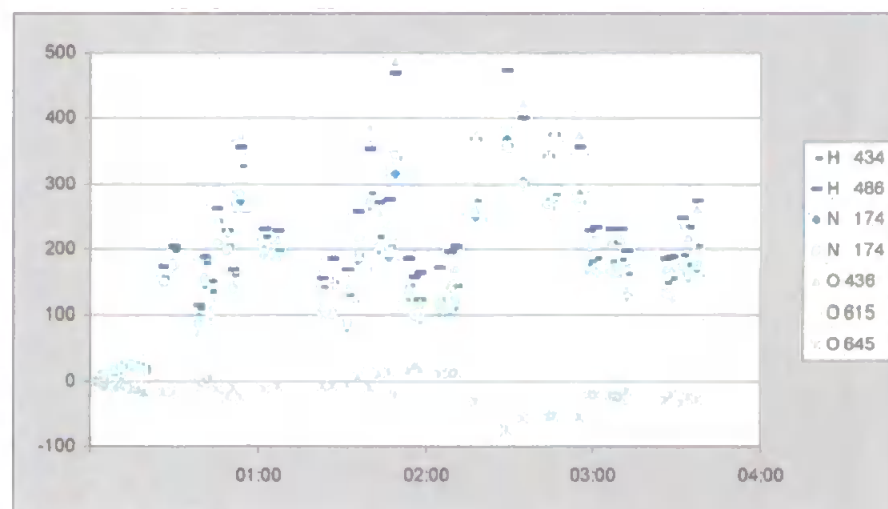
Lines excluded: Ni ^{231} Pb ^{220} Zn ^{208}

FIGURE 5.17: DRIFT PLOTS OBTAINED FROM THE HIGH CONCENTRATION SOLUTION ON THE SOIL MATRIX WORKING AT ROBUST CONDITIONS

A) ATOMIC LINES DRIFT PATTERNS

B) ARGON LINES DRIFT PATTERNS
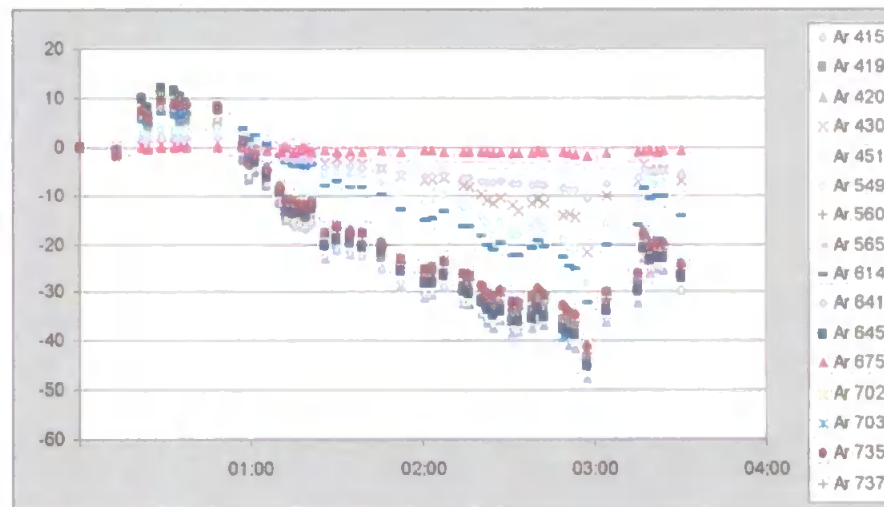
C) IONIC LINES DRIFT PATTERNS
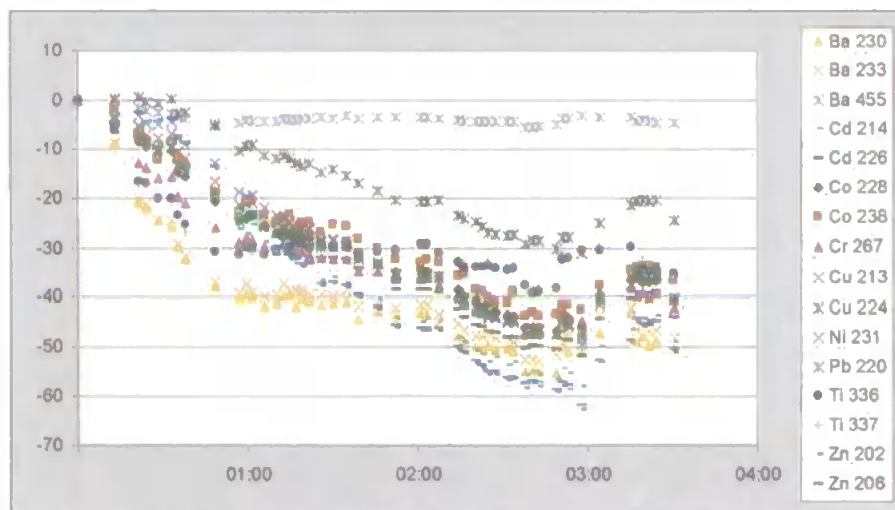
D) OTHER INTRINSIC PLASMA LINES DRIFT PATTERNS
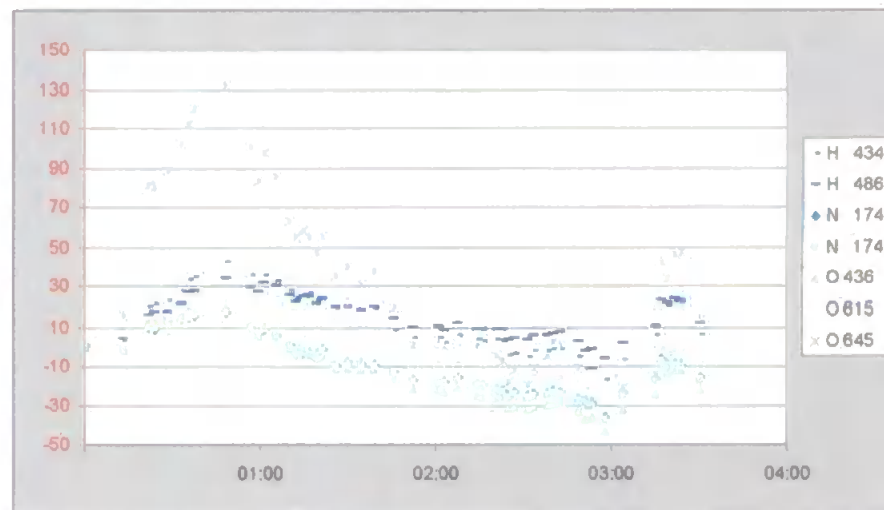
No lines were excluded

FIGURE 5.18: DRIFT PLOTS OBTAINED FROM THE LOW CONCENTRATION SOLUTION
ON THE SOIL MATRIX WORKING AT ROBUST CONDITIONS

A) ATOMIC LINES DRIFT PATTERNS
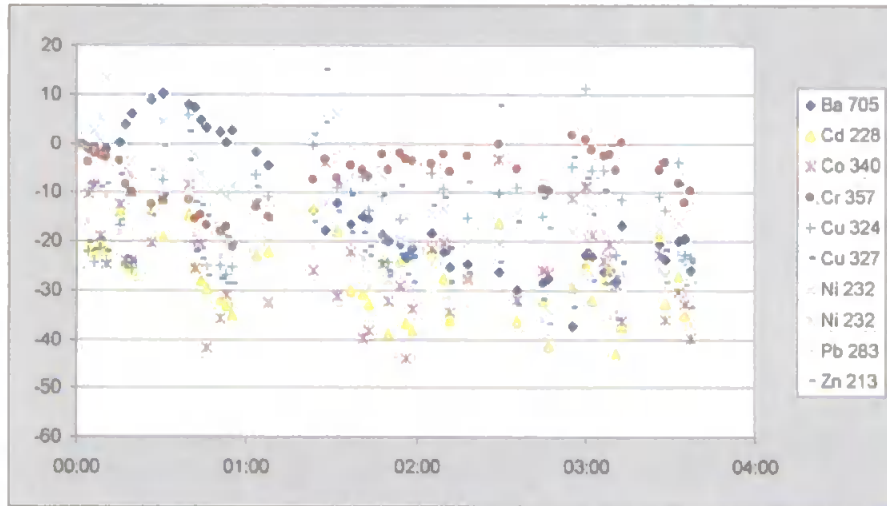
B) ARGON LINES DRIFT PATTERNS
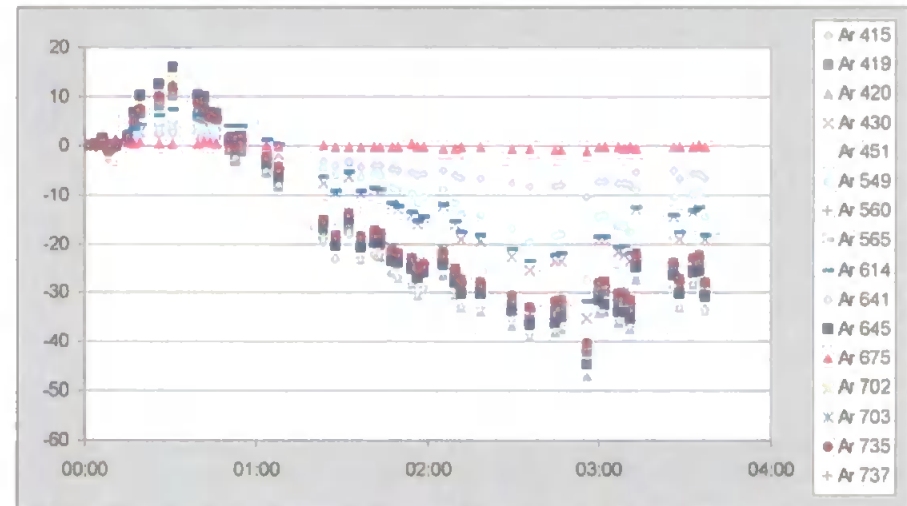
C) IONIC LINES DRIFT PATTERNS
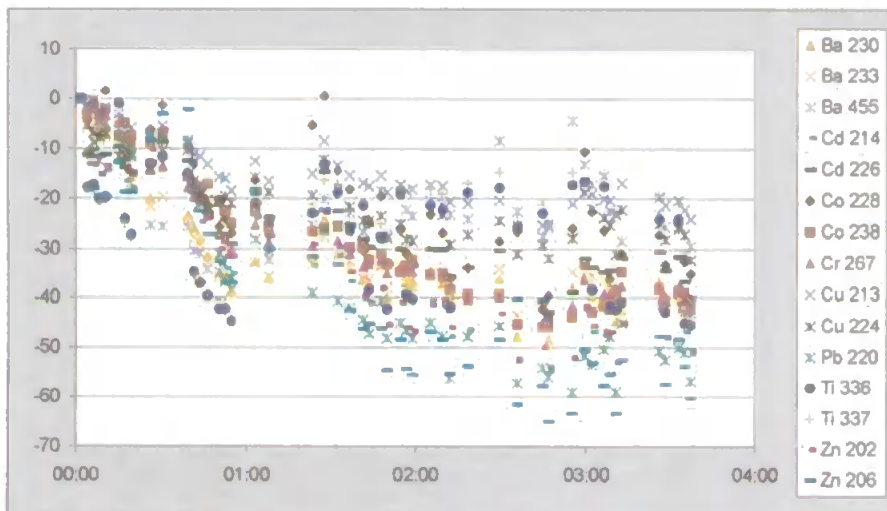
D) OTHER INTRINSIC PLASMA LINES DRIFT PATTERNS
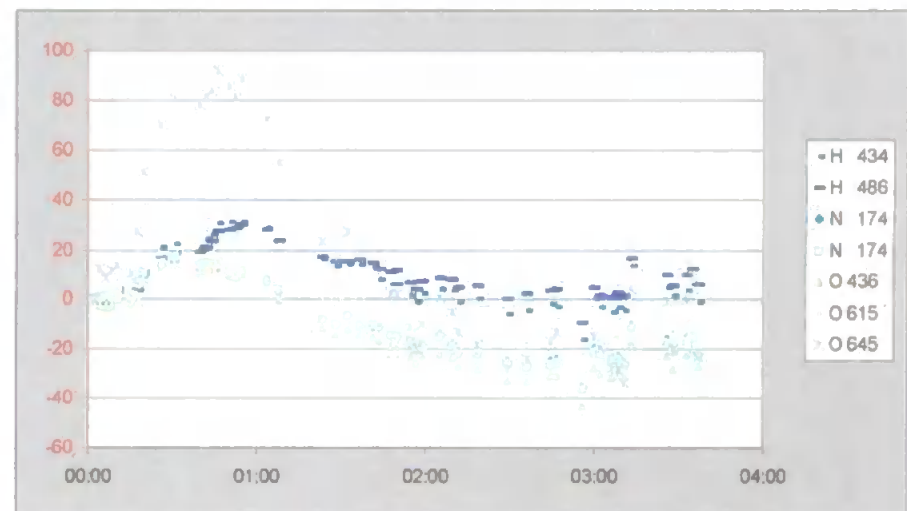
Lines excluded: Co [240] Ni [231] Pb [217] Zn [334]

5.3.3 SUMMARY OF RESULTS

A study of the drift patterns presented in Figure 5.7 - Figure 5.18 allows the influence of a number of different factors that may effect on the long-term stability of ICP-AES to be discussed.

Influence of the Type of Matrix

As may be expected, the soil matrix had the greatest effect on the long-term stability of the emission lines. Figure 5.15 to Figure 5.18 show the drift patterns obtained when the multi-element solutions were matched with the soil matrix. Instability is clearly visible when the standard conditions are employed (i.e. drift values up to 500%). When the robust conditions were selected, the intensity fluctuations, although still high, were more ordered. The water matrix seems to have little effect on the emission intensities when working at standard conditions. Figure 5.11 and Figure 5.12 show the drift patterns obtained when using the water matrix matched solutions. A very stable drift plot is observed for both concentrations. When working at the more robust setting, drift values were higher but a more marked common drift pattern was also recorded.

Finally, the nitric acid matrix gave the most stable responses at both conditions. However, the results are considerably different to those obtained previously (Section 3.3) for the Optima instrument. For example, very stable patterns are recorded when working at standard conditions. In addition, quite similar drift behaviour was observed for analyte and argon lines when working at robust conditions. This different behaviour may be related to the axial position of the torch.

Influence of the Instrumental Conditions

The results obtained indicate that the use of more robust conditions minimised the intensity suppressions due to the presence of a complex chemical matrix, however such condition do

not improve the long-term stability of the emission intensities. In two of the three cases studied, higher drift values were obtained when working at robust conditions, i.e. when using the nitric acid and the water matrices. However, when the more robust conditions were employed, the drift patterns are more ordered and higher inter-element correlation is observed. In such cases a drift correction procedure would be probably more efficient.

Influence of Concentration Level

In every case, similar drift patterns were observed independent of the concentration level of the analytes. This will be of importance when attempting drift correction. However, intensity fluctuations were slightly more chaotic when using the lower concentration solution due to working at values close to the determination limit for many of the lines monitored.

Nature of the Lines

The plots obtained show similar drift patterns regardless of the nature of the line. For instance, atomic and ionic lines followed similar patterns, even when the standard conditions, i.e. less energetic plasma, were employed. In terms of the intrinsic plasma lines, the results need to be interpreted carefully. The correlation matrix for each data set was calculated for a better comparison of line behaviour. These matrices show low or no correlation between argon lines and the analytes when working at standard conditions. Exceptions are found for the soil matrix, where some correlation was observed among all the lines. From the other plasma lines, the nitrogen and oxygen emissions show more similar behaviour to the analyte lines. At robust conditions, the plasma lines show different drift trends during the first hour of analysis associated with the instrument warming up period. The intrinsic plasma lines then remain more stable than the analyte lines, which tend to move towards lower emission intensities. This will certainly limit the use of plasma lines to correct for drift bias. In addition as observed when using the Optima instrument (Section 3.3.3), the argon lines show high negative correlation with most of the analyte lines, (the same applies also to nitrogen lines).

However, oxygen and hydrogen lines show a high positive correlation. In the case of the water and soil matrices, moderate positive correlation was found between analyte lines and most of the plasma lines.

5.4 CONCLUSIONS

As expected, the soil matrix gave rise to a stronger suppression effect than the water matrix reflecting the higher concentrations of concomitant elements involved. Ionic lines were found to be more sensitive to matrix effects than atomic lines, particularly when standard conditions were selected. It is important to note that the use of more robust conditions provided only a slight improvement in terms of matrix suppressions, with reductions of around 50% still observed.

From these results, the use of intrinsic plasma lines to overcome matrix effects would seem to offer little practical benefit. The enhancements and suppression observed for these lines are considerably different to those observed for most analyte lines, then their use for drift correction will be of help if a matrix matching step or other sort of matrix correction is previously undertaken.

CHAPTER 6

OVERALL CONCLUSIONS

Although manufacturers have made an effort to provide ICP-AES instruments with improved performances, this thesis shows that long-term stability continues to be relatively poor when working over a period of several hours. The long-term stability of three commercially available ICP-AES instruments has been studied, and in each case, severe drift bias was recorded. Drift may give rise intensity errors of up to 25% of the value at the beginning of the analysis. Therefore, long-term drift in ICP-AES instruments needs to be minimised by regularly recalibration or "corrected" in order to achieve analytically acceptable performance standards.

From the results reported in this study, it can be seen that the drift phenomenon is qualitatively reproducible although very dependent on the instrumental parameters set for the analysis. Variations in the long-term behaviour of the emission intensities were observed depending on the instrumental conditions. The analyst should consider this when deciding upon the instrumental parameters to be used for their determination. Figure 3.17 may provide a quick reference to the expected long-term behaviour of emission signals under a determined set of conditions.

The study of the drift patterns at different instrumental conditions facilitated the identification of the main causes of drift. Moreover, it was observed that the evolution of the drift patterns from one set of instrumental conditions to another was not random.

The effectiveness of a drift correction procedure will also be subject to the instrumental conditions employed. The fundamental limitations of using an internal standard method has been demonstrated in this studied. Only when working at robust conditions may a single internal standard be used to correct for drift. At such conditions, variations in the nebulisation efficiency is the main source of instability, and therefore high correlation is observed in the fluctuations of all the analyte lines independently of their nature. Thus any analyte line can be used to compensate for this source of noise. However, it has also been shown that the use of such conditions seriously reduces the sensitivity of the technique. At standard conditions, emission intensities are very vulnerable to drift, mainly due to fluctuations in the excitation process and therefore, complex drift patterns were recorded. A novel correction procedure has been developed for drift correction when working at standard conditions. The procedure, that utilises the drift pattern of an argon line, successfully removes most of the drift on the data. However, the application of such a procedure is still subject to practical limitations and further work would be required to make it universally applicable. Overall it is suggested that the use of "centre conditions" be adopted when possible to achieve reasonable detection limits in conjunction with stable instrument conditions over time.

The potential of using intrinsical plasma lines to monitor and correct for drift has been evaluated throughout this project. Among the possible intrinsic plasma lines, argon emissions are the most suitable for use when monitoring drift. However, limitations on the use of such lines have also been identified. First, such lines are much more stable than analyte line with regard to matrix effects. Secondly, argon is not necessarily involved in the nebulisation process, therefore, when drift is mainly due to variations in the nebulisation efficiency, argon emissions show a complete different drift pattern to that of the analyte lines.

In terms of data handled, several chemometrics methods have been applied to the study of drift phenomena. The use of time series provided a simple operation to mathematically identify the presence of a trend in data series. The correlation matrices help to quantify the similarities in the long-term fluctuations of the emission signals. PCA was also employed with the same objective; however no further information from the data was obtained and the physical characteristics of the new principal components could not be resolved. Among the chemometrics methods employed in this work, of special interest was the use of parallel factor analysis. PARAFAC compressed a three dimension data array in only two condensed factors. The interpretation of the new factors was achieved using physical parameters related to the system.

Overall, this study has helped to better characterise the drift phenomenon in ICP-AES systems. The origin of the problem as well as its magnitude have been determined at different working conditions. It is now possible to predict the type of drift pattern expected when analysing samples by ICP-AES at a particular set of instrumental parameters, and when the use of internal standards will be appropriate.

A number of areas can be identified from this study for future work. For example, work should continue to provide a universal methodology to correct for drift at standard conditions using argon lines. In addition, the effect on other long-term drift of other instrumental parameters such as the use of different instrumental devices also needs to be studied.

REFERENCE LIST

(1)   Greenfield, S.; Jones, I. L. I.; Berry, C. T. High Pressure Plasmas As a Spectroscopic Emission Sources. *Analyst* **1964**, *89*, 713-720.

(2)   Wendt, R. H.; Fassel V.A. Induction Coupled Plasma Spectrometric Excitation Source. *Anal. Chem.* **1965**, *37*, 920-922.

(3)   Ishii, I.; Tan, H. M.; Chan, S. K.; Montaser, A. Helium ICP AES - Effects of Induction Frequency and Forward Power on Plasma Formation and Analytical and Fundamental Properties. *Spectrochimica Acta Part B-Atomic Spectroscopy* **1991**, *46*, 901-916.

(4)   Iacone, L. A.; Masamba, W. R. L.; Nam, S. H.; Zhang, H.; Minnich, M. G.; Okino, A.; Montaser, A. Formation and Fundamental Characteristics of Novel Free-Running Helium Inductively Coupled Plasmas. *J. Anal. At. Spectrom.* **2000**, *15*, 491-498.

(5)   Nam, S. H.; Zhang, H.; Cai, M. X.; Lim, J. S.; Montaser, A. Status Report on Helium Inductively Coupled Plasma Mass Spectrometry. *Fresenius Journal of Analytical Chemistry* **1996**, *355*, 510-520.

(6)   Zhang, H.; Nam, S. H.; Cai, M. X.; Montaser, A. Atmospheric-Pressure Helium Inductively Coupled Plasmas for Elemental Mass Spectrometry. *Appl. Spectrosc.* **1996**, *50*, 427-435.

(7)   Sesi, N. N.; Mackenzie, A.; Shanks, K. E.; Yang, P. Y.; Hieftje, G. M. Fundamental-Studies of Mixed-Gas Inductively-Coupled Plasmas. *Spectrochimica Acta Part B-Atomic Spectroscopy* **1994**, *49*, 1259-&.

(8)   Wagatsuma, K.; Hirokawa, K. Characterization of Argon-Helium Mixed Gas Inductively Coupled Plasma Based on Spectroscopic Analysis of the Argon and Zinc Emission-Lines. *Anal. Sci.* **1993**, *9*, 83-88.

(9)   Boumans, P. W. J. M. Comment on a Proposed Excitation Mechanism in Argon ICPs. *Spectrochimica Acta Part B-Atomic Spectroscopy* **1982**, *37*, 82.

(10)   Goldwasser, A.; Mermet, J. M. Contribution of the Charge-Transfer Process to the Excitation Mechanisms in Inductively Coupled Plasma Atomic Emission-Spectroscopy. *Spectrochimica Acta Part B-Atomic Spectroscopy* **1986**, *41*, 725-739.

(11) deRegt, J. M.; deGroote, F. P. J.; vanderMullen, J. A. M.; Schram, D. C. Comparison of Active and Passive Spectroscopic Methods to Investigate Atmospheric Inductively Coupled Plasmas. *Spectrochimica Acta Part B-Atomic Spectroscopy* **1996**, *51*, 1371-1383.

(12) Jonkers, J.; deRegt, J. M.; vanderMullen, J. A. M.; Vos, H. P. C.; deGroote, F. P. J.; Timmermans, E. A. H. On the Electron Temperatures and Densities in Plasmas Produced by the "Torche a Injection Axiale". *Spectrochimica Acta Part B-Atomic Spectroscopy* **1996**, *51*, 1385-1392.

(13) Schram, D. C.; vanderMullen, J. A. M.; deRegt, J. M.; Benoy, D. A.; GEy, G. H. A. G.; DeGrootte, F.; Jonkers, J. Fundamental Description of Spectrochemical Inductively Coupled Plasmas. *J. Anal. At. Spectrom.* **1996**, *11*, 623-632.

(14) Mermet, J. M. Fundamental Principles of Inductively Coupled Plasmas. In *Inductively Coupled Plasma Spectrometry and Its Applications*; Hill, S. J., Ed.; Sheffield Academic Press: 1999; Chapter 2.

(15) Mermet, J. M. Ionic to Atomic Line Intensity Ratio and Residence Time in Inductively Coupled Plasma Atomic Emission-Spectrometry. *Spectrochimica Acta Part B-Atomic Spectroscopy* **1989**, *44*, 1109-1116.

(16) Mermet, J. M. Use of Magnesium As a Test Element for Inductively Coupled Plasma Atomic Emission-Spectrometry Diagnostics. *Anal. Chim. Acta* **1991**, *250*, 85-94.

(17) Novotny, I.; Farinas, J. C.; Wan, J. L.; Poussel, E.; Mermet, J. M. Effect of Power and Carrier Gas Flow Rate on the Tolerance to Water Loading in Inductively Coupled Plasma Atomic Emission Spectrometry. *Spectrochimica Acta Part B-Atomic Spectroscopy* **1996**, *51*, 1517-1526.

(18) Romero, X.; Poussel, E.; Mermet, J. M. The Effect of Sodium on Analyte Ionic Line Intensities in Inductively Coupled Plasma Atomic Emission Spectrometry: Influence of the Operating Conditions. *Spectrochimica Acta Part B-Atomic Spectroscopy* **1997**, *52*, 495-502.

(19) Parisi, A. F.; Rayson, G. D.; Hieftje, G. M. Utilization of RF Power Modulation for Fundamental Investigation of the ICP. *Abstracts of Papers of the American Chemical Society* **1985**, *190*, 96-ANL.

(20) Olesik, J. W.; Bradley, K. R. Analyte Excitation in the Inductively Coupled Plasma Studied by Power Modulation. *Spectrochimica Acta Part B-Atomic Spectroscopy* **1987**, *42*, 377-392.

(21) Parisi, A. F.; Hieftje, G. M. Fundamental-Studies in the ICP Using a Sinusoidally Modulated Power Input. *Appl. Spectrosc.* **1986**, *40*, 181-185.

(22) Parisi, A. F.; Rayson, G. D.; Hieftje, G. M.; Olesik, J. W. Temporally and Spatially Resolved Studies in an Amplitude Modulated Inductively Coupled Plasma. *Spectrochimica Acta Part B-Atomic Spectroscopy* **1987**, *42*, 361-376.

(23) Huang, M.; Lehn, S. A.; Andrews, E. J.; Hieftje, G. M. Comparison of Electron Concentrations, Electron Temperatures, Gas Kinetic Temperatures, and Excitation Temperatures in Argon ICPs Operated at 27 and 40 MHz. *Spectrochimica Acta Part B-Atomic Spectroscopy* **1997**, *52*, 1173-1193.

(24) Angleys, G.; Mermet, J. M. Theoretical Aspects and Design of a Low-Power, Low-Flow-Rate Torch in Inductively Coupled Plasma Atomic Emission-Spectroscopy. *Appl. Spectrosc.* **1984**, *38*, 647-653.

(25) Rezaaiyaan, R.; Hieftje, G. M.; Anderson, H.; Kaiser, H.; Meddings, B. Design and Construction of a Low-Flow, Low-Power Torch for Inductively Coupled Plasma Spectrometry. *Appl. Spectrosc.* **1982**, *36*, 627-631.

(26) Ross, B. S.; Yang, P. G.; Hieftje, G. M. The Investigation of a 13-MM Torch for Use in Inductively Coupled Plasma Mass-Spectrometry. *Appl. Spectrosc.* **1991**, *45*, 190-197.

(27) Ross, B. S.; Chambers, D. M.; Vickers, G. H.; Yang, P. G.; Hieftje, G. M. Characterization of a 9-MM Torch for Inductively Coupled Plasma Mass-Spectrometry. *J. Anal. At. Spectrom.* **1990**, *5*, 351-358.

(28) Weiss, A. D.; Savage, R. N.; Hieftje, G. M. Development and Characterization of a 9-MM Inductively-Coupled Argon Plasma Source for Atomic Emission-Spectrometry. *Anal. Chim. Acta* **1981**, *124*, 245-258.

(29) Hieftje, G. M. Mini, Micro, and High-Efficiency Torches for the ICP - Toys or Tools. *Spectrochimica Acta Part B-Atomic Spectroscopy* **1983**, *38*, 1465-1481.

(30) Rezaaiyaan, R.; Hieftje, G. M. Analytical Characteristics of a Low-Flow, Low-Power Inductively Coupled Plasma. *Anal. Chem.* **1985**, *57*, 412-415.

(31) Rezaaiyaan, R.; Olesik, J. W.; Hieftje, G. M. Interferences in a Low -Flow, Low-Power Inductively Coupled Plasma. *Spectrochimica Acta Part B-Atomic Spectroscopy* **1985**, *40*, 73-83.

(32) Evans, E. H.; Ebdon, L. Comparison of Normal and Low-Flow Torches for Inductively Coupled Plasma Mass-Spectrometry Using Optimized Operating-Conditions. *J. Anal. At. Spectrom.* **1991**, *6*, 421-430.

(33) Michaudpoussel, E.; Mermet, J. M. Influence of the Generator Frequency and the Plasma Gas Inlet Area on Torch Design in Inductively Coupled Plasma Atomic Emission- Spectrometry. *Spectrochimica Acta Part B-Atomic Spectroscopy* **1986**, *41*, 125-132.

(34) Horner, J. A.; Hieftje, G. M. Characterization of a 22 Mm Torch for ICP-AES. *Appl. Spectrosc.* **1999,** *53,* 713-718.

(35) Mermet, J. M. Improvement in the Limits of Detection in Inductively Coupled Plasma Atomic Emission Spectrometry. *Annali di Chimica* **1997,** *87,* 211-219.

(36) Schron, W.; Liebmann, A. Experimental Studies for the Characterization of Analytical Performance in Axially-Observed Inductively Coupled Plasma Atomic Emission Spectrometry. *Fresenius Journal of Analytical Chemistry* **1998,** *361,* 207-210.

(37) Brenner, I. B.; Zander, A.; Cole, M. Comparison of Axially and Radially Viewed Inductively Coupled Plasmas for Multi-Element Analysis: Effect of Sodium and Calcium. *J. Anal. At. Spectrom.* **1997,** *12,* 897-906.

(38) Dubuisson, C.; Poussel, E.; Mermet, J. M. Comparison of Axially and Radially Viewed Inductively Coupled Plasma Atomic Emission Spectrometry in Terms of Signal-to-Background Ratio and Matrix Effects - Plenary Lecture. *J. Anal. At. Spectrom.* **1997,** *12,* 281-286.

(39) Brenner, I. B.; LeMarchand, A.; Daraed, C.; Chauvet, L. Compensation of Ca and Na Interference Effects in Axially and Radially Viewed Inductively Coupled Plasmas [Full Text Delivery]. *Microchem. J.* **1999,** *63,* 344-355.

(40) Dewit, M.; Blust, R. Determination of Metals in Saline and Biological Matrices by Axial Inductively Coupled Plasma Atomic Emission Spectrometry Using Microconcentric Nebulization. *J. Anal. At. Spectrom.* **1998,** *13,* 515-520.

(41) OHanlon, K.; Ebdon, L.; Foulkes, M. Effect of Easily Ionizable Elements on Solutions and Slurries in an Axially Viewed Inductively Coupled Plasma. *J. Anal. At. Spectrom.* **1996,** *11,* 427-436.

(42) Brenner, I. B.; Zander, A. T. Axially and Radially Viewed Inductively Coupled Plasmas - a Critical Review. *Spectrochimica Acta Part B-Atomic Spectroscopy* **2000,** *55,* 1195-1240.

(43) Olesik, J. W.; Bates, L. C. Characterization of Aerosols Produced by Pneumatic Nebulizers for Inductively-Coupled Plasma Sample Introduction - Effect of Liquid and

Gas Flow Rates on Volume Based Drop Size Distributions. *Spectrochimica Acta Part B-Atomic Spectroscopy* **1995**, *50*, 285-303.

(44) Jankowski, K.; Dreger, M. Study of an Effect of Easily Ionizable Elements on the Excitation of 35 Elements in an Ar-MIP System Coupled With Solution Nebulization. *J. Anal. At. Spectrom.* **2000**, *15*, 269-276.

(45) Sayama, Y. Studies on Rapid and High-Performance Analytical Systems for the Process Quality and Quantity Control of the Nonferrous Metal-Refining Industry. *Bunseki Kagaku* **1997**, *46*, 407-408.

(46) Botto, R. I.; Zhu, J. J. Universal Calibration for Analysis of Organic Solutions by Inductively Coupled Plasma Atomic Emission Spectrometry. *J. Anal. At. Spectrom.* **1996**, *11*, 675-681.

(47) Botto, R. I. Applications of Ultrasonic Nebulization in the Analysis of Petroleum and Petrochemicals by Inductively Coupled Plasma Atomic Emission- Spectrometry. *J. Anal. At. Spectrom.* **1993**, *8*, 51-57.

(48) Anderson, J. The Analysis of Drinking-Water by Icp-Aes/Ultrasonic Nebulization. *Atomic Spectroscopy* **1992**, *13*, 99-104.

(49) Masson, P.; Orignac, D.; Vives, A.; Prunet, T. Matrix Effects During Trace Elements Analysis in Plant Samples by Inductively Coupled Plasma Atomic Emission Spectrometry With Axial View Configuration and Ultrasonic Nebulizer. *Analusis* **1999**, *27*, 813-820.

(50) Budic, B. Matrix Effects in Inductively Coupled Plasma Atomic Emission Spectrometry Using an Ultrasonic Nebulizer. *J. Anal. At. Spectrom.* **1998**, *13*, 869-874.

(51) Hoenig, M.; Docekalova, H.; Baeten, H. Study of Matrix Interferences in Trace Element Analysis of Environmental Samples by Inductively Coupled Plasma Atomic Emission Spectrometry With Ultrasonic Nebulization. *J. Anal. At. Spectrom.* **1998**, *13*, 195-199.

(52) Carre, M.; Lebas, K.; Marichy, M.; Mermet, M.; Poussel, E.; Mermet, J. M. Influence of the Sample Introduction System on Acid Effects in Inductively-Coupled Plasma-Atomic Emission-Spectrometry. *Spectrochimica Acta Part B-Atomic Spectroscopy* **1995**, *50*, 271-283.

(53) Fisher, A.; Hill, S. J. Instrumentation for ICP-AES. In *Inductively Coupled Plasma Spectrometry and Its Applications*; Hill, S. J., Ed.; Sheffield Academic Press: 1999; Chapter 3.

(54) Hoenig, M.; Baeten, H.; Vanhentenrijk, S.; Ploegaerts, G.; Bertholet, T. Evaluation of Various Commercially Available Nebulization Devices for Inductively Coupled Plasma Atomic Emission Spectrometry. *Analusis* **1997,** *25,* 13-19.

(55) Sharp, B. L. Pneumatic Nebulizers and Spray Chambers for Inductively Coupled Plasma Spectrometry - A Review. 1. Nebulizers. *J. Anal. At. Spectrom.* **1988,** *3,* 613-652.

(56) Sharp, B. L. Pneumatic Nebulizers and Spray Chambers for Inductively Coupled Plasma Spectrometry - A Review. 2. Spray Chambers. *J. Anal. At. Spectrom.* **1988,** *3,* 939-963.

(57) Legere, G.; Salin, E. D. Fast-Clearing Spray Chamber for Icp-Aes. *Appl. Spectrosc.* **1994,** *48,* 761-765.

(58) Gervais, L. S.; Salin, E. D. Heated Sample Introduction System for the Analysis of Slurries by Inductively Coupled Plasma Atomic Emission-Spectrometry. *J. Anal. At. Spectrom.* **1991,** *6,* 41-47.

(59) Schron, W.; Muller, U. Influence of Heated Spray Chamber Desolvation on the Detectability in Inductively Coupled Plasma Atomic Emission Spectrometry. *Fresenius Journal of Analytical Chemistry* **1997,** *357,* 22-26.

(60) Maestre, S.; Mora, J.; Todoli, J. L.; Canals, A. Evaluation of Several Commercially Available Spray Chambers for Use in Inductively Coupled Plasma Atomic Emission Spectrometry. *J. Anal. At. Spectrom.* **1999,** *14,* 61-67.

(61) Olesik, J. W. Echelle Grating Spectrometers for Inductively Coupled Plasma- Optical Emission Spectrometry - A Review of Basic Equations and Operating Principles. *Spectroscopy* **1999,** *14,* 36-41.

(62) Barnard, T. W.; Crockett, M. I.; Ivaldi, J. C.; Lundberg, P. L. Design and Evaluation of an Echelle Grating Optical-System for Icp- Oes. *Anal. Chem.* **1993,** *65,* 1225-1230.

(63) Barnard, T. W.; Crockett, M. I.; Ivaldi, J. C.; Lundberg, P. L.; Yates, D. A.; Levine, P. A.; Sauer, D. J. Solid-State Detector for Icp-Oes. *Anal. Chem.* **1993,** *65,* 1231-1239.

(64) Belchamber, R. M.; Horlick, G. Correlation Study of Internal Standardization in Inductively Coupled Plasma Atomic Emission-Spectrometry. *Spectrochimica Acta Part B-Atomic Spectroscopy* **1982,** *37,* 1037-1046.

(65) Myers, S. A.; Tracy, D. H. Improved Performance Using Internal Standardization in Inductively- Coupled Plasma Emission-Spectroscopy. *Spectrochimica Acta Part B-Atomic Spectroscopy* **1983,** *38,* 1227-1253.

(66) Mermet, J. M.; Ivaldi, J. C. Real-Time Internal Standardization for Inductively-Coupled Plasma- Atomic Emission-Spectrometry Using a Custom Segmented-Array Charge-Coupled-Device Detector. *J. Anal. At. Spectrom.* **1993,** *8,* 795-801.

(67) Belchamber, R. M.; Horlick, G. Effect of Signal Integration Period on Measurement Precision in Inductively Coupled Plasma Emission-Spectrometry. *Spectrochimica Acta Part B-Atomic Spectroscopy* **1982,** *37,* 71-74.

(68) Belchamber, R. M.; Horlick, G. Correlation of Fluctuations in Emission Signals From an Inductively Coupled Plasma With Fluctuations in the Nebulizer Spray Chamber Pressure. *Spectrochimica Acta Part B-Atomic Spectroscopy* **1982,** *37,* 1075-1078.

(69) Romero, X.; Poussel, E.; Mermet, J. M. Influence of the Operating Conditions on the Efficiency of Internal Standardization in Inductively Coupled Plasma Atomic Emission Spectrometry. *Spectrochimica Acta Part B-Atomic Spectroscopy* **1997,** *52,* 487-493.

(70) Mermet, J. M.; Poussel, E. Icp Emission Spectrometers - 1995 Analytical Figures of Merit. *Appl. Spectrosc.* **1995,** *49,* A12-A18.

(71) Poussel, E.; Mermet, J. M.; Samuel, O. Simple Experiments for the Control, the Evaluation and the Diagnosis of Inductively-Coupled Plasma Sequential Systems. *Spectrochimica Acta Part B-Atomic Spectroscopy* **1993,** *48,* 743-755.

(72) Carre, M.; Poussel, E.; Mermet, J. M. Drift Diagnostics in Inductively Coupled Plasma Atomic Emission- Spectrometry. *J. Anal. At. Spectrom.* **1992,** *7,* 791-797.

(73) Lalchev, M.; Ionov, I.; Daskalova, N. Application of Inductively Coupled Plasma Atomic Emission Spectrometry in Forensic Science. *J. Anal. At. Spectrom.* **1997,** *12,* 21-24.

(74) Cave, M.; Butler, O.; Cook, J. M.; Cresser, M. S.; Garden, L. M.; Miles, D. L. Environmental Analysis. *J. Anal. At. Spectrom.* **2000,** *15,* 181-235.

(75) Fairman, B.; Hinds, M. W.; Nelms, S. M.; Penny, D. M.; Goodall, P. Industrial Analysis: Metals, Chemicals and Advance Materials. *J. Anal. At. Spectrom.* **2000,** *15,* 1606-1631.

(76) Taylor, A.; Branch, S.; Halls, D. J.; Owen, L. M. W.; White, M. Clinical and Biological Materials, Food and Beverages. *J. Anal. At. Spectrom.* **2000,** *15,* 451-487.

(77) Velichkov, S.; Kostadinova, E.; Daskalova, N. Spectral Interferences in the Determination of Traces of Scandium, Yttrium and Rare Earth Elements in "Pure" Rare Earth Matrices by Inductively Coupled Plasma Atomic Emission Spectrometry. Part IV. Lutetium and Yttrium. **1998,** *53.*

(78) Bae, Z. U.; Lee, S. H.; Lee, S. H. Line Selection and Interference Correction for the Analysis of Tungsten Alloy by Inductively Coupled Plasma Atomic Emission Spectrometry. *Talanta* **1997**, *44*, 47-51.

(79) Conte, R. A.; Mermet, J. M.; Rodrigues, J. D.; DiMartino, J. L. Analysis of Tantalum Products by Inductively Coupled Plasma Atomic Emission Spectrometry. *J. Anal. At. Spectrom.* **1997**, *12*, 1215-1220.

(80) Daskalova, N.; Boevski, I. Spectral Interferences in the Determination of Trace Elements in Environmental Materials by Inductively Coupled Plasma Atomic Emission Spectrometry. *Spectrochimica Acta Part B-Atomic Spectroscopy* **1999**, *54*, 1099-1122.

(81) vanVeen, E. H.; deLoosVollebregt, M. T. C. Application of Mathematical Procedures to Background Correction and Multivariate Analysis in Inductively Coupled Plasma-Optical Emission Spectrometry. *Spectrochimica Acta Part B-Atomic Spectroscopy* **1998**, *53*, 639-669.

(82) Nolte, J. Minimizing Spectral Interferences With an Array ICP Emission Spectrometer Using Different Strategies for Signal Evaluation. *Atomic Spectroscopy* **1999**, *20*, 103-107.

(83) Danzaki, Y.; Takada, K.; Wagatsuma, K.; Oku, M. Accurate and Rapid Estimation on Spectral Interferences in Routine Analysis by ICP-AES: Use of Mutual Interference Coefficients. *Fresenius Journal of Analytical Chemistry* **1998**, *361*, 410-418.

(84) Todoli, J. L.; Mermet, J. M.; Canals, A.; Hernandis, V. Acid Effects in Inductively Coupled Plasma Atomic Emission Spectrometry With Different Nebulizers Operated at Very Low Sample Consumption Rates. *J. Anal. At. Spectrom.* **1998**, *13*, 55-62.

(85) Todoli, J. L.; Mermet, J. M. Effect of the Spray Chamber Design on Steady and Transient Acid Interferences in Inductively Coupled Plasma Atomic Emission Spectrometry. *J. Anal. At. Spectrom.* **2000**, *15*, 863-867.

(86) Fernandez, A.; Murillo, M.; Carrion, N.; Mermet, J. M. Influence of Operating-Conditions on the Effects of Acids in Inductively-Coupled Plasma-Atomic Emission-Spectrometry. *J. Anal. At. Spectrom.* **1994**, *9*, 217-221.

(87) Dubuisson, C.; Poussel, E.; Mermet, J. M.; Todoli, J. L. Comparison of the Effect of Acetic Acid With Axially and Radially Viewed Inductively Coupled Plasma Atomic Emission Spectrometry: Influence of the Operating Conditions. *J. Anal. At. Spectrom.* **1998**, *13*, 63-67.

(88) Todoli, J. L.; Mermet, J. M. Minimization of Acid Effects at Low Consumption Rates in an Axially Viewed Inductively Coupled Plasma Atomic Emission Spectrometer by Using Micronbulizer-Based Sample Introduction Systems. *J. Anal. At. Spectrom.* **1998**, *13*, 727-734.

(89) Catasus, M.; Todoli, J. L.; Gras, L.; Hernandis, V. Selection of the Operating Conditions for Overcoming Acids and Sodium Chloride Non-Spectroscopic Interferences in Inductively Coupled Plasma Atomic Emission Spectrometry: Effect of the Liquid-to-Vapor Mass Ratios. *J. Anal. At. Spectrom.* **2000**, *15*, 1203-1206.

(90) Todoli, J. L.; Mermet, J. M. Acid Interferences in Atomic Spectrometry: Analyte Signal Effects and Subsequent Reduction. *Spectrochimica Acta Part B-Atomic Spectroscopy* **1999**, *54*, 895-929.

(91) Blades, M. W.; Horlick, G. Interference From Easily Ionizable Element Matrices in Inductively Coupled Plasma Emission-Spectrometry - a Spatial Study. *Spectrochimica Acta Part B-Atomic Spectroscopy* **1981**, *36*, 881-900.

(92) AlAmmar, A. S.; Barnes, R. M. Inelastic Collisional Deactivation in Plasma-Related Non- Spectroscopic Matrix Interferences in Inductively Coupled Plasma Atomic Emission Spectrometry. *Spectrochimica Acta Part B-Atomic Spectroscopy* **1999**, *54*, 1063-1076.

(93) Olesik, J. W.; Williamsen, E. J. Easily and Noneasily Ionizable Element Matrix Effects in Inductively Coupled Plasma Optical Spectrometry. *Appl. Spectrosc.* **1989**, *43*, 1223-1232.

(94) Holclajtnerantunovic, I. D.; Tripkovic, M. R. Study of the Matrix Effect of Easily and Non-Easily Ionizable Elements in Inductively Coupled Argon Plasma .2. Equilibrium Plasma Composition. *J. Anal. At. Spectrom.* **1993**, *8*, 359-365.

(95) Hanselman, D. S.; Sesi, N. N.; Huang, M.; Hieftje, G. M. The Effect of Sample Matrix on Electron-Density, Electron-Temperature and Gas Temperature in the Argon Inductively-Coupled Plasma Examined by Thomson and Rayleigh-Scattering. *Spectrochimica Acta Part B-Atomic Spectroscopy* **1994**, *49*, 495-526.

(96) Galley, P. J.; Glick, M.; Hieftje, G. M. Easily Ionizable Element Interferences in Inductively-Coupled Plasma- Atomic Emission-Spectroscopy .1. Effect on Radial Analyte Emission Patterns. *Spectrochimica Acta Part B-Atomic Spectroscopy* **1993**, *48*, 769-788.

(97) Xu, Q.; Mattu, G.; Agnes, G. R. Influence of Droplets With Net Charge in Inductively Coupled Plasma Atomic Emission Spectroscopy and Implications for the Easily Ionizable Element Chemical Matrix Effect. *Appl. Spectrosc.* **1999**, *53*, 965-973.

(98) Hobbs, S. E.; Olesik, J. W. The Influence of Incompletely Desolvated Droplets and Vaporizing Particles on Chemical Matrix Effects in Inductively Coupled Plasma Spectrometry: Time-Gated Optical Emission and Laser-Induced Fluorescence Measurements. *Spectrochimica Acta Part B-Atomic Spectroscopy* **1997**, *52*, 353-367.

(99) Galley, P. J.; Hieftje, G. M. Easily Ionizable Element (Eie) Interferences in Inductively-Coupled Plasma-Atomic Emission-Spectrometry .2. Minimization of Eie Effects by Choice of Observation Volume. *Spectrochimica Acta Part B-Atomic Spectroscopy* **1994**, *49*, 703-724.

(100) Dubuisson, C.; Poussel, E.; Todoli, J. L.; Mermet, J. M. Effect of Sodium During the Aerosol Transport and Filtering in Inductively Coupled Plasma Atomic Emission Spectrometry. *Spectrochimica Acta Part B-Atomic Spectroscopy* **1998**, *53*, 593-600.

(101) Mermet, J. M. Revisitation of the Matrix Effects in Inductively Coupled Plasma Atomic Emission Spectrometry: the Key Role of the Spray Chamber - Invited Lecture. *J. Anal. At. Spectrom.* **1998**, *13*, 419-422.

(102) Budic, B.; Hudnik, V. Matrix Effects of Potassium Chloride and Phosphoric Acid in Argon Inductively Coupled Plasma Atomic Emission Spectrometry. *J. Anal. At. Spectrom.* **1994**, *9*, 53-57.

(103) Thompson, M.; Ramsey, M. H. Matrix Effects Due to Calcium in Inductively Coupled Plasma Atomic- Emission Spectrometry - Their Nature, Source and Remedy. *Analyst* **1985**, *110*, 1413-1422.

(104) Sesi, N. N.; Hieftje, G. M. Studies into the Interelement Matrix Effect in Inductively Coupled Plasma Spectrometry. *Spectrochimica Acta Part B-Atomic Spectroscopy* **1996**, *51*, 1601-1628.

(105) Sadler, D. A.; Sun, F.; Howe, S. E.; Littlejohn, D. Comparison of Procedures for Correction of Matrix Interferences in the Multi-Element Analysis of Soils by ICP-AES With a CCD Detection System. *Mikrochim. Acta* **1997**, *126*, 301-311.

(106) Ramsey, M. H.; Thompson, M. A Predictive Model of Plasma Matrix Effects in Inductively Coupled Plasma Atomic Emission-Spectrometry. *J. Anal. At. Spectrom.* **1986**, *1*, 185-193.

(107) Thompson, M.; Ramsey, M. H.; Coles, B. J.; Du, C. M. Correction of Matrix Effects in Inductively Coupled Plasma Atomic Emission-Spectrometry by Interactive Power Adjustment. *J. Anal. At. Spectrom.* **1987, 2,** 185-188.

(108) Thompson, M.; Ramsey, M. H. Extrapolation to Infinite Dilution - a Method for Overcoming Matrix Effects. *J. Anal. At. Spectrom.* **1990, 5,** 701-704.

(109) AlAmmar, A. S.; Barnes, R. M. Correction for Drift in ICP-OES Measurements by Internal Standardization Using Spectral Lines of the Same Analyte As Internal Reference. *Atomic Spectroscopy* **1998, 19,** 18-22.

(110) AlAmmar, A. S.; Barnes, R. M. Correction for Non-Spectroscopic Matrix Effects in Inductively Coupled Plasma-Atomic Emission Spectroscopy by Internal Standardization Using Spectral Lines of the Same Analyte. *Spectrochimica Acta Part B-Atomic Spectroscopy* **1998, 53,** 1583-1593.

(111) Villanueva, M.; Pomares, M.; Catasus, M.; Diaz, J. Application of Factorial Desingns for the Description and Correction of Combined Matrix Efects in ICP-AES. *Quimica Analitica* **2000, 19,** 39-42.

(112) Massart, D. L.; Vandeginste, B. G. M.; Deming S.N.; Michotte Y.; Kaufman, L., Chemometrics: a Textbook; Elsevier: 1988.

(113) Massart, D. L.; Kaufman, L., Interpretation of Analytical Data by the Use of Cluster Analysis; Wiley, New York: 1983.

(114) Einax, J. W.; Zwanziger, H. W.; Geis, S., Chemometrics in Environmental Analysis; VCH: 1997.

(115) Brereton, R. G., Chemometrics: Application of Mathematics and Statistics to Laboratory Systems; Ellis Horwood: 1990.

(116) Vandeginste, B. G. M.; Massart, D. L.; Buydens, L. C. M.; Jong, S.; Lewi, P. J.; Smeyers-Verbeke, J., Handbook of Chemometrics and Qualimetrics: Part B; Elsevier: 1998.

(117) Vandeginste, B. G. M.; Massart, D. L.; Buydens, L. C. M.; Jong, S.; Lewi, P. J.; Smeyers-Verbeke, J., Handbook of Chemometrics and Qualimetrics: Part A; Elsevier: 1998.

(118) Atkinson A.C.; Donev A.N., Optimum Experimental Designs; Oxford Science Publications: 1996.

(119) D.C Montgomery, Design and Analysis of Experiments; John Wiley & Sons.: 1997.

(120) Malinowski, E. R., Factor Analysis in Chemistry; 1991.

(121) Brereton, R. G. Introduction to Multivariate Calibration in Analytical Chemistry. *Analyst* **2000**, *125*, 2125-2154.

(122) Brown, S. D. The Kalman Filter in Analytical Chemistry. *Anal. Chim. Acta* **1986**, *181*, 1-26.

(123) Chatfield, C., The Analysis of Time Series: An Introduction; Chapman & Hall: 1997.

(124) Smilde, A. K. 3-Way Analyses - Problems and Prospects. *Chemometrics and Intelligent Laboratory Systems* **1992**, *15*, 143-157.

(125) Bro, R. PARAFAC. Tutorial and Applications. *Chemometrics and Intelligent Laboratory Systems* **1997**, *38*, 149-171.

(126) Harshman, R. A.; Lundy, M. E. Parafac - Parallel Factor-Analysis. *Computational Statistics & Data Analysis* **1994**, *18*, 39-72.

(127) Bro, R. Multi-way Analysis in the Food Industry. Models, Algorithms, and Applications. 1998. University of Amsterdam (NL) & Royal Veterinary and Agricultural University (DK).
Ref Type: Thesis/Dissertation

(128) Bro, R. N-way on-line course on PARAFAC and PLS. 1998.
Ref Type: Internet Communication

(129) Tucker, L. Some Mathematics Notes on the Three Mode Factor Analysis. *Psychometrika* **1966**, *31*, 279-311.

(130) Andersson, C. A. Interactive introduction to the Tucker3 model in chemometrics. 1999.
Ref Type: Internet Communication

(131) Bro, R. Multiway Calibration. Multilinear PLS. *Journal of Chemometrics* **1996**, *10*, 47-61.

(132) Smilde, A. K. Comments on Multilinear PLS. *Journal of Chemometrics* **1997**, *11*, 367-377.

(133) Salin, E. D.; Winston, P. H. Machine Learning and Artificial-Intelligence - an Introduction. *Anal. Chem.* **1992**, *64*, A49.

(134) Bos, M.; Bos, A.; Vanderlinden, W. E. Data-Processing by Neural Networks in Quantitative Chemical-Analysis. *Analyst* **1993**, *118*, 323-328.

(135) Brereton, R. G. CHEMOMETRICS IN ANALYTICAL-CHEMISTRY - A REVIEW. *Analyst* **1987**, *112*, 1635-1657.

(136) Araujo, P. W.; Brereton, R. G. Experimental Design .1. Screening. *Trac-Trends in Analytical Chemistry* **1996**, *15*, 26-31.

(137) Araujo, P. W.; Brereton, R. G. Experimental Design .2. Optimization. *Trac-Trends in Analytical Chemistry* **1996**, *15*, 63-70.

(138) Araujo, P. W.; Brereton, R. G. Experimental Design .3. Quantification. *Trac-Trends in Analytical Chemistry* **1996**, *15*, 156-163.

(139) Marcos, A.; Fisher, A.; Rea, G.; Hill, S. J. Preliminary Study Using Trace Element Concentrations and a Chemometrics Approach to Determine the Geographical Origin of Tea. *J. Anal. At. Spectrom.* **1998**, *13*, 521-525.

(140) Webster, L.; Simpson, P.; Shanks, A. M.; Moffat, C. F. The Authentication of Olive Oil on the Basis of Hydrocarbon Concentration and Composition. *Analyst* **2000**, *125*, 97-104.

(141) Haswell, S. J.; Walmsley, A. D. Multivariate Data Visualisation Methods Based on Multi- Elemental Analysis of Wines and Coffees Using Total Reflection X-Ray Fluorescence Analysis. *J. Anal. At. Spectrom.* **1998**, *13*, 131-134.

(142) Sun, L. X.; Danzer, K.; Thiel, G. Classification of Wine Samples by Means of Artificial Neural Networks and Discrimination Analytical Methods. *Fresenius Journal of Analytical Chemistry* **1997**, *359*, 143-149.

(143) Yasui, A.; Shindoh, K. Determination of the Geographic Origin of Brown-Rice With Trace-Element Composition. *Bunseki Kagaku* **2000**, *49*, 405-410.

(144) Kokot, S.; Phuong, T. D. Elemental Content of Vietnamese Rice - Part 2. Multivariate Data Analysis. *Analyst* **1999**, *124*, 561-569.

(145) Bruno, P.; Caselli, M.; Curri, M. L.; Genga, A.; Striccoli, R.; Traini, A. Chemical Characterisation of Ancient Pottery From South of Italy by Inductively Coupled Plasma Atomic Emission Spectroscopy (ICP-AES) Statistical Multivariate Analysis of Data. *Anal. Chim. Acta* **2000**, *410*, 193-202.

(146) Cave, M. R.; Harmon, K. Determination of Trace Metal Distributions in the Iron Oxide Phases of Red Bed Sandstones by Chemometric Analysis of Whole Rock and Selective Leachate Data. *Analyst* **1997**, *122*, 501-512.

(147) Cave, M. R.; Wragg, J. Measurement of Trace Element Distributions in Soils and Sediments Using Sequential Leach Data and a Non-Specific Extraction System With Chemometric Data Processing. *Analyst* **1997**, *122*, 1211-1221.

(148) Praisler, M.; Dirinck, I.; Van Bocxlaer, J.; De Leenheer, A.; Massart, D. L. Pattern Recognition Techniques Screening for Drugs of Abuse With Gas Chromatography-Fourier Transform Infrared Spectroscopy. *Talanta* **2000**, *53*, 177-193.

(149) Crisponi, G.; Cristiani, F.; Leardi, R.; Nurchi, V. M. Inorganic Pollution in the Soil of an Industrial Plant. A Chemometric Study. *Annali di Chimica* **2000**, *90*, 201-208.

(150) Cave, M. Improvement of Short-Term Precision in Inductively Coupled Plasma Atomic Emission Spectrometry by Principal Component Analysis Modelling. *J. Anal. At. Spectrom.* **1998**, *13*, 125-129.

(151) Huhn, G.; Schulz, H.; Stark, H. J.; Tolle, R.; Schuurmann, G. Evaluation of Regional Heavy Metal Deposition by Multivariate-Analysis of Element Contents in Pine Tree Barks. *Water Air and Soil Pollution* **1995**, *84*, 367-383.

(152) Candolfi, A.; De Maesschalck, R.; Massart, D. L.; Hailey, P. A.; Harrington, A. C. E. Identification of Pharmaceutical Excipients Using NIR Spectroscopy and SIMCA. *Journal of Pharmaceutical and Biomedical Analysis* **1999**, *19*, 923-935.

(153) Kramer, K.; Ebel, S. Application of NIR Reflectance Spectroscopy for the Identification of Pharmaceutical Excipients. *Anal. Chim. Acta* **2000**, *420*, 155-161.

(154) Al Jowder, O.; Defernez, M.; Kemsley, E. K.; Wilson, R. H. Mid-Infrared Spectroscopy and Chemometrics for the Authentication of Meat Products. *J. Agric. Food Chem.* **1999**, *47*, 3210-3218.

(155) Sadler, D. A.; Littlejohn, D. Use of Multiple Emission Lines and Principal Component Regression for Quantitative Analysis in Inductively Coupled Plasma Atomic Emission Spectrometry With Charge Coupled Device Detection. *J. Anal. At. Spectrom.* **1996**, *11*, 1105-1112.

(156) Coscione, A. R.; de Andrade, J. C.; Poppi, R. J.; Mello, C.; van Raij, B.; de Abreu, M. F. Multivariate Calibration Applied to a Highly Interfering Chemical System - The Simultaneous Spectrophotometric Determination of Aluminium and Iron in Plants Using Xylenol Orange and Partial Least-Squares Regression. *Anal. Chim. Acta* **2000**, *423*, 31-40.

(157) Cladera, A.; Alpizar, J.; Estela, J. M.; Cerda, V.; Catasus, M.; Lastres, E.; Garcia, L. Resolution of Highly Overlapping Differential Pulse Anodic Stripping Voltammetric Signals Using Multicomponent Analysis and Neural Networks. *Anal. Chim. Acta* **1997**, *350*, 163-169.

(158) Andrew, K. N.; Rutan, S. C.; Worsfold, P. J. Application of Kalman Filtering to Multivariate Calibration and Drift Correction. *Anal. Chim. Acta* **1999**, *388*, 315-325.

(159) Rutan, S. C.; Bouveresse, E.; Andrew, K. N.; Worsfold, P. J.; Massart, D. L. Correction for Drift in Multivariate Systems Using the Kalman Filter. *Chemometrics and Intelligent Laboratory Systems* **1996**, *35*, 199-211.

(160) vanVeen, E. H.; deLoosVollebregt, M. T. C. Kalman Filtering for Data Reduction in Inductively Coupled Plasma Atomic Emission-Spectrometry. *Anal. Chem.* **1991**, *63*, 1441-1448.

(161) Harshman, R. A. Foundations of the PARAFAC Procedure: Model and Conditions for an 'Explanatory' Multi-Mode Factor Analysis. *UCLA Working Papers in Phonetics* **1970**, *16*, 1.

(162) Bro, R. Exploratory Study of Sugar Production Using Fluorescence Spectroscopy and Multi-Way Analysis. *Chemometrics and Intelligent Laboratory Systems* **1999**, *46*, 133-147.

(163) Beltran, J. L.; Ferrer, R.; Guiteras, J. Multivariate Calibration of Polycyclic Aromatic Hydrocarbon Mixtures From Excitation-Emission Fluorescence Spectra. *Anal. Chim. Acta* **1998**, *373*, 311-319.

(164) Norgaard, L. Spectral Resolution and Prediction of Slit Widths in Fluorescence Spectroscopy by Two- and Three-Way Methods. *Journal of Chemometrics* **1996**, *10*, 615-630.

(165) Hindmarch, P.; Kavianpour, K.; Brereton, R. G. Evaluation of Parallel Factor Analysis for the Resolution of Kinetic Data by Diode-Array High-Performance Liquid Chromatography. *Analyst* **1997**, *122*, 871-877.

(166) Smilde, A. K.; Doornbos, D. A. 3-Way Methods for the Calibration of Chromatographic Systems - Comparing Parafac and 3-Way Pls. *Journal of Chemometrics* **1991**, *5*, 345-360.

(167) Westerhuis, J. A.; Kourti, T.; Macgregor, J. F. Comparing Alternative Approaches for Multivariate Statistical Analysis of Batch Process Data. *Journal of Chemometrics* **1999**, *13*, 397-413.

(168) Boque, R.; Smilde, A. K. Monitoring and Diagnosing Batch Processes With Multiway Covariates Regression Models. *AIChE J.* **1999**, *45*, 1504-1520.

(169) Dahl, K. S.; Piovoso, M. J.; Kosanovich, K. A. Translating Third-Order Data Analysis Methods to Chemical Batch Processes. *Chemometrics and Intelligent Laboratory Systems* **1999**, *46*, 161-180.

(170) Louwerse, D. J.; Smilde, A. K. Multivariate Statistical Process Control of Batch Processes Based on Three-Way Models. *Chemical Engineering Science* . **2000**, 1225-1235.

(171) Westerhuis, J. A.; Kourti, T.; Macgregor, J. F. Comparing Alternative Approaches for Multivariate Statistical Analysis of Batch Process Data. *Journal of Chemometrics.* **1999**, 397-413.

(172) Webb, D. P.; Salin, E. D. Line Selection Expert System for Control of Scanning Inductively Coupled Plasma Atomic Emission Spectrometers. *J. Anal. At. Spectrom.* **1989**, *4*, 793-796.

(173) Webb, D. P.; Salin, E. D. An Electronic Aid for Line Selection for Scanning Inductively Coupled Plasma Atomic Emission Spectrometers. *Spectrochimica Acta Part B-Atomic Spectroscopy* **1992**, *47*, E1587-E1594.

(174) Webb, D. P.; Hamier, J.; Salin, E. D. The Autonomous Instrument - a Design. *Trac-Trends in Analytical Chemistry* **1994**, *13*, 44-53.

(175) Branagh, W.; Whelan, C.; Salin, E. D. System for Automatic Selection of Operating Conditions for Inductively Coupled Plasma Atomic Emission Spectroscopy. *J. Anal. At. Spectrom.* **1997**, *12*, 1307-1315.

(176) Sartoros, C.; Alary, J. F.; Salin, E. D.; Mermet, J. M. An Expert System Program for ICP-AES System Diagnosis. *Spectrochimica Acta Part B-Atomic Spectroscopy* **1997**, *52*, 1923-1927.

(177) Blank T.B.; Brown, S. D. Data Processing Using Neural Networks. *Anal. Chim. Acta* **1993**, *277*, 273-287.

(178) Glick, M.; Hieftje, G. M. Classification of Alloys With an Artificial Neural Network and Multivariate Calibration of Glow-Discharge Emission-Spectra. *Appl. Spectrosc.* **1991**, *45*, 1706-1716.

(179) Brown, S. D. Information and Data Handling in Chemistry and Chemical Engineering: the State of the Field From the Perspective of Chemometrics. *Computers & Chemical Engineering* **1998**, *23*, 203-216.

(180) Ramsey, M. H.; Thompson, M. Improved Precision in Inductively Coupled Plasma Atomic-Emission Spectrometry by a Parameter-Related Internal Standard Method. *Analyst* **1984,** *109,* 1625-1626.

(181) Ramsey, M. H.; Thompson, M. Correlated Variance in Simultaneous Inductively Coupled Plasma Atomic-Emission Spectrometry - Its Causes and Correction by a Parameter-Related Internal Standard Method. *Analyst* **1985,** *110,* 519-530.

(182) Mark, H. and Workman, J.; Statistics in Spectroscopy; Academy Press: San Diego, 1991.

(183) Salin, E. D.; Horlick, G. Signal-to-Noise Ratio Performance Characteristics of an Inductively Coupled Plasma. *Anal. Chem.* **1980,** *52,* 1578-1582.

(184) Rezaaiyaan, R.; Hieftje, G. M. Correlation of Sample-Introduction System With the Nature and Magnitude of Interferences in ICP. *Abstracts of Papers of the American Chemical Society* **1985,** *190,* 94-ANL.

(185) Zhiglinsky, A. G.; Bodin, N. S.; Kalmakov, A. A.; Tsaryev, V. I. The Use of Correlations to Improve the Precision and Accuracy of Emission Spectral-Analysis. *Spectrochimica Acta Part B-Atomic Spectroscopy* **1982,** *37,* 1029-1035.

(186) Karanassios, V.; Drouin, P. J.; Spiers, G. A. Automated Detection and Interpretation of Spectral Information Using Cross-Correlation, Millilitre Volumes, Pneumatic Nebulization Sample Introduction and Inductively Coupled Plasma-Atomic Emission Spectrometry With Photodiode Array Detection. *Spectrochimica Acta Part B-Atomic Spectroscopy* **1998,** *53,* 1149-1166.

(187) Chausseau, M.; Poussel, E.; Mermet, J. M. Effect of the Operating Parameters on Second Scale Time Correlation Between Lines of the Same Element Using Axially Viewed Inductively Coupled Plasma-Multichannel-Based Emission Spectrometry. *Spectrochimica Acta Part B-Atomic Spectroscopy* **2000,** *55,* 1431-1450.

(188) Lopezmolinero, A.; Caballero, A. V.; Castillo, J. R. Classification of Emission Spectral-Lines in Inductively-Coupled Plasma-Atomic Emission-Spectroscopy Using Principal Component Analysis. *Spectrochimica Acta Part B-Atomic Spectroscopy* **1994,** *49,* 677-682.

(189) Moreda-Piñeiro, A.; Marcos, A.; Fisher, A.; Hill, S. J. Chemometrics approaches for the study of systematic error in inductivaly coupled plasma emission spectrometry and mass spectrometry. Journal of Analytical Atomic Spectrometry . 2001. Ref Type: In Press

(190) Lorber, A.; Goldbart, Z. Application of the Generalized Internal Reference Method for the Characterization of Parameters Causing Drift in Inductively-Coupled Plasma Emission-Spectrometry. *Anal. Chim. Acta* **1984**, *161*, 163-173.

(191) Bro, R. The N-Way Toolbox for Matlab. 1998. Ref Type: Computer Program

(192) Bro, R.; Kiers, H. A. L. A New Efficient Method for Determining the Number of Components in PARAFAC Models. *Journal of Chemometrics* **2000**.

(193) Barnett W.B.; Fassel V.A.; Kniseley R.N. Theorical Principles of Internal Standardisation in Analytical Emission Spectrometry. *Spectrochimica Acta Part B-Atomic Spectroscopy* **1968**, *23*, 643-664.

(194) Barnett W.B.; Fassel V.A.; Kniseley R.N. An Experimental Study of Internal Standardisation in Analytical Atomic Spectroscopy. *Spectrochimica Acta Part B-Atomic Spectroscopy* **1970**, *25*, 139-161.

(195) Lorber, A.; Goldbart, Z. Generalized Internal Reference Method for Simultaneous Multichannel Analysis. *Anal. Chem.* **1984**, *56*, 37-43.

(196) Lorber, A.; Goldbart, Z.; Eldan, M. Correction for Drift by Internal Reference Methods in Inductively Coupled Plasma Simultaneous Multielement Analysis. *Anal. Chem.* **1984**, *56*, 43-48.

(197) Lorber, A.; Eldan, M.; Goldbart, Z. Improved Detection Limits in Inductively Coupled Plasma Multichannel Spectrometry of Uranyl-Nitrate Solutions by Compensation of Nonrandom Background Fluctuations. *Anal. Chem.* **1985**, *57*, 851-857.

(198) Lorber, A.; Goldbart, Z.; Harel, A. Compensation for Background Variation by Generalized Background Subtraction. *Anal. Chem.* **1985**, *57*, 2537-2540.

(199) Lorber, A.; Goldbart, Z.; Harel, A.; Sharvit, E.; Eldan, M. Application of the Generalized Internal Reference Method to High- Accuracy Assay of Metallurgical Samples by Icp. *Spectrochimica Acta Part B-Atomic Spectroscopy* **1986**, *41*, 105-113.

(200) AlAmmar, A. S.; Hamid, H. A.; Rashid, B. H. Elimination of Interferences and Effects From Drift in Working Parameters in Inductively Coupled Plasma Atomic Emission-Spectrometry by Using a Combination of the Generalized Standard Addition Method and the Generalized Internal Reference Method. *Spectrochimica Acta Part B-Atomic Spectroscopy* **1990**, *45*, 359-366.

(201) AlAmmar, A. S.; Gupta, R. K.; Barnes, R. M. Correction for Non-Spectroscopic Matrix Effects in Inductively Coupled Plasma-Mass Spectrometry by Common Analyte Internal Standardization. *Spectrochimica Acta Part B-Atomic Spectroscopy* **1999**, *54*, 1849-1860.

(202) AlAmmar, A. A.; Gupta, R. K.; Barnes, R. M. Universal Calibration for Analysis of Organic Solutions of Medium and Low Volatility by Inductively Coupled Plasma-Atomic Emission Spectrometry. *J. Anal. At. Spectrom.* **1999**, *14*, 801-807.

(203) AlAmmar, A. S.; Gupta, R. K.; Barnes, R. M. Correction for Volatility Differences Between Organic Sample Analytes and Standards in Organic Solutions Analyzed by Inductively Coupled Plasma-Atomic Emission and Mass Spectrometry. *J. Anal. At. Spectrom.* **1999**, *14*, 793-799.

(204) Catasus, M.; Branagh, W.; Salin, E. D. Improved Calibration for Inductively-Coupled Plasma-Atomic Emission- Spectrometry Using Generalized Regression Neural Networks. *Appl. Spectrosc.* **1995**, *49*, 798-807.

(205) Boss, C. B.; Fredeen, K., Concepts, Instrumentation and Techniques in Inductively Coupled Plasma Optical Emission Spectrometry; Perkin Elmer: 1997.

(206) Boumans, P. W. J. M.; Broekaert, J. A. C.; Bubert, H.; Hagenah, W.; Hieftje, G. M.; Olesik, J. W., Boumans, P. W. J. M.; Inductively Coupled Plasma Emission Spectroscopy. Part 1; John Wiley & Sons: 1987.

(207) Zander, A. T.; Chien, R. L.; Cooper, C. B.; Wilson, P. V. An Image-Mapped Detector for Simultaneous ICP-AES. *Anal. Chem.* **1999**, *71*, 3332-3340.

(208) Masson, P. Matrix Effects During Trace Element Analysis in Plant Samples by Inductively Coupled Plasma Atomic Emission Spectrometry With Axial View Configuration and Pneumatic Nebulizer. *Spectrochimica Acta Part B-Atomic Spectroscopy* **1999**, *54*, 603-612.

MEETINGS ATTENDED

RSC ASG/ASU Meeting on Chemometrics,

University of Nottingham, 27 March 1998

RSC Analytical Division, R&D Young Researcher's Meeting,

University of Durham, 6-8 April 1998

A poster was presented entitled:

Finger printing ot tea using trace metal profile and pattern recognition techniques.

9th BNASS,

University of Bath, 8-10 July 1998

Two posters were presented:

Authentication of the origin of tea using trace metal profile and pattern recognition techniques

A chemometrics approach to correct drift in ICP-AES.

European Workshop in Chemometrics

University of Bristol, 13-18 December 1998

European Winter Conference on Plasma Spectrochemistry

Pau, France, 10-15 January 1999

A poster was presented entitled:

Drift diagnosis in ICP-AES Systems

RSC Analytical Division, R&D Young Researcher's Meeting,

University of Greenwich, 12-14 April 1999

An oral presentation was given entitled:

Stability Studies in ICP-AES Systems

The Plasma Winter Conference,

Florida, USA, January 2000.

A poster was sent entitled:

Characterisation of long-term drift phenomenon in ICP-AES

RSC Analytical Division, R&D Young Researcher's Meeting,

UMIST, University of Manchester, 16-17 April 2000

Two posters were presented entitled:

Characterisation of long-term drift phenomena in ICP-AES

The influence of matrix effects on stability in ICP-AES

10th BNASS,

University of Sheffield, 17-20 July 2000

A contributed lecture was given entitled:

A study of long-term stability in ICP-AES

Two posters were presented entitled:

Application of chemometric approaches for the study of systematic error in ICP-AES/MS

Study of systematic error in ICP-AES/MS by Parallel Factor Analysis (PARAFAC)

PUBLICATIONS

1. Preliminary Study Using Trace Element Concentrations and a Chemometrics Approach to Determine the Geographical Origin of Tea.
   Marcos, A.; Fisher, A.; Rea, G.; Hill, S. J.
   J. Anal. At. Spectrom. **1998,** *13,* 521-525.

2. A Drift Correction Procedure for ICP-AES Systems.
   Marcos, A.; Hill, S. J.
   Analyst **2000,** *125,* 1015-1020.

3. Application of a multi-way method to study long-term stability in ICP-AES
   Marcos, A.; Foulkes M; Hill, S.J.
   J. Anal. At. Spectrom. **2001,** 16, 105-114.

4. Parallel Factor Analysis for the study of systematic error in inductively coupled plasma atomic emission spectrometry and mass spectrometry.
   Moreda-Piñeiro, A.; Marcos, A.; Fisher, A.; Hill, S. J.
   J. Anal. At. Spectrom. **2001,** 16, 360-369.

5. Chemometrics approaches for the study of systematic error in inductivaly coupled plasma emission spectrometry and mass spectrometry.
   Moreda-Piñeiro, A.; Marcos, A.; Fisher, A.; Hill, S. J.
   J. Anal. At. Spectrom. **2001,** 16, 350-359.

6. Evaluation of the effect of data pre-treatment procedures on classical pattern recognition and principal components analysis approaches.
   Moreda-Piñeiro, A.; Marcos, A.; Fisher, A.; Hill, S. J.
   Submitted to Analytical Chimica Acta, 2001.

COPY OF THE PUBLISHED PAPERS

Application of a multi-way method to study long-term stability in ICP-AES†

Ana Marcos, Michael Foulkes and Steve J. Hill*

Department of Environmental Sciences, Plymouth Environmental Research Centre, University of Plymouth, Drake Circus, Plymouth, UK PL4 8AA

www.rsc.org/jaas

Although major advantages have been made in developing robust, easy-to-use ICP-AES instruments offering sub µg g^{-1} detection limits and relative interference free operation, long-term drift of the analytical signal continuous to be problematic and necessitates regular re-calibration. The work presented here focuses on the effect of two instrumental parameters, i.e. the rf power and the nebuliser gas flow rate, on the robustness of the signals. The effects on the long-term stability when varying these two factors was systematically studied using an experimental design protocol. A "*drift diagnosis*" on thirty emission lines was performed at 12 different sets of operating conditions by repeated determination of a multi-element solution over several hours. The results were studied using standard parameters, i.e., Mg ratio, sensitivity, drift error, drift patterns and multi-way analysis. Parallel factor analysis (PARAFAC) was employed to analyse the 3-way data array *generated*: "*emission lines × replicates × operating conditions*". The physical interpretation of the new PARAFAC-factors is shown to enable a better understanding of the drift phenomenon by mathematically characterising the causes of long-term instability. Finally, the robustness of the technique using different operating conditions is evaluated and the appropriate use of internal standards to correct for drift is discussed.

Introduction

Inductively coupled plasma atomic emission spectrometry (ICP-AES) is a well established technique for routine analysis.[1] Multi-element determinations, high selectivity and limits of detection below the µg g^{-1} level have led to a wide range of applications in the areas of food sciences, environmental and clinical analysis. Although most of the disadvantages once associated with ICP-AES have now been well characterised and can often be eliminated, long-term stability phenomenon may necessitate the analyst to recalibrate the instrument at regular intervals.

The causes of such instability are not fully understood. Initial studies[2-8] have identified the presence of flicker noise, mainly related to the sample introduction system, as the origin of the problem, i.e., long-term instability is caused by slight fluctuations in the instrumental parameters. Further work[6,9] identified three areas of instability: variation of the nebulisation efficiency; changes in the energy transfer from the plasma to the sample; and degradation of the optics system. In many modern instruments, software routines control the stability of the optical system and allow it to be monitored during the analysis. However, the operator usually has little or no information about the state of the sample transport system nor the stability of the plasma. The objective of this study was, therefore, to better characterise the drift phenomena by studying the two instrumental parameters most likely to have an effect on these parts of the system. The nebuliser gas flow rate and the rf power were chosen since these two settings are directly related to the nebulisation process and the energy transfer.

To carry out the study, the evolution of emission signals with time at different rf powers and nebuliser gas flow rates was monitored. In order to approach the problem in a systematic way, the selection of the instrumental settings was achieved

using an experimental design protocol. The robustness of the technique at different operating conditions is evaluated using standard parameters: long-term error, drift patterns, magnesium ratio[10,11] and correlation degrees[12] to identify similarities and differences between the emission lines i.e., analyte and argon lines, atomic and ionic emission lines. However, for data handling purposes, a multi-way approach[13] was necessary to facilitate the three dimension structure of the results. Our data can be arranged in a cubic array, indexed: emission lines × replicates × instrumental conditions.

A multi-way decomposition method, parallel factor analysis, PARAFAC,[14,15] was then performed on the data set. Two PARAFAC-factors were calculated and their physical relevance investigated in terms of energy data, drift patterns and instrumental conditions.

Background

In essence, six parameters need to be set before running an ICP-AES analysis: the three argon flows (plasma, nebuliser and auxiliary flow), the sample uptake rate, the rf power and the viewing height. In addition to these, the size of the entrance slit, the integration time and the type of background correction employed will determine the nature of the mathematical process used to convert the raw signal into usable data. When trying to identify the effect of small variations in the instrumental parameters on the signals, there is a problem in isolating each function since the working parameters are inter-related. For instance, an increase in the nebuliser flow rate may improve the transport efficiency by creating a finer aerosol, such that more drops will reach the plasma, and thus the intensity of the signal could be enhanced. However, at the same time, a higher nebuliser flow will decrease the residence time of the sample aerosol in the plasma, so that less energy will be transferred to the sample, with the potential loss of some emissions lines. Although the transport of the sample to the plasma will be largely influenced by the sample uptake rate and

DOI: 10.1039/b008759i

J. Anal. At. Spectrom., 2001, 16, 105–114 **105**

the nebuliser gas flow rate, other factors will also have an effect on the type of aerosol created, e.g., the viscosity of the sample, type of nebuliser and spray chamber employed, as well as the room temperature. In terms of energy transfer, the instrumental parameters with most influence are the rf power supply, the three argon flows and the sample uptake rate. Since these instrumental parameters are interrelated, a systematic study of the influence of the variation of each parameter on the robustness of the emission signal would lead to a high number of experiments. For example, if the six instrumental parameters mentioned above (i.e., rf power, sample uptake rate, the three argon flows and the viewing high) are considered for just two different settings of each parameter, 64 experiments would be required to study all the interactions. For this reason, we have limited the number of instrumental parameters to be modified to the rf power and the nebuliser gas flow rate.

The power delivered to the plasma will determine its temperature, with higher power resulting in higher temperatures. Higher temperatures enhance emission for all ionic lines, however, the effect on atomic lines depends on the relative excitation and ionisation energies of the emitting atom: short wavelengths atomic lines are enhanced; long wavelength atomic lines are suppressed; and moderate wavelength atomic lines remain relatively unaffected.

The nebuliser flow affects the average size of the aerosol droplets, but also the residence time of the sample in the plasma and the plasma temperature. At low nebuliser flow, the average size of the aerosol droplets increases, reducing the transport efficiency of the spray chamber. Thus, every line will partially decrease its emission intensity as less sample reaches the plasma. However, a lower nebuliser flow will also increase the residence time of the aerosol in the plasma and the plasma temperature. This could enhance the emission of any ionic line. For atomic lines, the increased residence time provides energy to promote two competing pathways: the excitation, which leads to emission enhancement, and ionisation, which leads to emission suppression. Therefore the net effect will depend on the relative energies of the two processes such that: (1) high-energy atomic emission lines emitted by elements that resist ionisation (e.g., Zn) show enhanced emission with increased residence time; (2) low-energy atomic emission lines emitted by elements that are easily ionised (e.g., Na) show suppressed emission with increased residence time; and (3) moderate-energy atomic emission lines emitted by atoms of moderate ionisation energy (e.g., Cu) remain unaffected by residence time.

Clearly, even when considering only two factors, an ICP is a complex system and, for this reason, a systematic approach to the problem is essential. We have used an experimental protocol to plan our experiments. The experimental design strategy[16,17] gathers together experimental knowledge. It can be applied to investigate a phenomenon in order to gain further understanding or to improve performance. When planning experiments, the influence of different parameters can be studied simultaneously. In this study the experimental design was used to evaluate the effect of each instrumental parameter individually as well as the interactions between them.

The N-way approach: PARAFAC

Many analytical chemist have introduced multivariate methods such as principal component analysis (PCA), principal component regression (PCR) or partial least squares (PLS) to further study their results.[18] In standard multivariate analysis. data are arranged in a two-way structure, a table or a matrix. An example could be a data matrix which has different samples along the rows with the concentration of several elements along the columns. However sometimes, a third dimension is necessary to describe the data. Consider for instance, using the example above, the determination of a

number of metals in various samples and at different pH. Such data could be arranged in a three-way structure, indexed by sample, element and pH.

In this study, we have produced data matrices in which each row represents an emission line and each column a replicate of its intensity over time. As we repeat the experiment under different working conditions, we can arrange all the data in an array, a cube of data, indexed by line, replicate and experiment (Fig. 1). In such a cube, one dimension will contain the different emission lines, the second dimension the replicates and the third dimension the different experimental conditions employed. We therefore produce a 3-way data set and, thereby, multi-way methods can be applied.

We have employed PARAFAC[14] (parallel factor analysis) to describe the data. Although PARAFAC was originally employed in psychometrics,[19] several applications of PARAFAC in chemical systems have been reported. Most of them corresponded to decomposition processes in excitation–emission fluorescence spectroscopy for data treatment[20,21] and also for instrument optimisation.[22] Applications of PARAFAC to high-performance liquid chromatography (HPLC) coupled with different detectors[23,24] have also been found. Applications in the chemical industry have also been reported.[25–27]

PARAFAC is a decomposition method for 3 or higher orders arrays, which could be compared to principal component analysis (PCA). The aim of decomposition is to retain the maximum amount of information from the data but represent it in a smaller number of components or factors. Using PARAFAC, instead of working with a 2-way data set, the algorithm is extended to higher modes, 3, 4 or in general N-way data sets. The structural model of a two-way PCA is a bilinear model [eqn. (1)], and likewise a PARAFAC model of a three-way array is defined by the structural model described in eqn. (2):[14]

$$x_{ij} = \sum_{f=1}^{F} a_{if} b_{jf} + e_{ij} \tag{1}$$

$$x_{ijk} = \sum_{f=1}^{F} a_{if} b_{jf} c_{kf} + e_{ijk} \tag{2}$$

where x_{ijk} represents data in object i of variable j at condition k; i,j,k are variables respectively along the first, second and third dimension (Objects, Variables, Conditions); f, F are principal components or factors; a,b,c is the model loading on first, second and third dimension; and e is the model error.

A decomposition of the data is made into triads or trilinear components. The results of a PARAFAC analysis are given as N-loading matrices, one for each mode studied. In our case, we are dealing with a three way data set, and three loading matrices will be obtained A, B and C. The trilinear model is found to minimise the sum of squares of the residuals e_{ijk} in the model. Eqn. (2) may be represented graphically as in Fig. 2.

It should be stressed that the reason for using a multi-way method is not to obtain a better fit for the data, but rather more adequate, robust and interpretable models, based on a smaller number of parameters. For example, in order to calculate an F-component PCA model to a $I \times J \times K$ array, we would need first to unfold the data to a $I \times JK$ matrix and then apply a PCA, the solution of which will consist of $F(I+JK)$ parameters
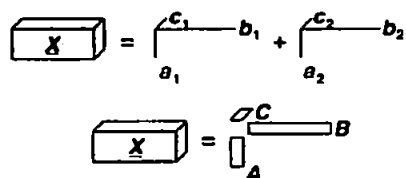

Fig. 1 3-Way arrangement of data sets.

Fig. 2 Geometrical representation of a PARAFAC analysis.

Fig. 3 Differences in the data disposition to perform a PARAFAC or a PCA.

(Fig. 3). A corresponding PARAFAC model with an equal number of components would consist of only $F(I+J+K)$ parameters. Clearly the PCA model will be more difficult to interpret because a much higher number of parameters are implied. In our case, we are dealing with an array of *30 emission lines* × *100 replicates* × *12 instrumental conditions. Each PAR-AFAC factor will be defined by (30+100+12)→142 parameters.*

If we want to explain the same data set by a PCA, we first need to unfold the data sets to a matrix which dimension will be *30 emission lines* × *(100 replicates* × *12 instrumental conditions) giving 30 emission lines* × *1200 variables. Each PCA factor will be defined by (30+1200)→1230 parameters.*

Another advantages of PARAFAC *versus* unfolded PCA is the uniqueness of the solution. In bilinear methods, the solutions present rotational freedom. This is not the case with PARAFAC, where the estimated model cannot be rotated without a loss of fit.

Experimental

Methodology

To generate the data set, a multi-element solution ($10\ \mu g\ g^{-1}$) containing 15 analytes (see Table 1) was repeatedly analysed

over a period of 8 h without recalibration. In order to ensure stable starting conditions, 2 h were allowed to warm up the instrument prior to starting the measurements. The evolution of the intensities from 30 emission lines was then followed over time. The lines studied are reported in Table 1 and represent one atomic and one ionic line for most elements and four argon lines.

Instrumentation

The instrument employed was an Optima 3000 (Perkin-Elmer Corporation, Norwalk, USA). This ICP-AES instrument combines an echelle polychromator with a solid state detector which allows simultaneous acquisition of over 5000 lines with simultaneous background measurements. The instrumental parameters employed are shown in Table 2. The settings for the nebuliser gas flow rate and rf power were defined using an experimental design.

Table 1 Emission lines used in this study

Element	λ/nm	Intensity I_a/I_b[a]	EE[b] = λ/eV	IP[c]/eV	EP + IP[d]/eV
Al (I)	396.152	10.5	3.13	—	3.1
Ba (II)	230.424	73.0	5.38	5.21	≥10.6
Ba (II)	233.527	75.0	5.31	5.21	11.2
Ca (I)	422.673	1.5	2.99		2.9
Ca (II)	317.933	1.5	3.90	6.11	13.1
Cd (I)	228.802	110	5.42	—	5.4
Cd (II)	226.502	120	5.47	8.99	14.4
Co (I)	340.512	NO DATA	3.64	—	4.0
Co (II)	228.616	43.0	5.42	7.88	14.3
Cr (I)	357.869	13.0	3.46	—	≥3.46
Cr (II)	267.716	42.0	4.63	6.77	≥11.4
Cu (I)	324.754	56.0	3.82	—	3.8
Cu (II)	224.700	39.0	5.52	7.73	15.9
Fe (II)	259.940	48.0	4.77	7.90	≥12.7
Mg (I)	285.213	NO DATA	4.35	—	4.3
Mg (II)	279.079	1.0	4.44	7.65	≥12.1
Mn (I)	403.076	6.8	3.08	—	3.1
Mn (II)	257.610	220	4.81	7.43	12.2
Na (I)	589.592	43.0	2.10	—	2.1
Ni (I)	232.003	20.0	5.34	—	≥5.34
Ni (II)	231.604	15.0	5.35	7.64	≥13.0
Pb (II)	220.353	70.0	5.62	7.42	14.7
Ti (II)	379.280	NO DATA	3.27	6.83	≥10.1
Zn (I)	213.856	170	5.80	—	5.8
Zn (II)	202.548	75.0	6.12	9.39	15.5
Ar (I)	357.229	2.3	3.47	—	≥3.47
Ar (I)	404.597	2.5	3.06	—	≥3.06
Ar (I)	420.068	50	2.95	—	≥2.95
Ar (I)	451.074	21	2.75	—	≥2.75

[a]I_a/I_b, Ratio of net analyte intensity to background intensity (from Handbook of ICP-AES, CRC Press, 1981). [b]EE Transition emitted energy (calculated converting the nm^{-1} to eV). [c]IP First ionisation potential (from Handbook of Physics and Chemistry, CRC Press, 77th Edition, 1997). [d]EP + IP Excitation potential (Handbook of Spectroscopy Vol.1, PW Robinson CRC Press, 1974).

Table 2 Instrumental settings used in experimental work

Rf power	Designed variable
Injector diameter	2 mm
Nebuliser type	Cross flow pneumatic nebuliser
Nebuliser flow	Designed variable
Plasma flow	$15\,l\,min^{-1}$
Auxiliary flow	$0.8\,l\,min^{-1}$
Sample uptake rate	$1.0\,l\,min^{-1}$
Viewing height	12 mm
Read time	10–20 s

Experimental design settings

A combination of two full-factorial designs was employed: a full-factorial experiment of two factors at three levels (Table 3) → *9 experiments*; and a full-factorial experiment of two factors at two levels (Table 4) → *4 experiments*.

The centre conditions (*point (0,0): rf power 1250 W and nebuliser flow rate 0.9 l min⁻¹*) were replicated three times. A graphic representation of the experimental points is shown in Fig. 4. In total, 15 experiments were planned and, for each experimental point, a data set was produced, *i.e.*, the intensity of the selected emission lines was measured 99 times (approximately 8 h).

An overview of the final experimental protocol is presented in Table 5. The robustness of the instrument at the different instrumental conditions employed is also reported on Table 5. The robustness of the plasma is referred to[28] as "*its ability to keep the variation of the analytical signal to a minimum when changing the sample matrix*". To quantify robustness, Mermet[1] introduced the magnesium ionic-to-atomic line intensity ratio where values over 10 provide a robust plasma, whilst a Mg ratio below 10 indicates that any changes in the sample matrix would highly affect the emission intensities. Although in this work we have not matched the test solution with a complex chemical matrix to simplify the problem, the Mg ratio at each instrumental setting was determined to provide an additional factor to evaluate the operating conditions selected for this study.

N-way data handling

Matlab software (Mathworks, Inc.; Version 5.1) and the N-Way Toolbox for Matlab[29] were employed to perform the 3-way analysis. Before running a PARAFAC analysis, the data was scaled to unit squared variation. Scaling in multi-way analysis has to be done taking the trilinear model into account. If variable *i* of the first mode is to be scaled (compared to the rest of the variables in the first mode), it is necessary to scale all rows where variable *i* occurs by the same scalar. This means that whole matrices instead of rows were scaled. Mathemati-

Fig. 4 Graphical representation of the experimental design.

Table 3 Experimental designed levels, block 1

Factor 1			Factor 2		
Rf power/W			Nebuliser flow rate/l min⁻¹		
−1	0	+1	−1	0	+1
1000	1250	1500	0.6	0.9	1.2

Table 4 Experimental designed levels, block 2

Factor 1		Factor 2	
Rf power/W		Nebuliser flow rate/l min⁻¹	
−0.5	+0.5	−0.5	+0.5
1125	1375	0.75	1.05

cally scaling within the first mode can be described as:

$$x_{ijk}^{scal} = \frac{x_{ijk}}{S_i} \tag{3}$$

Where S_i will scale to unit squared variation:

$$S_i = \sqrt{\left(\sum_{j=1}^{J} \sum_{k=1}^{K} x_{ijk}^2 \right)} \tag{4}$$

The core consistence and the explained variance were the two parameters employed to optimise the number of components to use in the PARAFAC model. The core consistence diagnosis is a percentage below or equal to 100%. A value of 80–100% means that the model is valid, while a value below 40% means that the model is not valid. A core consistency between 40 and 80% means that the model is probably valid but somehow difficult to estimate, *e.g.*, due to slight mis-specification or high correlation. The core consistency may decrease with the number of components, but very sharply where the correct number of components is exceeded. Hence, the appropriate number of components is the model with the highest number of components, highest explained variation and a valid core consistency. Four PARAFAC models were calculated using one, two, three and four components. The explained variance increased continuously with the number of components, see Fig. 5(A). The core consistency fell to values around 10%, when more than two components were calculated, Fig. 5(B). Therefore, a two components PARAFAC model was employed in this analysis.

Table 5 Experiment plan

| Experiment	Rf power/ W	Nebuliser flow rate/ l min⁻¹	Room temperature/ °C	Magnesium ratio (MgII/MgI)
Central conditions (1)	1250	0.90	26–27	10.5
Experiment 1	1125	1.05	27.5–28.5	8.9
Experiment 2	1125	0.75	28	8.4
Experiment 3	1375	1.05	29.5–29	10.9
Experiment 4	1375	0.75	28.5–29.5	11.1
Central conditions (2)	1250	0.90	28.5–27	10.5
Experiment 5	1000	0.90	26	6.7
Experiment 6	1250	1.2	26–26.5	8.6
Experiment 7	1250	0.6	26–25	10.1
Experiment 8	1500	0.9	25–25.5	12.5
Central conditions (3)	1250	0.90	24.5–24	10.5
Experiment 9	1000	1.2	23–26	5.8
Experiment 11	1500	1.2	25–26.5	10.3
Experiment 12	1500	0.6	26–28	11.6
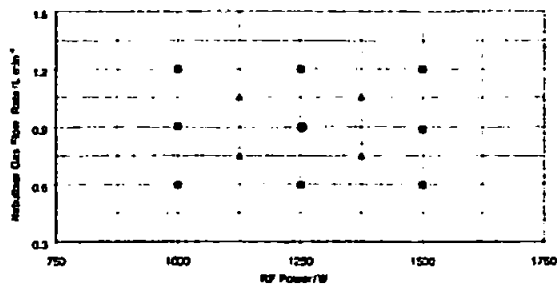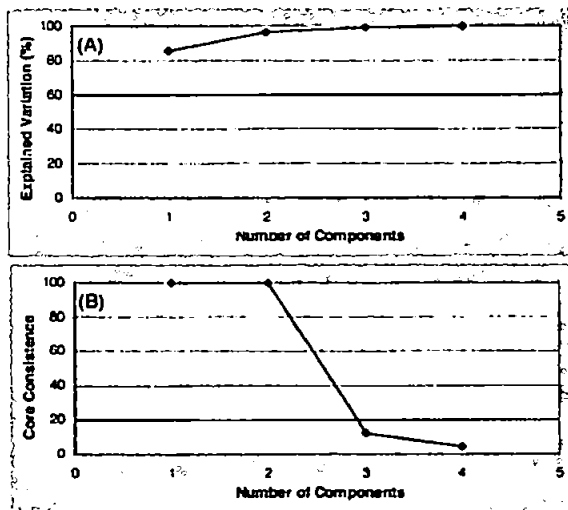
Fig. 5 Optimisation of the number of PARAFAC components. (A) Variance explained depending on the number of components and (B) core consistencies depending on the number of components.

Results and discussion

Classical analysis

One data set was obtained for each experiment with the exception of where the experimental conditions were such that the plasma could not be sustained, i.e., rf power 1000 W and nebuliser gas flow rate 0.6 l min⁻¹. As expected, the intensity levels of every line changed from one set of experimental conditions to another, and so did the sensitivity. Table 6 shows the limits of detection for every line at the different operating condition selected for this study and reflects a degradation of

sensitivity when robust conditions are employed, and more precisely when low nebuliser flows are set.

In order to check the stability of the instrument from one day to another, an intensity check using the central conditions (rf, 1250 W; nebuliser gas flow, 0.9 l min⁻¹) was performed prior to each experiment. Very similar intensity values were obtained over the whole period of experimental work (RSD between 1.7 and 6.1%).

The reproducibility of the experimental protocol was also checked for the above conditions, by replicating the procedure three times. The three data sets obtained are comparable, particularly in terms of their characteristic drift patterns and the magnitude of the drift (Fig. 6).

The drift bias on each line and at every replicate was plotted for each set of conditions. These plots are presented in the Electronic Supplementary Information in the file.† Different drift patterns were found depending on the instrumental parameters, and also the magnitude of drift error varied with the instrumental settings. Some of the operating conditions produced very stable signals with drift values below 3% over the entire experiment, as was the case when using the central conditions, i.e., rf power 1250 W and nebuliser flow rate 0.9 l min⁻¹, and the moderate conditions, rf power 1125 W and nebuliser flow rate 0.75 l min⁻¹. In other cases, the magnitude of the drift can reach values over 20%, i.e., experimental conditions: rf power 1375 W, nebuliser flow rate 1.05 l min⁻¹. However, the most interesting observation from the results obtained is the evolution of the trends with the changes in the instrumental parameters. In Fig. 7, we have replaced each experimental point (described in Fig. 4) by a plot of the drift data set obtained at the corresponding experimental conditions. One can easily identify that some plots could be grouped together. For instance, in the right-bottom corner, the plots show two trends, one grouping all the analyte lines and the other containing the four argon lines. This was found under robust or at least moderately robust conditions: 1500 W, 0.60 l min⁻¹; 1375 W, 0.75 l min⁻¹; 1250 W, 0.60 l min⁻¹ for

Table 6 Limit of detection of studied lines at different operating conditions (ppb). Figures in bold represent values which lie outside the 95% confidence interval

Experiment No. Rf power/W Nebuliser gas flow/l min⁻¹	CC 1250 0.9	Ex. 1 1125 1.05	Ex. 2 1125 0.75	Ex. 3 1375 1.05	Ex. 4 1375 0.75	Ex. 5 1000 0.9	Ex. 6 1250 1.2	Ex. 7 1250 0.6	Ex. 8 1500 0.9	Ex. 9 1000 1.2	Ex. 11 1500 1.2	Ex. 12 1500 0.6
Al - 396.152 - (I)	57	11	43	19	48	14	19	170	59	3	15	140
Ba - 230.424 - (II)	4	3	8	3	7	3	3	22	1.6	5	2	20
Ba - 233.527 - (II)	3	1.3	4	1.6	4	3	2	13	2	3	1.6	23
Ca - 317.933 - (II)	6	4	6	3	6	5	4	35	5	3	2	60
Ca - 422.673 - (I)	17	3	15	4	9	7	5	35	8	1.4	3	120
Cd - 226.502 - (II)	3	2	3	2	3	3	1.6	10	1.8	4	1.8	14
Cd - 228.802 - (I)	6	5	8	4	9	5	5	20	6	7	4	31
Co - 228.616 - (II)	11	9	25	7	15	15	7	52	8	6	4	69
Co - 340.512 - (I)	75	23	63	24	110	29	21	190	33	12	21	840
Cr - 267.716 - (II)	6	2	6	2	2	4	3	9	1.8	4	1.5	33
Cr - 357.869 - (I)	15	4	21	7	41	5	6	100	11	2	7	240
Cu - 224.700 - (II)	10	6	12	4	16	4	3	45	7	1.5	6	65
Cu - 324.754 - (I)	3	1.0	5	1.3	8	1.1	1.3	26	3	0.5	1.4	45
Fe - 259.940 - (II)	3	1.2	3	1.8	5	3	1.7	13	1.3	1.2	1.0	19
Mg - 279.079 - (II)	30	11	25	9	21	14	14	82	18	8	13	260
Mg - 280.270 - (II)	0.5	0.2	0.5	0.5	0.6	4	0.5	1.5	0.6	0.2	1.2	1.4
Mg - 285.213 - (I)	1.1	0.6	1.9	1.0	2	5	0.6	6	1.2	0.5	1.1	13
Mg 279.553 - (II)	0.6	0.3	0.4	0.5	0.6	4	0.5	0.8	0.5	0.2	1.1	1.5
Mn - 257.610 - (II)	0.6	0.3	1.2	0.3	0.6	0.4	0.3	3	0.6	0.3	0.3	3
Mn - 403.076 - (I)	120	14	56	44	55	19	23	430	130	4	20	520
Na - 589.592 - (I)	40	7	31	8	30	15	14	110	32	3	11	360
Ni - 231.604 - (II)	6	3	11	2	13	8	6	32	5	6	7	64
Ni - 232.003 - (I)	16	11	34	13	26	11	9	69	12	9	11	77
Pb - 216.999 - (I)	160	72	250	87	220	81	77	520	110	41	46	690
Pb - 220.353 - (II)	36	32	55	25	52	45	37	88	34	20	36	230
Ti - 337.280 - (II)	3	1.2	4	0.7	5	1.5	0.8	5	2	0.8	0.8	17
Zn - 202.548 - (II)	4	3	5	1.7	3	6	4	12	2	8	2	16
Zn - 213.856 - (I)	1.8	1.2	3	1.8	3	2	1.4	6	1.4	1.8	1.1	6

Fig. 7 Drift patterns at different experimental conditions. Details of the plots are available as Electronic Supplementary Information.†

A final group of plots can be recognised on the top left corner of Fig. 7. When using a low rf power and a high nebuliser gas flow (i.e., 1000 W, 1.2 l min⁻¹ or 1125 W, 1.05 l min⁻¹) a warming up effect is observed. Under such conditions, the plasma is slightly cooler due to the low power employed and the high setting for the nebuliser gas, which also contributes to the cooling effect. Finally, when setting the instrument at 1000 W and 0.9 l min⁻¹, i.e., operating conditions which are very similar to the so called standard conditions, (1000 W and 1.0 l min⁻¹), high values of drift were observed. Under such settings, the emission signal drifts to progressively higher values.

Correlation and internal standardisation. The correlation coefficient is a measure of the linear relationship between fluctuations in the analyte and internal standard signals. Thus, high correlation between analyte lines and internal standards is necessary. In order to investigate the potential for internal

the rf power and the nebuliser gas flow rate, respectively. A deficiency in the transport system due to a low nebuliser flow may cause this separation between the argon lines, since such conditions may lead to a partial blocking of the nebuliser tip, thus deteriorating its performance. This problem will only affect the analyte lines, while the argon lines, which are not necessarily involved in the nebulisation process, will remain unaffected.

Another set of similar patterns can be found in the right-top area of Fig. 7. This zone corresponds to unusual instrumental conditions, i.e., high rf power and high nebuliser gas flow, and is therefore not of great practical interest. However, in a similar way to the results in the right-bottom area discussed above, two of the plots shows similar trends. The experiments run at rf power 1375 W, nebuliser flow rate 1.05 l min⁻¹ and at rf power 1500 W, nebuliser flow rate 1.20 l min⁻¹ present similar patterns, with very unstable signals during half of the experiment, prior to a stabilising of the signals.

In the middle area, near the central conditions, various plots show considerably robust data with low drift values, but relatively noisy signals, i.e., the experimental settings 1250 W, 1.2 l min⁻¹ and 1125 W, 0.75 l min⁻¹; 1250 W, 1.2 l min⁻¹; 0.9 l min⁻¹;

Fig. 6 Drift patterns at central conditions, three replicates: rf power, 1250 W and nebuliser gas flow, 0.9 l min⁻¹.
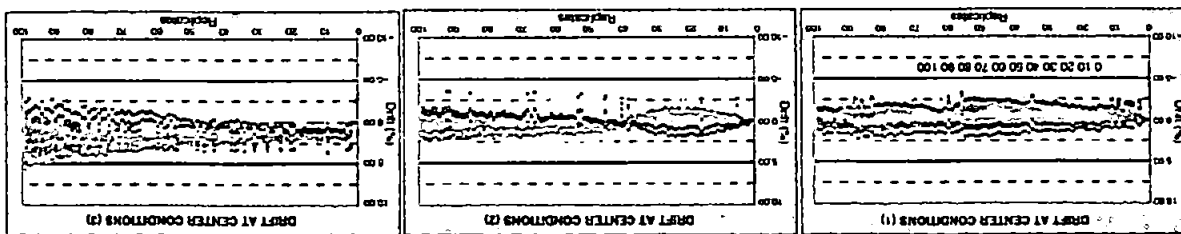
Table 7 Summary of results

	Rf power/W	1000			1125		1250			1375		1500		
	Nebuliser flow rate/l min⁻¹	0.60	0.90	1.20	0.75	1.05	0.60	0.90	1.20	0.75	1.05	0.60	0.90	1.20
Drift after 8 h (%)	Average	—	7.32	1.14	1.08	3.20	0.53	0.87	2.89	3.17	8.89	3.47	2.18	3.75
	Minimum	—	0.24	0.02	0.02	0.12	0.07	0.01	0.49	1.98	0.11	0.35	0.01	0.36
	Maximum	—	17.46	5.59	2.59	9.01	1.48	1.61	5.79	6.45	21.17	8.83	4.56	9.79
Correlation[a]	Average	—	0.71	0.62	0.54	0.40	0.95	0.41	0.61	0.98	0.53	0.97	0.64	0.55
	Atomic–Atomic	—	0.58	0.58	0.44	0.18	0.91	0.35	0.50	0.98	0.39	0.97	0.68	0.36
Analyte–Analyte	Ionic–Ionic	—	0.89	0.69	0.83	0.88	0.98	0.61	0.86	0.98	0.77	0.97	0.66	0.91
	Atomic–Ionic	—	0.66	0.59	0.42	0.21	0.94	0.32	0.52	0.97	0.46	0.97	0.61	0.42
Correlation[a]	Average	—	0.79	0.70	0.54	0.40	−0.74	0.28	0.62	−0.87	0.63	−0.80	−0.05	0.28
	Argon–Atomic	—	0.64	0.62	0.23	0.04	−0.73	0.08	0.40	−0.89	0.52	−0.79	−0.06	0.09
Argon–Analyte	Argon–Ionic	—	0.92	0.76	0.80	0.71	−0.75	0.46	0.81	−0.86	0.72	−0.80	−0.04	0.44
Remarks	Trends	—	Yes	?	No	?	Yes	No	No	Yes	Yes	Yes	Yes	Yes

[a]Pearson's correlation.

standard methods to correct for long-term drift error at each of the operating conditions tested, the correlation matrices of each data set have been calculated. The correlation matrices are presented in the Electronic Supplementary Information in the file "CORR-MAT.doc".† These matrices quantify the similarities and differences observed from the drift plots in Fig. 7. Correlation between emission lines changes from one set of experimental conditions to another, as well as the type (*i.e.*, atomic, ionic, argon) of lines showing good correlation. Likewise, we only observed very high inter-analyte correlation when working at robust or moderately robust conditions, independent of the nature of the emission line, *i.e.*, atomic or ionic line. Table 7 summarises the information obtained by studying the correlation matrices.

The different patterns identified when varying the instrumental conditions highlight the difficulties when trying to optimise a general correction method for drift. The use of internal standardisation has been a common approach to minimise the drift from the early work of Barnett *et al.*[30,31] and Myers and Tracy[32] to more recent and complicated approaches.[7,33–40] Our results are in agreement with those of

Romero *et al.*[9] and indicate that whilst internal standardisation may be an option when working under robust conditions, the approach is of very little value when softer settings are employed. Of particular interest is the possibility of correcting for drift by employing an argon line, as is the case when moderate robust conditions (rf power 1375 W, nebuliser flow rate 1.05 l min⁻¹) are employed.

Fig. 8 and Fig. 9 show the changes in the shape of the drift patterns before and after internal standardisation under two different operating conditions: rf power 1500 W, nebuliser flow
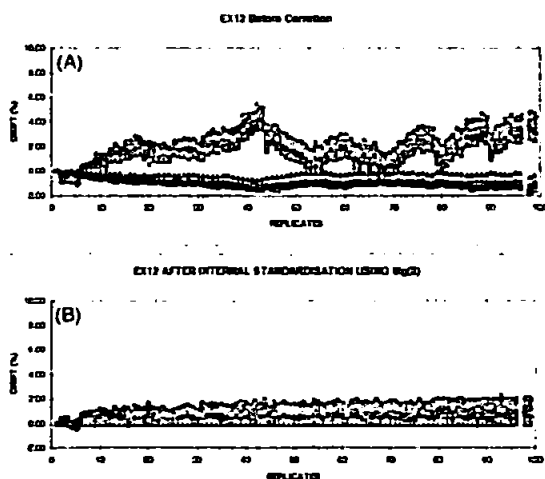

Fig. 8 Drift correction by internal standardisation using experimental conditions as for Experiment 12; rf power = 1500 W and nebuliser gas flow = 0.6 l min⁻¹. At robust conditions any analyte line can alleviate long term drift (example using MgII line). (A) Two groups of lines are observed, one containing all the analyte lines (on the top of the plot) and the other containing only the four argon lines. (B) When MgII is employed as internal standard, using $A_n^{corr} = A_n + [(I_0 - I_n)/I_n] \times A_n$ which expects similar drift errors in the analyte line and internal standard line, most of the long-term noise is removed.
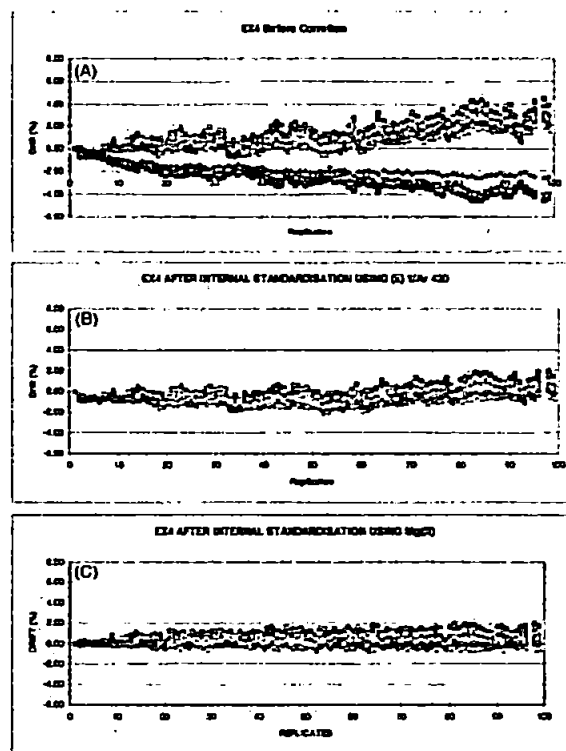
Fig. 9 Drift correction by internal standardisation using experimental conditions as in Experiment 4; rf power = 1375 W, nebuliser gas flow = 0.75 l min⁻¹. (A) Drift pattern before correction. High correlation between analyte lines is observed and the four argon lines. High negative correlation between both groups can be observed. (B) Drift on the analyte lines using the inverse of Ar[420.063 nm] as an internal standard and using the formula $A_n^{corr} = A_n - 0.5[(I_0 - I_n)/I_n] \times A_n$. The 0.5 factor was introduced to optimise the correction. (C) Drift on the analyte lines using the Mg[279.079 nm] line as internal standard using the formula $A_n^{corr} = A_n + [(I_0 - I_n)/I_n] \times A_n$.

Table 8 Improvement factors obtained when correcting drift by internal standardisation at robust conditions: rf power 1500 W, nebuliser gas flow rate 0.6 l min⁻¹

	Drift before correction (%)	Drift after correction by Mg (II) line (%)	Factor of improvement, IF
Al - 396.152 - (I)	3.04	0.55	5
Ba - 230.424 - (II)	4.02	1.51	3
Ba - 233.527 - (II)	4.05	1.54	3
Ca - 317.933 - (II)	2.89	0.41	7
Ca - 422.673 - (I)	3.89	1.38	3
Cd - 226.502 - (II)	4.16	1.65	3
Cd - 228.802 - (I)	3.89	1.39	3
Co - 228.616 - (II)	4.38	1.86	2
Co - 340.512 - (I)	2.89	0.41	7
Cr - 267.716 - (II)	3.55	1.06	3
Cr - 357.869 - (I)	2.76	0.28	10
Cu - 224.700 - (II)	4.27	1.76	2
Cu - 324.754 - (I)	3.58	1.08	3
Fe - 259.940 - (II)	3.89	1.38	3
Mg - 279.079 - (II)	2.47	0.10	25
Mg - 285.213 - (I)	3.05	0.57	5
Mn - 257.610 - (II)	3.70	1.20	3
Mn - 403.076 - (I)	3.56	1.06	3
Na - 589.592 - (I)	8.83	6.21	1
Ni - 231.604 - (II)	3.08	0.60	5
Ni - 232.003 - (I)	4.37	1.86	2
Pb - 220.353 - (II)	4.63	2.11	2
Ti - 379.280 - (II)	3.18	0.69	5
Zn - 202.548 - (II)	4.45	1.93	2
Zn - 213.856 - (I)	3.79	1.29	3

rate 0.6 l min⁻¹ and rf power 1375 W, nebuliser flow rate 0.75 l min⁻¹. The improvement factors for each case are shown in Tables 8 and 9.

Multi-way analysis

From Fig. 7, the variation of the drift patterns from one set of conditions to another is not random. Groups of settings with similar drift patterns are observed, reflecting the progressive
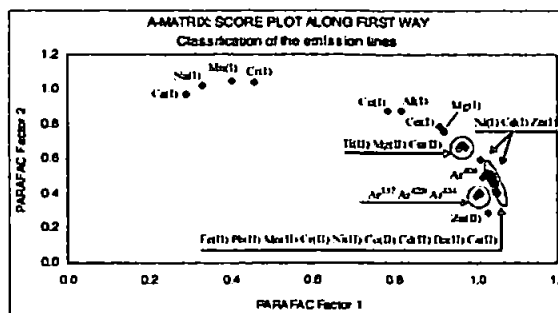

Fig. 10 PARAFAC score plot along the first mode.

change in drift patterns when varying the instrumental conditions. The complete array of data as described in previous sections was analysed simultaneously by performing a parallel factor analysis.

The use of PARAFAC found that the best model resulted when only two factors were calculated (96.8% of the total variance was explained). Clearly, this was expected since we are altering just two instrumental parameters in this study, and it may indicate that the model is working well.

The "PARAFAC-score plots" have been plotted in Fig. 10. A partial separation can be noticed between atomic and ionic lines and especially between soft and hard lines. Closer to the right hand side bottom corner of the plot, i.e., high score on PARAFAC factor 1 and low on PARAFAC factor 2, the emission line is the hardest. In a similar way, Fig. 11 represents the loadings of factor 1 and 2 along the second dimension versus replicates, i.e., time. The drift patterns of some specific instrumental conditions have clearly conditioned the formation of theses factors.

Finally, Fig. 12 shows the PARAFAC loading plot along the third mode. The distribution of the experiment points on the new axes is nearly linear, with a remarkable trend to robust
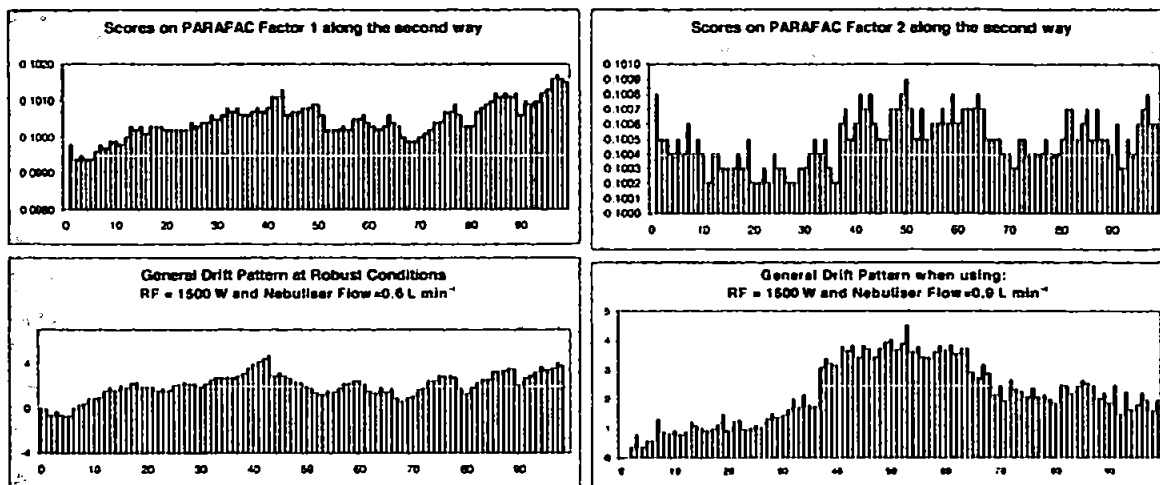
Table 9 Improvement factors obtained when correcting drift by internal standardisation at moderately robust conditions: rf power 1375 W, nebuliser gas flow rate 0.75 l min⁻¹

	Drift before correction (%)	Drift after correction by Ar line (%)	Drift after correction by Mg (II) line (%)	Factor of improvement when using Ar IF	Factor of improvement when using Mg (II) IF
Al - 396.152 - (I)	3.0	0.6	0.8	5	4
Ba - 230.424 - (II)	2.6	0.3	0.5	10	5
Ba - 233.527 - (II)	2.3	0.0	0.2	80	11
Ca - 317.933 - (II)	2.2	−0.2	0.0	11	51
Ca - 422.673 - (I)	3.9	1.5	1.8	3	2
Cd - 226.502 - (II)	2.9	0.5	0.8	5	4
Cd - 228.802 - (I)	2.0	−0.4	−0.1	6	17
Co - 228.616 - (II)	2.8	0.4	0.7	7	4
Co - 340.512 - (I)	2.4	0.1	0.3	42	8
Cr - 267.716 - (II)	2.6	0.2	0.5	12	6
Cr - 357.869 - (I)	3.9	1.5	1.7	3	2
Cu - 224.700 - (II)	2.9	0.5	0.8	6	4
Cu - 324.754 - (I)	3.2	0.8	1.0	4	3
Fe - 259.940 - (II)	2.3	0.1	0.2	60	11
Mg - 279.079 - (II)	2.1	−0.2	0.1	9	21
Mg - 285.213 - (I)	2.1	−0.3	0.0	8	177
Mn - 257.610 - (II)	2.2	−0.2	0.1	13	27
Mn - 403.076 - (I)	4.4	2.0	2.2	2	2
Na - 589.592 - (I)	6.5	4.0	4.3	2	2
Ni - 231.604 - (II)	1.9	−0.5	−0.2	4	8
Ni - 232.003 - (I)	3.3	0.9	1.1	4	3
Pb - 220.353 - (II)	2.8	0.4	0.6	7	4
Ti - 379.280 - (II)	3.1	0.7	1.0	4	3
Zn - 202.548 - (II)	1.4	−0.9	−0.7	2	2
Zn - 213.856 - (I)	2.7	0.3	0.6	8	5

Fig. 11 PARAFAC factors along the second mode. Similarities to the drift patterns at some specific instrumental conditions.

conditions, i.e., high rf power and low nebuliser gas flow rate. In order to quantify these graphic observations, the degree of correlation, r, between the loadings of the new PARAFAC factors and several physical parameters of our data has been calculated. Thus, the scores of the new components in the first mode (A-matrix) were correlated to the energy data of the lines studied: excitation energy, ionisation energy and emission energy of the monitored lines. The B-loading matrix was compared to the shape of the drift patterns, and the C-loadings were correlated to the levels of the rf power and the nebuliser flow rate set in each experiment. Importantly, the correlation levels found in this exercise enables the interpretation of the physical significance of the PARAFAC factors. The results are summarised below:

Within the 1st mode: emission lines. Factor 1: some correlation was found between the emission energy of the emission lines and the scores of PARAFAC factor 1, ($r = 0.58$). Factor 2: the scores of the second factor are highly correlated to the inverse of the excitation energy of the emission lines ($r = 0.90$).

Within the 2nd mode: replicates/time. Factor 1: the loadings of this factor are highly correlated to the general (average) analyte drift patterns at robust and moderately robust conditions ($r = 0.92$). Factor 2: some correlation was found ($r \approx 0.6$) between this factor and the average drift pattern when using 1500 W and 0.9 l min^{-1} and when using default conditions, 1000 W and 0.9 l min^{-1} (Fig. 11).

Within the 3rd mode: experimental conditions. Factor 1: the nebuliser gas flow rate employed in the different drift diagnoses was highly correlated to the loadings of PARAFAC factor 1 along the third mode ($r = 0.93$). Factor 2: the loadings of factor 2 were found very highly correlated ($r = 0.97$) to the ratio: (rf power)/(nebuliser flow rate).

It is important to note that although no analytical information was incorporated into the matrix when performing the PARAFAC analysis, the new factors are highly correlated to some of the physical parameters investigated. This strong association suggests that the two instrumental parameters modified in our study are related to the cause of most of the variation in the data set and so are intrinsic to the drift phenomenon.

Conclusions

The results presented here are in agreement with and complementary to previous work indicating that the rf power and the nebuliser gas flow rate settings have a fundamental effect on the robustness of the data.

The results shown in Fig. 7 could provide the analyst with a quick reference to better optimise instruments for long-term stability. In addition, this study facilitates the appropriate use of internal standards for drift correction. (1) Soft conditions, low power (rf power $\approx$ 1000 W) with medium to high nebuliser flow (> 1.0 l min^{-1}) give very unstable signals over time and complex drift patterns. Under these conditions, the use of an internal standard to compensate for instrument drift will not lead to an improvement on the quality of the data. For such conditions, the authors have developed a new correction procedure.[41] (2) With medium power (rf power = 1250 W), the data obtained indicate that the instrument is generally quite stable, showing drift values below 5% and complex drift patterns. Although drift correction under such conditions might be not necessary, internal standardisation methods will not be appropriate. (3) Under robust conditions, the instability is highly correlated between all the analyte lines and any line
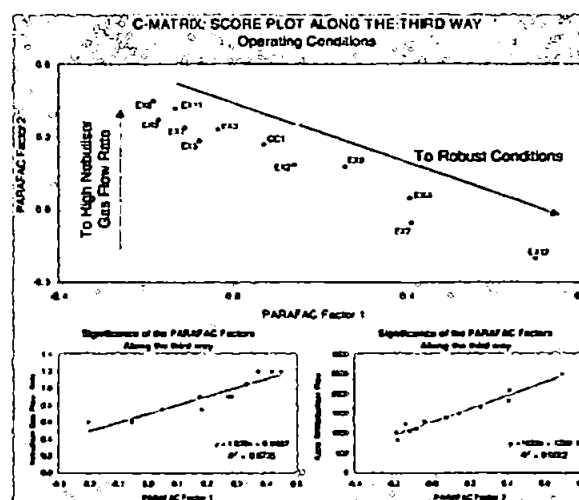

Fig. 12 PARAFAC score plot along the third mode. Physical interpretation of the model factors.

can be employed to correct for drift. Of specific interest are the so called "moderate robust conditions" (rf power 1375 W, nebuliser flow rate 1.05 l min^{-1}) where argon lines could be used as internal standards.

The use of the multi-way approach, PARAFAC, has also been shown to be a powerful tool to describe the system. The results are easier to interpret than those obtained using PCA due to the smaller number of parameters implied in the formation of the PARAFAC factors. A mathematically agreed interpretation of the tri-dimensional factors has been achieved by using physical parameters related to the system.

However, the full potential of this technique has not yet been realised and work in this area will continue, particularly in the area of multi-way regression[42] to correct for drift. Matrix effects and the influence of concentration levels on long-term stability of signals will also be the subject of further work.

Acknowledgements

References

1 S. J. Hill, *Inductively Coupled Plasma Spectrometry and its Applications*, Sheffield Academic Press, UK, 1999.
2 E. D. Salin and G. Horlick, *Anal. Chem.*, 1980, 52, 1578.
3 R. M. Belchamber and G. Horlick, *Spectrochim. Acta, Part B*, 1982, 37, 71.
4 R. M. Belchamber and G. Horlick, *Spectrochim. Acta, Part B*, 1982, 37, 17.
5 M. H. Ramsey and M. Thompson, *Analyst*, 1985, 110, 519.
6 M. Carre, E. Poussel and J. M. Mermet, *J. Anal. At. Spectrom.*, 1992, 7, 791.
7 J. M. Mermet and J. C. Ivaldi, *J. Anal. At. Spectrom.*, 1993, 8, 795.
8 G. J. Schmidt and W. Slavin, *Anal. Chem.*, 1982, 54, 2491.
9 X. Romero, E. Poussel and J. M. Mermet, *Spectrochim. Acta. Part B*, 1997, 52, 487.
10 J. M. Mermet, *Spectrochim. Acta, Part B*, 1989, 44, 1109.
11 J. M. Mermet, *Anal. Chim. Acta*, 1991, 250, 85.
12 A. Lopezmolinero, A. V. Caballero and J. R. Castillo, *Spectrochim. Acta, Part B*, 1994, 49, 677.
13 A. K. Smilde, *Chemometrics and Intelligent Laboratory Systems*, 1992, 15, 143.
14 R. Bro, *Chemometrics and Intelligent Laboratory Systems*, 1997, 38, 149.
15 R. A. Harshman and M. E. Lundy, *Computational Statistics & Data Analysis*, 1994, 18, 39.
16 A. C. Atkinson and A. N. Donev, *Optimum Experimental Designs*, Oxford Science Publications, UK, 1996.
17 D. C. Montgomery, *Design and Analysis of Experiments*, John Wiley & Sons, Chichester, UK, 1997.
18 B. G. M. Vandeginste, D. L. Massart, L. C. M. Buydens, S. DeJong, P. J. Lewi and J. Smeyers-Verbeke, *Handbook of Chemometrics and Qualimetrics*, Elsevier Science B. V, 1998.
19 R. A. Harshman, *UCLA Working Papers in Phonetics*, 1970, 16, 1.
20 J. L. Beltran, R. Ferrer and J. Guiteras, *Anal. Chim. Acta*, 1998, 373, 311.
21 R. Bro, *Chemometrics and Intelligent Laboratory Systems*, 1999, 46, 133.
22 L. Norgaard, *J. Chemom.*, 1996, 10, 615.
23 P. Hindmarch, K. Kavianpour and R. G. Brereton, *Analyst*, 1997, 122, 871.
24 A. K. Smilde and D. A. Doornbos, *J. Chemom.*, 1991, 5, 345.
25 R. Boque and A. K. Smilde, *AIChE Journal*, 1999, 45, 1504.
26 K. S. Dahl, M. J. Piovoso and K. A. Kosanovich, *Chemometrics and Intelligent Laboratory Systems*, 1999, 46, 161.
27 J. A. Westerhuis, T. Kourti and J. F. Macgregor, *J. Chemometr.*, 1999, 13, 397.
28 J. L. Todoli and J. M. Mermet, *Spectrochim. Acta Part B*, 1999, 54, 895.
29 The *N*-way toolbox for MATLAB, ver. 1.02, KVL, Denmark, 1999. http://newton.foodsci.kvl.dk/Matlab/nwaytoolbox/index.htm.
30 W. B. Barnett, V. A. Fassel and R. N. Kniseley, *Spectrochim. Acta Part B*, 1968, 23, 643.
31 W. B. Barnett, V. A. Fassel and R. N. Kniseley, *Spectrochim. Acta Part B*, 1970, 25, 139.
32 S. A. Myers and D. H. Tracy, *Spectrochim. Acta Part B*, 1983, 38, 1227.
33 A. S. AlAmmar, H. A. Hamid and B. H. Rashid, *Spectrochim. Acta Part B*, 1990, 45, 359.
34 A. Lorber, Z. Goldbart and M. Eldan, *Anal. Chem.*, 1984, 56, 43.
35 A. Lorber and Z. Goldbart, *Anal. Chim. Acta*, 1984, 161, 163.
36 A. S. AlAmmar and R. M. Barnes, *At. Spectrosc.*, 1998, 19, 18.
37 M. H. Ramsey and M. Thompson, *Analyst*, 1984, 109, 1625.
38 J. N. Walsh, *Chem. Geol.*, 1992, 95, 113.
39 V. Kanicky, *Collection Czechoslovak Chem. Commun.*, 1993, 58, 2905.
40 D. A. Sadler, F. Sun, S. E. Howe and D. Littlejohn, *Mikrochim. Acta*, 1997, 126, 301.
41 A. Marcos and S. J. Hill, *Analyst*, 2000, 125, 1015.
42 R. Bro, *J. Chemom.*, 1996, 10, 47.

A drift correction procedure for ICP-AES systems

Ana Marcos and Steve J. Hill

Department of Environmental Sciences, Plymouth Environmental Research Center, University of Plymouth, Drake Circus, Plymouth, UK PL4 8AA

A method is reported for correction of long-term drift in ICP-AES measurements. The change in the intensity of thirty emission lines was monitored over eight hours without recalibration of the instrument. Drift values were found to give errors of up to 20% with respect to the first measurement. The suggested procedure utilises the drift pattern of an intrinsic plasma line, Ar 404.597 nm, and the results of a principal component analysis to remove the drift error. After correction, the drift values drop to less than ±2%.

match samples with one or several internal standards to be able to correct some of the drift error. Both options are time consuming. The correcting method suggested here avoids recalibration and or sample matching with an internal standard element, by use of an intrinsic plasma line.

Previous work[2,3] on ICP-AES systems has shown the convenience of working at robust conditions, low nebuliser gas flow rate and high rf power. At these conditions, signals are more stable and their drift patterns are highly correlated between all the analyte lines and so, internal standardisation methods may correct for long-term drift error. Unfortunately,

Introduction

Inductively coupled plasma atomic emission spectrometry (ICP-AES) is a well established technique for routine analysis.[1] Multi-element determinations, high selectivity and limits of detection below the μg g^{-1} level have led to a wide range of applications in areas such as food science, environmental and clinical analysis.

However, in routine use, long-term drift may be a disadvantage of the ICP-AES technique, and in practice requires the analyst to either regularly recalibrate the instrument or

Table 2 ICP-AES operating conditions

Rf power	1000 W
Injector diameter	2 mm
Nebuliser type	Cross flow pneumatic nebuliser
Nebuliser flow	0.9 L min^{-1}
Plasma flow	15 L min^{-1}
Auxiliary flow	0.8 L min^{-1}
Sample uptake rate	1.0 L min^{-1}
Viewing height	12 mm
Read time	10–20 s

Table 1 Emission lines used in study

Element	λ/nm	Intensity, I_a/I_b[a]	EE = λ^b/eV	IP[c]/eV	EP + IP[d]/eV
Al (I)	396.152	10.5	3.13	—	3.1
Ba (II)	230.424	73.0	5.38	5.21	≥10.6
Ba (II)	233.527	75.0	5.31	5.21	11.2
Ca (I)	422.673	1.5	2.99	—	2.9
Ca (II)	317.933	1.5	3.90	6.11	13.1
Cd (I)	228.802	110	5.42	—	5.4
Cd (II)	226.502	120	5.47	8.99	14.4
Co (I)	340.512	No data	3.64	—	14.0
Co (II)	228.616	43.0	5.42	7.88	14.3
Cr (I)	357.869	13.0	3.46	—	≥3.46
Cr (II)	267.716	42.0	4.63	6.77	≥11.4
Cu (I)	324.754	56.0	3.82	—	3.8
Cu (II)	224.700	39.0	5.52	7.73	15.9
Fe (II)	259.940	48.0	4.77	7.90	≥12.7
Mg (I)	285.213	No data	4.35	—	4.3
Mg (II)	279.079	1.0	4.44	7.65	≥12.1
Mn (I)	403.076	6.8	3.08	—	3.1
Mn (II)	257.610	220	4.81	7.43	12.2
Na (I)	589.592	43.0	2.10	—	2.1
Ni (I)	232.003	20.0	5.34	—	≥5.34
Ni (II)	231.604	15.0	5.35	7.64	≥13.0
Pb (II)	220.353	70.0	5.62	7.42	14.7
Ti (II)	379.280	No data	3.27	6.83	≥10.1
Zn (I)	213.856	170	5.80	—	5.8
Zn (II)	202.548	75.0	6.12	9.39	15.5
Ar (I)	357.229	2.3	3.47	—	≥3.47
Ar (I)	404.597	2.5	3.06	—	≥3.06
Ar (I)	420.068	50	2.95	—	≥2.95
Ar (I)	451.074	21	2.75	—	≥2.75

[a] Ratio of net analyte intensity to background intensity (*Handbook of ICP-AES*, CRC Press, 1981). [b] Transition emitted energy (calculated by converting nm^{-1} to eV). [c] First ionisation potential (*Handbook of Physics and Chemistry*, CRC Press, 77th Edition, 1997). [d] Excitation potential (P. W. Robinson, *Handbook of Spectroscopy Vol.1*, CRC Press, 1974).

many ICP-AES users employ soft conditions to perform their analyses,[4–8] i.e., the so called 'default conditions' which imply low rf power (~ 1000 W) and a medium nebuliser flow rate (~ 1.0 Lmin⁻¹). These values facilitate the use of both soft and hard emission lines and are thus more versatile. In addition, 'standard conditions' are often promoted by manufacturers.[9] However, when using such working parameters, the ICP-AES technique can give very unstable signals over time and complex drift patterns. For this reason, an attempt has been made to monitor and correct the instability when using the more routine soft conditions.

The approach reported here requires the analyst only to monitor the drift of one argon line. A polynomial regression trendline is then fitted to the argon drift, and the long-term drift on the other lines is estimated using the trendline of the argon emission once modified by a correction factor, f_i, which is specific for each emission line. To date, this correction factor has been estimated by employing the results of a principal component analysis performed on the data set. However, the ideal case will be to estimate f_i by using only physical properties of the emission lines.

Methodology

Experimental

A multi-element solution containing 15 analytes was repeatedly analysed over a period of 8 h without recalibration (100 replicates). In order to ensure stable starting conditions, 2 h were allowed for the instrument to 'warm up'. The change in the intensities from 30 emission lines was then followed over the time. Table 1 details the lines monitored in this study. In most cases, one atomic and one ionic line were used, in addition to four argon emission lines.

Instrumentation

The instrument employed was an OPTIMA 3000 (Perkin Elmer Corporation, Norwalk, CT, USA). This ICP-AES combines an echelle polychromator with a solid state detector, which allows simultaneous acquisition. The plasma was viewed radially. The operating conditions are described in Table 2.

Table 3 Polynomial regressions of the emission lines studied

| Emission lines	Polynomial parameters						Statistics	
	β_0	β_1	β_2	β_3	β_4	β_5	s	r
Al (I)	0.107	0.313	−0.014	3.5E-04	−3.7E-06	1.4E-08	0.23	0.992
Ca (I)	0.033	0.071	−0.0038	1.1E-04	−1.3E-06	5.5E-09	0.13	0.886
Cd (I)	−0.048	0.316	−0.0133	3.2E-04	−3.4E-06	1.2E-08	0.31	0.989
Co (I)	−0.074	0.196	−0.0095	0.00026	−3.0E-06	1.2E-08	0.25	0.981
Cr (I)	0.016	0.045	−0.0027	8.9E-05	−1.2E-06	5.4E-09	0.13	0.865
Cu (I)	0.011	0.124	−0.0062	1.7E-04	−2.0E-06	8.2E-09	0.16	0.973
Mg (I)	0.047	0.257	−0.0116	2.9E-04	−3.1E-06	1.1E-08	0.20	0.990
Mn (I)	−0.026	0.047	−0.0029	9.2E-05	−1.2E-06	5.4E-09	0.13	0.859
Na (I)	0.070	0.039	−0.0026	6.8E-05	−8.4E-07	3.7E-09	0.14	0.958
Ni (I)	0.047	0.319	−0.0145	3.6E-04	−3.8E-06	1.4E-08	0.30	0.986
Zn (I)	0.254	0.462	−0.02	4.7E-04	−4.8E-06	1.7E-08	0.35	0.992
Ba (II)	−0.012	0.885	−0.0382	9.0E-04	−9.0E-06	3.1E-08	0.66	0.993
Ba (II)	0.321	0.832	−0.0348	8.1E-04	−8.1E-06	2.8E-08	0.58	0.994
Ca (II)	0.075	0.447	−0.0194	4.7E-04	−4.9E-06	1.8E-08	0.31	0.994
Cd (II)	0.122	0.238	−0.0108	2.7E-04	−2.9E-06	1.1E-08	0.22	0.988
Co (II)	−0.003	0.404	−0.0171	4.1E-04	−4.3E-06	1.6E-08	0.44	0.985
Cr (II)	−0.068	0.606	−0.0267	6.4E-04	−6.5E-06	2.3E-08	0.41	0.994
Cu (II)	0.053	0.381	−0.0169	4.1E-04	−4.4E-06	1.6E-08	0.25	0.993
Fe (II)	0.271	0.423	−0.0188	4.6E-04	−4.8E-06	1.8E-08	0.29	0.993
Mg (II)	−0.204	0.233	−0.01	2.5E-04	−2.8E-06	1.1E-08	0.23	0.988
Mn (II)	0.334	0.540	−0.0234	5.5E-04	−5.7E-06	2.0E-08	0.36	0.994
Ni (II)	−0.206	0.282	−0.0126	3.1E-04	−3.3E-06	1.2E-08	0.28	0.984
Pb (II)	0.534	0.016	−0.0016	5.8E-05	−7.6E-07	3.2E-09	0.43	0.442
Ti (II)	0.193	0.353	−0.0154	3.7E-04	−3.9E-06	1.4E-08	0.23	0.994
Zn (II)	1.031	0.503	−0.0215	5.2E-04	−5.5E-06	2.0E-08	0.53	0.988
³⁵⁷Ar	0.048	0.617	−0.0239	5.1E-04	−4.6E-06	1.4E-08	0.56	0.993
⁴⁰⁴Ar	−0.011	0.415	−0.0187	4.4E-04	−4.4E-06	1.6E-08	0.32	0.991
⁴²⁰Ar	0.033	0.593	−0.0249	5.5E-04	−5.2E-06	1.7E-08	0.34	0.996
⁴⁵¹Ar	0.004	0.588	−0.0242	5.3E-04	−4.9E-06	1.6E-08	0.36	0.996
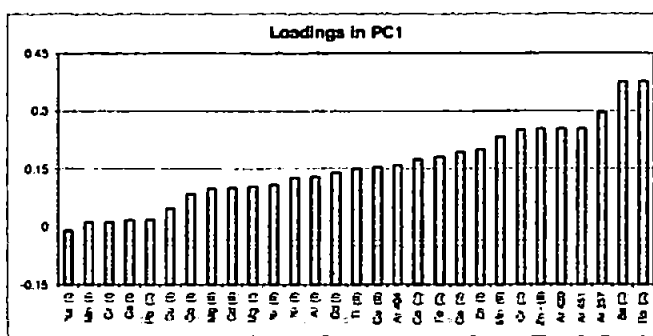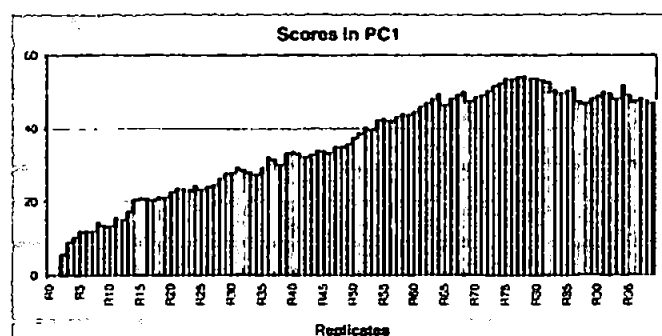
Fig. 1 Details of the principal component analysis performed to the data. Data employed, drift values; samples, the 100 replicates; variables, the 30 emission lines monitored; pretreatment, none; results, PC1 accounts for − 100% of the variation.

The correction procedure

The different steps employed in the correction procedure are described below:

1. The trendline of one of the argon lines (404.597 nm)† is calculated by employing a polynomial model up to the 5th order:

---

† This argon line was chosen because of all the argon lines monitored, the drift pattern most closely resembled that of the analyte lines.

$$y = \beta_0 + \beta_1 n + \beta_2 n^2 + \beta_3 n^3 + \beta_4 n^4 + \beta_5 n^5 \qquad (1)$$

Where y refers to the measured drift error and n refers to the replicate number.

2. A correction factor, f_i, specific for each emission line is determined using the results of a principal component analysis, PCA, performed on the data:

$$f_i = \frac{L_{\text{Anal}_i}}{L_{\text{Ar}_{404}}} \qquad (2)$$

Table 4 Comparison of the polynomial parameters. Where to apply the specific correction factor?

| Emission lines | Ratio[a] | | | | | | From the PCA | |
	β_0	β_1	β_2	β_3	β_4	β_5	Loadings ratio Ratio (analyte/Ar)	Loadings in PC1
Al (I)	−9.47	0.76	0.75	0.79	0.84	0.89	0.82	0.13
Ca (I)	−2.91	0.17	0.20	0.24	0.29	0.35	0.11	0.02
Cd (I)	4.25	0.76	0.71	0.74	0.77	0.79	0.89	0.14
Co (I)	6.51	0.47	0.50	0.59	0.68	0.76	0.53	0.08
Cr (I)	−1.40	0.11	0.15	0.20	0.27	0.35	0.08	0.01
Cu (I)	−0.97	0.30	0.33	0.39	0.46	0.52	0.30	0.05
Mg (I)	−4.13	0.62	0.62	0.65	0.69	0.73	0.65	0.10
Mn (I)	2.34	0.11	0.15	0.21	0.27	0.34	0.07	0.01
Na (I)	−6.19	0.09	0.14	0.15	0.19	0.24	−0.06	−0.01
Ni (I)	−4.13	0.77	0.77	0.82	0.87	0.92	0.80	0.12
Zn (I)	−22.48	1.11	1.07	1.08	1.10	1.10	1.26	0.19
Ba (II)	1.05	2.13	2.04	2.04	2.03	2.01	2.37	0.37
Ba (II)	−28.44	2.01	1.86	1.84	1.83	1.81	2.38	0.37
Ca (II)	−6.64	1.08	1.03	1.06	1.10	1.13	1.21	0.19
Cd (II)	−10.84	0.57	0.58	0.62	0.66	0.71	0.63	0.10
Co (II)	0.31	0.97	0.91	0.93	0.96	0.99	1.10	0.17
Cr (II)	6.05	1.46	1.43	1.45	1.47	1.47	1.57	0.24
Cu (II)	−4.71	0.92	0.90	0.94	1.00	1.05	0.98	0.15
Fe (II)	−23.95	1.02	1.00	1.05	1.10	1.14	1.13	0.18
Mg (II)	18.09	0.56	0.53	0.58	0.64	0.70	0.62	0.10
Mn (II)	−29.53	1.30	1.25	1.26	1.28	1.29	1.46	0.23
Ni (II)	18.24	0.68	0.67	0.70	0.74	0.77	0.68	0.11
Pb (II)	−47.21	0.04	0.08	0.13	0.17	0.20	0.12	0.02
Ti (II)	−17.11	0.85	0.82	0.85	0.88	0.91	0.95	0.15
Zn (II)	−91.23	1.21	1.14	1.19	1.24	1.27	1.60	0.25
^{357}Ar	−4.22	1.49	1.27	1.16	1.03	0.89	1.87	0.29
^{404}Ar	1.00	1.00	1.00	1.00	1.00	1.00	1.00	0.15
^{420}Ar	−2.91	1.43	1.33	1.25	1.17	1.09	1.60	0.25
^{451}Ar	−0.32	1.42	1.29	1.20	1.10	1.00	1.60	0.25

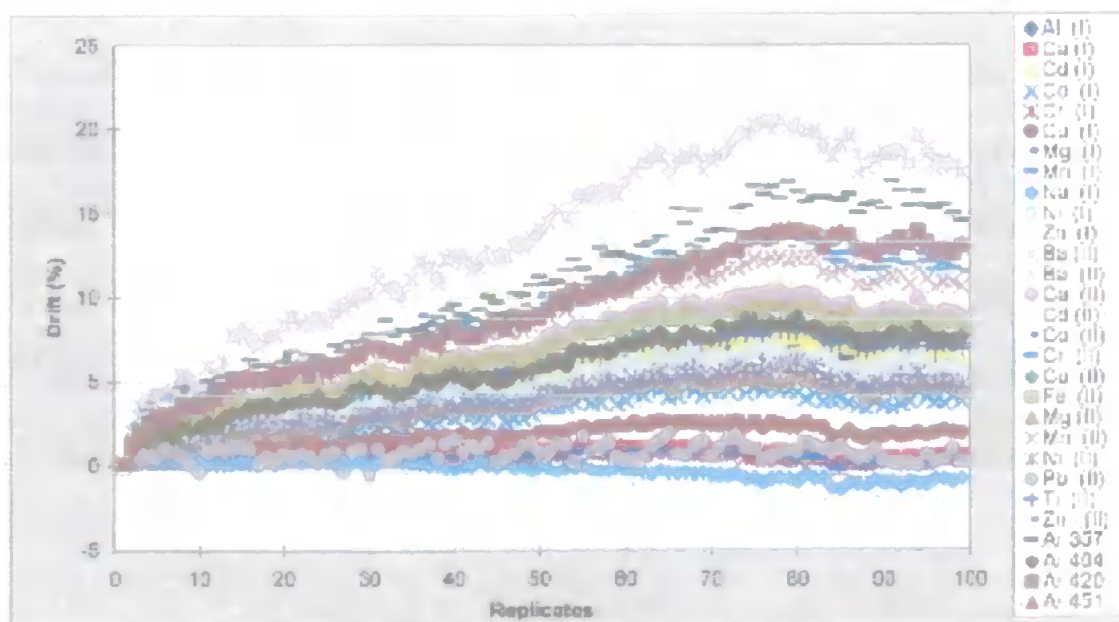[a] Parameters of the analyte trendline/parameters of the ^{404}Ar.

Fig. 2 Drift patterns over 8 h of analysis.

Where L_{Anal_i} refers to the loading of analyte line i on PC1, and $L_{Ar_{404}}$ refers to the loading of argon line 404.597 nm on PC1.

3. The drift on each emission line is then estimated using the trendline of the argon, and the correction factor specific for the line, f_i. All the parameters, β, of the argon trendline in n; (i.e., β_1, β_2, β_3, β_4, β_5, not β_0) are multiplied by f_i:

$$y_{Anal_i} = \beta_0^{Ar_{404}} + f_i\beta_1^{Ar_{404}}n + f_i\beta_2^{Ar_{404}}n^2 + f_i\beta_3^{Ar_{404}}n^3 + f_i\beta_4^{Ar_{404}}n^4 + f_i\beta_5^{Ar_{404}}n^5 \qquad (3)$$

4. The estimated drift is removed from the measured data to create the 'corrected data set'.

5. The long-term drift on the corrected data set is calculated and compared to the drift of the data before correction.

Calculation of the trendlines. Any curve can be fitted using a polynomial regression to the nth order. Increasing the order has the effect of improving the fit, i.e., the regression coefficient, r, will tend to one. In this study, the drift patterns have been regressed to polynomial curves up to the 5th order, which gives an improved regression coefficient but with a practical number of parameters: six [eqn. (1)]. The polynomial

equations were calculated using the software 'CurveExpert, version 1.3' (Daniel Hyams & Microsoft Corporation, Redmond, WA, USA).

Although, only the trendline of argon 404.597 nm is used in the correction procedure, the polynomial regressions of all the other lines studied were also calculated. This facilitated a comparison of the polynomial parameters of every line to those of the argon trendline, and thus allowed us to determine where the specific correction factor should be applied. The parameters found are reported in Table 3.

The correction factor. The specific correction factors have been calculated by employing the loadings of a principal component analysis (Fig. 1) performed on the data set. The loading in the first principal component of every emission line is compared to the loading of the argon line [eqn. (2)]. The 'loading ratios' have been employed as *specific correction factors*.

In order to investigate where to apply the specific correction factor, the polynomial parameters of all the fitted curves were compared. It was observed that the ratio of all parameters
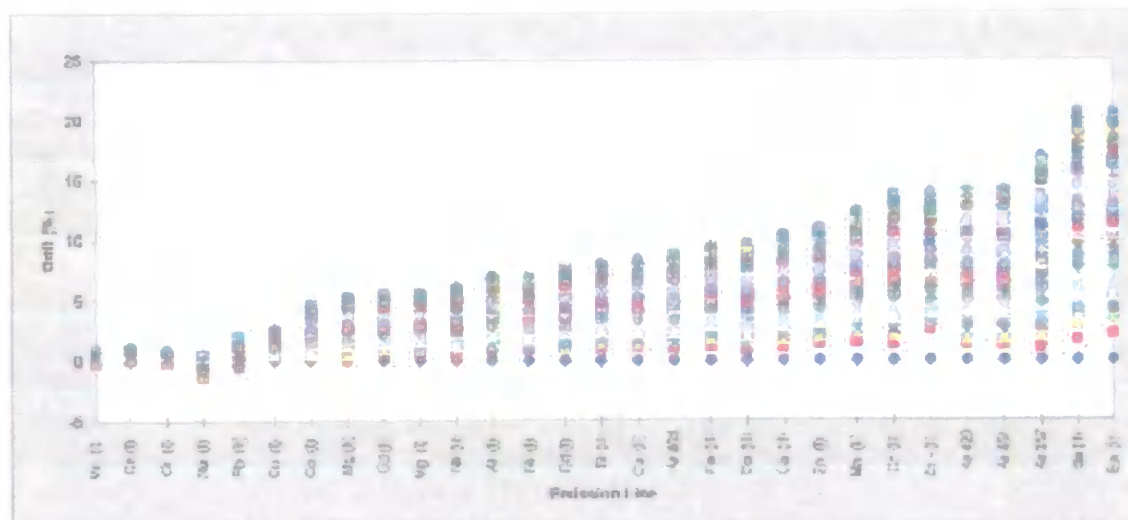

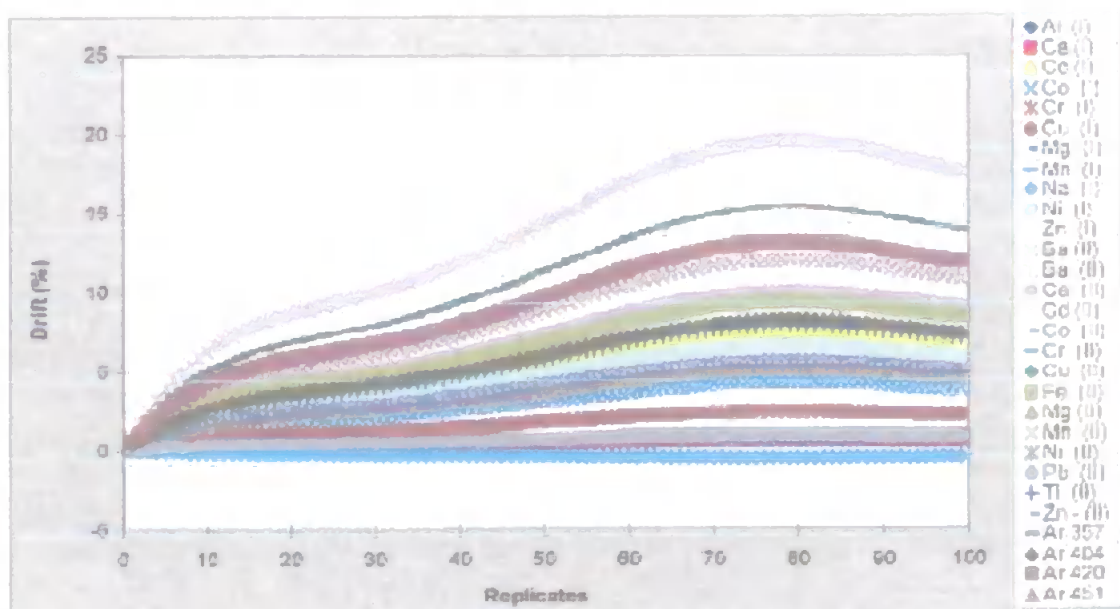Fig. 3 Ranges of variation for each monitored emission line.

Fig. 4 Estimated drift using the suggested correction procedure.

multiplying the replicates n of the analyte line to those of the argon line were constant, and this ratio was indeed similar to the ratio of the PCA loadings (Table 4). Thus, the correction factors were calculated using the PCA loading ratios and applied to the argon trendline by multiplying every parameter, except the intercept, β_0. The drift on each analyte line was then estimated by eqn. (3).

Results and discussion

Fig. 1 shows the evolution of the drift on the 30 emission lines monitored during 8 h of repeated determinations. It can be seen that the drift patterns are similar for all the lines, but with a different gradient at the beginning of the analysis.

If the range of variation of each emission line is plotted, Fig. 2, it can be seen how some lines remain very stable during the whole experiment whilst others have drift values up to 20%. In general, the atomic lines are more stable than the ionic lines, a feature almost certainly due to the low rf power employed (1000 W), which tends to make hard lines more vulnerable to drift. Certainly, the variation in the sequence of lines is not random (Fig. 3), and so some physical characteristic of the emission lines probably accounts for these differences. A number of fundamental properties of the lines have been correlated to the variation sequence, e.g., emission energy, excitation energy and intensity of the lines, in order to estimate the correction factor. To date however, we have not found good correlation with any of the physical characteristics tested, and thus the loading ratio has been retained as the best approximation to calculate the specific correction factors.

The 'estimated drift' for each emission line monitored is shown in Fig. 4. This was calculated using the polynomial fit for the emission line of argon 404.597 nm and the specific correction factors. The remaining drift error after correction has been plotted in Fig. 5. It can be observed that the long-term drift drops from around 20% in the original data set, Fig. 2, to better than 2% after applying the correction procedure, Fig. 5. The factors of improvement are detailed in Table 5.

The suggested correction procedure has been shown to successfully remove most of the drift from the data when using 'typical' default instrumental conditions. The procedure employs the drift pattern of an intrinsic plasma line, the emission line of argon at 404 nm, instead of an added internal standard,

and only requires the results of a previous principal component analysis to estimate the specific correction factors.

The phenomenon which cause the sequence described above are still being investigated as are the potential effects due to the addition of a more complex chemical matrix.

Table 5 Improvement in drift obtained by employing the suggested correction procedure after 8 h of analysis

Emission lines	Long-term drift after 8h of analysis Measured (%)	After correction (%)	F_t^a	Maximum drift observed Measured (%)	After correction (%)	F_t
Al (I)	6.0	−0.1	55	7.0	0.6	11
Ca (I)	0.5	−0.3	2	1.2	0.4	3
Cd (I)	6.3	−0.3	21	7.7	0.9	8
Co (I)	3.9	0.0	98	4.8	0.6	8
Cr (I)	0.3	−0.2	1	1.0	0.5	2
Cu (I)	1.9	−0.2	8	2.7	0.4	6
Mg (I)	4.6	−0.3	17	5.6	0.6	10
Mn (I)	0.4	−0.1	3	0.9	0.4	2
Na (I)	−0.8	−0.3	3	0.5	0.7	1
Ni (I)	5.6	−0.3	19	7.1	0.7	11
Zn (I)	9.0	−0.3	27	11.0	0.6	17
Ba (II)	17.4	−0.2	109	20.5	1.3	16
Ba (II)	17.5	−0.1	136	20.6	1.3	16
Ca (II)	8.8	−0.2	43	10.4	0.8	14
Cd (II)	4.4	−0.3	16	5.6	0.5	10
Co (II)	8.2	0.0	750	9.8	1.0	10
Cr (II)	11.5	−0.1	84	13.8	0.9	16
Cu (II)	7.2	−0.1	70	8.3	0.7	12
Fe (II)	8.2	−0.2	42	9.6	0.8	12
Mg (II)	4.4	−0.2	20	5.4	0.5	11
Mn (II)	10.6	−0.2	56	12.4	0.8	16
Ni (II)	4.8	−0.3	18	6.2	0.6	10
Pb (II)	0.2	−0.6	0	2.0	1.1	2
Ti (II)	6.9	−0.1	58	8.1	0.6	13
Zn - (II)	11.4	−0.4	30	13.9	1.6	9
357Ar	14.5	0.6	25	16.9	1.9	9
404Ar	7.7	0.2	34	8.8	0.5	16
420Ar	12.9	1.0	13	13.9	1.5	10
451Ar	13.1	1.2	11	14.1	1.5	9

a Factors of improvement.
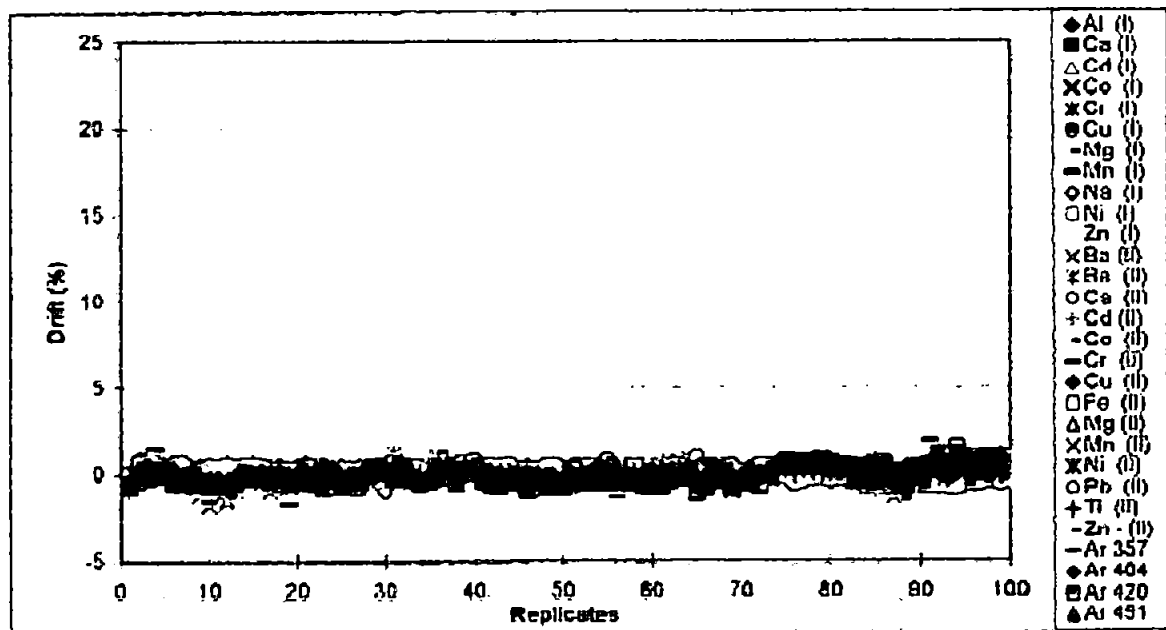
Fig. 5 Drift error remaining after correction.

References

1 *Inductively Coupled Plasma Spectrometry and Its Applications*, ed. S. J. Hill, Sheffield Academic Press, 1999.
2 X. Romero, E. Poussel and J. M. Mermet, *Spectrochim. Acta, Part B*, 1997, 52B, 487.
3 A. Marcos, M. Foulkes and S. J. Hill, *J. Anal. At. Spectrom.*, submitted for publication.
4 I. Rodushkin, T. Ruth and A. Huhtasaari, *Anal. Chim. Acta*, 1999, 378, 191.
5 O. Abollino, M. Aceto, M. C. Bruzzoniti, E. Mentasti and C. Sarzanini, *Anal. Chim. Acta*, 1998, 375, 293.
6 J. A. Nobrega, Y. Gelinas, A. Krushevska and R. M. Barnes, *J. Anal. At. Spectrom.*, 1997, 12, 1243.
7 T. Piippanen, J. Rautiainen and J. Tummavuori, *Anal. Chim. Acta*, 1997, 349, 327.
8 E. H. VanVeen, S. Bosch and M. T. C. de Loos-Vollebregt, *Spectrochim. Acta, Part B*, 1997, 52, 321.
9 C. B. Boss and K. J. Fredeen, *Concepts, Instrumentation and Techniques in ICP-OES*, Perkin Elmer Corporation, 1997.